AN EXPERIMENTAL STUDY OF PROTON–EXCHANGED LITHIUM NIOBATE OPTICAL WAVEGUIDES

A Thesis,
Submitted To The
Faculty Of Engineering
Of The University Of Glasgow
By

Armando Loni, BSc(Nat. Phil.)

CONTENTS

Dedicated To My Wife, Linda.

ACKNOWLEDGEMENTS.

I am extremely grateful to Professor John Lamb for the interest he has shown in my work, and the encouragement he has given me over the last three years.

I would like to thank Prof. S.J. Thomson, now retired, for allowing me to use the many facilities of the Chemistry Department.

I express sincere gratitude to my academic supervisors (and friends) Professor Richard De La Rue and Doctor John Winfield (Chemistry Department) for their encouragement, help, and ideas, and for the many useful discussions.

The help and assistance of members of the Mechanical and Electronic Workshops, for realising and improving many of my designs, is much appreciated. Thanks also to Mr. Kas Piechowiak for cutting and polishing my lithium niobate.

I would like to acknowledge the following members of the Chemistry Department:

* Mr. J. McCaig (for familiarising me with analysis by atomic absorption spectroscopy),

Mrs. Frieda Laurie and Mr. George McCulloch (for their help in the infrared absorption studies),

Members of the Glassblowing Workshop and Mechanical Workshop (for their help in the construction and repair of my equipment in the Chemistry laboratory)

and,

Messrs. Larry McGhee, David Wilson, and Jim McIver (for their friendship).

Finally, my thanks to Barr and Stroud Ltd., not only for supplying me with lithium niobate, but also for their financial assistance over the last three years.

* *Now with Motherwell Technical College.*

THESIS OUTLINE

The object of this thesis is to form an understanding of the origin of the problems associated with proton–exchanged waveguides, and to investigate possible solutions.

Chapter 1 gives a brief introduction to the properties of lithium niobate, and discusses the methods available for fabricating optical waveguides in the bulk material, with particular emphasis on waveguide fabrication by the proton–exchange process. Some of the devices which have been fabricated by proton–exchange are discussed. The problems associated with proton–exchanged waveguides are reviewed.

Chapter 2 deals with the physical and chemical characterisation of proton–exchanged waveguides fabricated using neat benzoic acid melts. The extent of proton–exchange is determined as a function of fabrication time and temperature using optical waveguide prism–coupler measurements, infrared absorption spectroscopy, and atomic absorption spectroscopy.

Chapter 3 is concerned with the problem of waveguide mode–index stability. Using a hydrogen isotopic–exchange reaction, the extent of which is observed via infrared absorption spectroscopy, information on the (room–temperature) mobility of protons within the guiding layer is obtained for waveguides fabricated using neat benzoic acid melts. The recently reported process of fabricating waveguides in lithium niobate by deuterium–exchange is investigated. The behaviour of proton–exchanged and deuterium–exchanged waveguides with respect to reaction with atmospheric water vapour is investigated, and the optical properties of deuterium–exchanged waveguides are studied.

In Chapter 4, a study of annealed and dilute–melt proton–exchanged waveguides is presented. It is shown, using prism–coupler measurements and infrared absorption spectroscopy, that annealed and dilute–melt waveguides can have very similar optical properties, depending on the amount of annealing and the lithium benzoate mole–fractions used. The extent of proton–exchange is determined with time (between 215°C and

235°C) for dilute–melt waveguides produced using lithium benzoate mole–fractions of up to 1.1%. Isotopic–exchange in annealed and dilute–melt waveguides is also investigated, both at room–temperature and at temperatures commonly used for annealing. A possible explanation for the poor optical properties of (neat–melt) proton–exchanged waveguides is given.

Chapter 5 deals with a study of propagation losses (using the two–prism method) and the electro–optic effect in x– and z–cut proton–exchanged waveguides. Measurements of r_{33} (in proton–exchanged waveguides) and r_{22} (in titanium–indiffused waveguides) are carried out using an external interferometric method designed by the author. The results of Chapter 4 are used to establish a method by which losses below 0.5dB/cm and a substantially restored electro–optic effect can be achieved (using a combination of dilute–melt fabrication with post–exchange annealing). Prior to the waveguide measurements, the bulk electro–optic effect is investigated for congruent, incongruent, MgO–doped, and annealed (high–temperature) crystals.

Finally, in Chapter 6, a summary of the thesis is presented, and suggestions for future work are given.

CHAPTER 1

An Introduction to Lithium Niobate Integrated Optics Technology.

1.1. LITHIUM NIOBATE.

1.1.1. Crystal Structure.

The materials aspect of lithium niobate has been studied by Nassau *et al*[1,2] and Abrahams *et al*[3,4,5]. Additional observations on the structure are reviewed in the papers by Rauber[6] and Weis *et al*[7]. The most recent investigation of the structure of congruent lithium niobate has been carried out by Abrahams *et al*[8].

The structure of congruent lithium niobate above its Curie temperature (1210°C), i.e. in its paraelectric state, consists of planar sheets of oxygen atoms in a hexagonal–close–packing configuration (Figure 1.1). Below the Curie temperature, i.e. in its ferroelectric state, the lithium and niobium cations are displaced along the c–axis direction by (respectively) 0.71Å and 0.26Å[6]. The displacement can take place either above or below the oxygen planes, giving multi–domain material (unpoled). Poling the crystal (as discussed in Section 1.1.2) gives single–domain crystals.

Due to its displacement out of the oxygen layer (in the ferroelectric state), the lithium ion has a distorted octahedral environment, leaving another octahedral site vacant. Therefore, the octahedral interstices formed in the structure are one–third filled by lithium atoms (Li), one third filled by niobium atoms (Nb), and one–third vacant (V)[8]. In the c–direction, the stacking sequence of atoms in these interstices is[8]:

.....Nb V Li Nb V Li Nb V Li.....

In the model of congruent lithium niobate presented by Abrahams *et al*[8], one niobium ion in approximately every three unit cells occupies a lithium ion site, leaving a corresponding niobium site vacant. A unit cell with a vacant niobium site and with all other sites occupied has a net charge of −5. A unit cell with a vacant niobium site but with niobium at the lithium site has a net −1 charge, and a unit cell with both sites occupied by niobium, a net +4 charge. Abrahams showed that each of the latter combinations necessarily occurred and that the corresponding formula of congruent lithium niobate was:

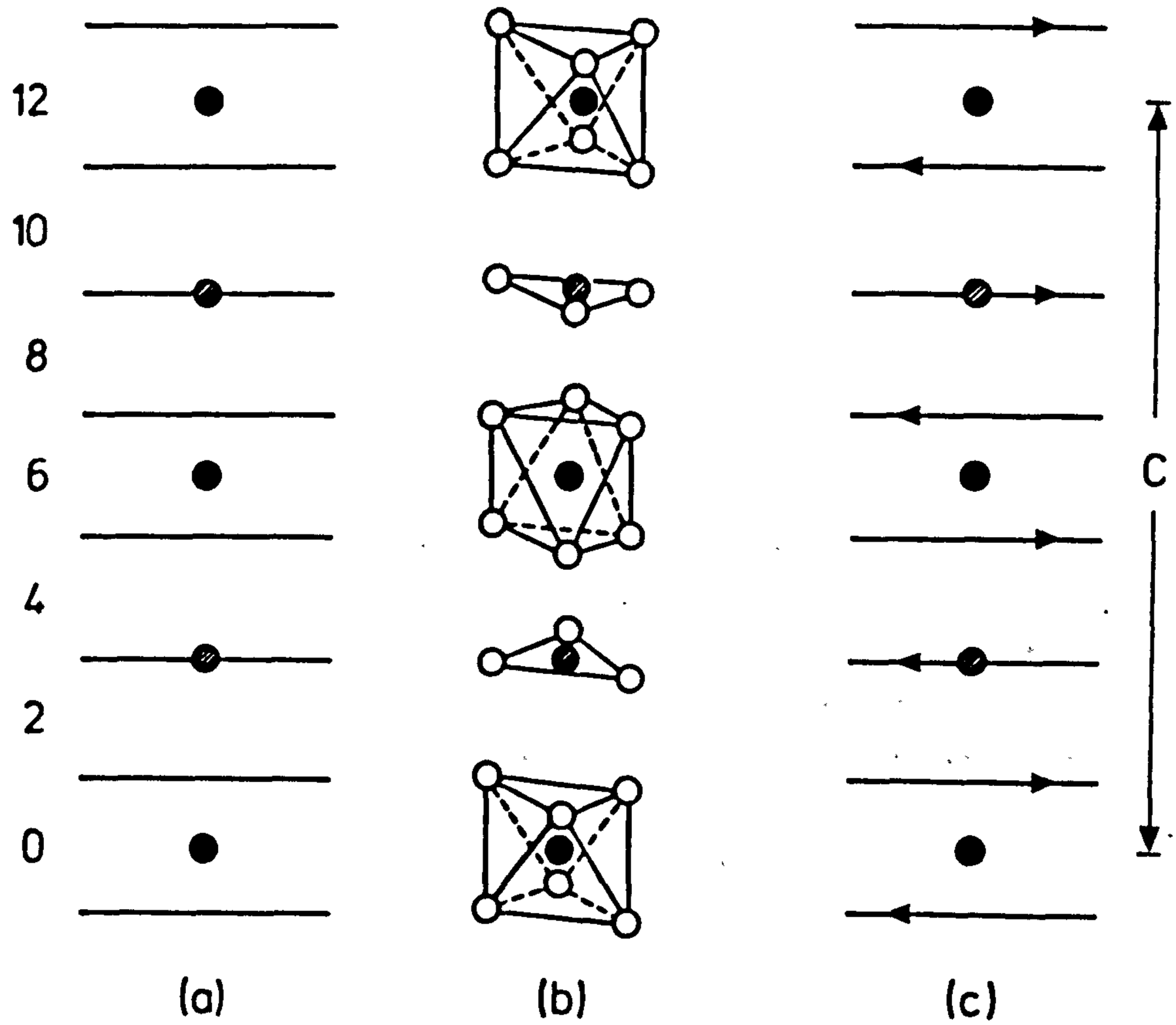

Figure 1.1. The Crystal Structure Of Lithium Niobate Above The Curie Temperature (A. Rauber[6]).

$Li_{0.941}Nb_{1.012}O_3$

By convention[7], the Cartesian coordinate system is related to the hexagonal unit cell coordinates of lithium niobate as follows: the z–axis coincides with c_{hex} and the x–axis is chosen to coincide with any of the equivelent a_{hex} axes; the y–axis lies in a plane of mirror symmetry, orthogonal to x and z.

1.1.2. Crystal Growth By The Czochralski Technique.

The growth of lithium niobate by the Czochralski technique was reported independently by Ballman[9] and Fedulov *et al*[10] in 1964. Since then, all commercially available lithium niobate has been grown by this method.

The starting compounds used for the growth of lithium niobate ($LiNbO_3$) are lithium carbonate (Li_2CO_3) and niobium pentoxide (Nb_2O_5). Appropriate amounts of the starting compounds are weighed and homogenised in a platinum crucible and the mixture is heated (in ambient atmosphere) to approximately 1160°C for 12hr, to ensure that reaction of the constituents occurs[11]:

$$Li_2CO_3 + Nb_2O_5 \longrightarrow 2LiNbO_3 + CO_2.$$

The axis generally used for crystal growth is the z–axis, although both x– and y–axis growth can be used. The Czochralski technique enables the growth of good–quality crystal boules, with uniform composition. Boules with diameters of 75mm are now being produced[12].

To obtain single–domain crystals, the boules must be electrically poled[2]. Poling consists of applying a d.c. electric field along the z–axis of the boule either during or after growth. The z–axis faces are coated with platinum paste electrodes and the boule is heated to above the Curie temperature (1210°C), after which a poling current of approximately

$2mA/cm^2$ is passed for 30min to 60min[2]. During this time, the boule is cooled to below the Curie temperature. The current is then switched off and the boule is allowed to cool to room–temperature[2].

1.1.3. Non–Stoichiometry In Lithium Niobate.

The combination of piezo–electric and optical properties has made lithium niobate one of the most extensively studied materials in recent years. As a consequence, it has been widely used for the fabrication of bulk and integrated optical devices. However, when Abrahams *et al* determined the crystal structure in 1966, the large possible deviations in stoichiometry in the lithium niobate system were generally unknown.

The phase diagram of the system $Li_2O–Nb_2O_5$ has been examined by many workers. The version given by Svaasand *et al*[13] is shown in Figure 1.2a. An extended view of the central part of the diagram is reproduced in Figure 1.2b. There are at least four compounds in the $Li_2O–Nb_2O_5$ system, namely $Li_2Nb_{28}O_{71}$, $LiNb_3O_8$, $LiNbO_3$, and Li_3NbO_4. Besides $LiNbO_3$, only $LiNb_3O_8$ has been grown in single–crystal form[13]. Lithium niobate has a solid–solution range from 44 mole% to 50 mole% Li_2O (Figure 1.2a and 1.2b) and tends to grow with variable composition, depending on the ratio of starting compounds used[11,14]. Carruthers *et al*[11] have determined the variation in the solid (crystal) composition as a function of the melt composition (Figure 1.3). The congruent melting composition is 48.6 mole% Li_2O[11].

At temperatures above approximately 900°C, the solid–solution range is large and the range gets smaller at lower temperatures[14] (Figure 1.2b). Svaasand *et al*[13] showed that the $LiNb_3O_8$ phase precipitated from an originally homogeneous $LiNbO_3$ phase after annealing congruent composition crystals at 600°C–900°C for 170hr[13]. The precipitated phase led to an increase in optical scattering in the samples[13]. The rate of precipitation was temperature–dependent and reached a maximum at 800°C, after 10hr[13]. The cooling rates used in the growth of commercially available lithium niobate are sufficiently rapid (>3°C/min)[12] that precipitation of $LiNb_3O_8$ does not occur. However, the occurrence of the latter phase should always be considered when

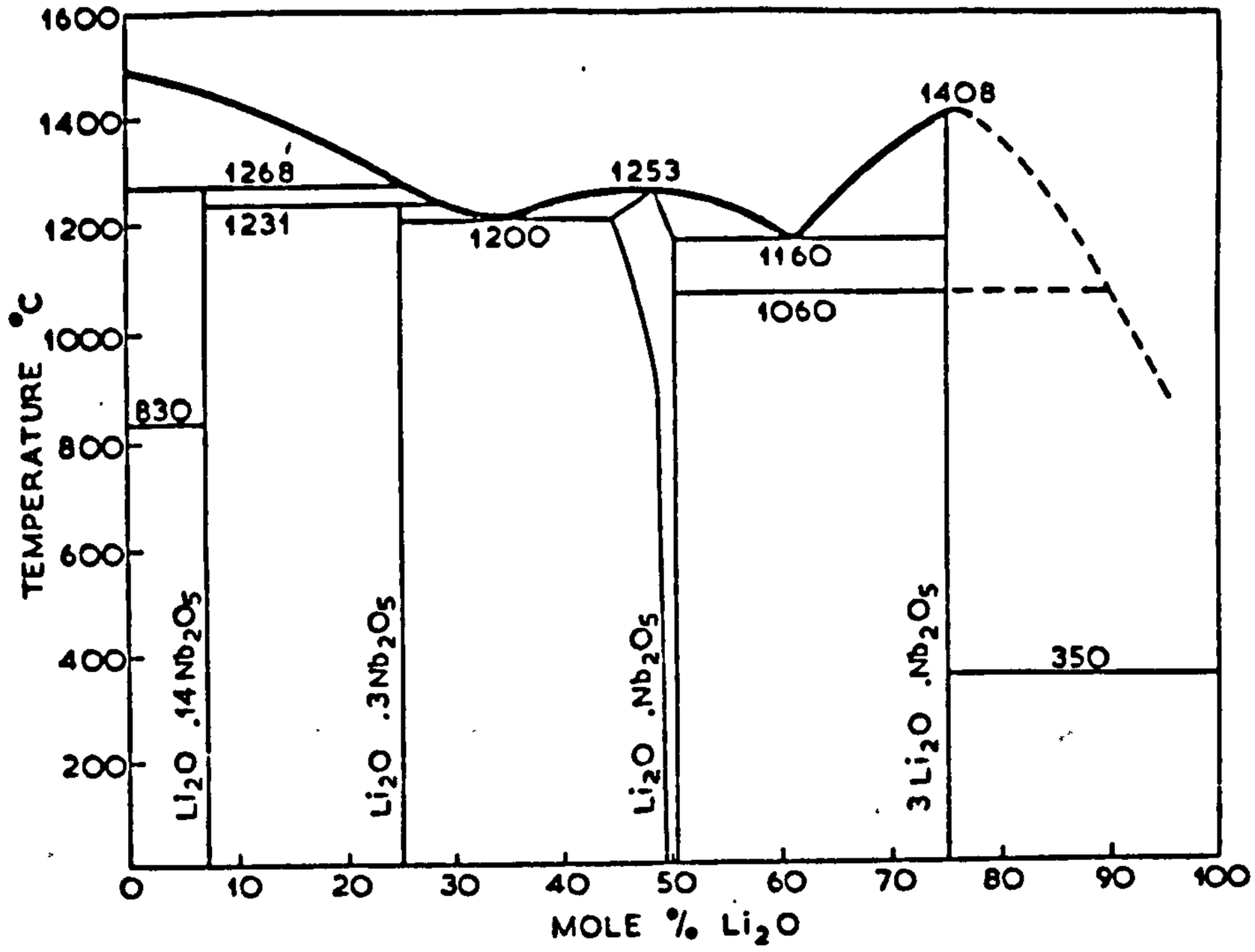

Figure 1.2a. Phase Diagram For The $Li_2O-Nb_2O_5$ System (Svaasand *et al*[14]).

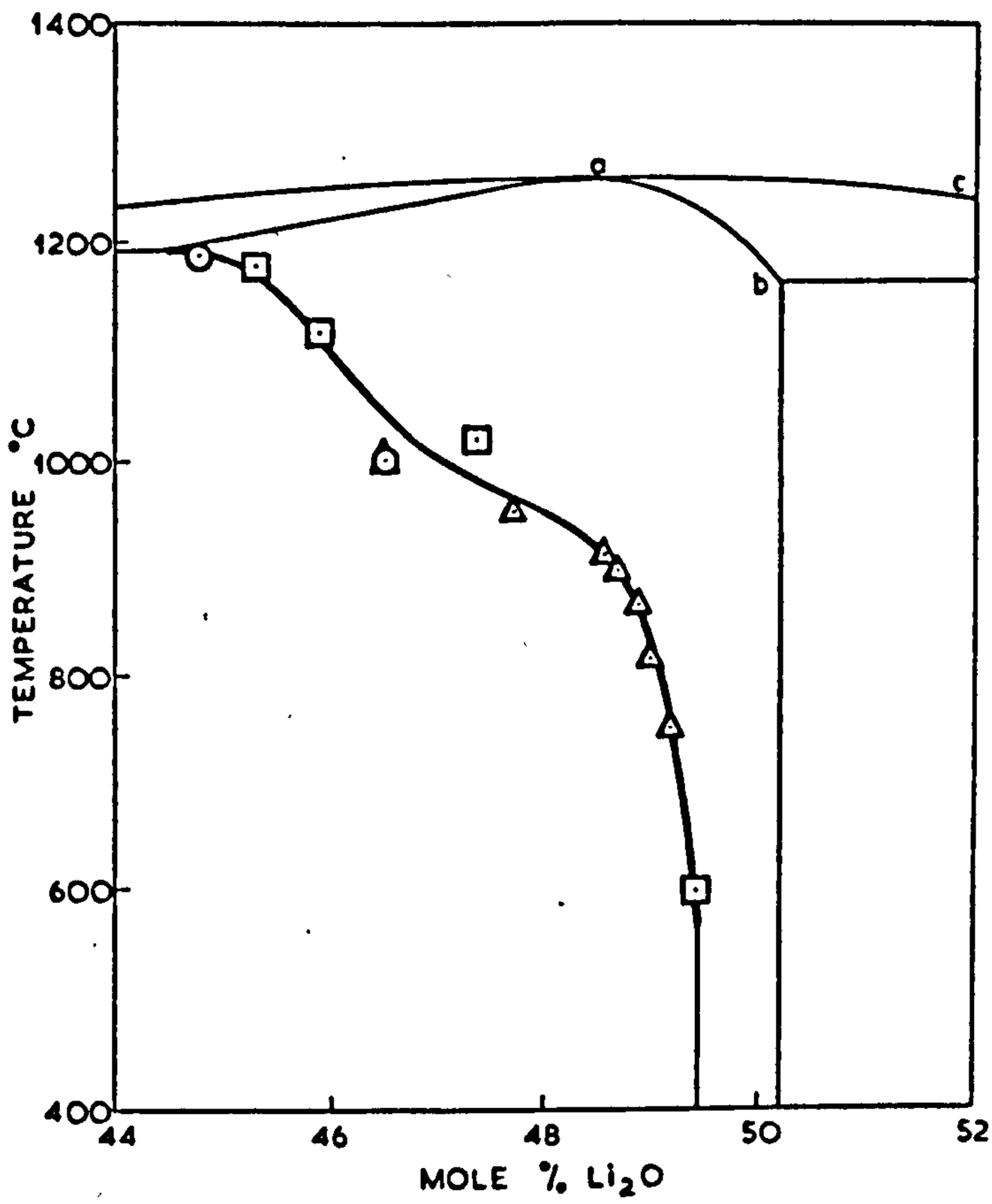

Figure 1.2b. Extended Phase Diagram For The $Li_2O-Nb_2O_5$ System (Svaasand *et al*[13]).

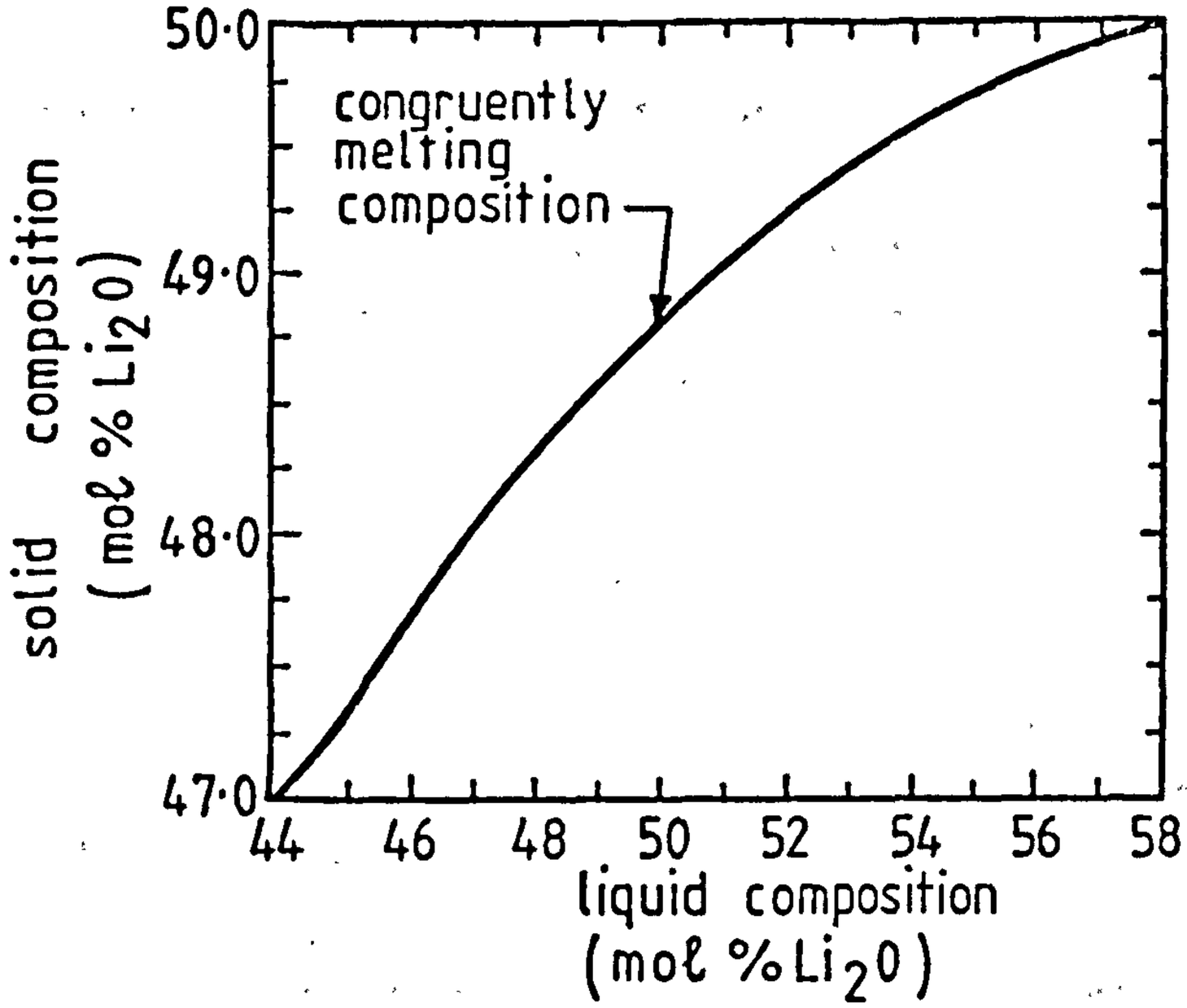

Figure 1.3. Solid (Crystal) Composition Versus Melt Composition For Lithium Niobate (Carruthers *et al*[11]).

undertaking heat–treatment of lithium niobate crystals, for example, in fabricating titanium–indiffused waveguides (Section 1.2.3).

Several properties of bulk lithium niobate, for example, the Curie temperature[15,16] and birefringence[15,16,17,18], are strongly dependent on the composition. Other properties, such as the electro–optic effect[19], the dielectric constant[19], and the unit–cell parameters[8,20,21], show only minor variations.

1.2. OPTICAL WAVEGUIDE FORMATION IN LITHIUM NIOBATE.

Five methods which have been used to form optical waveguides in lithium niobate are: (1) lithium oxide (Li_2O) outdiffusion, (2) ion–implantation, (3) metal indiffusion, (4) proton–exchange and, (5) titanium–indiffusion combined with proton–exchange.

1.2.1. Lithium Oxide (Li_2O) Outdiffusion.

It has been reported[15–18] that the ordinary refractive index (n_o) of lithium niobate is independent of the crystal stoichiometry whereas the extraordinary refractive index (n_e) increases (approximately linearly) as the lithium/niobium mole–ratio decreases. Hence, by reducing the lithium concentration at the surface of the crystal, an optical waveguiding layer can be formed. Kaminow *et al*[22] and Carruthers *et al*[23] have showed that heating lithium niobate at temperatures greater than 800°C resulted in the outdiffusion of lithium oxide (Li_2O) and, therefore, produced outdiffused waveguiding regions. The refractive index profile of an outdiffused waveguide is graded in form with a maximum index change (Δn_e) of between 10^{-2} and 10^{-3} ($\lambda = 0.6328\mu m$), depending on the amount of outdiffusion[22,23].

1.2.2. Ion–Implantation.

Ion–implantation is an alternative technology for the fabrication of optical waveguides in lithium niobate[24]. Workers at Surrey University[25] have studied the characteristics of waveguides fabricated by the implantation of high energy (1MeV) He^+. The process involves implanting lithium niobate

substrates with He^+ to form a buried (damaged) layer whose refractive indices are lower than that of the bulk crystal. The damaged layer forms the walls of the waveguide. The depth of the layer is determined by the ion energy and the refractive index reduction depends on the ion dose[24]. The implantation process is followed by a low-temperature (100°C to 220°C) annealing stage. Annealing removes the ion-induced damage from the guiding layer and, therefore, reduces scattering and propagation losses[25].

The amount of reduction of the refractive index can be as much as 5%, depending on the ion dose[24,25]. Instabilities in the refractive index have been observed at room-temperature, although it was shown that the instabilities could be avoided by annealing[26]. Waveguide losses as low as 1dB/cm ($\lambda = 0.6328\,\mu m$) have been reported for multi-mode waveguides[26], although the electro-optic coefficients (r_{33}) have been shown to be reduced by approximately 20%[27].

1.2.3 Metal-Indiffusion.

The most common method of producing optical waveguides in lithium niobate is by metal-indiffusion. The metal which has been the most widely used is titanium[28,29]. The fabrication process involves coating the lithium niobate substrate (after cleaning) with a thin-film of the metal. The thickness of the film ranges between 250Å and 1000Å. The substrate is heated at temperatures in the range 850°C to 1150°C for times of a few hours or longer, depending on the depth of waveguide required. During heating, the metal oxidises and diffuses into the substrate[29].

The refractive index profile of a metal-indiffused waveguide is graded in form and the values of n_o and n_e are increased, enabling both TE and TM modes to be supported. The highest index changes are achieved with titanium metal (with the values $\Delta n_e = 0.025$, $\Delta n_o = 0.01$)[28,29]. Other metals, such as vanadium and nickel, give changes of ($\Delta n_e = 2x10^{-3}$, $\Delta n_o = 5x10^{-4}$), and ($\Delta n_e 5x10^{-3}$; $\Delta n_o = 2x10^{-3}$), respectively[29]. Losses of approximately 1dB/cm ($\lambda = 0.6328\,\mu m$) have been reported[30], with no reduction in the electro-optic effect.

Due to the high temperatures involved in the diffusion process there is a tendency to lose Li_2O from the substrate[22,23]. This is undesirable for the following reason: since the loss of Li_2O occurs over the whole of the substrate, a planar waveguiding region is formed. Light confinement in stripe waveguides can therefore be lost via the outdiffused planar waveguide, and unwanted coupling between stripe waveguides can take place.

Several methods have been proposed to compensate for the loss of Li_2O at the surface of the substrate, and therefore to eliminate the outdiffused waveguide modes[31,32,33,34,35]. The methods rely on the treatment of the substrate with Li_2O vapour during the diffusion process. Sources of vapour are $LiNbO_3$ and Li_2CO_3 powders[32–34]. It has been reported[35] that the presence of lithium niobate crystals also compensates for loss of Li_2O. The above methods may introduce excess Li_2O into the crystal so that the change in n_e is negative rather than positive, and the outdiffused waveguide is not formed.

1.2.4. Proton–Exchange.

The proton–exchange process was introduced by Jackel *et al*[36,37] as a means of producing the compounds hydrogen niobate ($HNbO_3$) and hydrogen tantalate ($HTaO_3$) from lithium niobate and lithium tantalate, respectively. The process consists of[38] chemical reaction between lithium niobate (or lithium tantalate) and an acid at temperatures between 150°C and 250°C (or higher, if using sealed vessels[39]) for periods of a few minutes or longer, depending on the depth of waveguide required.

The proton–exchange process involves exchange between lithium ions in the substrate and protons (hydrogen) from the acid. Complete exchange (in powders) eventually results in a transformation from the rhombohedral lithium niobate structure to the cubic hydrogen niobate structure[36,37]. However, partially exchanged materials can be prepared which allow the preparation of thin layers at the surface of the lithium niobate substrate[38]. These layers have an increased extraordinary refractive index and, therefore, act as waveguiding layers[38]. The acid most widely used for proton–exchange is benzoic acid ($C_6H_5CO_2H$), for reasons

which are discussed in Chapter 2.

The refractive index profile of a proton–exchanged waveguide is approximately step–like, with a large increase in n_e ($\Delta n_e = 0.1257$ at $\lambda = 0.6328\,\mu m$)[38], and a reduction in n_o ($\Delta n_o = -0.04$ at $\lambda = 0.6328\,\mu m$)[40]. Therefore, in x– and y–cut material only TE modes are supported and in z–cut material only TM modes are supported.

Shah[41] and Jackel[42] have demonstrated waveguide formation in lithium niobate by immersion in molten silver nitrate ($AgNO_3$) and molten thallium nitrate ($TlNO_3$). It was thought that the waveguides so formed were a result of silver–lithium or thallium–lithium ion exchange. The high index change observed was of the same value as that observed in proton–exchanged waveguides. However, the waveguides had a high degree of irreproducibility for apparently identical treatment[41,42]. The latter effects lead them, and others[43], to believe that the formation process was not due to silver or thallium ions exchanging with lithium ions, but to exchange between hydrogen and lithium ions, i.e. proton–exchange. The source of hydrogen was found to be water impurities in the melts.

Many problems have been associated with proton–exchange. These include time–varying effective mode–indice[44], relatively high propagation losses (2dB/cm to 5dB/cm, Chapter 4), severe in–plane scattering[45,46], surface damage induced on y–cut substrates[47], and a reduced electro–optic effect[48].

As is discussed in Chapter 4, some of the latter problems can be avoided either by post–fabrication annealing or by using what are known as dilute–melts[49]. When a small percentage of lithium benzoate ($C_6H_5CO_2Li$) is added to the benzoic acid the extent of proton–exchange is reduced[49]. Waveguide fabrication by this method is commonly referred to as dilute–melt fabrication, and forms part of the work described in Chapter 4.

1.2.5. Titanium–Indiffusion Combined With Proton–Exchange.

Titanium–indiffusion and proton–exchange were successfully combined for the first time by De Micheli *et al*[40, 50]. Such waveguides are formed by the proton–exchange of titanium–indiffused lithium niobate. The combined process (TIPE) offers several advantages which include the tailoring of waveguide birefringence[51] (using either neat– or dilute–melts and/or annealing), realising proton–exchanged y–cut waveguides with no surface damage[40], and the formation of buried (TM) waveguides (due to the reduced value of n_o caused by proton–exchange)[40].

1.3. DEVICE FABRICATION BY PROTON–EXCHANGE.

The proton–exchange process has been used to fabricate a wide range of passive and active integrated optical devices. Passive structures include various types of gratings and planar lenses[52,53,54,55], and (using the TIPE process) polarisers[56,57]. Polarisers fabricated by the TIPE process exploit the fact that proton–exchange increases n_e and decreases n_o, while titanium–indiffusion increases *both* n_e and n_o. In a TIPE z–cut stripe waveguide, TE and TM modes can be supported in the titanium–indiffused region but only TM modes can be supported in the proton–exchanged region. Therefore, the TE mode can be rejected. A TE–pass polariser can be produced using x–cut material.

Other applications of proton–exchanged waveguides include electro–optic phase modulators[58,59] and intensity modulators[48], acousto–optic devices[60], interferometric temperature sensors[61], and various non–linear devices[62,63,64].

Becker[48] compared the performance of titanium–indiffused and proton–exchanged Mach–Zehnder intensity modulators. He concluded that, for the proton–exchanged devices, the electro–optic effect was reduced, but that there was no significant reduction for the titanium–indiffused devices. More recently, Minakata *et al*[59] reported an approximate ten–fold reduction in the electro–optic coefficient r_{33} for z–cut proton–exchanged (neat–melt) waveguides. In marked contrast,

Wong[65] has obtained V_π values for proton–exchanged Mach–Zehnder modulators comparable to those for titanium–indiffused counterparts. He noted, however, that annealing had probably taken place during the deposition of SiO_2 buffer layers.

1.4. DISCUSSION.

The advantages of proton–exchange over titanium–indiffusion are that the waveguide formation process can be carried out at much lower temperatures, single–mode waveguides can be formed after only a few minutes, the refractive index profile is step–like with a large waveguide (surface) index, the refractive index profiles can be modified by annealing (if required), no photo–refractive effects have been reported for short wavelengths[66], and the process is compatible with state–of–the–art photolithographic techniques.

Clearly, proton–exchange is an attractive (possible) alternative to titanium–indiffusion, provided that the major problems discussed earlier can be overcome or avoided. Perhaps the most important problems yet to be resolved are the reduction in the electro–optic performance and the high propagation losses.

REFERENCES.

(1) K. Nassau, H.J. Levinstein, G.M. Loiacono, *Ferroelectric Lithium Niobate 1: Growth, Domain Structure, Dislocations & Etching*, J. Phys. Chem. Solids, 27, 983, (1966).

(2) K. Nassau, H.J. Levinstein, G.M. Loiacono, *Ferroelectric Lithium Niobate 2: Preparation of Single–Domain Crystals*, J. Phys. Chem. Solids, 27, 989, (1966).

(3) S.C. Abrahams, J.M. Reddy, J.L. Bernstein, *Ferroelectric Lithium Niobate 3: Single–Crystal X–Ray Diffraction Study at 24°C*, J. Phys. Chem. Solids, 27, 997, (1966).

(4) S.C. Abrahams, W.C. Hamilton, J.M. Reddy, *Ferroelectric Lithium Niobate 4: Single–Crystal Neutron Diffraction Study at 24°C*, J. Phys. Chem. Solids, 27, 1013, (1966).

(5) S.C. Abrahams, H.J. Levinstein, J.M. Reddy, *Ferroelectric Lithium Niobate 5: Polycrystal X–Ray Diffraction Study Between 24°C and 1200°C*, J. Phys. Chem. Solids, 27, 1019, (1966).

(6) A. Rauber, *Chemistry and Physics of Lithium Niobate*, (Current Topics in Materials Science, Volume 1, Ed. E. Kaldis, North–Holland, 1978).

(7) R.S. Weis, T.K. Gaylord, *Lithium Niobate: Summary of Physical Properties and Crystal Structure*, Appl. Phys. A, 37, 191, (1985).

(8) S.C. Abrahams, P. Marsh, *Defect Structure Dependence on Composition in Lithium Niobate*, Acta Cryst., B42, 61, (1986).

(9) A.A. Ballman, *Growth of Piezo–Electric and Ferroelectric Materials by the Czochralski Technique*, J. Amer. Ceram. Soc., 48, 112, (1965).

(10) S.A. Fedulov, Z.I. Shapiro, *The Growth of Crystals of $LiNbO_3$, $LiTaO_3$, and $NaNbO_3$ by the Czochralski Method*, P.B. Ladyzhinskii, Sov. Phys. Cryst. 10, 218, (1965).

(11) J.R. Carruthers, G.E. Peterson, M. Grasso, P.M. Bridenbaugh, *Nonstoichiometry and Crystal Growth of $LiNbO_3$*, J. Appl. Phys., 42, 1846, (1971).

(12) Personal Communication with Technical Staff, Barr & Stroud Ltd.

(13) L.O. Svaasand, M. Eriksrud, A.P. Grale, F. Mo, *Crystal Growth and Properties of $LiNb_3O_8$*, J. Cryst. Growth, 18, 179, (1973).

(14) L.O. Svaasand, M. Eriksrud, G. Nakken, A.P. Grale, *Solid–Solution Range of Lithium Niobate*, J. Cryst. Growth, 22, 239, (1974).

(15) J.G. Bergman, A. Ashkin, A.A. Ballman, J.M. Dziedzic, H.J. Levinstein, R.G. Smith, *Curie Temperature, Birefringence, and Phase–Matching Temperature Variations as Functions of Melt Stoichiometry*, Appl. Phys. Lett., 12, 92, (1968).

(16) R.L. Byer, J.F. Young, R.S. Feigelson, *Growth of High–Quality Lithium Niobate Crystals From the Congruent Melt*, J. Appl. Phys., 41, 2320, (1970).

(17) J.E. Midwinter, *Assesment of Lithium Meta–Niobate for Non–Linear Optics*, Appl. Phys. Lett., 11, 128, (1967).

(18) J.E. Midwinter, *Lithium Niobate: Effects of Composition on the Refractive Indices & Optical Second Harmonic Generation*, J. Appl. Phys., 39, 3033, (1969).

(19) E.H. Turner, F.R. Nash, P.M. Bridenbaugh, *Dependence of Linear Electro–Optic Effect & Dielectric Constant on Melt Composition in Lithium Niobate*, J. Appl. Phys., 41, 5278, (1970).

(20) P. Lerner, C. Legras, J.P. Duman, *Stoechiometrie Des Monocristaux De Metaniobate De Lithium*, J. Cryst. Growth, 3/4, 231, (1968).

(21) J.T. Milek, M. Neuberger, *Linear Electro–Optic Modulator Materials*, (IFI/Plenum, New York, 1972).

(22) I.P. Kaminow, J.R. Carruthers, *Optical Waveguiding Layers in $LiNbO_3$ and $LiTaO_3$*, Appl. Phys. Lett., 22(7), 326, (1973).

(23) J.L. Carruthers, I.P. Kaminow, L.W. Stultz, *Diffusion Kinetics and Optical Waveguiding Properties of Outdiffused Layers in $LiNbO_3$ and $LiTaO_3$*, Appl. Opt., 13, 2333, (1974).

(24) G.L. Destefauis, J.P. Gailliard, E.L. Ligeon, S. Vallette, B.W. Farmery, P.D. Townsend, A. Perez, *The Formation Of Waveguides And Modulators In Lithium Niobate By Ion–Implantation*, J. Appl. Phys., 50, 7818, (1979).

(25) J.M. Naden, B.L. Weiss, J. Light. Tech., LT–3, 855, (1985).

(26) J.M. Naden, B.L. Weiss, *The Annealing Of He^+ Implanted Optical Waveguides In Lithium Niobate*, J. Light. Tech., LT–4, 1402, (1986).

(27) G.T. Reed, B.L. Weiss, *Electro–Optic Effect In He^+ Implanted Optical Waveguides In Lithium Niobate*, Elect. Lett., 23, 424, (1987).

(28) R.J. Esdaile, PhD Thesis, University of Glasgow, 1979.

(29) R.V. Schmidt, I.P. Kaminow, *Metal–Diffused Optical Waveguides in $LiNbO_3$*, Appl. Phys. Lett., 25(8), 458, (1974).

(30) M.J. Li, M. De Micheli, D.B. Ostrowsky, M. Papuchon, *High Index Low–Loss $LiNbO_3$ Waveguides*, Opt. Commun., 62(1), 17, (1987).

(31) W.K. Burns, C.H. Bulmer, E.J. West, *Application of Li_2O Compensation Techniques to TI:$LiNbO_3$ Planar and Channel Waveguides*, Appl. Phys. Lett., 33(1), 70, (1978).

(32) T.R. Ranganath, S. Wang, *Suppresion of Li_2O Outdiffusion From TI:$LiNbO_3$ Optical Waveguides*, Appl. Phys. Lett., 30, 376, (1977).

(33) B. Chen, A.C. Pastor, *Elimination of Li_2O Outdiffused Waveguides in $LiNbO_3$*, Appl. Phys. Lett., 30, 570, (1977).

(34) S. Miyazawa, R. Gugliemi, A. Carenco, *A Simple Technique for Suppresing Li_2O Outdiffusion in TI:$LiNbO_3$ Optical Waveguides*, Appl. Phys. Lett., 31, 742, (1977).

(35) B. Schuppert, *Experimental Investigation of Outdiffusion in Lithium Niobate Substrates*, Proc. 4th European Conference on Integrated Optics (ECIO), 11th–13th May, Glasgow, (1987).

(36) J.L. Jackel, C.E. Rice, *Topotactic to Cubic Perovskite Structural Transformation in $LiNbO_3$ and $LiTaO_3$*, Ferroelectrics, 38, 801, (1982).

(37) C.E. Rice, J.L. Jackel, *$HNbO_3$ and $HTaO_3$: New Cubic Perovskites From $LiNbO_3$ and $LiTaO_3$*, J. Sol. St. Chem., 41, 308, (1982).

(38) J.L. Jackel, C.E. Rice, J.J. Veselka, *Proton–Exchange for High–Index Waveguides in Lithium Niobate*, Appl. Phys. Lett., 41(7), 607, (1982).

(39) M. De Micheli, M.J. Li, D.B. Ostrowsky, *The Double Proton–Exchange in Lithium Niobate: Low Loss & Quasi–Embedded Waveguides*, Proc. 4th European Conference on Integrated Optics, May 11th–13th, 1987, Glasgow.

(40) M. De Micheli, J. Botineau, P. Sibillot, D.B. Ostrowsky, M. Papuchon, *Fabrication and Characterisation of Titanium–Indiffused Proton–Exchanged (TIPE) Waveguides in $LiNbO_3$*, Opt. Commun., 42(2), 101, (1982).

(41) M.L. Shah, *Optical Waveguides in Lithium Niobate by Ion–Exchange Techniques*, Appl. Phys. Lett., 26, 652, (1975).

(42) J.L. Jackel, *Variation in Waveguides Fabricated by Immersion of $LiNbO_3$ in $AgNO_3$ and $TlNO_3$: The Role of Hydrogen*, Appl. Phys. Lett., 41(6), 505, (1982).

(43) Yi–Xin Chen, W.S. Chang, S.S. Lau, L. Weilunski, R.L. Holman, *Characterisation of Lithium Niobate Waveguides Exchanged in $TlNO_3$ Solutions*, Appl. Phys. Lett., 40, 10, (1982).

(44) A. Yi–Yan, *Index Instabilities in Proton–Exchanged Waveguides*, Appl. Phys. Lett., 42(8), 633, (1983).

(45) M.N. Armenise, S.M. Al–Shukri, A. Dawar, R.M. De La Rue, A.C.G. Nutt, *Optical Characterisation of Proton–Exchanged and Titanium–Indiffused Proton–Exchanged Slab Guides on Lithium Niobate*, IEEE International Workshop on Integrated Optical & Related Technologies for Signal Processing, Technical Digest, 21, September, 1984, Italy.

(46) S.M. Al–Shukri, J. Duffy, R.M. De La Rue, M.N. Armenise, C. Canali, A. Carnera, *Proton–Exchanged Optical Waveguides on Lithium Niobate: Devices, Characterisation, & Future Prospects*, SPIE Vol–578, Proc. Int. Opt. Cir. Eng. II, 2, (1985).

(47) A. Campari, G. Ferrari, G. Mazzi, C. Summonte, S.M. Al–Shukri, A. Dawar, R.M. De La Rue, A.C.G. Nutt, *Strain and Surface Damage Induced by Proton–Exchange in Y–Cut $LiNbO_3$*, J. Appl. Phys., 58(12), 4521, (1985).

(48) R.A. Becker, *Comparison of Guided–Wave Interferometric Modulators Fabricated on Lithium Niobate Via Titanium–Indiffusion and Proton–Exchange*, Appl. Phys. Lett., 43, 131, (1983).

(49) J.L. Jackel, C.E. Rice, J.J. Veselka, *Compositional Control in Proton–Exchanged Lithium Niobate*, Elec. Lett., 19(10), 387, (1983).

(50) M. De Micheli, *Non–Linear Effects in TIPE:$LiNbO_3$ Waveguides for Optical Communications*, J. Opt. Commun., 4, 25, (1983).

(51) V. Hinkov, E. Ise, *Control of Birefringence in TI:LiNbO$_3$ Optical Waveguides by the Proton–Exchange of Lithium Ions*, J. Light. Tech. 4(4), 444, (1986).

(52) C. Warren, S. Forouhar, W.S.C. Chang, *Double Ion–Exchanged Chirp Grating Lens in Lithium Niobate Waveguides*, Appl. Phys. Lett., 43, 424, (1983).

(53) T. Suhara, *Proton–Exchanged Fresnel Lenses in TI:LiNbO$_3$ Waveguides*, Appl. Opt., 25, 3379, (1983).

(54) D.Y. Zang, C.S. Tsai, *Titanium–Indiffused Proton–Exchanged Waveguide Lenses in LiNbO$_3$ for Optical Information Processing*, Appl. Opt., 25, 2264, (1983).

(55) Z.D. Yu, *Waveguide Optical Planar Lenses In Lithium Niobate–Theory And Experiments*, Opt. Commun., 47, 248, (1983).

(56) J.J. Veselka, G.A. Bogert, *Low–Loss TM–Pass Polariser Fabricated by Proton–Exchange for Z–Cut TI:LiNbO$_3$ Waveguides*, Elect. Lett., 23, 29, (1987).

(57) M. Papuchon, S. Vatoux, *Integrated Optical Polariser On Lithium Niobate:TI Channel Waveguides Using Proton–Exchange*, Elect. Lett., 19, 612, (1983).

(58) K.K. Wong, S. Wright, R.M. De La Rue, *Electro–Optic Waveguide Frequency Translator Fabricated by Proton–Exchange*, Opt. Lett., 7, 546, (1982).

(59) M. Minakata, K. Kumagai, S. Kawakami, *Lattice Constant Changes and Electro–Optic Effects in Proton–Exchanged LiNbO$_3$ Optical Waveguides*, Appl. Phys. Lett., 49(16), 992, (1986).

(60) J.F. Duffy, Ph.D. thesis, University of Glasgow, 1986.

(61) M. Haruna, *Optical π−arc Waveguide Interferometer for Temperature Sensing*, Appl. Opt., 24, 2483, (1985).

(62) A. Mahapatra, W.C. Robinson, *Integrated Optical Ring−Resonator Made by Proton−Exchange in Lithium Niobate*, Appl. Opt., 24, 2285, (1985).

(63) M. De Micheli, *Non−linear Interactions in Lithium Niobate Guides*, (New Directions in Guided Wave & Coherent Optics, Ed. Ostrowsky, Spitz, Martinuss Nijhoff, The Hague, 1984).

(64) S. Neveu, J.P. Barety, M. De Micheli, P. Sibillot, D.B. Ostrowsky, *Phase−Matched SHG Using The d_{33} Coefficient In Proton−Exchanged Guides*, Topical Meeting on Integrated & Guided Wave Optics, 24th−26th April, Orlando, Florida, (1984), PD−6.

(65) K.K. Wong, *An Experimental Study of Dilute−Melt Proton−Exchanged Waveguides in X− and Z−Cut $LiNbO_3$*, GEC J. Res., 3(4), 243, (1985).

(66) J. Jackel, A.M. Glass, G.E. Peterson, C.E. Rice, D.H. Olsen, J.J. Veselka, *Damage−Resistant $LiNbO_3$ Waveguides*, J. Appl. Phys., 55(1), 269, (1984).

CHAPTER 2

Characterisation Of Proton–Exchanged Planar Waveguides On X– And Z–Cut Lithium Niobate Using Prism–Coupler Measurements, Infrared Spectroscopy, And Atomic Absorption Spectroscopy

2.1. INTRODUCTION.

Since proton–exchange was first established as another means of producing optical waveguides on lithium niobate substrates[1], workers have been concerned mostly with the application of the technique to the fabrication of waveguide–based devices. Collaborators of the Department of Electronic and Electrical Engineering, Glasgow University, have studied some of the structural aspects of proton–exchanged lithium niobate using Rutherford backscattering[2] and nuclear reactions[2].

Problems associated with proton–exchanged waveguides, for example, mode–index instability[3,4], surface damage[5], high propagation losses[6], and a reduced electrooptic effect[7,8] should be avoided if proton–exchange is to be considered seriously for the production of integrated optical components. An understanding of the waveguide formation process might help to establish methods of avoiding these problems.

The present work is concerned with determining the extent of proton–exchange in x– and z–cut lithium niobate as a function of temperature and time using mode–index measurements (prism–coupling), infrared spectroscopy and atomic absorption spectroscopy.

2.2. THE PROTON–EXCHANGE PROCESS.

The proton–exchange technique involves chemical reaction between lithium niobate and acid at temperatures in the range 150°C to 249°C[1]. Temperatures as high as 300°C have been used[9], but the reactions were performed in a sealed ampoule to avoid evaporation of the acid.

A number of different acids have been found suitable for proton–exchange[10], the most convenient of which is benzoic acid ($C_6H_5CO_2H$). The reasons for using benzoic acid are: (a) it has a convenient working range (melting point ≃122°C, boiling point ≃249°C), (b) the toxicity is low, (c) it is relatively easy to handle at room temperature and in its molten state, and (d) it is inexpensive.

The overall reaction can be represented by the equation:

$$LiNbO_3 + xH^+ \longrightarrow Li_{1-x}H_xNbO_3 + xLi^+ \quad \text{.....(1).}$$

The extent of proton–exchange depends on the time and temperature of reaction, and only partial exchange is necessary for waveguide formation[11,12,13]. Complete exchange results in the formation of the compound $HNbO_3$ causing a structural transformation to take place in the crystal, from the hexagonal unit cell to the cubic unit cell[14,15,16,17].

Protons are incorporated within the crystal in the form of OH– hydroxyl groups (formally the result of bonding between H^+ and O^{2-} in the lattice). The extent of formation of OH– hydroxyl groups has been monitored using infrared spectroscopy (Section 2.5), and related to the depth of the exchanged regions as estimated from prism–coupling angles (Section 2.4). The percentage of lithium which is replaced by protons has been determined by chemical analysis of the benzoic acid (after waveguide fabrication) using atomic absorption spectroscopy (Section 2.6).

2.3. SAMPLE PROCESSING.

Congruent–composition x– and z–cut lithium niobate substrates were polished on both faces for the purpose of the infrared spectroscopic characterisation. The crystals were thoroughly cleaned and de–greased ultrasonically using a series of methanol and acetone baths. The dimensions of each sample, typically 1.5x1.0x0.1cm, were accurately measured to a precision limit of ±0.05mm using a Vernier gauge.

The samples were mounted in PTFE holders and placed in individual, covered, silica glass beakers which contained accurately weighed quantities of molten AnalaR benzoic acid. The silica glass beakers were used to avoid possible contamination of the acid with lithium, which often exists as an impurity in other types of glass. The PTFE holders were perforated with holes (diameter ≃5mm) to ensure an even flow of acid over the surface area of each sample. Acids were weighed to a precision of $\pm 10^{-4}$g using an Oertling LA 164 electronic balance. Each beaker held approximately 20g of acid.

The heating source used was a high–temperature oil bath which was controlled to ±0.25°C. The oil bath was covered to provide a well–isolated, temperature–stable environment. The waveguide fabrication time was defined as the time interval between total immersion and removal of the sample. The difference between oil bath and acid temperatures could be as much as 10°C and so the temperatures quoted in this work are *acid* temperatures. Temperatures were measured using a Pt–13%Rh/Pt thermocouple with a 0°C reference junction. Temperatures were recorded periodically throughout waveguide fabrication.

Benzoic acid which had re–crystallised on the sample surfaces as they cooled was removed by washing the samples in methanol. Acids were retained after proton–exchange for the purpose of analysis by atomic absorption spectroscopy. Tables 2.1 and 2.2 list the fabrication times and temperatures of the x– and z–cut waveguides, respectively.

2.4. OPTICAL CHARACTERISATION OF PROTON–EXCHANGED WAVEGUIDES.

The results presented in the following sections confirm much of what has already appeared in the published literature[18,19,20]. However, optical waveguide measurements have been included because they have been correlated with the results of infrared and atomic absorption spectroscopy. Another reason for repeating the waveguide measurements was that previous workers[18,19,20] have tended to quote oil bath temperatures rather than acid temperatures. The difference between the two temperatures caused discrepancies in calculating effective diffusion coefficients and activation energies.

2.4.1. Waveguide Measurements At $\lambda = 0.6328\,\mu m$

It has been shown[21] that proton–exchange increases the extraordinary refractive index of lithium niobate ($\Delta n_e \simeq 0.125$), and reduces the ordinary index ($\Delta n_o \simeq -4 \times 10^{-2}$). Therefore, waveguide modes are of the TE type in x– and y–cut proton–exchanged lithium niobate and of the TM type in z–cut material.

Sample	Fabrication Temperature (°C)	Fabrication Time (hr)
X1	168.6±0.8	1
XX13	"	2
X11	"	3
XX18	"	4.42
X12	"	6
X4	175.2±1.2	0.25
XX14	"	0.67
X10	"	1
XX16	"	2
X13	"	3
XX17	"	4.42
X20	"	6
X2	198.7±1.2	0.25
X5	"	1
X7	"	2
X15	"	3
X19	"	4.42
X22	"	6
XX8	207.5±1.0	0.12
X6	"	0.25
X8	"	1
X9	"	2
X14	"	3
X16	"	4.42
X17	"	6

Table 2.1. Fabrication Temperatures And Times For The X–Cut Proton–Exchanged Lithium Niobate Waveguides.

Sample	Fabrication Temperature (°C)	Fabrication Time (hr)
ZZ2	167.5±1.7	0.67
Z1	"	1
ZZ3	"	2
Z2	"	3
Z4	"	6
Z25	182.4±0.8	0.42
Z26	"	1
Z23	"	2
Z22	"	3
Z16	"	4.42
Z15	"	6
Z12	196.9±1.7	0.12
Z11	"	0.25
Z9	"	1
Z8	"	2
Z7	"	3
Z6	"	4.42
Z5	"	6
Z24	210.9±1.8	0.12
ZZ21	"	0.25
Z20	"	0.42
ZZ14	"	0.67
Z21	"	1
Z19	"	2
Z18	"	3
Z17	"	4.42
Z14	"	6

Table 2.2. Fabrication Temperatures And Times For The Z–Cut Proton–Exchanged Lithium Niobate Waveguides.

The standard prism–coupling technique[22] was employed to assess the optical properties of the waveguides. Measurements were made at the $\lambda = 0.6328\,\mu m$ He–Ne laser wavelength with rutile prisms ($n_e = 2.8719$, $n_o = 2.5837$). A prism–coupling rig with (x,y,z,θ,φ) movements was used. The light propagated along the y–axis of each waveguide. The input coupling angles (ξ) of the excited modes were measured to a precision of 0.01^o and were used to evaluate the effective refractive indices (N_{eff}) for each mode using the expression:

$$N_{eff} = n_p \sin[A + \sin^{-1}(\sin\xi / n_p)] \quad \ldots\ldots\ldots\ldots\ldots\ldots (2),$$

where A is the apex angle of the prism (degrees), and n_p is the relevent refractive index of the prism.

The effective mode–indices were used to define the refractive index/depth profile in the waveguides (n(x)) by applying the inverse WKB method[23,24]. The method assumes that n(x) can be represented approximately by a piece–wise linear function. The profile is determined by calculating the depth at which the refractive index in the guiding medium is equal to the effective index of the supported mode, using an area–minimising technique to estimate both the best–fit turning point depth of each mode and the waveguide depth.

A typical profile is depicted in Figure 2.1 for an x–cut proton–exchanged waveguide (sample X13, 175.2°C, 3hr). The profile is step–like in form with a waveguide (surface) index of 2.3273 (i.e. $\Delta n_e = 0.1248$), in agreement with previous work[1,18]. The values of N_{eff} were used as data input for a computer program based on normalised step–index equations[25] from which the waveguide (surface) refractive indices and the depths of exchanged layers were calculated. The substrate index used at $\lambda = 0.6328\,\mu m$ was $n_e = 2.2025$. For TE modes, a normalised waveguide index (b) is defined by[24]:

$$b = (N_{eff}^2 - n_f^2)/(n_f^2 - n_e^2) \quad \ldots\ldots\ldots (3),$$

where n_e is the substrate refractive index, n_f is the (unknown) guiding region refractive index, and N_{eff} is given by Equation (2). A normalised

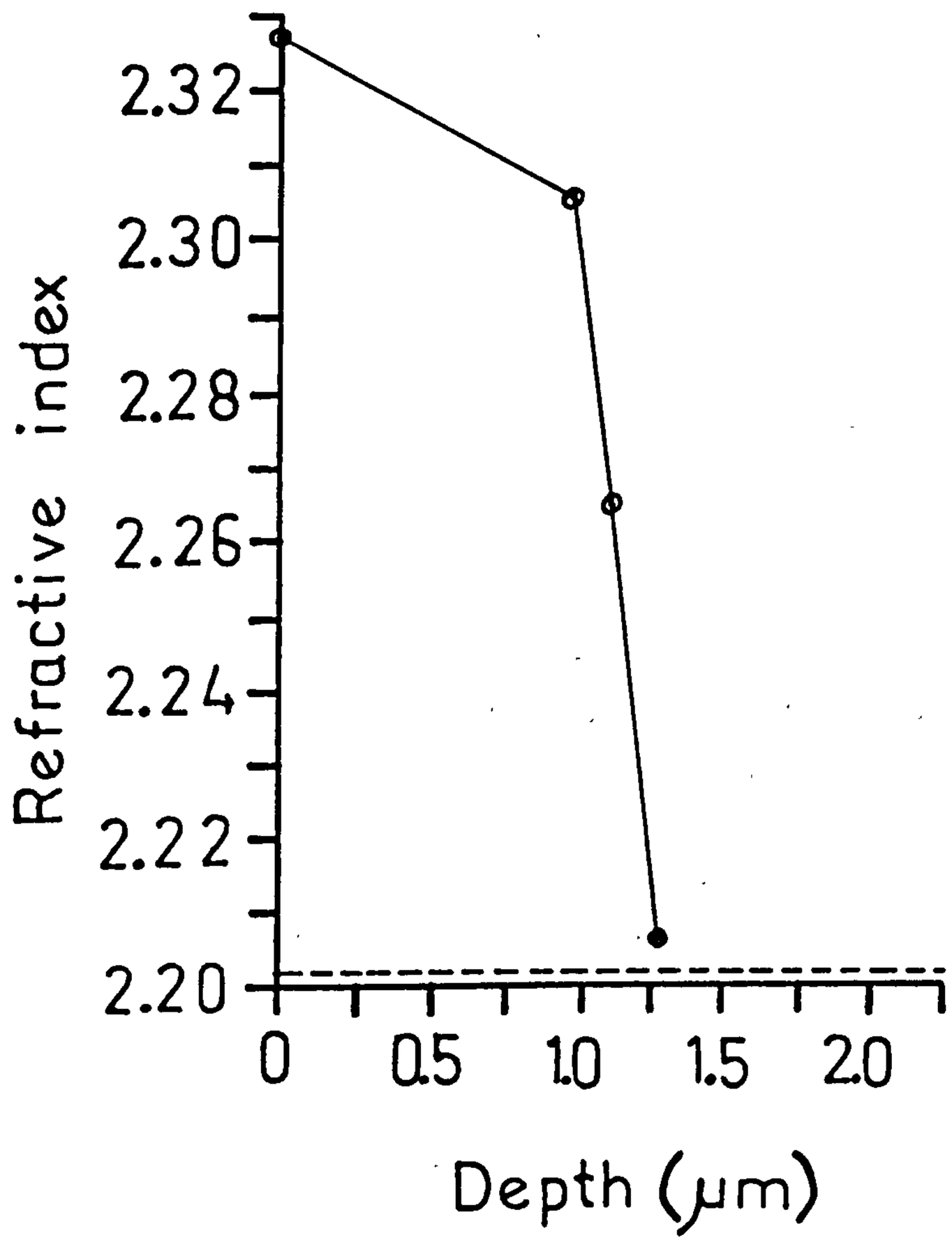

Figure 2.1. Refractive Index Profile Of An X−Cut Proton−Exchanged Lithium Niobate Waveguide Measured At $\lambda = 0.6328\mu m$. *The waveguide Was Fabricated At $T = 175^{o}C$ For $t = 3hrs$.*

waveguide thickness (V) is defined by[24]:

$$V = kd(n_f^2 - n_e^2)^{1/2} \quad \ldots\ldots\ldots\ldots (4),$$

where d is the guiding region thickness and k is the free-space propagation constant ($=2\pi/\lambda$). Plots of b versus V are obtained from solutions of the normalised dispersion equations with an asymmetry parameter (a) given by[24]:

$$a = (n_s^2 - n_c^2)/(n_f^2 - n_e^2) \quad \ldots\ldots\ldots\ldots (5),$$

where n_c is the cover refractive index ($n_c = 1$, for air). From a knowledge of the number of modes, a restricted range of values for V is defined. Within this region a computer scan is carried out to obtain an estimate of n_f for each mode, given an initial estimate of the asymmetry parameter (i.e. an initial choice of n_f).

The values of b are obtained from the theoretical plots and an initial choice of V. These, together with N_{eff}, are used to obtain sets of estimated n_f values. V is then adjusted (by an amount specified by the operator) until the standard deviation of the mean value of n_f is reasonably small ($\approx 10^{-4}$). The value of 'a' is adjusted at the same time. Having obtained an estimate of n_f and the corresponding V, the guide depth (d) follows immediately from Equation (4).

Using the waveguide indices calculated for the samples in Tables 2.1 and 2.2, the following mean values of Δn_e ($= n_f - n_e$) were calculated: $\Delta n_e = (0.1267 \pm 0.0026)$ for x-cut proton-exchanged waveguides, and $\Delta n_e = (0.1256 \pm 0.0016)$ for z-cut proton-exchanged waveguides. The difference between the values of Δn_e for x- and z-cut proton-exchanged waveguides has been reported elsewhere[6,19]. The values quoted in reference (19) were $\Delta n_e = 0.1267$ for x-cut and $\Delta n_e = 0.1259$ for z-cut, which are in close agreement with the values measured in the present study.

The assumption that the waveguide refractive index profile is step–like has been shown to be valid by Nutt[6]. Figures 2.2 and 2.3* are the dispersion curves at $\lambda = 0.6328\,\mu m$ for proton–exchanged waveguides on x– and z–cut lithium niobate, respectively. The waveguide depths were measured from IWKB plots. The experimental points closely agree with the superimposed theoretical dispersion curves obtained using the step–index equations[24], supporting the step–index assumption.

He also estimated the waveguide profiles at $\lambda = 1.15\,\mu m$[6]. Although the index change at the latter wavelength was $\Delta n_e = 0.096$, the waveguide depths estimated for several different samples agreed with depths measured for the same samples at $\lambda = 0.6328\,\mu m$ (to within 2%), supporting the assumption that proton–exchanged waveguides have a step–like refractive index profile. Rutherford backscattering and hydrogen–profiling have been used to estimate the depth of exchanged layers[2,6], and the values agree closely with those estimated from refractive index profiles.

The experimental relationship between the number of modes supported in a proton–exchanged waveguide and the waveguide fabrication time is shown in Figures 2.4 and 2.5 for x– and z–cut proton–exchanged waveguides, respectively. Using Figures 2.4 and 2.5, the experimental cut–off depth for each mode was estimated by substituting into Equations (9) and (10) (below) the value of 't' at which the relevant mode ceased to propagate. The value of 't' was defined as the time read–off at the point where the number of modes supported (M) was half–way between two integer values (e.g. M = 5.5). If the choice of time corresponded to a non–integer value of M, the value of M was rounded–off. The theoretical cut–off depths were calculated using Equation (4), assuming a waveguide (surface) refractive index of 2.3285. The cut–off depths for the TE and TM modes (Table 2.3) agree with the theoretical values (within the accuracy of measurement) supporting the step–index model.

* *These curves were re–produced from Reference (6).*

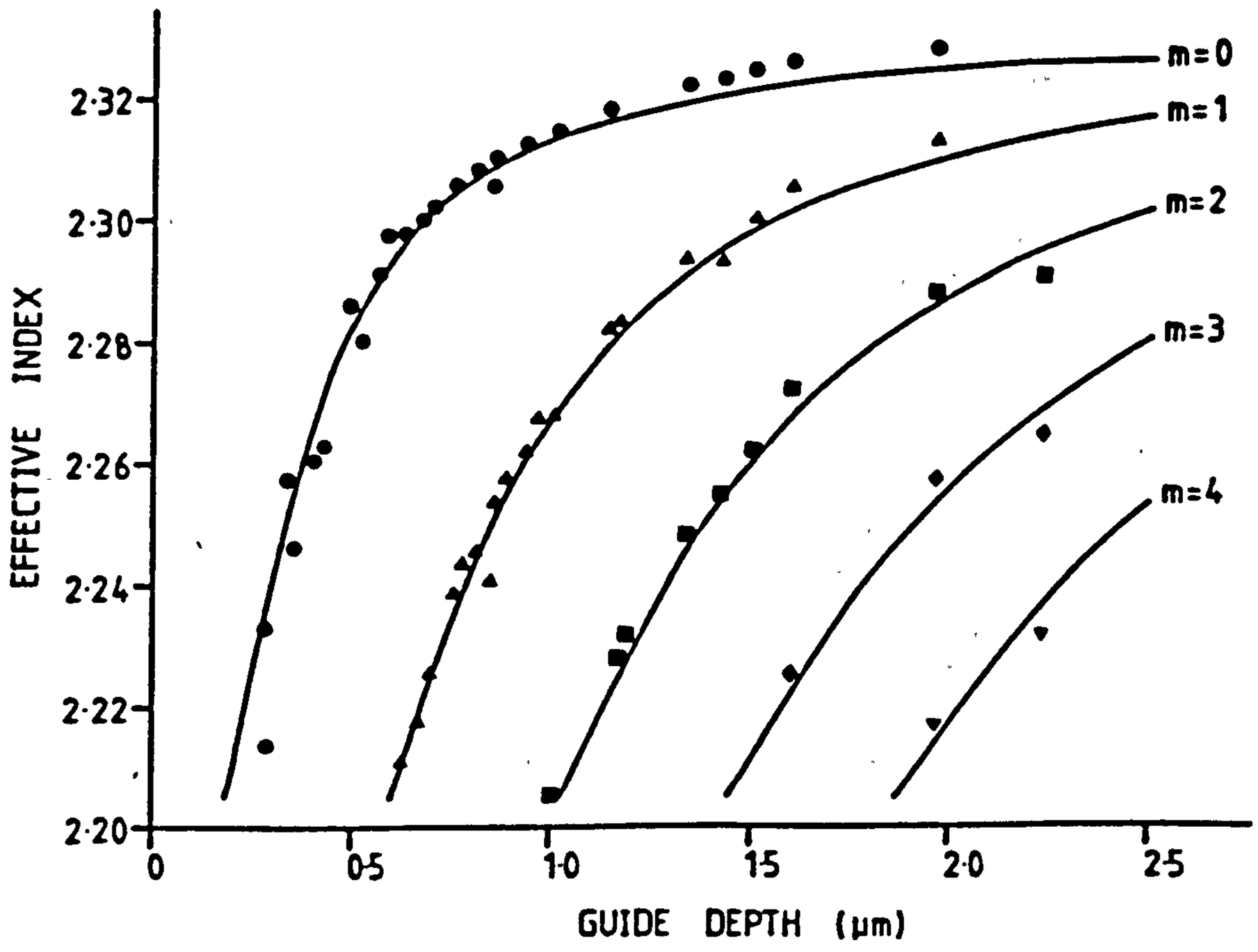

Figure 2.2. Experimental Points On Theoretical Dispersion Curves, For A Step–Index Change $\Delta n_e = 0.126$ ($\lambda = 0.6328\,\mu m$) In X–Cut Proton–Exchanged Planar Waveguides *(From Reference (6))*.

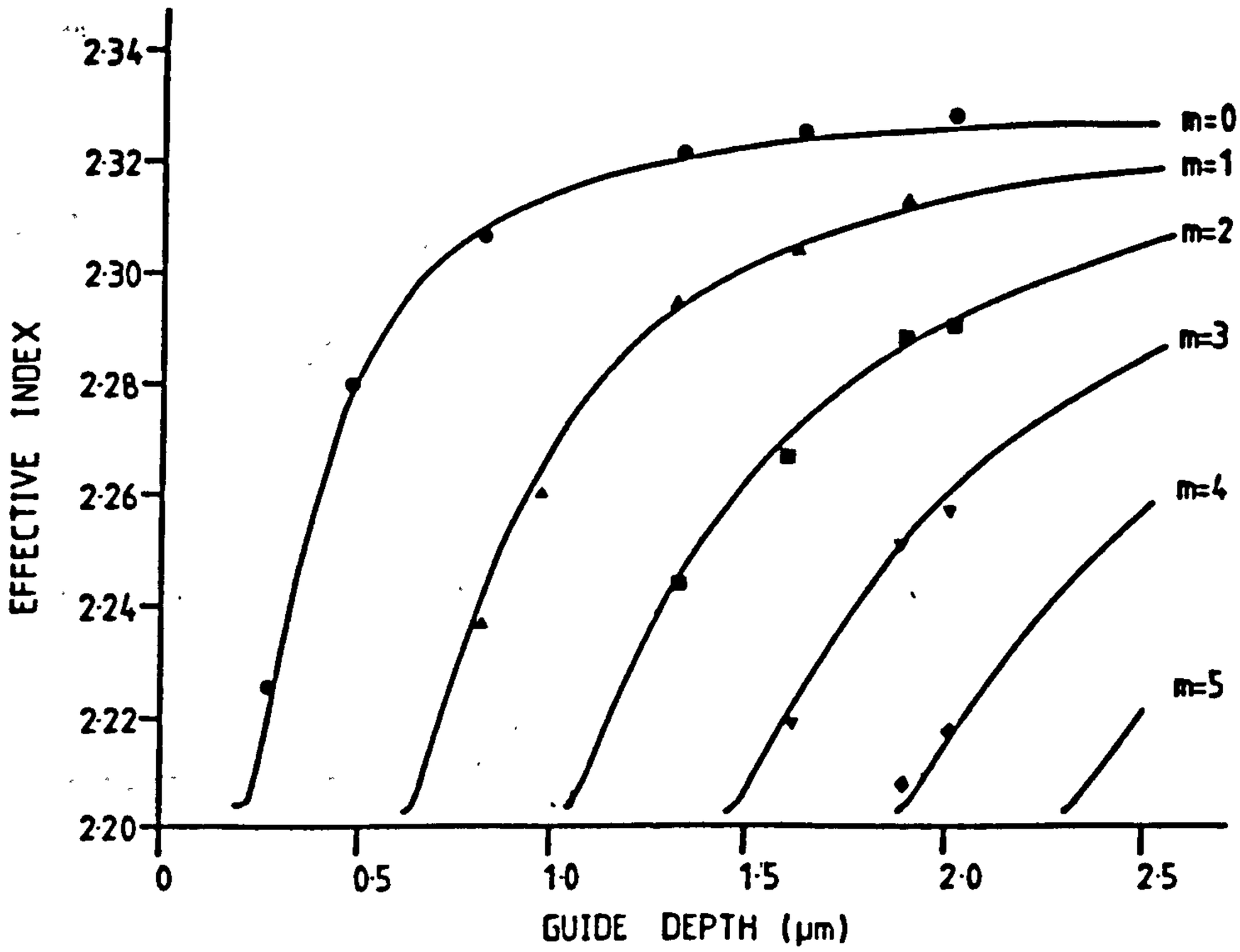

Figure 2.3. Experimental Points On Theoretical Dispersion Curves, For A Step–Index Change $\Delta n_e = 0.126$ ($\lambda = 0.6328\,\mu m$) In Z–Cut Proton–Exchanged Waveguides ***(From Reference (6).***

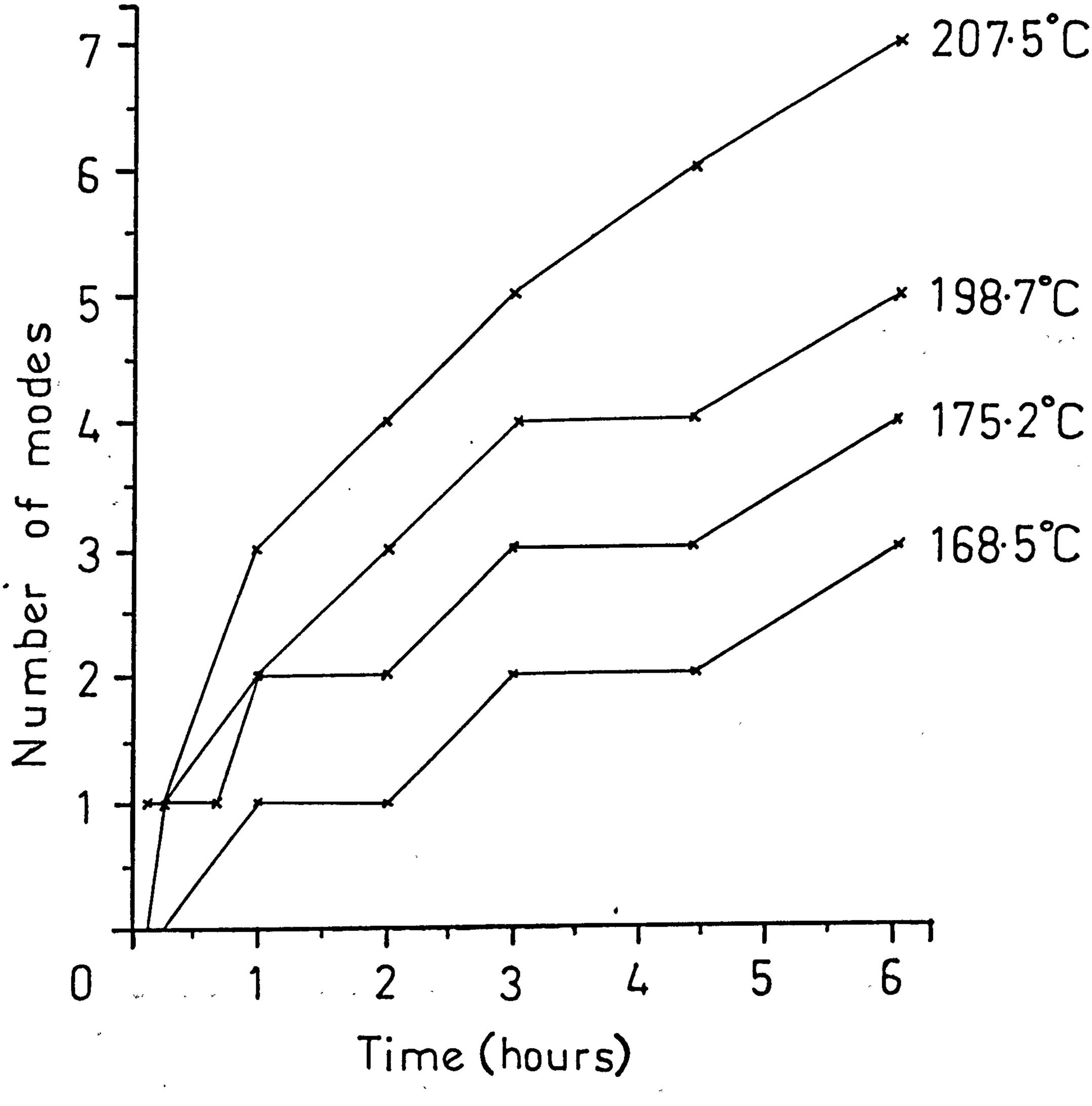

Figure 2.4. Number Of Modes Supported As A Function Of Fabrication Time And Temperature, For X−Cut Proton−Exchange Lithium Niobate ($\lambda = 0.6328\,\mu m$).

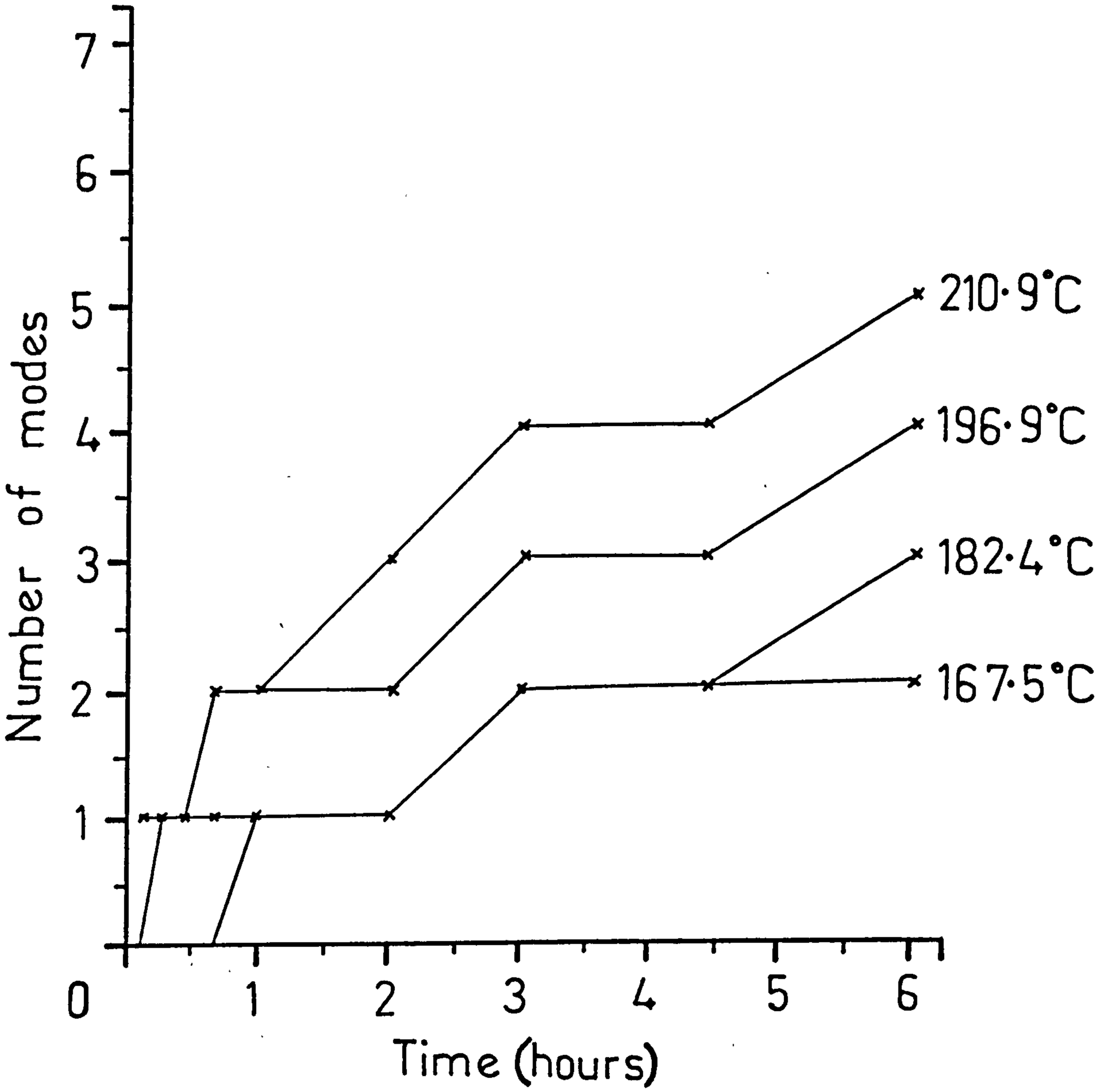

Figure 2.5. Number Of Modes Supported As A Function Of Fabrication Time And Temperature, For Z−Cut Proton−Exchanged Lithium Niobate ($\lambda = 0.6328\,\mu m$).

2.4.2. Estimation Of Effective Diffusion Coefficients And Activation Energies From Optical Waveguide Measurements.

Figures 2.6a and 2.6b show the relationship between waveguide depth and $t^{1/2}$ for x− and z−cut waveguides, respectively. The experimental points lie on a straight line indicating that proton−exchange can be represented by a diffusion model. Therefore, the equations of the lines can be represented by:[26]

$$d = 2[D(T)t]^{1/2} \ldots\ldots\ldots (5),$$

where T is the fabrication temperature (K), d is the guide depth (μm), t is the fabrication time (hr), and D(T) is the diffusion coefficient ($\mu m^2 hr^{-1}$) at temperature T.

In estimating the waveguide depths one is considering the combined process of lithium ions coming out of the substrate and protons going in. Therefore, D(T) in Equation (5) is an *effective* diffusion coefficient. The gradient of each line in Figures 2.6a and 2.6b was used to calculate D(T), assuming Equation (5). The effective diffusion coefficients for x− and z−cut waveguides are given in Table 2.4.

The relationship between the effective diffusion coefficient and temperature is given by the Arrhenius Law[27]:

$$D_i(T) = D_{oi} \exp(-Q_i/RT) \ldots\ldots\ldots\ldots\ldots (6),$$

where i denotes the direction of diffusion (along x, y, or z), Q_i is an effective activation energy for proton−exchange ($kJmol^{-1}$), D_{oi} ($\mu m^2 hr^{-1}$) is a pre−exponential term characteristic of the substrate orientation, and R is the universal gas constant ($8.31 Jmol^{-1}K^{-1}$). For x−cut waveguides $D_{ox} = 1.468 \times 10^8 \mu m^2 hr^{-1}$, and for z−cut waveguides $D_{oz} = 7.773 \times 10^8 \mu m^2 hr^{-1}$. If proton−exchange is a diffusion−limited process, then plotting the natural logarithm of the effective diffusion coefficients against the inverse of the absolute temperature should give straight−line plots from which the effective activation energy, Q_i, can be estimated.

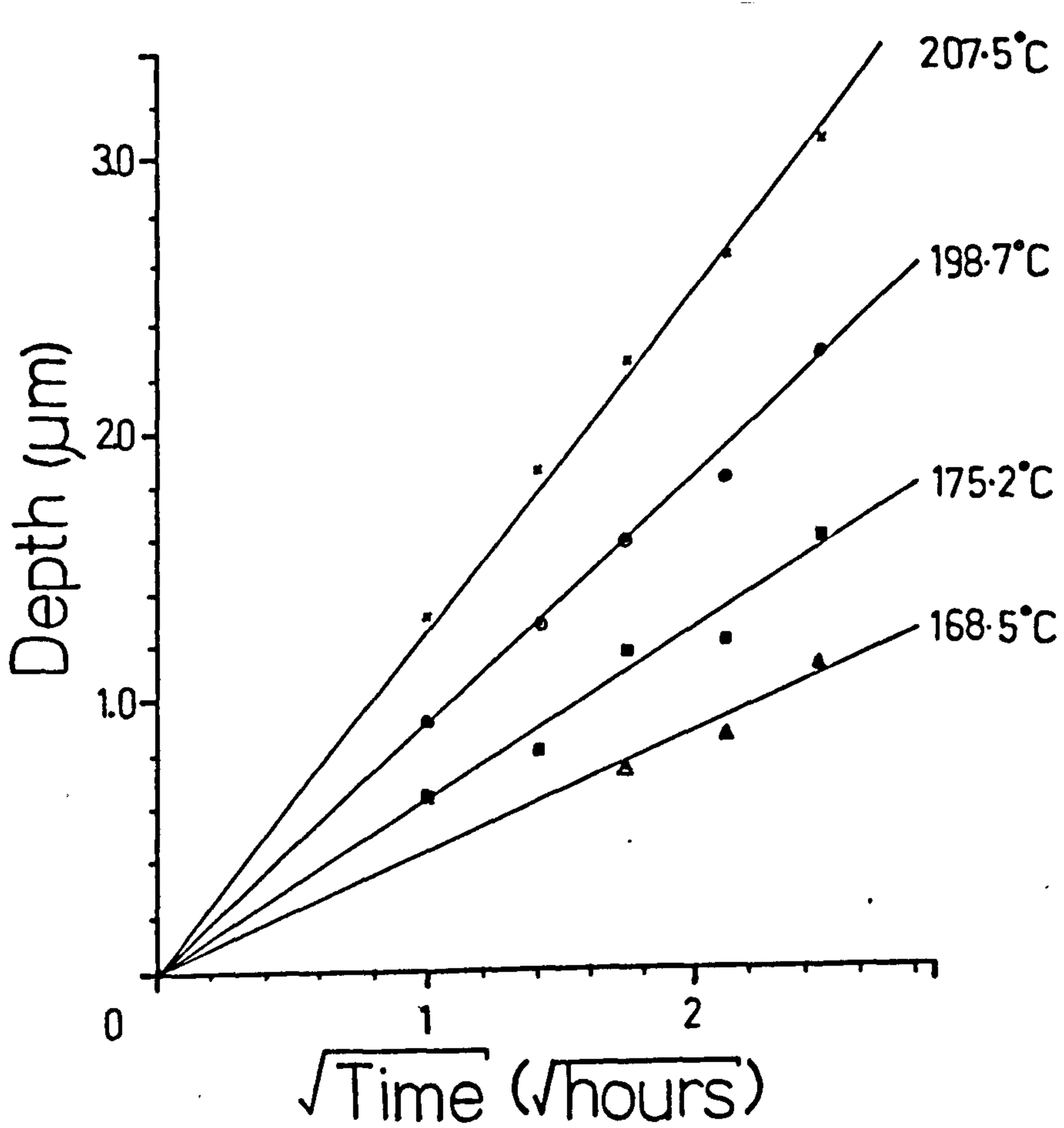

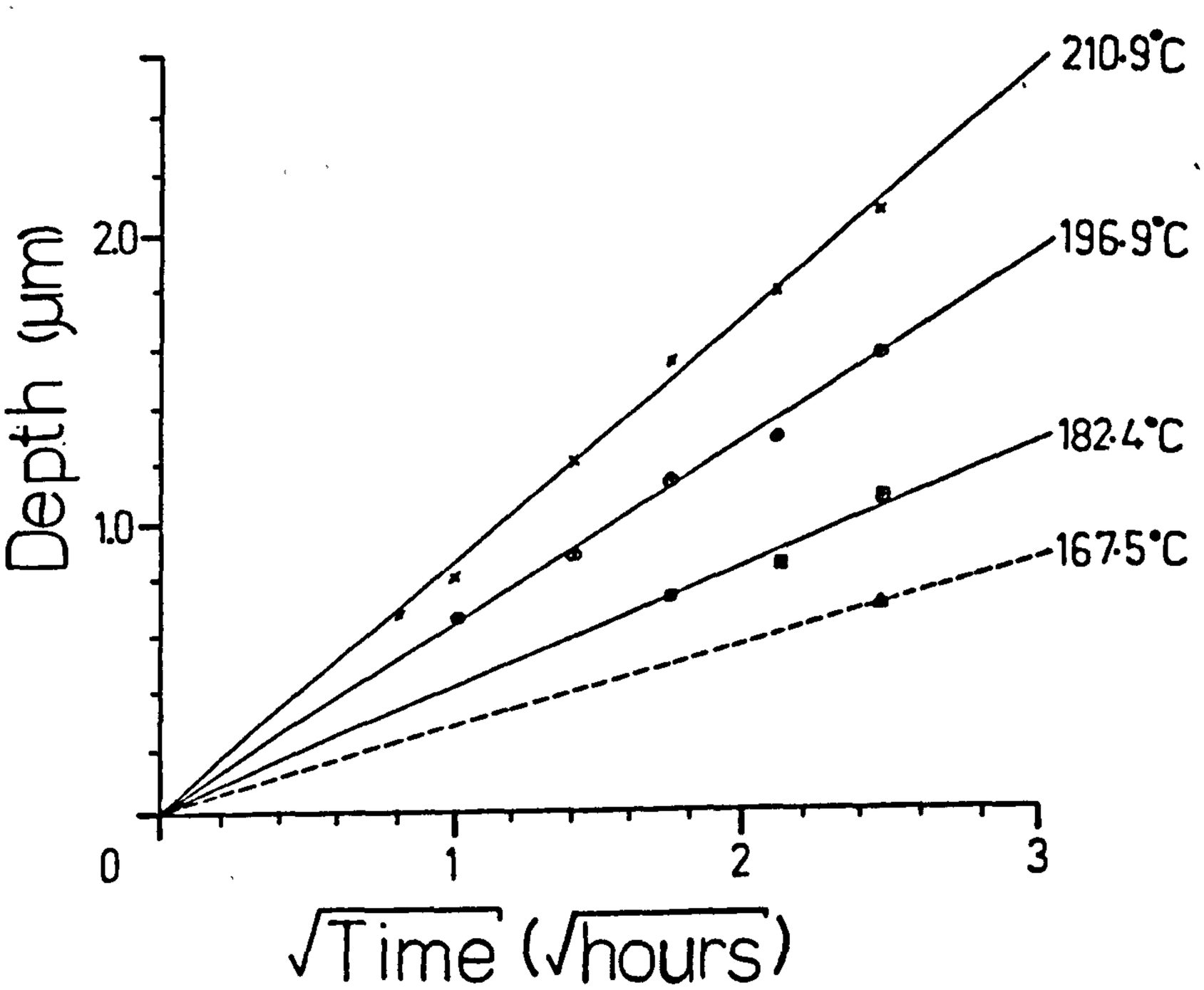

Figure 2.6a (*X–Cut, Above*) And 2.6b (*Z–Cut, Below*). Waveguide Depth As A Function Of $t^{1/2}$, At Four Temperatures.

Mode Number	Experimental cut–off depth (μm)	Theoretical cut–off depth (μm)
TE_0	0.34±0.15	0.16
TE_1	0.71±0.12	0.58
TE_2	1.07±0.11	1.00
TE_3	1.47±0.11	1.42
TE_4	2.08±0.16	1.84
TM_0	0.29±0.08	0.20
TM_1	0.60±0.09	0.62
TM_2	1.02±0.04	1.04
TM_3	1.42±0.07	1.46

Table 2.3. Experimental And Theoretical Cut–Off Depths For TE And TM Modes In X–Cut (TE) And Z–Cut (TM) Proton–Exchanged Waveguides.

Substrate Orientation	Fabrication Temperature T(°C)	Effective Diffusion Coefficients D(T) (μm^2/hr.)	Activation Energy* (kJmol^{-1}) Q_1	Q_2
x–cut	168.6	0.05	79.3	60.4
"	175.2	0.10		
"	198.7	0.21		
"	207.5	0.39		
z–cut	167.5	––	87.7	81.2
"	182.4	0.05		
"	196.9	0.10		
"	210.9	0.18		

Table 2.4. Effective Diffusion Coefficients And Activation Energies For X– And Z–Cut Proton–Exchanged Waveguides.

* *Q_1–calculated from prism–coupling data (section 2.4.2)*
Q_2–calculated from infrared spectroscopic measurement (section 2.5.3)

Figure 2.7 shows the linear relationship between lnD(T) and 1/T for x− and z− cut waveguides. The equations of the lines are:

$$\ln D(T) = -9545.413/T + 18.8047 \quad (x-\text{cut}) \ldots\ldots\ldots\ldots (7),$$

$$\ln D(T) = -10556.071/T + 20.4713 \quad (z-\text{cut}) \ldots\ldots\ldots\ldots (8),$$

where T is in Kelvin. From the gradients of the latter two lines the following activation energies were calculated: $Q_x = 79.3 kJ/mol^{-1}$, $Q_z = 87.7 kJ/mol^{-1}$ (Table 2.4). Equation (1) can now be written in the form:

$$d(\mu m) = 2.423 \times 10^{4} t^{1/2} \exp(-4.772 \times 10^{3}/T): \quad (x-\text{cut}) \ldots\ldots\ldots (9),$$

$$d(\mu m) = 5.576 \times 10^{4} t^{1/2} \exp(-5.278 \times 10^{3}/T): \quad (z-\text{cut}) \ldots\ldots\ldots (10).$$

The effective diffusion coefficients and activation energies listed in Table 2.4 do not agree with published work[18,19,20]. However, previous workers assumed that the acid temperature was the same as the oil bath temperature. The value of activation energy for the x− cut work was quoted to be[20] $Q_x = 84 kJmol^{-1}$. When the temperatures used in calculating Q_x were corrected (lowered by 10°C) the value was $Q_x = 80 kJmol^{-1}$, which is closer to the value of $79.3 kJmol^{-1}$ measured in the present study.

The information in this section is sufficient to allow proton− exchanged waveguides to be fabricated to any defined depth, with a choice of fabrication parameters.

2.5. INFRARED SPECTROSCOPIC STUDY OF PROTON− EXCHANGED WAVEGUIDES.

2.5.1. Introduction.

When an electromagnetic wave is incident on a vibrating molecule, energy

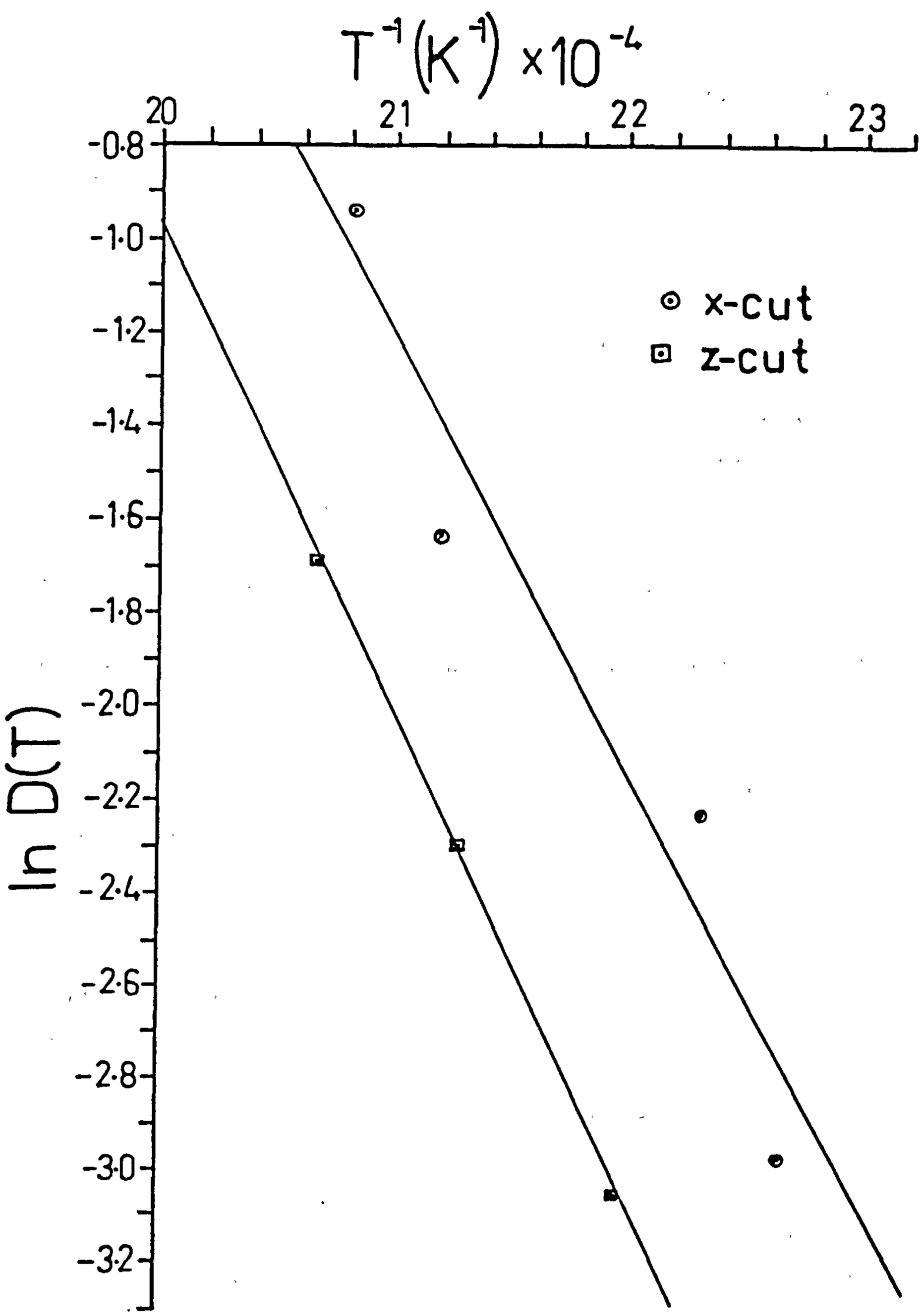

Figure 2.7. lnD(T) As A Function Of Temperature For X– And Z–Cut Proton–Exchanged Lithium Niobate.

is transferred to the molecule by the absorption of photons and the molecule is set into vibration[28]. The vibrational frequency (υ) is related to the mass of and the distance between the vibrating species, through the harmonic oscillator equation[28]:

$$\upsilon = (k/m)^{1/2} \ldots\ldots\ldots (11),$$

where k is a constant (dependent on the distance between the vibrating species), and m is the mass of the vibrating species. Molecular systems have characteristic vibrational frequencies. The present work is concerned with the absorption of radiative frequencies in the OH− stretching region of the electromagnetic spectrum ($\lambda = 2.8\mu m$ to $3.0\mu m$).

2.5.2. OH− Hydroxyl Group Formation In Bulk Lithium Niobate.

One of the consequences of growing lithium niobate by the Czochralski technique is that, whatever the ratio of the starting compounds, the solid crystal boule pulled from the melt is always deficient in lithium[29]. In the model of congruent lithium niobate presented by Abrahams *et al*[30] some of the lithium sites are occupied by niobium (Chapter 1, Section 1.1.3). To preserve charge neutrality, one niobium ion replaces five lithium ions.

Another mechanism by which charge neutrality is preserved is by the incorporation of hydrogen from atmospheric water vapour[30]. The hydrogen bonds to oxygen in the lattice to form OH− hydroxyl groups[31,32], the formation of which can be observed using infrared spectroscopy. The hydroxyl group in bulk lithium niobate has a characteristic absorption band at $\upsilon_{max} = 3484cm^{-1}$. This absorption band has been observed by many workers[31,32] and is depicted in Figure 2.8 for an x− cut crystal grown from a congruent melt ($(Li/Nb)_{melt} = (Li/Nb)_{crystal} = 0.945$[33]).

An interesting feature of the absorption band in x− cut material, is its dependence on the polarisation of the incident radiation. In Figure 2.8 the absorption band is present when the incident radiation is polarised perpendicular to the c− axis of the crystal and disappears when the

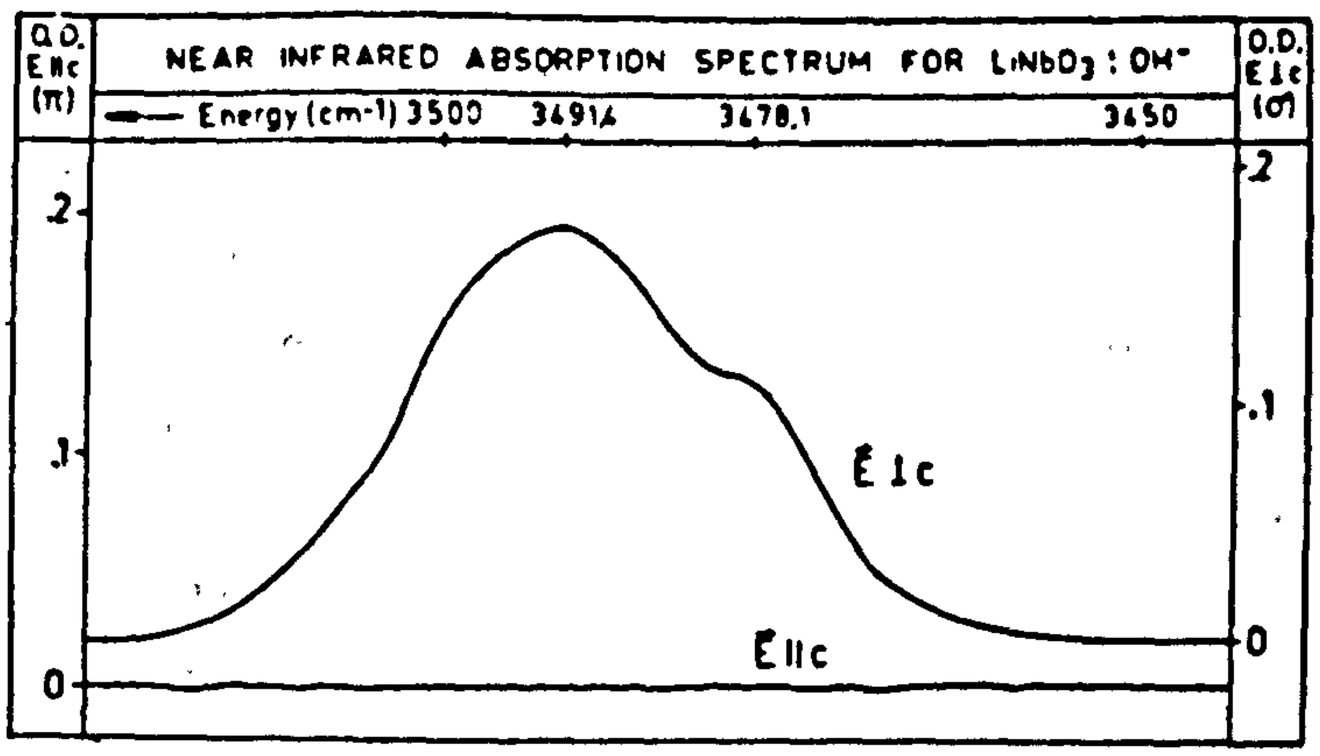

Figure 2.8. Polarised Infrared Spectra Of Congruent X–Cut Lithium Niobate (Herrington *et al*[32]. O.D.= Optical Density≡Absorbance).

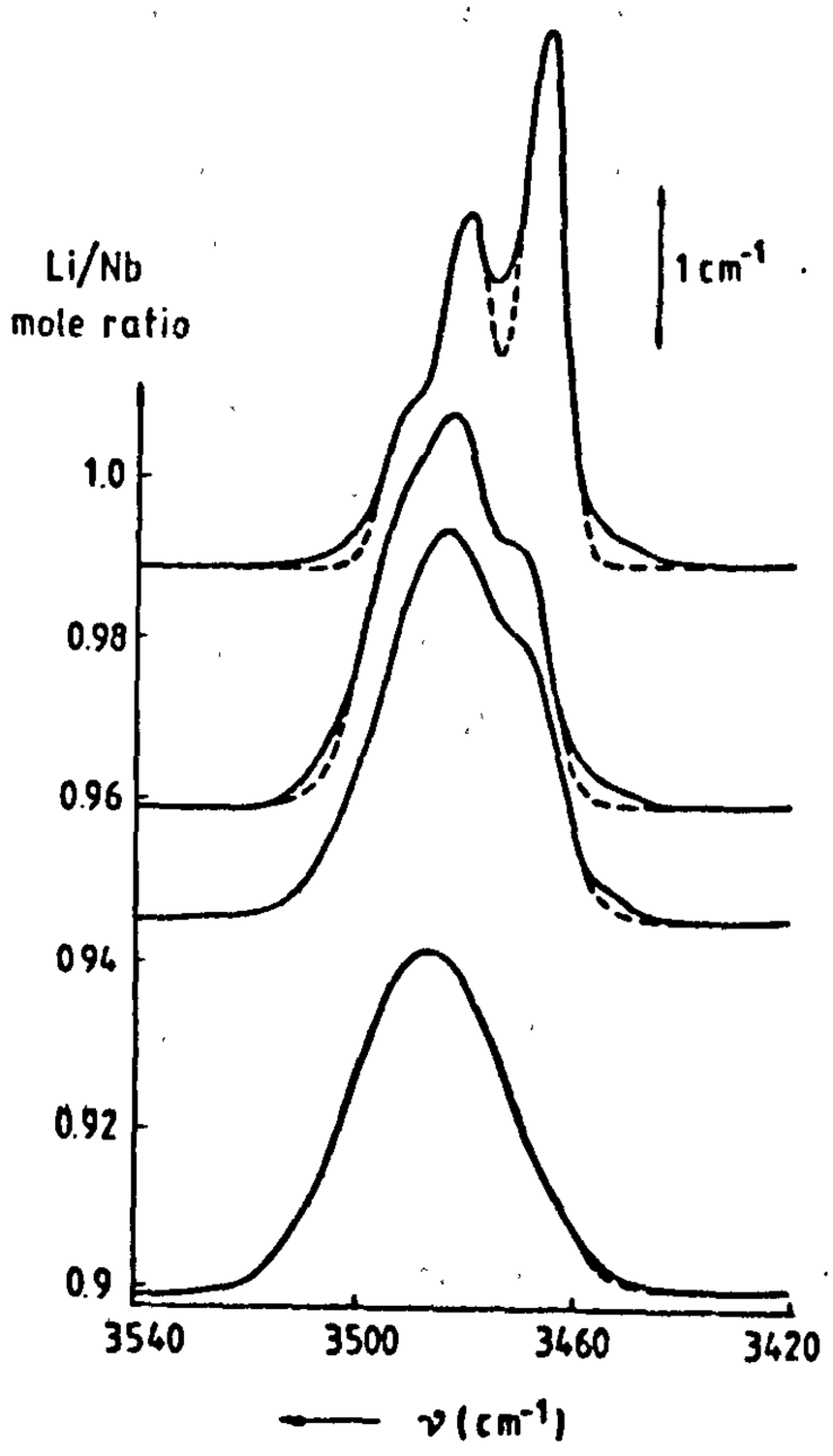

Infrared absorption bands of $LiNbO_3$ crystals of various compositions, dashed lines indicating the results of a Gaussian fitting. The spectra are measured at room temperature.

Figure 2.9. Infrared Spectra Of Bulk Lithium Niobate Of Varying Stoichiometry (Kovacs *et al*[33]).

incident radiation is polarised parallel to the c−axis, indicating that the OH− vibration is perpendicular to c. The absorption band consists of two overlapping sub− bands separated by 10cm^{-1}, indicating the presence of two slightly different OH− environments. The shape of the absorption band depends on the crystal stoichiometry[32], as shown in Figure 2.9 As the lithium deficiency increases, the broad band resolves into three relatively narrow sub− bands, suggesting the presence of *more* than two OH− environments.

2.5.3. Formation Of OH− Hydroxyl Groups In Proton− Exchanged Lithium Niobate Waveguides.

The present section is concerned with determining the extent of OH− formation in proton− exchanged waveguides as a function of waveguide fabrication times and temperatures. The waveguide fabrication conditions were described in Section 2.3 (Tables 2.1 and 2.2).

In recording infrared spectra of proton− exchanged waveguides, previous workers[6,11] did not consider the OH− absorption of the bulk material. This was unusual since it had been shown[32] that the bulk OH− absorption depended on the stoichiometry of the substrate, and the substrate stiochiometry varied from sample− to− sample[33]. In the present work, infrared spectra were recorded prior to fabrication so that the bulk OH− absorbance could be subtracted from the OH− absorbance of the proton− exchanged region.

The infrared absorption spectra of the x− cut waveguides fabricated at 198.7°C and the z− cut waveguides fabricated at 210.9°C are shown in Figures 2.10 and 2.11, respectively. The x− cut spectra consist of two overlapping OH− bands: a broad band at υ_{max}= 3250cm^{-1}, and a sharp band at υ_{max}= 3505cm^{-1}. The two bands indicate the existence of two different OH− environments. In the spectra of the z− cut waveguides only the sharp band at υ_{max}= 3505cm^{-1} is present, although the existence of the broad band is evident from the shoulder on the high− frequency side of the sharp band.

The shape of the absorption bands in the infrared spectra of x− and

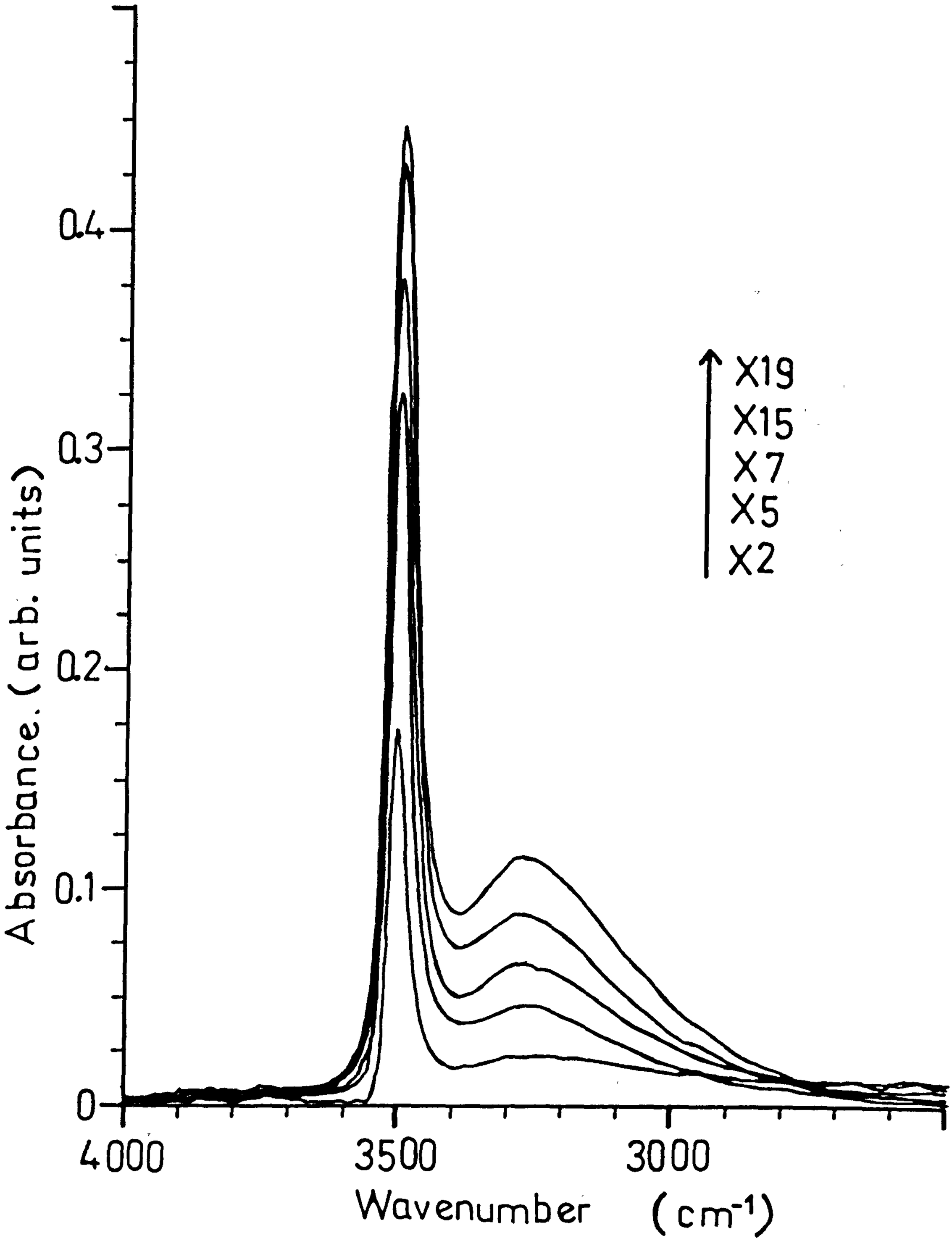

Figure 2.10. Infrared Spectra Of X–Cut Proton–Exchanged Lithium Niobate, Superimposed As A Function Of Fabrication Time *(The Fabrication Temperature Was T=198.7°C).*

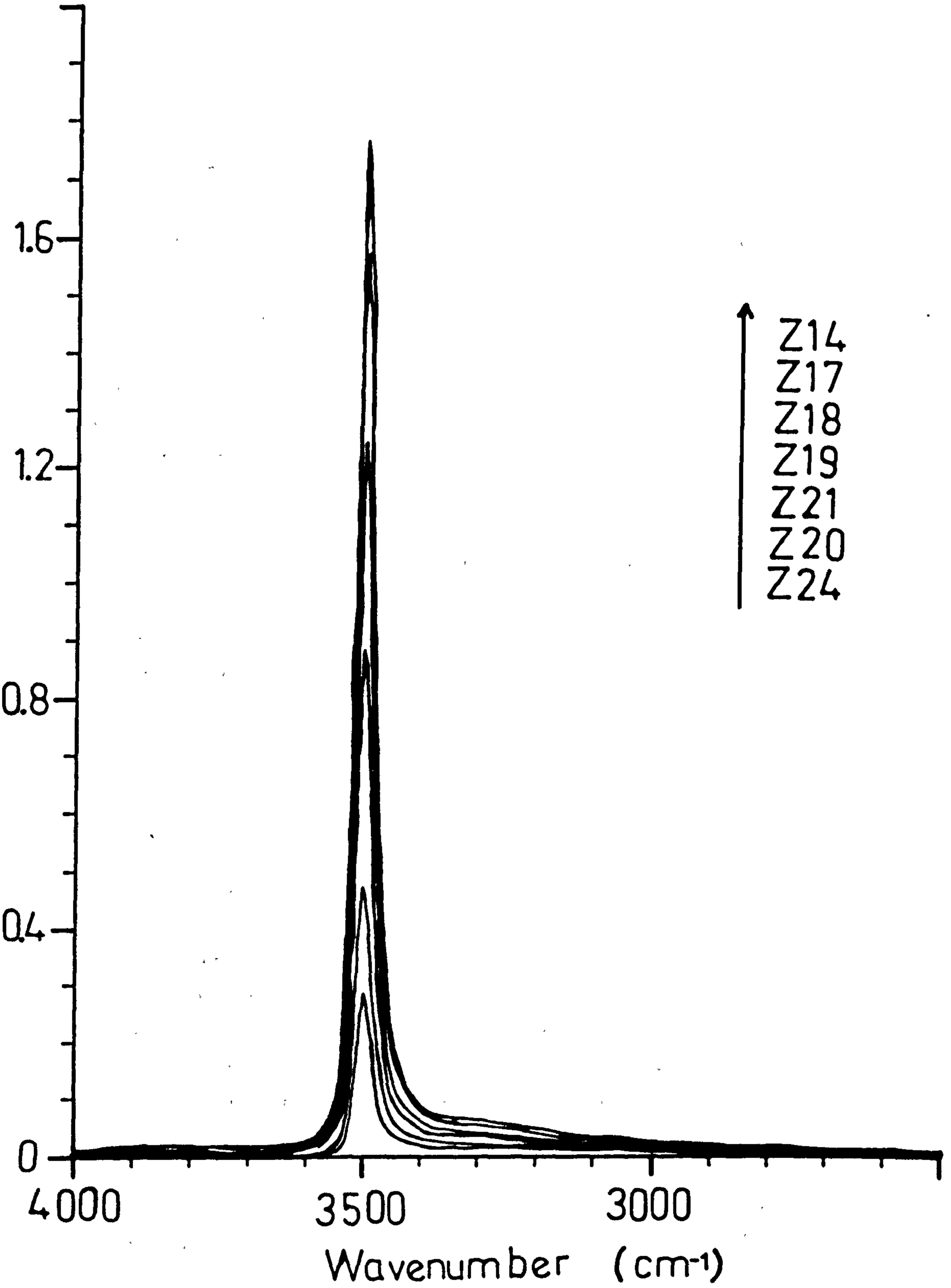

Figure 2.11. Infrared Spectra Of Z–Cut Proton–Exchanged Lithium Niobate, Superimposed As A Function Of Fabrication Time ***(The Fabrication Temperature Was T=210.9°C).***

z– cut proton– exchanged waveguides can be explained by considering the potential energy curves for the vibrating OH– groups[28,34,35]. A reasonable assumption to make when considering OH– bonds, is that the proton vibrates against the more massive and approximately stationary oxygen anion. A free OH– hydroxyl group has a narrow potential energy curve corresponding to a narrow potential well[34]. Such a potential gives rise to the sharp, well– defined band at υ_{max}= 3505cm^{-1} in x– y– and z– cut proton– exchanged waveguides. Hydrogen– bonded OH– hydroxyl groups have broad potential energy curves and give rise to the broad absorption band at υ_{max}= 3250cm^{-1} in x– and y– cut proton– exchanged waveguides[34].

The absence of the broad absorption band in z– cut material is because, no matter what the polarisation of the incident radiation, the vibration remains unexcited. If the proton is hydrogen– bonded to three oxygen anions and is located slightly above an oxygen triangle plane* (Chapter 1, Figure 1.1), the whole vibration can be resolved into three components along the x– y– and z– axes*. It can easily be shown by symmetry that the x– and y– components cancel and that the vibration lies solely along the z– axis. However, the presence of the shoulder on the high– frequency side of the z– cut band suggests that there is a vibrational component lying slightly out from the z– axis*.

By placing an infrared polariser in the path of the incident beam, information on the orientation– dependence of the OH– absorption bands was obtained (Figures 2.12a and 2.12b). However, the rotation of the polariser was unknown with respect to the axes of the waveguides. The polarisation of the incident radiation was determined by recording the infrared spectra of the nematic liquid crystal p– n– butyl– N– (p– methylbenzylidene)aniline (MBBA), orientated normal to the horizon, with the polariser set at 0° and 90°. Only certain absorption bands are present, depending on the incident polarisation**.

* *Thanks to Mr. M.A. Foad (Chemistry Department, University of Glasgow) for this suggestion.*

** *Thanks to Dr. R. Peacock (Chemistry Department, University of Glasgow) for carrying out this work.*

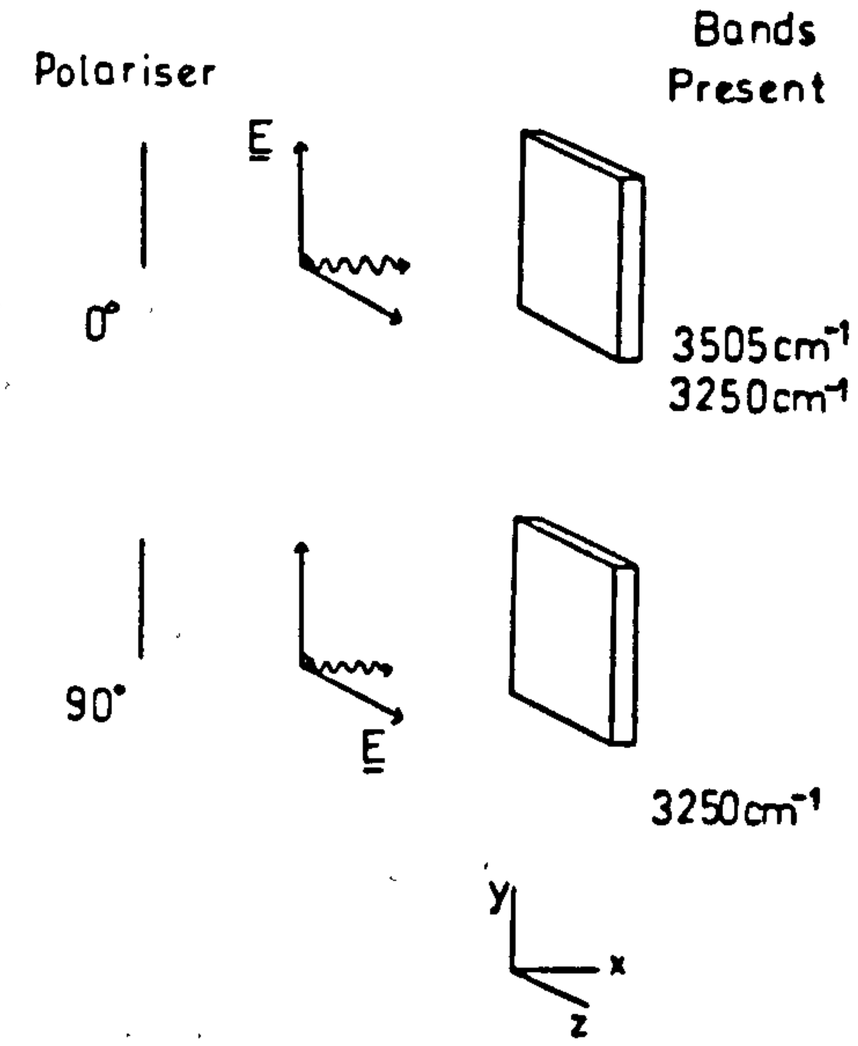

Figure 2.12a. Diagram Showing The Polarisation Dependence Of The OH Absorption Bands In X–Cut Proton–Exchanged Lithium Niobate.

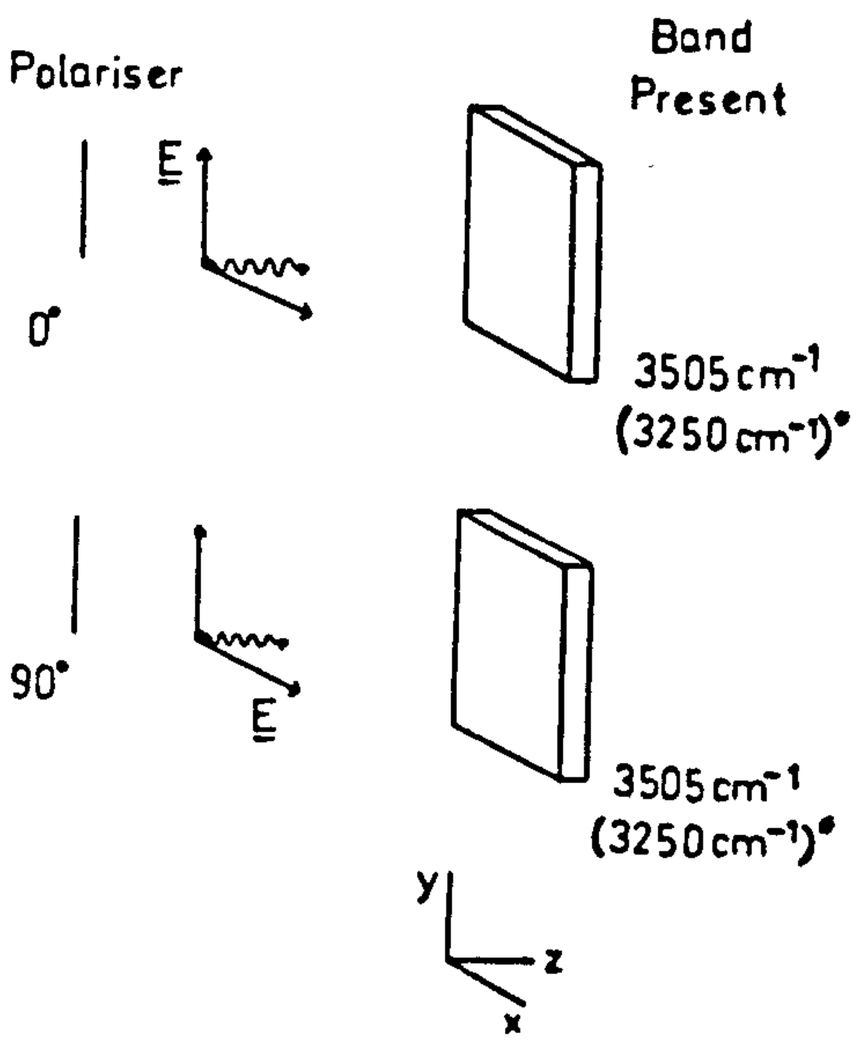

Figure 2.12b. Diagram Showing The Unpolarised Absorption Band In Z–Cut Proton–Exchanged Waveguides. (*_Broad Band Present To A Lesser Extent Than In X–Cut_).

E= Polarised Radiation Direction.

Comparison of the spectrum of MBBA with published literature[36] enabled the incident polarisation to be determined. With the polariser set at 0° the polarisation was vertical, i.e. parallel to the y–axis of the lithium niobate, and when set at 90° the polarisation was horizontal, i.e. parallel to the x, or z–axis, depending on the crystal orientation.

The sharp OH–absorption band at υ_{max}= 3505cm^{-1} in the x–cut spectra was strongly dependent on the polarisation of the incident radiation (Figure 2.12a). When the polarisation was perpendicular to the c–axis the band was present, and when the polarisation was parallel to c the band disappeared. However, the sharp band was *always* present in the z–cut material. These measurements indicate that free OH is confined to vibrate in the (x,y)–plane of the waveguide.

In the spectra of the x–cut waveguides the broad OH–absorption band at υ_{max}= 3250cm^{-1} was independent of the polarisation of the incident radiation, indicating that the vibration had equal components along the y– and z–axis of the substrate. However, in the spectra of the z–cut waveguides the broad absorption band did *not* have a component along the y–axis (or the x–axis), indicating that the vibration was solely along the z–axis. If the vibration *was* along the z–axis, there should have been no component along y. However, there was a y–component in the x–cut material. The reason for this discrepancy is unclear.

The x– and z–cut infrared spectra in Figures 2.10 and 2.11 indicate that the OH–absorbance increases with the waveguide fabrication time. Previous workers reported[6,20] that the extent of proton–exchange in x–cut material was non–linear at high temperatures (>200°C) and long times (>1hr.). The latter work[20] showed that in x–cut proton–exchanged lithium niobate, the absorbance of the OH–band at υ_{max}= 3505cm^{-1} increased non–linearly with temperature and time.

Figures 2.13a and 2.13b show the variation in peak absorbance with $t^{1/2}$ for the OH–absorption bands at υ_{max}= 3250cm^{-1} and υ_{max}= 3505cm^{-1}, respectively of x–cut proton–exchanged waveguides. The variation in the absorbance of both bands is non–linear with $t^{1/2}$, in agreement with the results published in references (6) and (20).

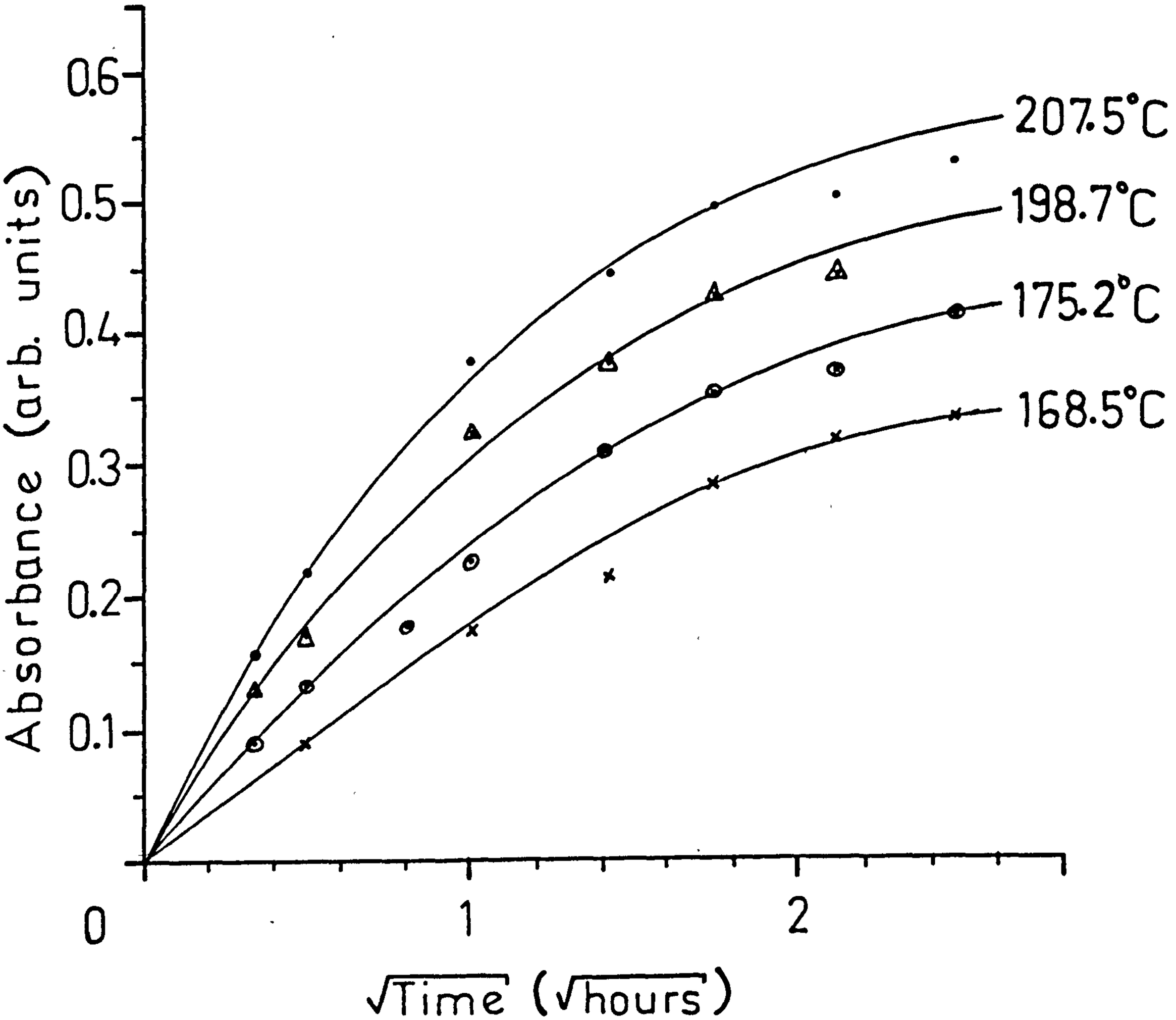

Figure 2.13a. Variation In Absorbance At υ_{max}= 3505cm^{-1} With $t^{1/2}$ For X– Cut Proton– Exchanged Lithium Niobate.

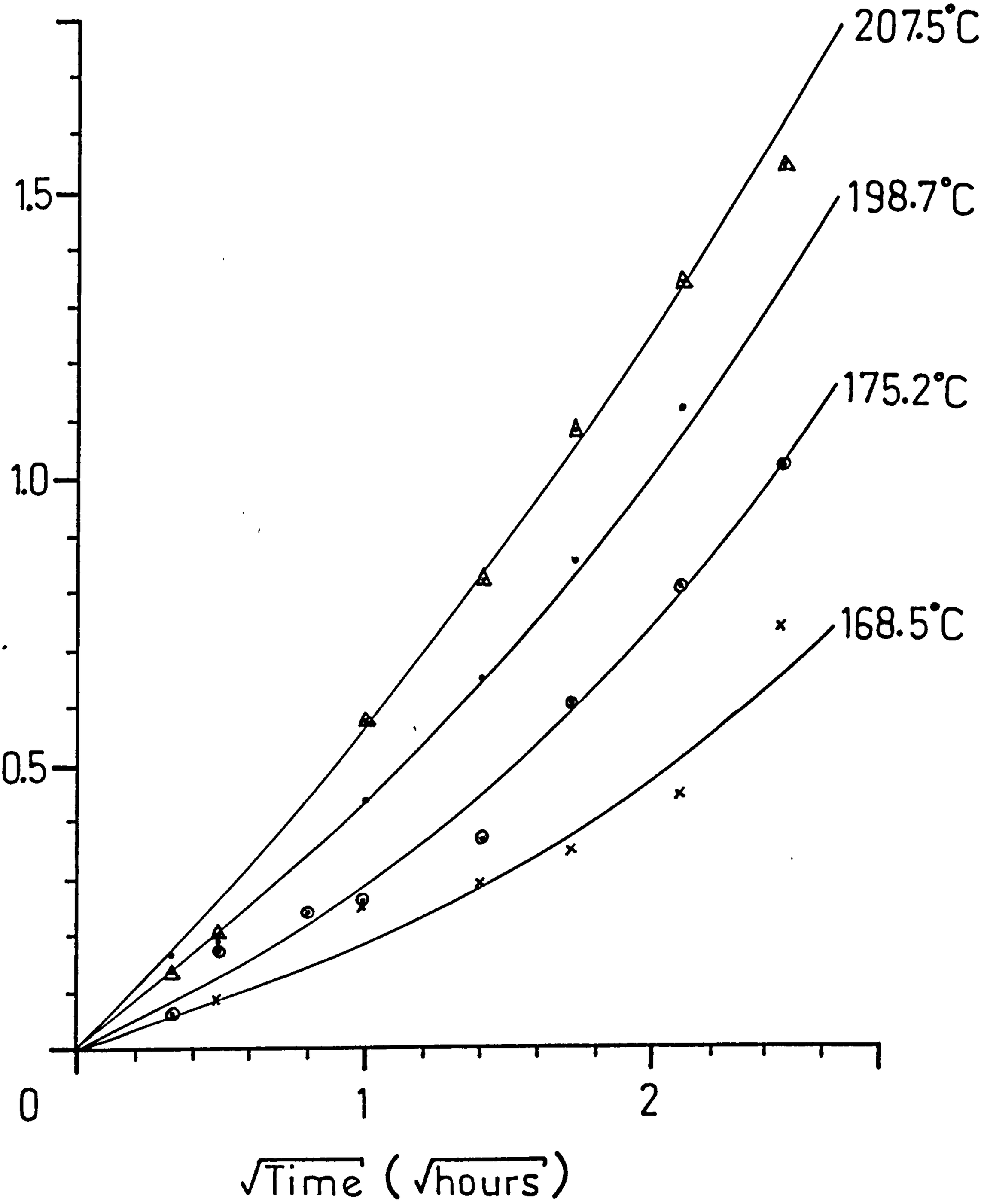

Figure 2.13b. Variation In Absorbance At υ_{max}= 3250cm^{-1} With $t^{1/2}$ For X– Cut Proton– Exchanged Lithium Niobate.

However, when describing an absorbance peak, two factors must be considered: height and width. Both are inter-dependent and one should not be used without the other. Therefore, the *area* of the OH-bands should be used in estimating the extent of proton-exchange.

The relationship between OH-absorption band area and $t^{1/2}$ is shown in Figures 2.14 and 2.15 for x- and z-cut waveguides, respectively. The integration was performed between $\upsilon = 2700cm^{-1}$ and $\upsilon = 3600cm^{-1}$ (x-cut), and from $\upsilon = 2900cm^{-1}$ to $\upsilon = 3650cm^{-1}$ (z-cut). The linear relationship between band area and $t^{1/2}$ indicates that the extent of OH formation is governed by diffusion. One can therefore write an equation which is analogous to Equation (5):

$$(area) = 2[M(T)t]^{1/2} \quad \ldots\ldots\ldots (13),$$

where M(T) is analogous to the effective diffusion coefficient D(T) in Equation (5).

The natural logarithm of M(T) was plotted as a function of 1/T to test for an Arrhenius law, resulting in the lines:

$$\ln M(T) = -7271.546/T + 20.951, \text{ for x-cut} \quad \ldots\ldots\ldots (14),$$

$$\ln M(T) = -10091.29/T + 26.923, \text{ for z-cut} \quad \ldots\ldots\ldots (15).$$

Equations (14) and (15) were used to calculate effective activation energies for the proton-exchange process. The values obtained were $Q_x = 60.4kJmol^{-1}$ and $Q_z = 81.2kJmol^{-1}$. Table 2.4 compares the activation energies estimated from mode angle measurements (Section 2.4.3) with those estimated from the results of infrared spectroscopy. Both methods are in agreement that the activation energy is higher in z-cut material. The values of Q_z calculated by the two methods are close. However, there is a large discrepancy between the values of Q_x.

The difference between the values of Q_x could be due to the overlapping absorption bands obtained with x-cut waveguides. To get a more precise estimate of the intensity of the absorption for OH-groups in x-cut

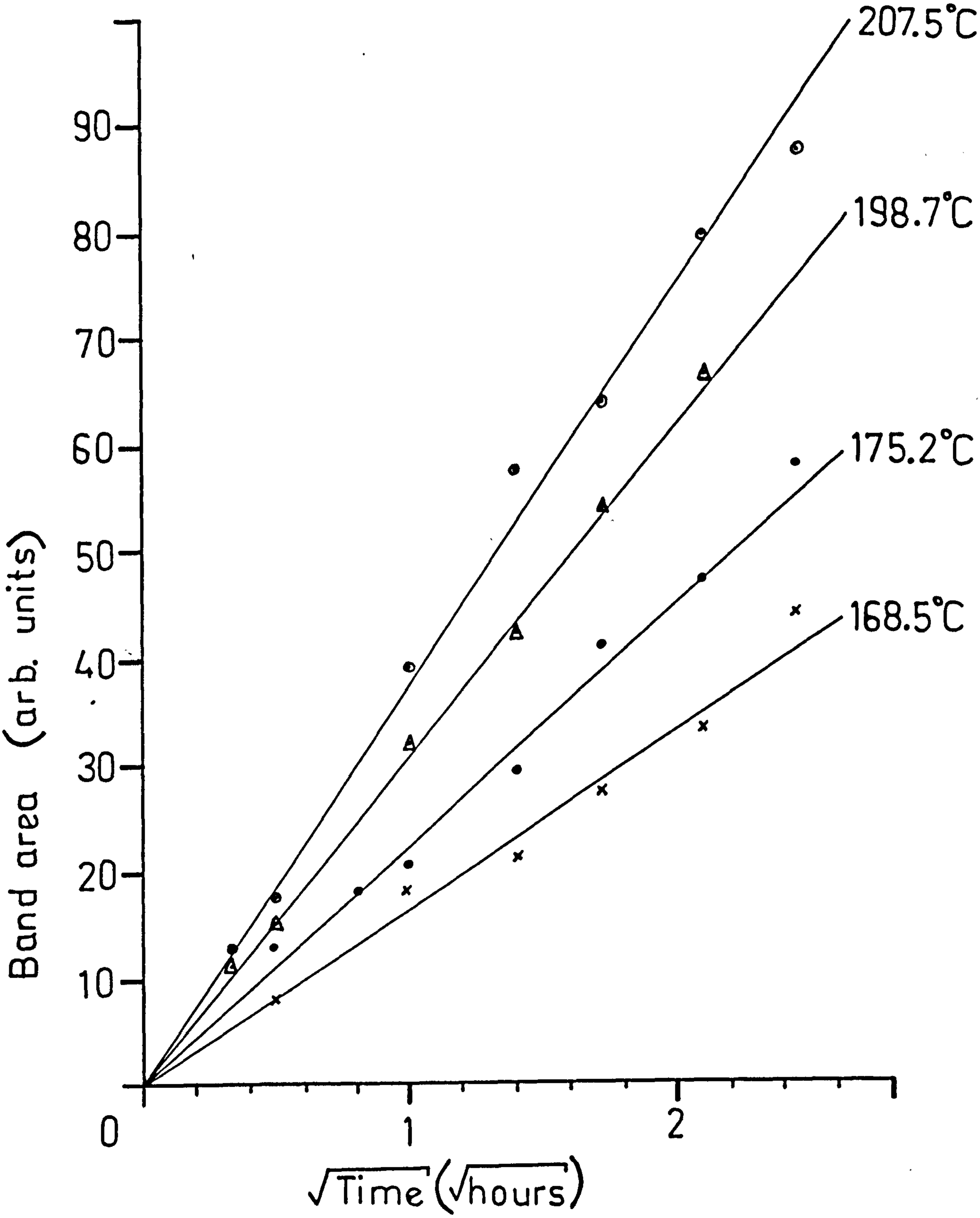

Figure 2.14. OH Area As A Function Of $t^{1/2}$ For X–Cut Proton–Exchanged Lithium Niobate.

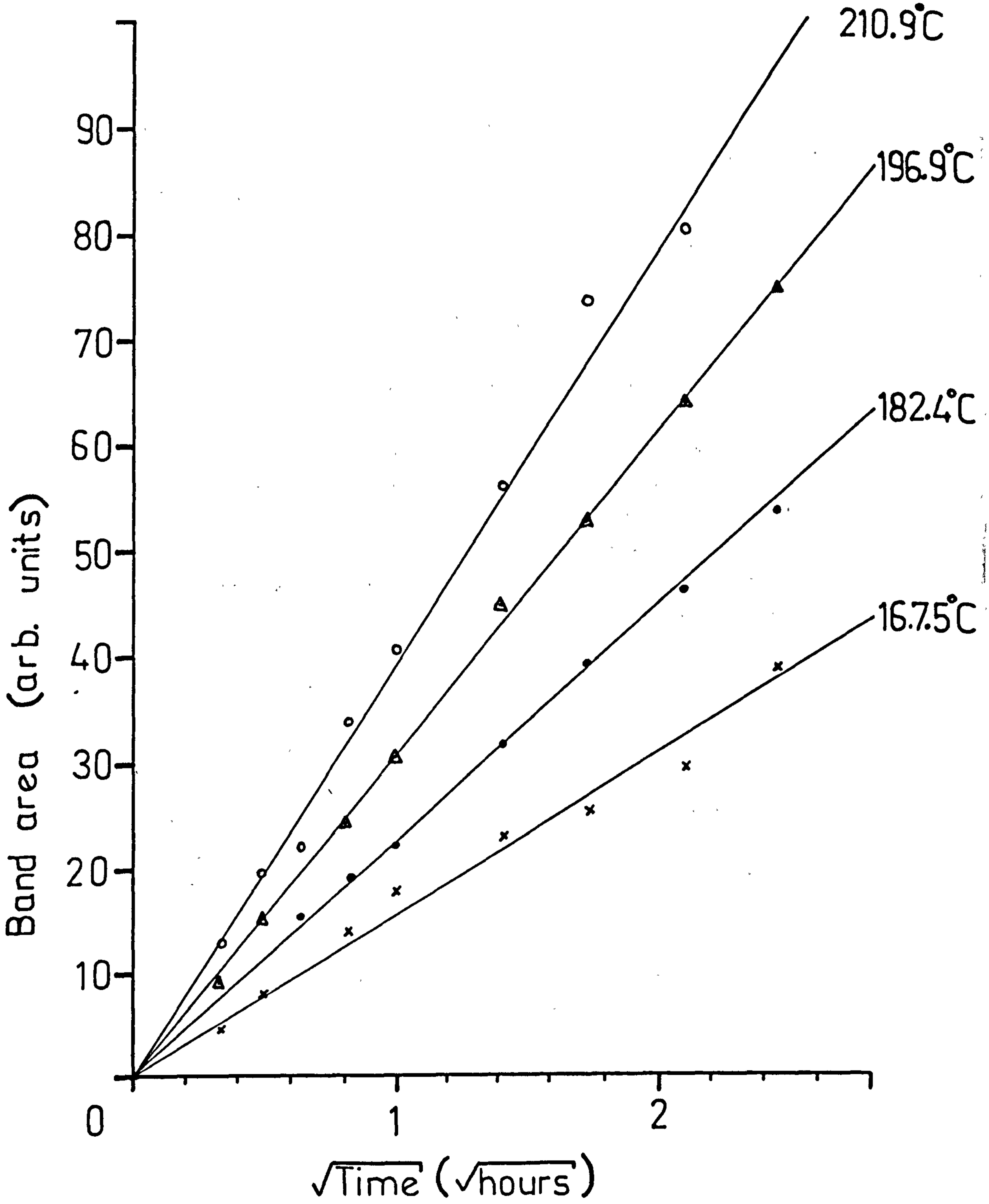

Figure 2.15. OH Area As A Function Of $t^{1/2}$ For Z–Cut Proton–Exchanged Lithium Niobate.

waveguides, the area of the absorption bands should be calculated separately. The total area would, in consequence, be larger and the estimated activation energy would therefore be larger.

Using Equations (13), (14), and (15), one can write:

$$(\text{Area}) = 7.111\text{x}10^{4}t^{1/2}\exp(-3.363\text{x}10^{3}/T),\ \text{x-cut} \quad \text{.....(16)},$$

$$(\text{Area}) = 9.826\text{x}10^{5}t^{1/2}\exp(-4.884\text{x}10^{3}/T),\ \text{z-cut} \quad \text{.....(17)}.$$

The linear relationships between absorption band area and $t^{1/2}$ and between waveguide depth and $t^{1/2}$ suggest that the absorption band area can be related to the depth of the waveguide region. The latter relationship was tested and verified by plotting the area as a function of depth for the x- and z-cut waveguides (Figures 2.16 and 2.17, respectively). The equations of the lines in Figures 2.16 and 2.17 are:

$$(\text{Area}) = 45.071d + 3.767\ (\text{x-cut}) \quad \text{.....(18)},$$

$$(\text{Area}) = 27.991d + 7.404\ (\text{z-cut}) \quad \text{.....(19)},$$

where d is in μm. The OH-absorption band areas can be estimated for any temperature and time using Equations (16) and (17). The depth of the exchanged region can, in consequence, be calculated using Equations (18) or (19).

The relationship between absorption band area and waveguide fabrication temperature is depicted in Figures 2.18 and 2.19 for x- and z-cut proton-exchanged waveguides, respectively. The latter two figures indicate that there is a minimum temperature at which proton-exchange occurs. The minimum temperature is defined at the point where the lines intercept the temperature axis.

The interception points are at $T = (140.6 \pm 3.3)^{\circ}C$ for z-cut, and $T = (131.9 \pm 8.3)^{\circ}C$ for x-cut. Values obtained by plotting the waveguide depth as a function of temperature at fixed times are $T = (148.5 \pm 7.5)^{\circ}C$ for z-cut, and $T = (145.4 \pm 3.4)^{\circ}C$ for x-cut. The estimated minimum

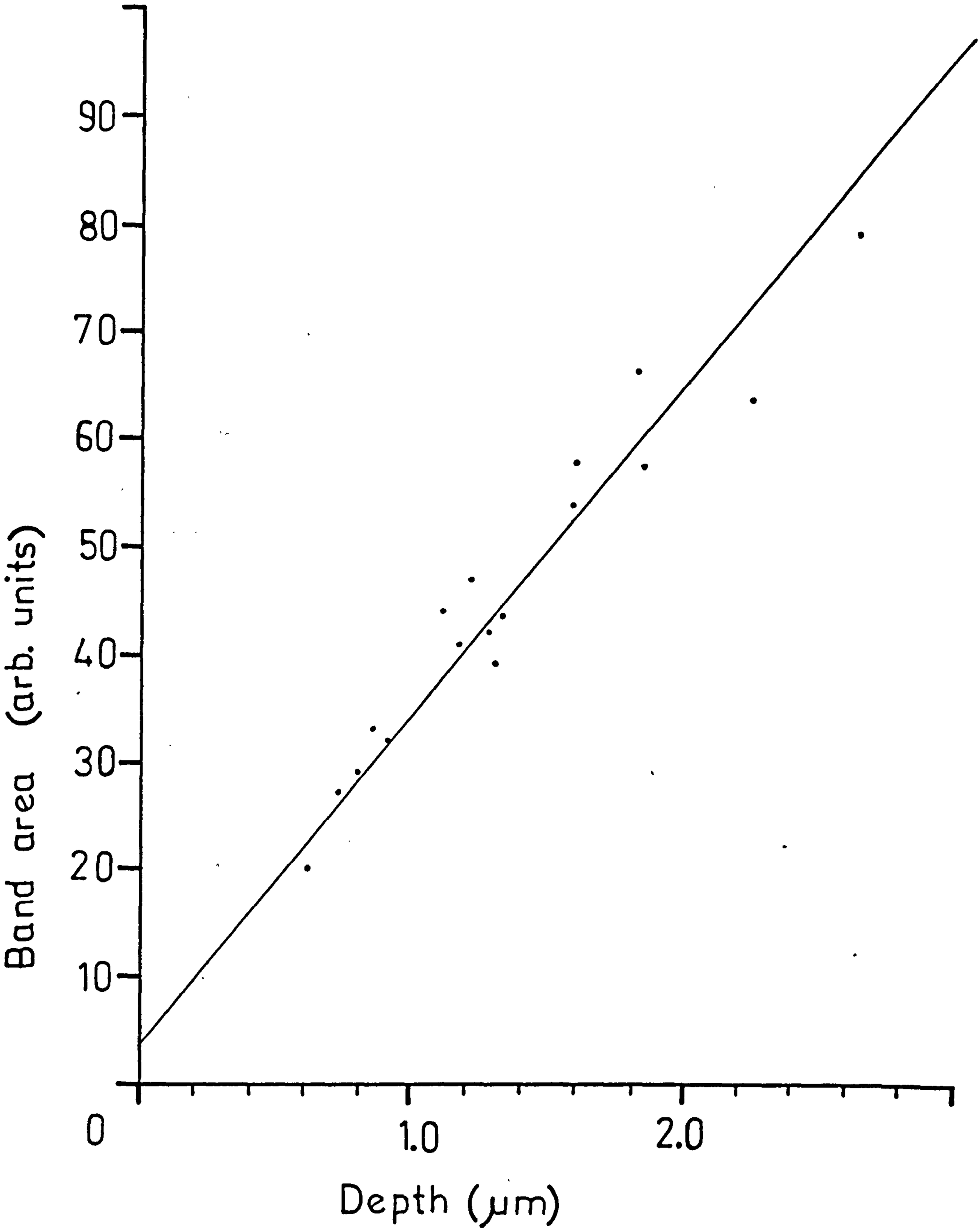

Figure 2.16. OH Area As A Function Of Depth For X–Cut Proton–Exchanged Lithium Niobate.

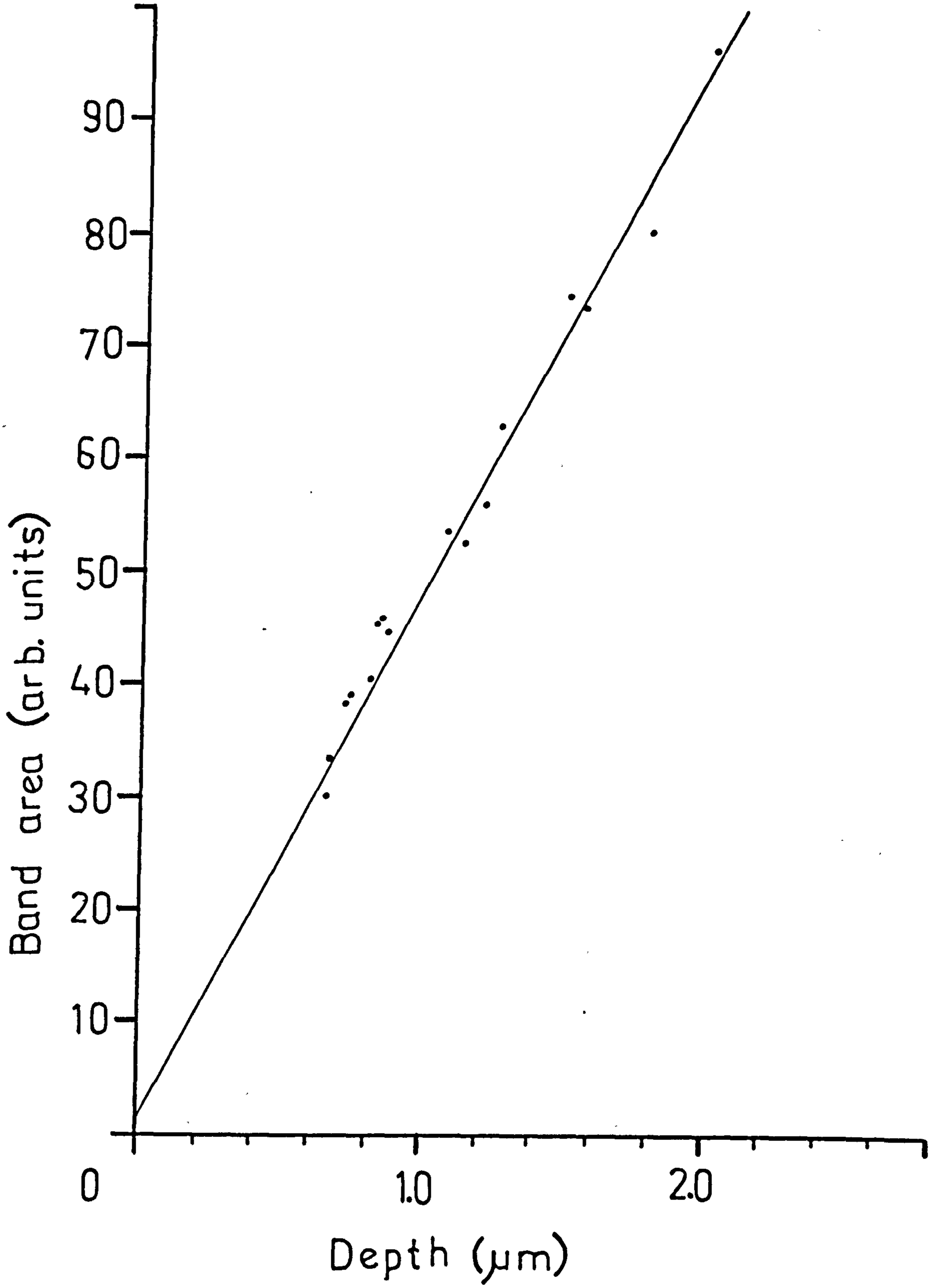

Figure 2.17. OH Area As A Function Of Depth For Z–Cut Proton–Exchanged Lithium Niobate.

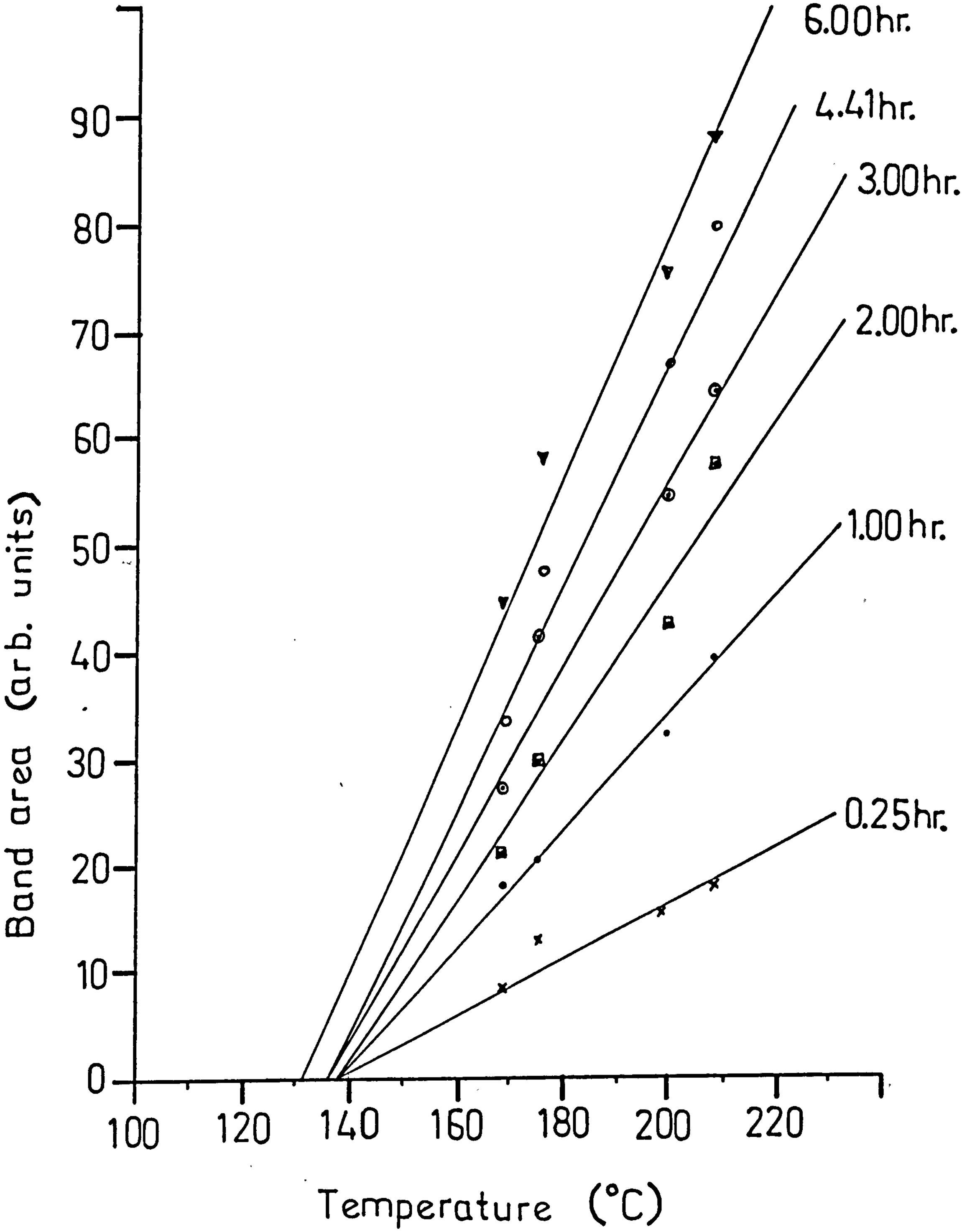

Figure 2.18. OH Area As A Function Of Fabrication Temperature (Fixed Times) For X–Cut Proton–Exchanged Lithium Niobate.

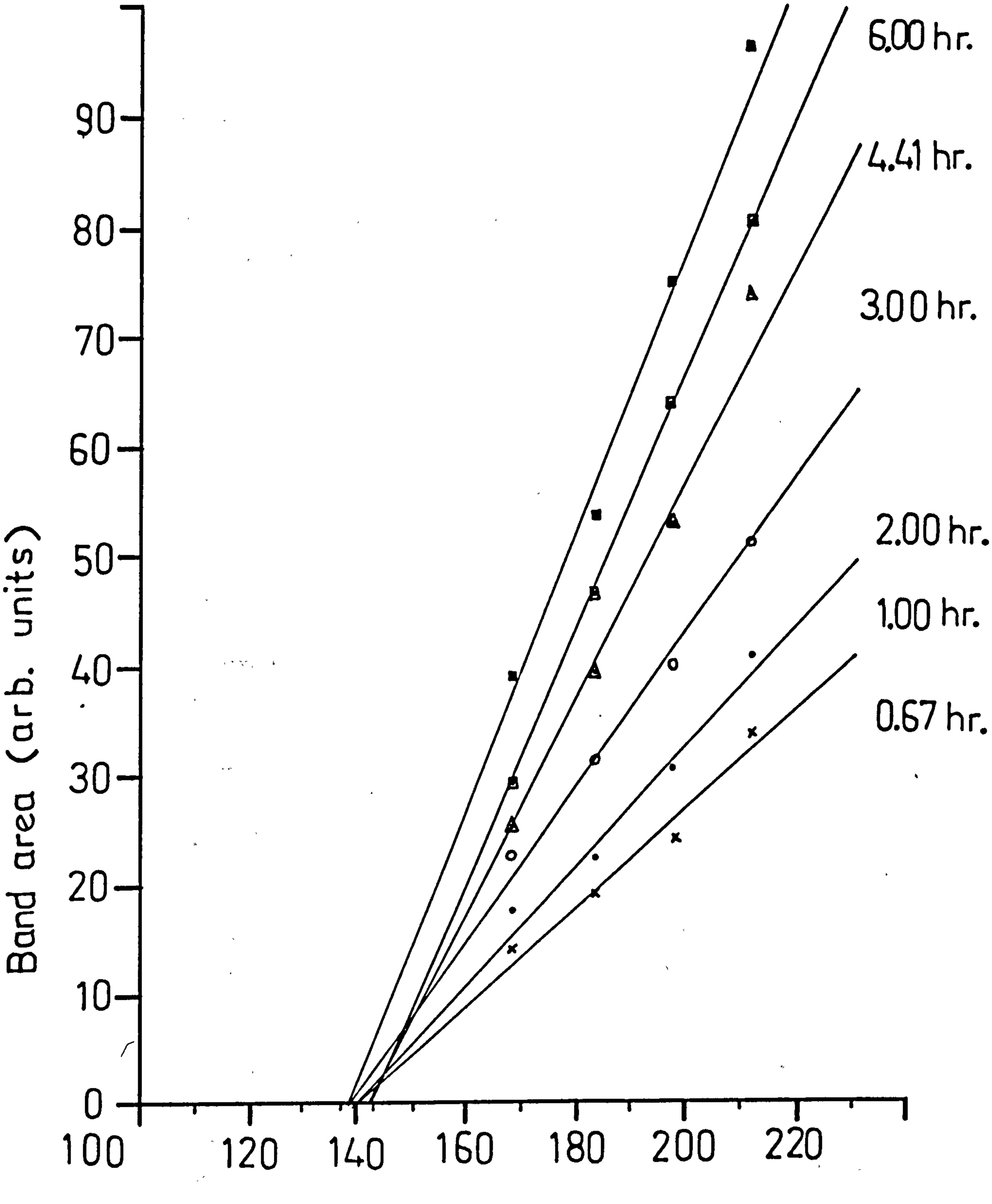

Figure 2.19. OH Area As A Function Of Fabrication Temperature Fixed Times) For Z–Cut Proton–Exchanged Lithium Niobate.

temperatures for proton–exchange are identical for x– and z–cut lithium niobate (within experimental error). It should be noted that the minimum exchange temperatures are higher than the melting point of the benzoic acid (122°C). Experiments to determine the importance of the fabrication temperature and the acidity of the acid are being carried out by Mr. M.A. Foad of the University of Glasgow Chemistry Department.

It has been demonstrated in this section that the extent of proton–exchange as a function of temperature and time can be observed using OH–absorption band areas. The depth of a proton–exchanged waveguide has been related to the areas under the OH–absorption bands. By using polarised infrared radiation the free OH–vibrations were found to be localised in the (x,y)–plane and the hydrogen–bonded OH–vibrations were shown to have components along the x, y, and z–axes.

2.6. DETERMINATION OF THE EXTENT OF PROTON–EXCHANGE USING ATOMIC ABSORPTION SPECTROSCOPY.

2.6.1. Introduction.

Atomic absorption spectroscopy is an analytical method for the determination of elements based on the absorption of radiation by free atoms[37]. The technique involves spraying a nebulised aqueous solution of an analyte sample into a high–temperature flame (1200°C to 1500°C), producing an atomic vapour in which most of the atoms are in an unexcited state[38].

Light of a selected wavelength passes through the flame and excites the ground state electrons of the atoms via the absorption of photons. The transmitted radiation is detected using a photomultiplier. By comparing the transmitted intensity to the initial intensity the absorption can be estimated. The absorption is directly proportional to the atomic population in the flame.

Atomic absorption spectroscopy requires using a set of standard (reference) solutions containing known concentrations of the element to be

determined. By measuring the absorbances of the standard solutions, a calibration curve can be plotted. Using the calibration curve and the absorbances of the analyte solutions, the concentrations in the analyte solutions can be determined. The following section is concerned with the determination of lithium in benzoic acid as a function of the temperature and time of proton–exchange[39].

2.6.2. Preparation Of Standard And Analyte Solutions For Atomic Absorption Spectroscopy.

The acids used for analyses were retrieved after proton–exchange with x– and z–cut lithium niobate under the conditions outlined in Section 2.3 and Tables 2.1 and 2.2. The surface areas of the samples (dimensions measured with a Vernier guage) were estimated to within $\pm 0.05 cm^2$ of one another. The re–crystallised acids were crushed and homogenised using an agate mortar and pestle.

Accurately weighed portions of each acid ($1 \pm 10^{-4} g$) were dissolved in absolute alcohol (50ml), in 100ml volumetric flasks. The solutions were made up to 100ml with distilled water. The standard solutions were prepared by serial dilution of Spectrosol lithium nitrate (1000ppm), added to absolute alcohol (50ml) in which portions ($1 \pm 10^{-4} g$) of AnalaR benzoic acid had been dissolved. The solutions were made up to 100ml with distilled water. The concentrations of lithium in the standard solutions were 0 (blank), 0.05, 0.08, 0.1, 0.5, 1.0, 1.5, and 2.0μg/ml.

Absorption signals were measured on a Perkin–Elmer 306 spectrometer. The radiation source was a lithium hollow cathode lamp ($\lambda = 0.678 \mu m$). The sensitivity of the spectrometer was approximately 0.035μg/ml for 1% absorption[40,41].

2.6.3. The Determination Of Lithium In Benzoic Acid After Proton–Exchange.

The calibration curve of the standard solutions is shown in Figure 2.20. Errors were calculated for the concentrations using estimated errors in weighing of the acid ($\pm 10^{-4} g$), the solution volumes ($\pm 0.12 ml$[42]), and

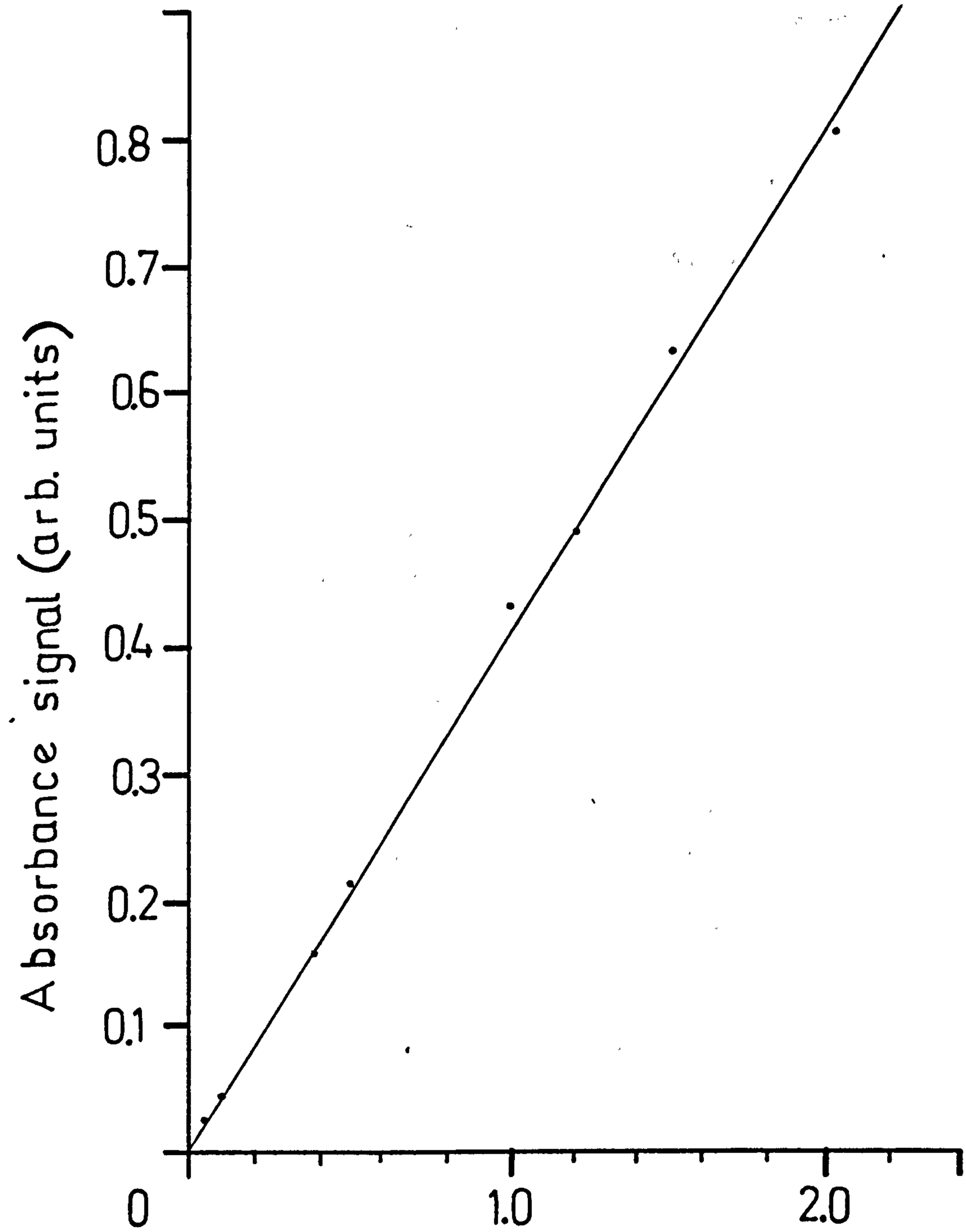

Figure 2.20. Atomic Absorption Calibration Curve.

using the standard deviation of absorbances (the absorbance of each analyte solution was measured six times).

Tables 2.5 and 2.6 list the molals of lithium (moles of lithium/kg of benzoic acid) as a function of exchange time and temperature for the x– and z– cut waveguides, respectively. The variation of lithium molality with $t^{1/2}$ is shown in Figures 2.21 and 2.22 for x– and z– cut proton– exchanged waveguides, respectively.

The concentration of lithium in benzoic acid increased with time and temperature. The higher concentrations for x– cut proton– exchanged lithium niobate indicated that the extent of proton– exchange in x– cut material was greater than in z– cut, for equivalent times and temperatures. For example, the lithium molals determined after proton– exchange at T= 210°C for six hours were 29.34×10^{-4} and 12.07×10^{-4} for x– and z– cut waveguides, respectively.

Figures 2.21 and 2.22 indicate that the relationship between the lithium concentration in benzoic acid and $t^{1/2}$ is non– linear. However, this does not necessarily imply that the migration of lithium *in the crystal* during proton– exchange is not governed by diffusion. Lithium reaches the acid as a result of three separate processes: (i) migration of lithium ions to the surface of the crystal, (ii) exchange between lithium ions and protons at the surface, (iii) migration of lithium ions into the melt. Neither of these processes can be followed individually by atomic absorption spectroscopy. Therefore, atomic absorption spectroscopy can only be used to determine the overall extent of reaction as a function of temperature or time.

It was assumed that, in using one gram aliquots of acid, the distribution of lithium in the recrystallised acids was homogeneous. This assumption was tested by taking seven different aliquots per acid sample, from four samples reacted at the same temperature for different times. The portions were taken from the samples which had previously been used for proton– exchange at 198.7°C for 0.25hr, 1hr, 3hr, and 6hr (samples X4, X10, X13, and X20, respectively). The lithium concentration in each aliquot was calculated as described above.

Sample	Fabrication Temperature (°C)	Fabrication Time (hr)	Lithium Molality ($x10^{-4}$)
X1	168.6±0.8	1	2.16±0.34 (0.16)
XX13	"	2	2.57±0.74 (0.14)
X11	"	3	3.96±0.17 (0.18)
XX18	"	4.42	5.80±0.73 (0.21)
X12	"	6	5.97±0.01 (0.19)
X4	175.2±1.2	0.25	0.99±0.17 (0.13)
XX14	"	0.67	2.07±0.43 (0.17)
X10	"	1	3.08±0.17 (0.21)
XX16	"	2	5.47±0.84 (0.26)
X13	"	3	6.18±0.01 (0.24)
XX17	"	4.42	8.40±0.15 (0.27)
X20	"	6	11.56±0.17 (0.30)
X2	198.7±1.2	0.25	1.31±0.17 (0.10)
X5	"	1	4.73±0.17 (0.18)
X7	"	2	7.10±0.18 (0.19)
X15	"	3	9.84±0.01 (0.21)
X19	"	4.42	10.60±0.01 (0.18)
X22	"	6	16.68±0.84 (0.23)
XX8	207.5±1.0	0.12	2.90±0.49 (0.25)
X6	"	0.25	2.32±0.17 (0.14)
X8	"	1	9.22±0.68 (0.25)
X9	"	2	13.76±0.01 (0.28)
X14	"	3	16.88±0.36 (0.28)
X16	"	4.42	22.07±0.19 (0.33)
X17	"	6	29.34±0.18 (0.33)

Table 2.5. Lithium Concentration In Benzoic Acid After Proton–Exchange With X–Cut Lithium Niobate

('x'–factors are in parentheses).

Sample	Fabrication Temperature (°C)	Fabrication Time (hr)	Lithium Molality (x10⁻⁴)
ZZ2	167.5±1.7	0.67	1.50±0.43
Z1	"	1	2.24±0.42
ZZ3	"	2	2.94±0.83
Z4	"	6	4.34±0.34
Z25	182.4±0.8	0.42	0.42±1.46
Z26	"	1	1.03±0.48
Z23	"	2	3.08±1.33
Z22	"	3	3.45±0.78
Z16	"	4.42	4.60±0.82
Z15	"	6	6.42±0.76
Z12	196.9±1.7	0.12	0.07±0.63
Z11	"	0.25	0.79±0.46
Z9	"	1	3.97±0.64
Z7	"	3	7.07±0.60
Z6	"	4.42	9.00±0.45
Z5	"	6	10.05±0.60
ZZ21	210.9±1.8	0.25	5.14±1.55
Z20	"	0.42	0.08±0.56
ZZ14	"	0.67	4.53±0.53
Z21	"	1	2.87±0.67
Z19	"	2	5.93±0.30
Z18	"	3	9.13±0.84
Z17	"	4.42	10.12±0.73
Z14	"	6	12.07±0.42

Table 2.6. Lithium Concentration In Benzoic Acid After Proton–Exchange With Z–Cut Lithium Niobate.

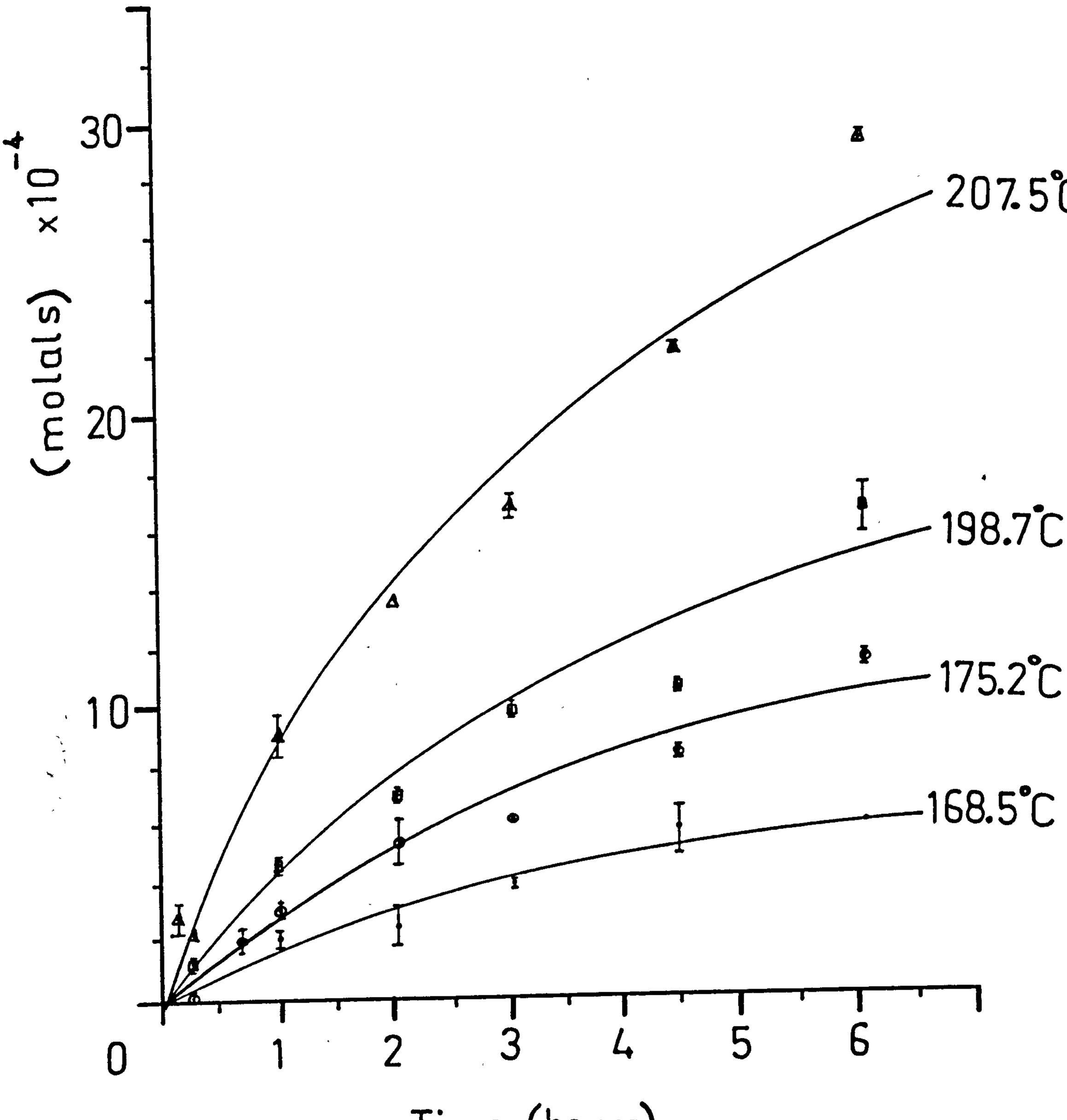

Figure 2.21. Lithium Molals As A Function Of $t^{1/2}$ (X-Cut Proton-Exchange)

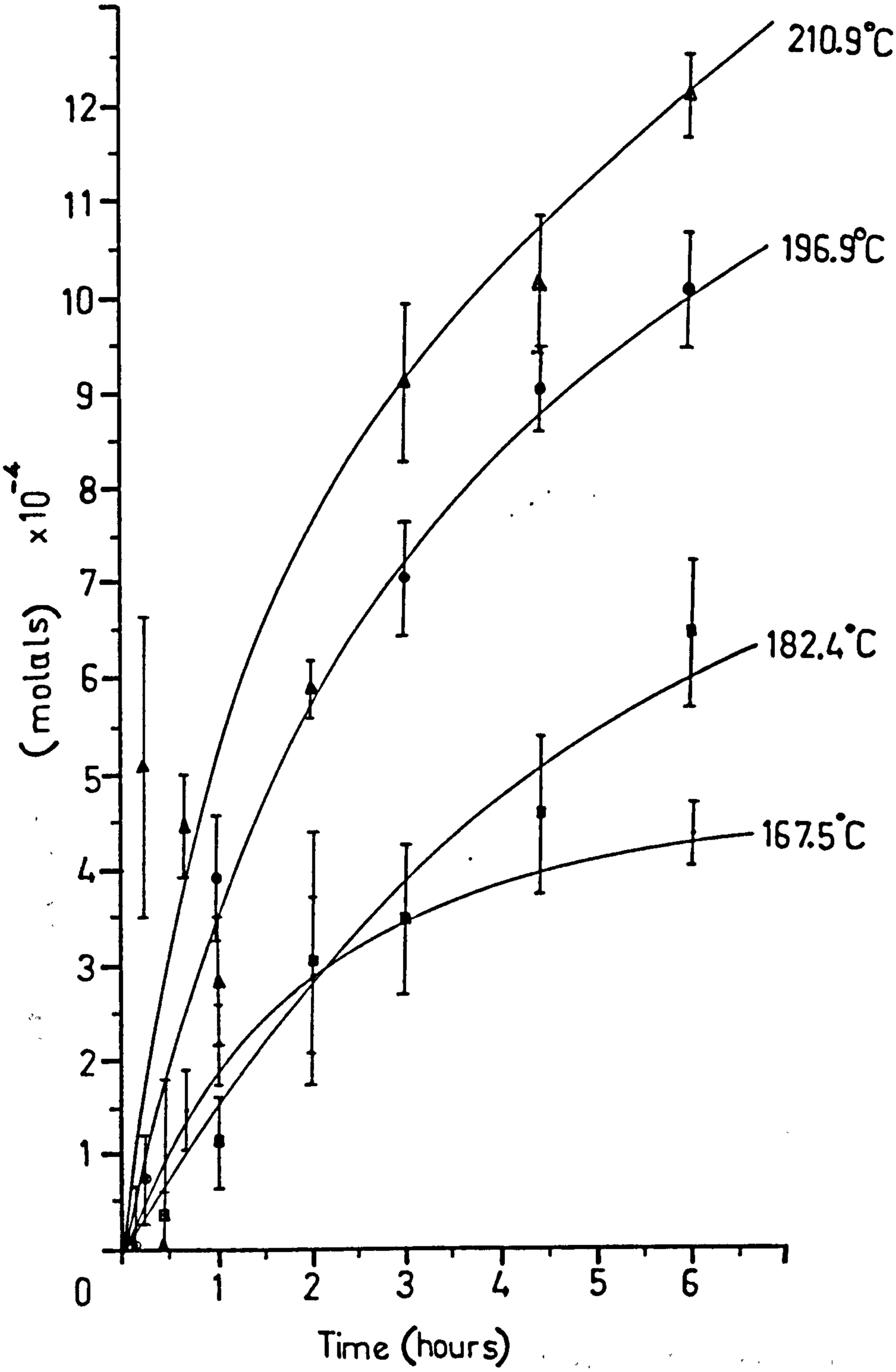

Figure 2.22. Lithium Molals As A Function Of $t^{1/2}$ (Z– Cut Proton– Exchange).

Sample	Number of replications	Molals ($x10^{-4}$)	Mean (σ)	95% confidence limit (error as %)
X4	7	0.99 0.67 0.82 0.82 1.14 1.14 1.15	0.96 (0.19)	0.82 to 1.10 (14%)
X10	7	3.08 3.53 3.55 3.42 3.84 4.45 4.02	3.70 (0.45)	3.37 to 4.03 (8.9%)
X13	6	6.18 6.96 7.05 7.20 7.16 7.30	6.98 (0.41)	6.68 to 7.28 (4.3%)
X20	7	11.56 10.34 10.77 9.98 10.39 11.14 10.02	10.60 (0.59)	10.16 to 11.04 (4.2%)

Table 2.7. Lithium Concentration Of Different Aliquots Taken From The Same Benzoic Acid Samples.

The molal ranges were calculated for a 95% confidence limit (the waveguides were fabricated at 198.7°C for, respectively, 0.25hr (X4), 1hr (X10), 3hr (X13), and 6hr (X20)).

The 95% confidence limits[43] calculated for each concentration are given in Table 2.7.

The results presented in Table 2.7 indicate that the lithium distribution in the recrystallised acids is uniform and that concentrations can be determined with a precision between 4% and 14%. The determination is less precise for low lithium concentrations because of the difficulty in measuring low absorbances.

One can estimate the percentage of Li−H substitution within the waveguide layer, i.e. the factor 'x' in Equation (1), from the lithium concentration in the acid and the waveguide depth. The value of 'x' was calculated as follows: the dimensions (x,y,z) of the lithium niobate wafers were measured; the total exchangable volume (V_{ex}) was then estimated using:

$$V_{ex}= 2xyd_z+ 2xzd_y+ 2yzd_x \quad \text{.....(20)},$$

where d_i (i= x,y,z) was the depth of the exchanged region along the x−, y−, and z− directions.

The mass of lithium niobate in the exchangable volume was estimated using the density (ρ) of congruent lithium niobate (ρ= 4.64g/cm^3[44,45]) and the equation:

$$\text{(mass of exchangable lithium niobate)}= W= \rho V_{ex} \quad \text{.....(21)}.$$

The mass of *lithium* in the exchangable volume was:

$$6.94W/147.85 \quad \text{.....(22)},$$

where 6.94 is the molecular weight of lithium, and 147.85 is the molecular weight of lithium niobate. The total mass of lithium determined by atomic absorption spectroscopy was W'. Therefore, the percentage of Li−H exchange, i.e. 'x', was estimated using:

$$'x'= (W'/W)x100\% \quad \text{.....(23)}.$$

The values of 'x' for the x−cut waveguides in Table 2.5 indicated that up to 33% of lithium in the exchangable volume had been replaced by protons (sample X17), and that the percentage increased with time. For example, 'x'≃25% (T= 210.5°C, t= 0.12hr) and 'x'≃33% (T= 210.5°C, t= 6hr). The minimum percentage of Li−H exchange was 10% (sample X2). Values calculated by Rice *et al*[13] (see also Chapter 1) and Canali *et al*[2] agree that 65% to 75% of the lithium ions are replaced by protons.

The low percentages could be explained if lithium were lost at some point during proton−exchange. Lithium could be lost, for example, either by evaporation, adsorption onto the surface of the silica glass, or absorption by the PTFE holders. One method of testing for loss of lithium is by studying changes in the lithium content of benzoic acid into which lithium benzoate has been added (with no lithium niobate wafer being present), after heating at temperatures typically used for proton−exchange. By comparing the concentrations before and after reaction, it may be possible to determine if lithium is lost.

To use this method, three different quantities of lithium benzoate were dissolved in molten benzoic acid at 235°C for 4.5hr (Table 2.8). The quantities were chosen to correspond to lithium concentrations determined after proton−exchange with lithium niobate at 210°C for times of up to 6hr. After 4.5hr the acids were allowed to cool and the concentrations of lithium were determined by atomic absorption spectroscopy.*

The results in Table 2.8 indicate that, at low concentrations, 57% to 60% of the lithium was detected, and at high concentrations, all the lithium was detected. The results of Section 2.6.3 (the determination of lithium in benzoic acid after proton−exchange) indicate that the error in determining concentrations corresponding to less than 0.96×10^{-4} molals (i.e. samples 1a,b and 2a,b in Table 2.8) was approximately 14%. Therefore, assigning the maximum 14% error to low concentration samples, the *corrected* percentage of lithium detected in samples 1a,b and 2a,b is (60±6)% and the percentage of Li−H exchange in the low concentration waveguides in Table 2.5 would therefore be ≃33%, which is almost identical to the values calculated for higher concentrations (for

* Thanks to Mr. M.A. Foad (Chemistry Dept., G.U.) for helping with this work.

Sample	Weight of Lithium Benzoate (g)	Experimental Concentration in Lithium Benzoate (μg)	Theoretical Concentration in Lithium Benzoate (μg)	% of Detected Lithium
1a	9×10^{-4}	22.7±12.9	48.8	57
1b		26.4±13.0		
2a	28×10^{-4}	86.7±25.6	151.7	60
2b		96.6±26.9		
3a	101×10^{-4}	557.3±33.0	547.4	100
3b		548.6±39.8		

Table 2.8. Comparison Between Experimental And Theoretical Lithium Concentrations In Lithium Benzoate.

example, sample X17, Table 2.5). Without further detailed work, one cannot conclusively say that lithium is lost to the immediate environment during proton–exchange. Mr. M.A. Foad of the University of Glasgow Chemistry Department is carrying out further work using higher concentrations of lithium benzoate to test for loss of lithium.

2.7. Discussion.

Hydrogen–bonded OH in proton–exchanged waveguides has been attributed to the presence of $HNbO_3$[10]. Fourquet *et al*[16] have studied the structure of cubic $HNbO_3$ and showed that there was an infrared absorption band at $\upsilon_{max}=3250cm^{-1}$, as observed in proton–exchanged waveguides. They presented evidence indicating the existence of two different OH–environments[16] in $HNbO_3$ and, using results of nuclear magnetic resonance experiments, suggested that protons could jump between the two available OH–environments.

The structural transformation from $LiNbO_3$ to cubic $HNbO_3$ was shown to occur via a topotactic exchange reaction[15], i.e. the NbO_6 octahedra became tilted due to hydrogen–bonding between OH groups and adjacent

oxygen anions and the tilting caused the unit cell length to double in value. The combination of a structural transformation and protonic jumps could be the cause of both the strain and the poor optical properties observed in proton–exchanged waveguides[2,5].

It has been shown that the percentage of Li–H exchange, as calculated by atomic absorption spectroscopy, is lower than the percentages calculated by Rice *et al*[13] and Canali *et al*[2]. Rice *et als* calculations[13] were based on thermo–gravimetric measurements on proton–exchanged lithium niobate powders heated to between 800°C and 1000°C. The weight–loss on heating was attributed to loss of OH from the powder. By measuring the maximum weight loss, the hydrogen (proton) concentration in the proton–exchanged powder was determined. However, at temperatures greater than 800°C, there could be loss of Li_2O[46]. The experimental description did not mention if Li_2O losses were taken into account. If they were not, the estimated percentage of Li–H exchange would be high.

The method of Canali *et al*[2] involved hydrogen–profiling via the nuclear reaction[47]:

$$^{15}N + {}^{1}H \longrightarrow {}^{12}C + \alpha + 4.43MeV\ \gamma\text{–ray} \quad \text{.....(24).}$$

During this reaction, a narrow resonance is formed at 6.385MeV. To use this technique for hydrogen–profiling the energy of the incident beam must be greater than the resonance energy. On travelling through the exchanged layer the beam is attenuated. After reaching the energy where the resonance forms, the resonance decays into the products in Equation (24). Increasing the energy enables the incident beam to travel deeper in the crystal, and the decrease to the resonance energy occurs at a greater depth.

The depth of penetration into the waveguide region is determined by referring to energy loss calibration tables[47]. By measuring the γ–ray yield as a function of the incident energy (penetration depth) the proton concentration in the guiding layer can be determined. The precision of the nuclear reaction technique is 0.1 at%, corresponding to a proton

concentration of $5x10^{19}cm^{-3}$[2]. The depth resolution is 0.01μm to 0.02μm[47]. The independent results of Rice *et al*[13] and Canali *et al*[2] agree that 65% to 75% of the original lithium ions present in the lithium niobate lattice exchange with protons.

To determine the amount of lithium left in the waveguiding region after proton–exchange, a second nuclear reaction technique was used[2,6]. The reaction, established by Chu *et al*[48], was first applied to lithium niobate waveguides fabricated by exchange in $TINO_3$ solutions[49]. The reaction is:

$$^{1}H + ^{7}Li \longrightarrow ^{4}He + \alpha \quad \text{.....(25).}$$

The latter reaction is not a resonant reaction and the achievable depth resolution is poor, about 0.1μm. The target is bombarded with a 1.5MeV proton beam and the α–particle yield is measured. Using the latter reaction, it has been shown[2] that ≃30% of the original lithium concentration is left in the guiding region after proton–exchange. The approximate 70% lithium depletion in the exchanged layer is in broad agreement with the proton concentration values determined by Rice *et al*[13] and Canali *et al*[2].

The percentage of exchange estimated in the present work differs from the percentages estimated independently by other workers by as much as a factor of two. The difference may be a consequence of lithium being lost to the immediate environment during proton–exchange. A method of testing for loss of lithium has been investigated in the present work, although further measurements are required. Another method of testing for loss of lithium is to carry out proton–exchange in a sealed system, and to compare the resulting lithium concentrations with those obtained by proton–exchange in an unsealed system. Continuing work on the calibration of atomic absorption measurements for the detection of lithium is being carried out by Mr. M.A. Foad of the Glasgow University Chemistry Department.

Although proton–exchange has been optically well–defined for planar waveguides, there are still serious problems inherent with the process. For example, there is a reduction in both the electro–optic effect[7,8] and the acousto–optic effect[50]. There are also problems associated with d.c. drift[8], stability of waveguide mode–indices[3,4], and high propagation losses[6]. Recently, there has been considerable interest in proton–exchange using dilute–melts (Chapter 4). Waveguides produced using dilute–melts have improved scattering[4] and improved stability[4], and electro–optic device performance has been shown to be comparable with titanium indiffused waveguides[51].

In the following chapters, an attempt has been made to relate the undesirable effects in proton–exchanged waveguides to the waveguide formation process. Dilute–melt proton–exchanged waveguides are investigated in detail. Annealed proton–exchanged waveguides are shown to have improved optical properties, similar to dilute–melt waveguides.

REFERENCES.

(1) J.L. Jackel, C.E. Rice, J.J. Veselka, *Proton–Exchange for High Index Waveguides in $LiNbO_3$*, Appl. Phys. Lett., 41(7), 607, (1982).

(2) C. Canali, A. Carnera, G. Della Mea, R.M. De La Rue, A.C.G. Nutt, J.R. Tobin, *Proton–Exchanged $LiNbO_3$ Waveguides: Materials Analysis and Optical Characteristics*, Proc. SPIE–460, L.A. Symposium, Calif., 22nd–26th January, 1984.

(3) A. Yi–Yan, *Index Instabilities in Proton–Exchanged $LiNbO_3$ Waveguides*, Appl. Phys. Lett., 42(8), 633, (1983).

(4) J.L. Jackel, C.E. Rice, *Short– and Long–Term Stability in Proton–Exchanged Lithium Niobate Waveguides*, SPIE–460, "Processing of Guided Wave Optoelectronic Materials", 43, (1984).

(5) A. Campari, C. Ferrari, G. Mazzi, C. Summonte, S.M. Al–Shukri, A. Dawar, R.M. De La Rue, A.C.G. Nutt, *Strain and Surface Damage Induced By Proton–Exchange in Y–Cut Lithium Niobate*, J. Appl. Phys., 58(12), 4521, (1985).

(6) A.C.G. Nutt, PhD Thesis, University of Glasgow, (1985).

(7) R.A. Becker, *Comparison of Guided–Wave Interferometric Intensity Modulators Fabricated Via Titanium Indiffusion and Proton–Exchange*, Appl. Phys. Lett., 43(2), 131, (1983).

(8) K.K. Wong, R.M. De La Rue, S. Wright, *Electro–Optic Frequency Translator in $LiNbO_3$ Fabricated by Proton–Exchange*, Opt. Lett., 7(11), 1546, (1982).

(9) M. De Micheli, M.J. Li, D.B. Ostrowsky, M. Papuchon, *The Double Proton–Exchange in $LiNbO_3$: Low Loss & Quasi–Embedded Waveguides*, Proc. 4th European Conference on Integrated Optics, 11th–13th May, 1987, Glasgow.

(10) J.L. Jackel, C.E. Rice, *Topotactic to Cubic Perovskite Structural Transformation in $LiNbO_3$ and $LiTaO_3$*, Ferroelectrics, 38, 801, (1981).

(11) J.L. Jackel, C.E. Rice, J.J. Veselka, *Compositional Control in Proton–Exchanged $LiNbO_3$*, Elect. Lett., 19(10), 387, (1983).

(12) C.E. Rice, *The Structural Properties of $Li_{1-x}H_xNbO_3$*, J. Solid State Chem., 64, 188, (1986).

(13) C.E. Rice, J.L. Jackel, *Structural Changes with Composition and Temperature in Rhombehedral $Li_{1-x}H_xNbO_3$*, Mat. Res. Bull., 19, 591, (1984).

(14) C.E. Rice, J.L. Jackel, *$HNbO_3$ and $HTaO_3$: New Cubic Perovskites From $LiNbO_3$ and $LiTaO_3$ Via Ion Exchange*, J. Solid State Chem., 41, 308, (1982).

(15) J.L. Fourquet, M.F. Renou, R. De Pape, *La Reaction D'Echange Topotactique $LiNbO_3$–$HNbO_3$ En Milieu Acide*, Rev. Chim. Miner., 21, 383, (1984).

(16) J.L. Fourquet, M.F. Renou, R. De Pape, H. Theveneau, P.P. Man, O. Lucas, J. Pannetier, *$HNbO_3$: Structure and NMR Study*, Solid State Ionics, 9/10, 1011, (1983).

(17) M.T. Weller, P.G. Dickens, *Proton Motion in $HNbO_3$ and $HTaO_3$*, J. Sol. St. Chem., 60, 139, (1985).

(18) D.F. Clark, A.C.G. Nutt, K.K. Wong, P.J.R. Laybourn, R.M. De La Rue, *Characterisation of Proton–Exchanged Slab Optical Waveguides on Z–Cut $LiNbO_3$*, J. Appl. Phys., 54(11), 6218, (1983).

(19) A.C.G. Nutt, K.K. Wong, D.F. Clark, P.J.R. Laybourn, R.M. De La Rue, *Proton–Exchanged $LiNbO_3$ Slab and Stripe Waveguides: Characterisation and Comparisons*, Proc. 2nd European Conference on Integrated Optics, Florence, 1983.

(20) K.K. Wong, D.F. Clark, A.C.G. Nutt, J. Winfield, P.J.R. Laybourn, R.M. De La Rue, *Characterisation of Proton–Exchanged Slab Optical Waveguides on X–Cut $LiNbO_3$*, IEEE Proc. J–133, 113, (1986).

(21) M. De Micheli, J. Botineau, P. Sibillot, D.B. Ostrowsky, M. Papuchon, *Fabrication and Characterisation of Titanium Indiffused Proton–Exchanged (TIPE) Waveguides in $LiNbO_3$*, Opt. Commun., 42, 101, (1982).

(22) P.K. Tien, R. Ulrich, *Theory of Prism–Film Coupler and Thin–Film Light Guides*, J. Opt. Soc. Amer., 60, 1325, (1970).

(23) J. Finak, H. Jerominek, Z. Opilski, K. Wotjala, *Planar Diffusion Glass Waveguides Obtained by Immersing in Molten KNO_3*, Opt. Act., XII(1), 11, (1982).

(24) J.M. White, P.F. Heidrich, *Optical Waveguide Refractive Index Profiles Determined From Measurements of Mode Indices: A Simple Analysis*, Appl. Opt., 15(1), 151, (1976).

(25) H. Kogelnik, V. Ramaswamy, *Scaling Rules for Thin–Film Optical Waveguides*, Appl. Opt., 13(8), 1857, (1974).

(26) J.F. Crank, *Mathematics of Diffusion*, (O.U.P., 1956), Chapter 1.

(27) C.H. Bamford, C.F.H. Tipper, *Comprehensive Chemical Kinetics 2: The Theory of Kinetics*, (Elsevier, 1969).

(28) N. Colthup, S. Wiberley, L. Daly, *Introduction to Infrared and Raman Spectroscopy*, (A.P., 1964).

(29) J.R. Carruthers, G.E. Peterson, M. Grasso, P.M. Bridenbaugh, *Nonstoichiometry and Crystal Growth of $LiNbO_3$*, J. Appl. Phys., 42(5), 1846, (1971).

(30) S.C. Abrahams, P. Marsh, *Defect Structure Dependence on Composition in Lithium Niobate*, Acta Cryst., B42, 61, (1986).

(31) J.R. Herrington, B. Dischler, A. Rauber, J. Schneider, *An Optical Study of the Stretching Absorption Near 3μm From OH^- Defects in Lithium Niobate*, Sol. St. Commun., 12, 351, (1973).

(32) L. Kovacs, V. Szalay, R. Capelletti, *Stoichiometry Dependence of the OH^- Absorption Band in Lithium Niobate Crystals*, Sol. St. Commun., 52(12), 1029, (1984).

(33) Personal communication from technical–staff members, Pilkington Electro–Optic Materials, Barr and Stroud, Ltd.

(34) *Hydrogen Bonding* –papers presented at the Symposium on Hydrogen–Bonding, Ljubljana, 29th July–3rd August, 1957, Ed. D. Hadzi. See presentation by N. Sheppard, p.85.

(35) E.R. Lippincott, R. Schroeder, *One–Dimensional Model of the Hydrogen–Bond*, J. Chem. Phys., 23, 1099, (1955).

(36) R.J. Dudley, S.F. Mason, R.D. Peacock, *Electronic and Vibrational Linear and Circular Dichroism of Nematic and Cholestoric Systems*, J. Chem. Soc. Faraday II, 71, 997, (1975).

(37) G.F. Kirkbright, M. Sargent, *Atomic Absorption and Fluorescence Spectroscopy*, (A.P., 1974).

(38) W.J. Price, *Analytical Atomic Absorption Spectrometry*, (Heydon & Son, 1972).

(39) A. Loni, R.M. De La Rue, J.M. Winfield, *Proton–Exchanged $LiNbO_3$ Planar Optical Waveguides: Chemical and Optical Properties and Room–Temperature Hydrogen Isotopic–Exchange Reactions*, J. Appl. Phys., 61(1), 64, (1987).

(40) Perkin–Elmer 306 manual.

(41) Reference (37), p.620.

(42) *Handbook of Chemistry and Physics*, Ed. R. Weast (CRC Press, 55th Edition, 1974–1975).

(43) D.A. Skoog, D.M. West, *Fundamentals of Analytical Chemistry*, (Holt, Rinehart & Winston, 1976), p.60–66.

(44) *Current Topics in Materials Science Vol. 1*, Ed. E. Kaldis, (North Holland, 1978): see A. Rauber, *Chemistry and Physics of Lithium Niobate*, Chapter 3.

(45) R.S. Weiss, T.K. Gaylord, *$LiNbO_3$: Summary of Physical Properties and Crystal Structure*, Appl. Phys. A., 37, 191, (1985).

(46) I.P. Kaminow, J.R. Carruthers, *Optical Waveguiding Layers in $LiNbO_3$ and $LiTaO_3$*, Appl. Phys. Lett., 22(7), 326, (1973).

(47) W.A. Lanford, *^{15}N Hydrogen–Profiling: Scientific Applications*, Nucl. Instr. & Methods, 149, Part 1: Light–Element Profiling, 1, (1978).

(48) W.K. Chu, J.W. Mayer, M.A. Nicolet, *Principles and Applications of Ion Beam Technology for the Analysis of Solids and Thin–Films*, Thin Sol. Films, 77, 181, (1981).

(49) Y.X. Chen, W.S.C. Cheng, S.S. Lau, *Characterisation of $LiNbO_3$ Waveguides Exchanged in $TlNO_3$ Solution*, Appl. Phys. Lett., 40(1), 10, (1982).

(50) R.L. Davis, *Acousto–Optic Bragg Diffraction in Proton–Exchanged Waveguides*, Proc. SPIE–517, paper 10, (1984).

(51) K.K. Wong, N.J. Parsons, A.R. Olderoyd, A.C. O'Donnel, *High Quality Optical Waveguides in Lithium Niobate by Dilute Melt Proton–Exchange*, Proc. IOOC/ECOC '85,"Integrated Optical Waveguide Fabrication", Venice, 1985.

CHAPTER 3

Room–Temperature Hydrogen Isotopic–Exchange Reactions In Proton–Exchanged And Deuterium–Exchanged Lithium Niobate Waveguides Prepared From Neat Benzoic Acid Melts.

3.1. INTRODUCTION.

This work was in part motivated by the possibility that hydrogen isotopic–exchange in proton–exchanged waveguides might help in determining whether or not instabilities in effective mode indices[1] and increased scattering in the waveguide with time[2] are related to reaction between the guiding layer and the atmosphere.

The method of hydrogen isotopic–exchange used in the present study involves exchange between protons (^1H) in the proton–exchanged waveguide layer and deuterium (D) from D_2O vapour. The extent of proton–deuterium replacement has been observed using infrared spectroscopy in the OH and OD hydroxyl stretching regions ($\upsilon = 3600cm^{-1}$ to $\upsilon = 3000cm^{-1}$ and $\upsilon = 2700cm^{-1}$ to $\upsilon = 2200cm^{-1}$, respectively).

The following sections are concerned with hydrogen isotopic–exchange in x– and z–cut neat melt proton–exchanged waveguides carried out at room–temperature. The recently reported process of fabricating waveguides in lithium niobate by deuterium–exchange[3] has been investigated, using optical waveguide measurements and hydrogen isotopic–exchange. The comparison between proton–exchanged and deuterium–exchanged lithium niobate is discussed.

3.2. SAMPLE PREPARATION AND PROCESSING.

Experiments were carried out on x– and z–cut congruent lithium niobate wafers which had been polished on both faces for the infrared absorption studies. The samples and their treatment are summarised in Table 3.1. The waveguide fabrication procedure has been described in Chapter 2, Section 2.3, with the exception of the x–cut samples XC (deuterium–exchanged, 218°C, 8hr 11min) and XD (proton–exchanged, 218°C, 8hr 11min). The latter two samples were produced in sealed double limb Pyrex glass vessels under a dry argon atmosphere (water vapour $\leqslant$5ppm). One limb of each vessel contained the acid, and the other limb contained the wafer. When the acid was molten it was poured into the limb which contained the wafer.

The proton–exchanged samples XB and ZB (155°C, 2hr) were mounted in specially designed evacuable Pyrex glass cells fitted with calcium fluoride (CaF_2) windows for the purpose of recording infrared spectra as a function of the time of exposure of the samples in D_2O vapour or to ambient atmosphere. The D_2O was contained in a single limb Pyrex glass vessel.

Once the samples (XB and ZB) had been mounted and the cells evacuated, they were exposed to D_2O vapour for aggregate periods of time. Infrared spectra were recorded at the end of each period, immediately after the D_2O vapour had been removed from the cells. After deuteration by the above process the samples were exposed to ambient atmosphere for aggregate periods of time and their infrared spectrum was recorded at the end of each period, after the cells had been evacuated.

Sample	Fabrication Temperature (°C)	Fabrication Time	Treatment & Comments
XB	155	2hr	(a),(b)
ZB	155	2hr	(a),(b)
ZZ5	168	4hr 25min	(a),(b),
XC	218	8hr 11min.	(a),(c)
XD	218	8hr 11min.	(a),(b),(d)
XE	218	8hr 11min	(a),(b)

Table 3.1. Samples Used In The Isotopic–Exchange Experiments, Together With Their Prior Treatment.

(a) *virgin subtraction used in infrared spectra*
(b) *fabricated using neat benzoic acid*
(c) *fabricated by deuterium–exchange, argon atmosphere*
(d) *fabricated by proton–exchange, argon atmosphere*

The deuterated benzoic acid ($C_6H_5CO_2D$) used to fabricate the deuterium–exchanged waveguide (XC) was prepared by refluxing AnalaR benzoic acid with D_2O (99.8%) at 120°C over a period of seven days. The solid product was separated from the liquid by filtration through a sintered glass funnel. The acid was then placed in a vacuum line and dried by pumping overnight under vacuum (the vacuum line system consisted of a rotary vacuum pump connected in series with a mercury vapour diffusion pump and the vacuum achieved was $\simeq 10^{-6}$ Torr). The acid was then transferred to an argon filled glove box (water vapour $\leqslant$5ppm).

In order to determine the extent of deuteration an infrared mull was prepared enabling the infrared spectrum of the acid to be recorded. The mull was prepared by mixing a small portion of the acid with liquid paraffin to form a paste. The paste was sandwiched between two infrared transmitting potassium bromide (KBr) plates and the infrared spectrum was recorded. If the acid were completely deuterated, the OH hydroxyl groups would be replaced by OD hydroxyl groups and the spectrum would contain OD absorption bands. The infrared spectrum of the acid, recorded immediately after the infrared mull was prepared, indicated that deuteration was extensive but not complete.

The proton–exchanged waveguide XD (218°C, 8hr 11min) was produced under an essentially dry argon atmosphere to give a comparison with proton–exchange in ambient atmosphere and, therefore, to help to determine effects of water vapour during proton–exchange.

After fabrication, the deuterium–exchanged sample XC (218°C, 8hr 11min, argon atmosphere) and the proton–exchanged sample XD (218°C, 8hr 11min, argon atmosphere) were transferred to infrared cells in the argon filled glove box so that infrared spectra could be recorded before the waveguides were exposed to the atmosphere.

3.3. ROOM–TEMPERATURE HYDROGEN ISOTOPIC–EXCHANGE IN NEAT–MELT PROTON–EXCHANGED WAVEGUIDES.

Infrared spectra, superimposed as a function of the time of exposure of the samples in D_2O vapour, are shown in Figures 3.1 and 3.2 for the proton–exchanged samples XB and ZB (both fabricated at 155°C for 2hr), respectively. The overall exposure time was 1232min.

At t=0 (after fabrication, before D_2O exposure), the infrared spectra contained absorbance bands of the free (XB, ZB) and hydrogen–bonded (XB) hydroxyl groups which were discussed in Chapter 2, Section 2.5. Exposure of the proton–exchanged samples to D_2O vapour resulted in a steady decrease in the absorption of the OH–bands at υ_{max}=3505cm^{-1} (XB and ZB) and υ_{max}=3250cm^{-1} (XB). The reduction in the OH–bands was accompanied by a steady growth of OD counterparts at υ_{max}=2590cm^{-1} (XB and ZB) and υ_{max}=2410cm^{-1} (XB), indicating exchange between protons in the waveguides and deuterium from the D_2O vapour.

The positions of maximum absorbance for the OH and OD hydroxyl groups are summarised in Table 3.2. Due to the overlap of bands and different band envelopes, the positions of absorbance maxima are somewhat variable (±2cm^{-1}) for different samples.

Exposure of the proton–exchanged samples to D_2O vapour also resulted in the formation of a set of weak bands at $\upsilon\simeq$2800cm^{-1} (Figures 3.1 and 3.2) which were unidentifiable at the time of publication of reference (6). It is possible that these bands were due to the presence of D_2O vapour in the infrared cells. This possibility was tested* by filling the infrared cell with D_2O vapour and recording the infrared spectrum. The spectrum of D_2O vapour (Figure 3.3) consists of a set of absorption bands at $\upsilon\simeq$2800cm^{-1}. These bands are similar in appearance to the bands observed in the spectra of the deuterated samples XB and ZB, indicating that the latter bands were due to gaseous D_2O.

* *This work was carried out by G. Hay as part of his final year project, Department of Electronic & Electrical Engineering, 1987, under the supervision of the author.*

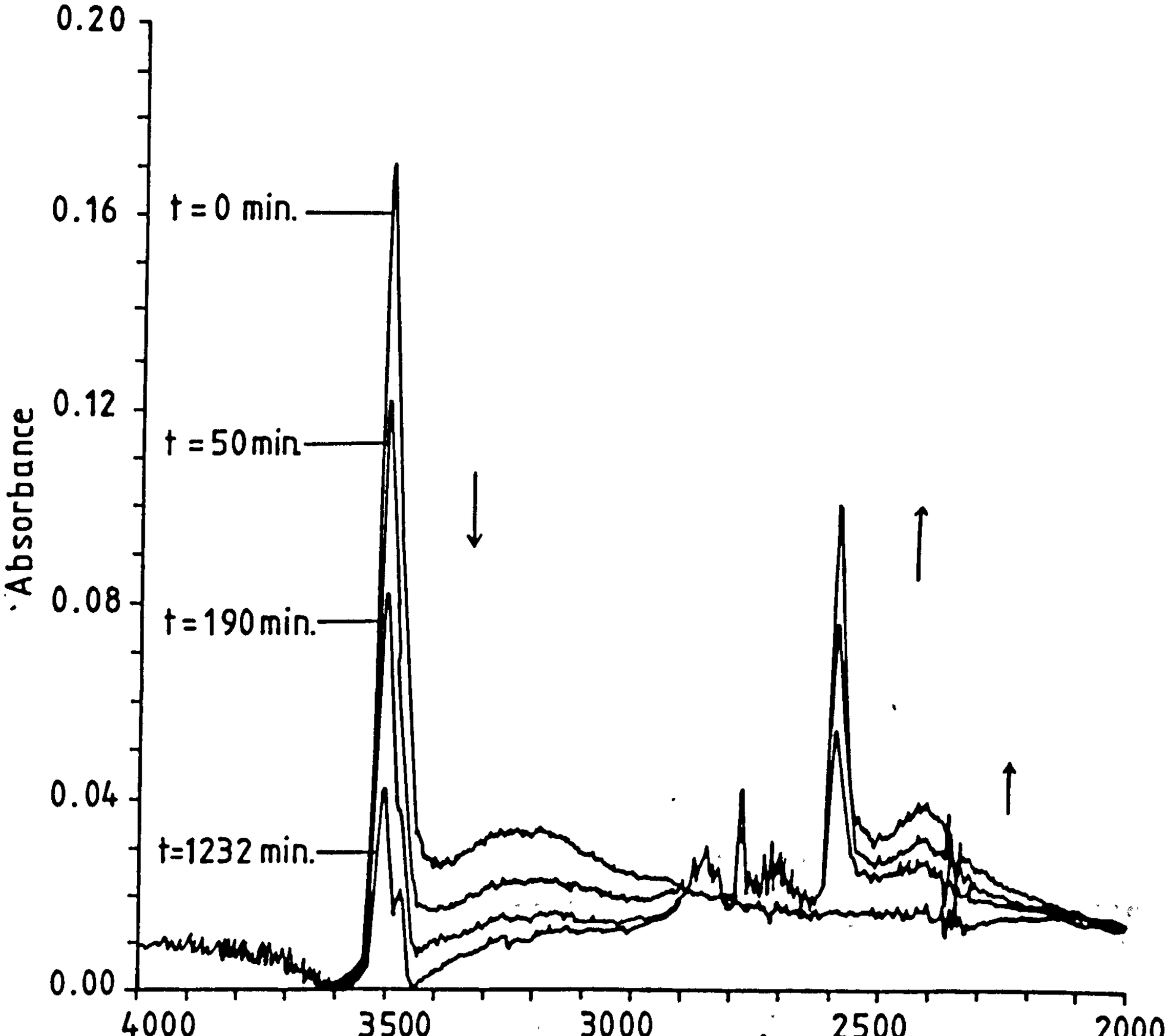

Figure 3.1. Infrared Spectra Of The X–Cut Proton–Exchanged Waveguide XB, Superimposed As A Function Of The Time Of Exposure Of The Sample In D_2O Vapour At Room–Temperature *(The Waveguide Was Fabricated At 155°C For 2hr).*

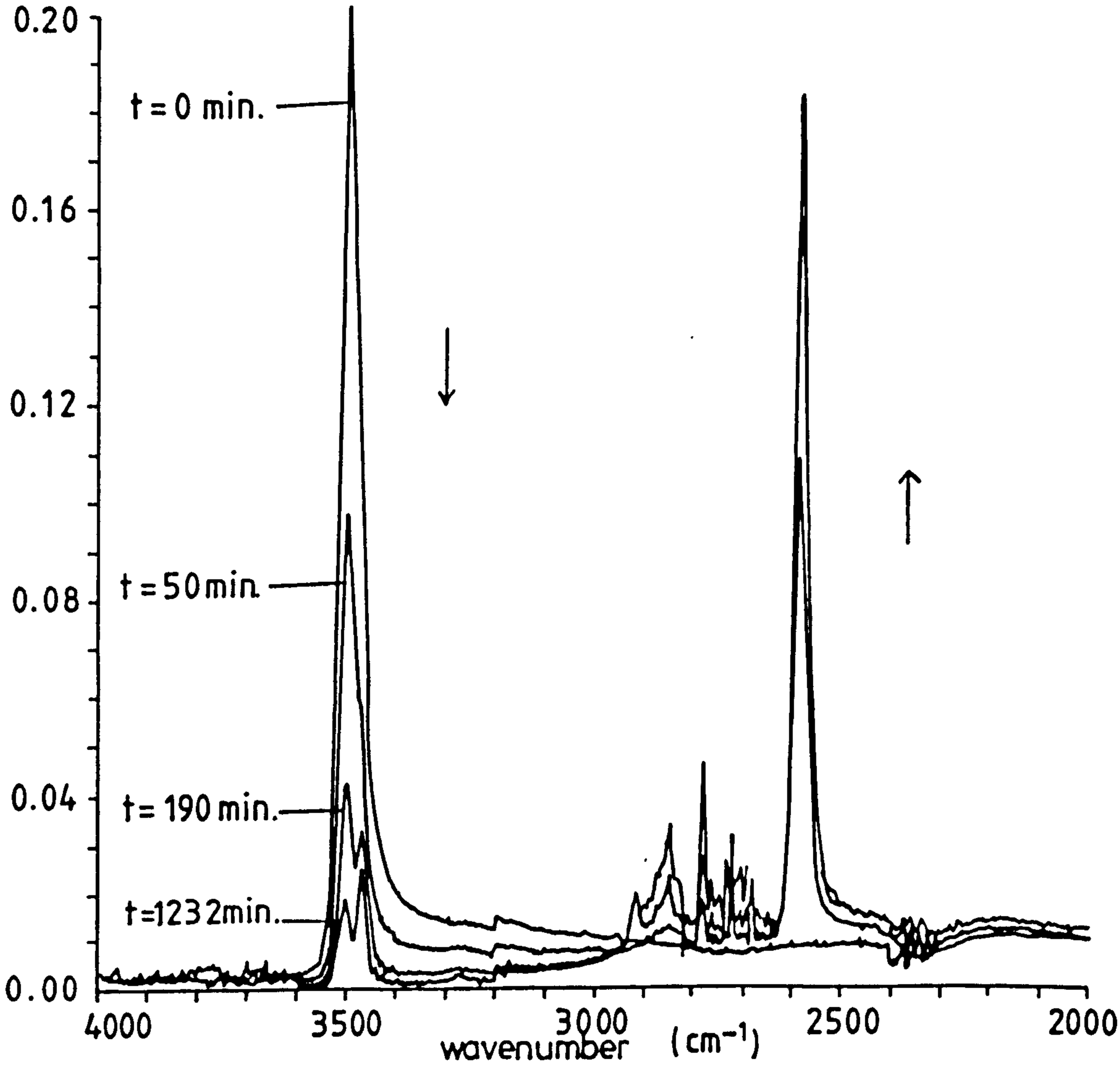

Figure 3.2. Infrared Spectra Of The Z–Cut Proton–Exchanged Waveguide ZB, Superimposed As A Function Of The Time Of Exposure Of The Sample In D_2O Vapour At Room–Temperature *(The Waveguide Was Fabricated At 155°C For 2hr).*

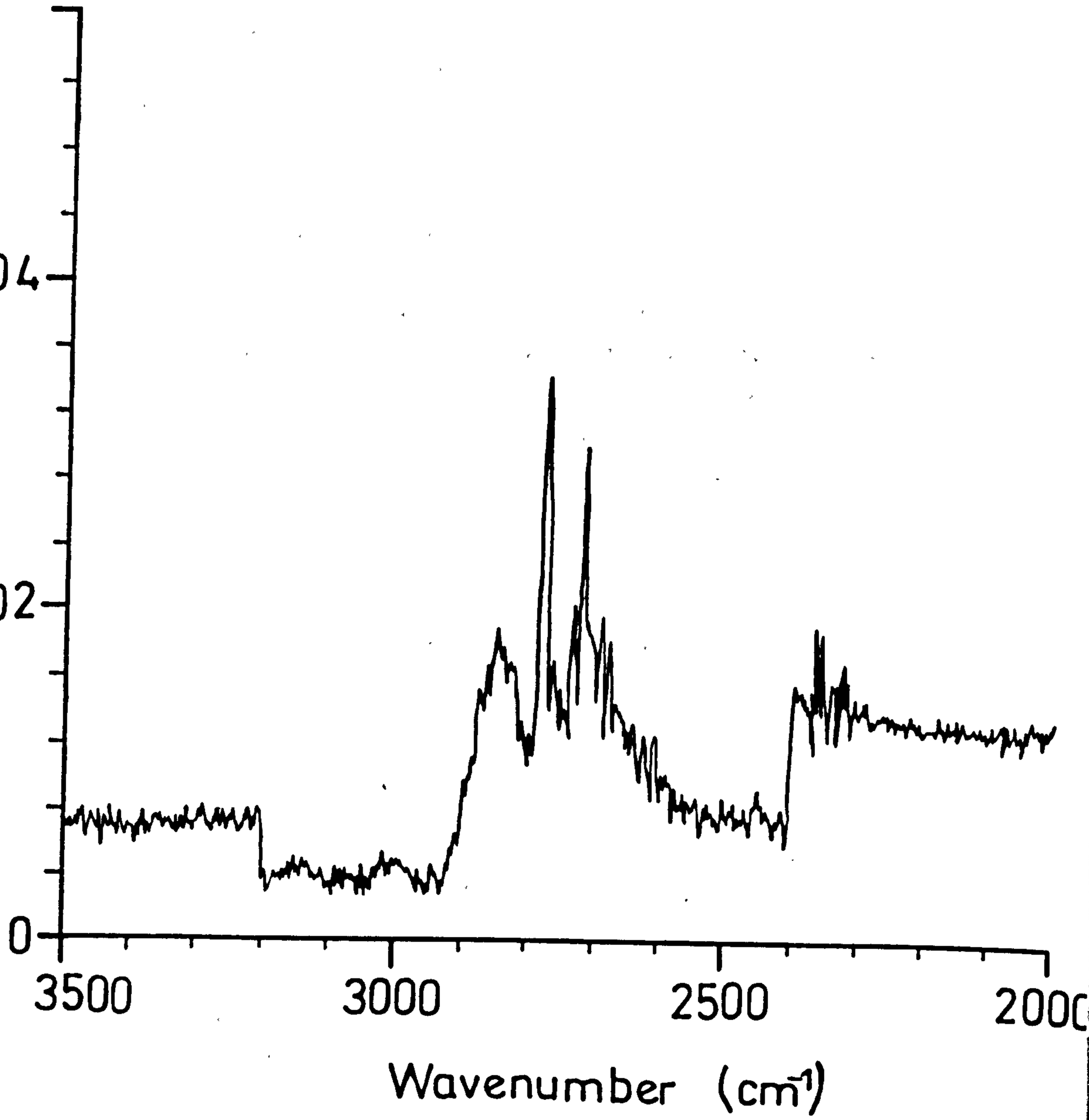

Figure 3.3. Infrared Absorption Spectrum Of D_2O Vapour.

An interesting feature of the spectra in Figures 3.1 and 3.2 is that the sharp OH− band at υ_{max}= 3505cm^{-1} is resolved into two closely−spaced bands at low hydroxyl concentrations, indicating the existence of two slightly different OH environments.

The existence of more than one OH environment is in accordance with observations on virgin lithium niobate[4,5], although the latter work[5] indicates that as many as three sharp bands may be observed depending on the crystal stoichiometry (see also Chapter 2, Section 2.5.2).Measurements using polarised infrared radiation on both x− and z−cut waveguides suggest[6] that the OD hydroxyl groups responsible for the sharp absorption band at υ_{max}= 2590cm^{-1} are localised in the (x,y)−plane, perpendicular to the crystallographic c−axis, while the OD

Sample[a]	IR spectra, hydroxyl group stretching frequencies υ_{max}(cm^{-1})[b]	
XD	3504(s)	3269(br)
XE	3506(s)	3276(br)
XC	3507(vw), 3473(vw),	3276(vw,br), 2591(m), 2416(br)
XC[c]	3504(m)	3276(br), 2591(m), 2406(br)
XB	3505(m)	≈3250(br)
XB[d]	3508(vw), 3474(vw),	≈3250(br), 2589(m), 2424(br)
ZB	3501(m)	
ZB[d]	3506(vw), 3470(vw)	2587(m)

Table 3.2. Hydroxyl Group Stretching Frequencies Of Proton−Exchanged (XB, ZB,XD, XE) And Deuterium−Exchanged (XC) Waveguides.

[a] *Samples prepared as described in text and Table I*
[b] *s: strong; m: medium; vw: very weak; br: broad*
[c] *After air exposure for 624hr.*
[d] *After D_2O vapour exposure for 20.5hr.*

hydroxyl groups responsible for the broad absorption band at $\upsilon_{max}=2410cm^{-1}$ have components along the x- y- and z-axis (these bands are analogous to the OH counterparts discussed in Chapter 2, Section 2.5.).

The extent of isotopic-exchange was determined as a function of time by calculating the areas of the OH- and OD-bands (shown in Chapter 2 to represent the concentration of the absorbing species). The areas of the absorption bands were calculated by integration over the band envelopes between the regions $\upsilon=3560cm^{-1}$ to $\upsilon=3100cm^{-1}$ (x- and z-cut), and $\upsilon=2400cm^{-1}$ to $\upsilon=2630cm^{-1}$ (x- and z-cut). The integration region for the OH-bands was limited due to the presence of the D_2O vapour absorption bands. The integration region for the OD-bands was limited because of the presence of a CO_2 stretching feature between $\upsilon=2300cm^{-1}$ and $\upsilon=2400cm^{-1}$. The latter effect was due to atmospheric CO_2 being present in the spectrometer reference beam but not in the evacuated infrared cells.

The variation in OH- and OD-band areas with exposure time in D_2O vapour is shown in Figures 3.4 and 3.5, respectively, for the proton-exchanged samples XB and ZB. Most of the proton-deuterium exchange took place during the first six hours. For example, the OH area reduced from 100% to 38% (XB) and from 100% to 12% (ZB) after six hours in D_2O vapour. After six hours the extent of isotopic-exchange with time decreased. No further isotopic-exchange was observed after a 20hr long exposure.

Prism-coupling measurements (after fabrication) indicated that the depth of the proton-exchanged region was greater in the x-cut sample. The depth of the proton-exchanged region was 0.49μm in sample XB and 0.35μm in sample ZB. Therefore, the concentration of OH hydroxyls in sample XB was greater than in sample ZB (Chapter 2, Section 2.5.3). At the point where no further isotopic-exchange was observed (after $\simeq$20hr) the OH area had reduced to 30% for XB and 10% for ZB, indicating that isotopic-exchange occurred to a lesser extent in the waveguide with the greater hydroxyl concentration (i.e. greater depth).

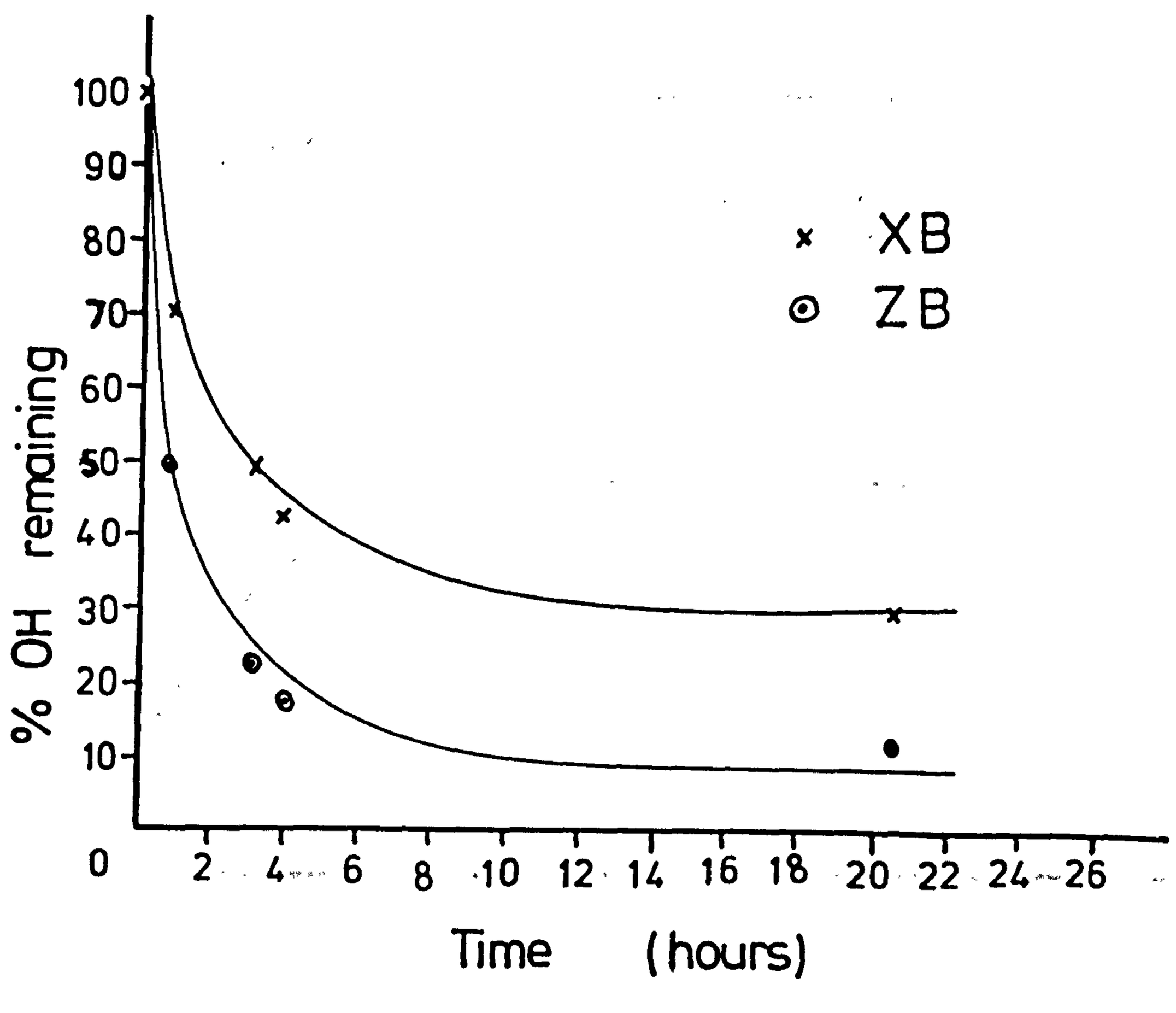

Figure 3.4. Variation In OH–Area With Exposure Time In D_2O Vapour, For The Proton–Exchanged Waveguides XB And ZB *(Both Waveguides Were Fabricated At 155°C For 2hr).*

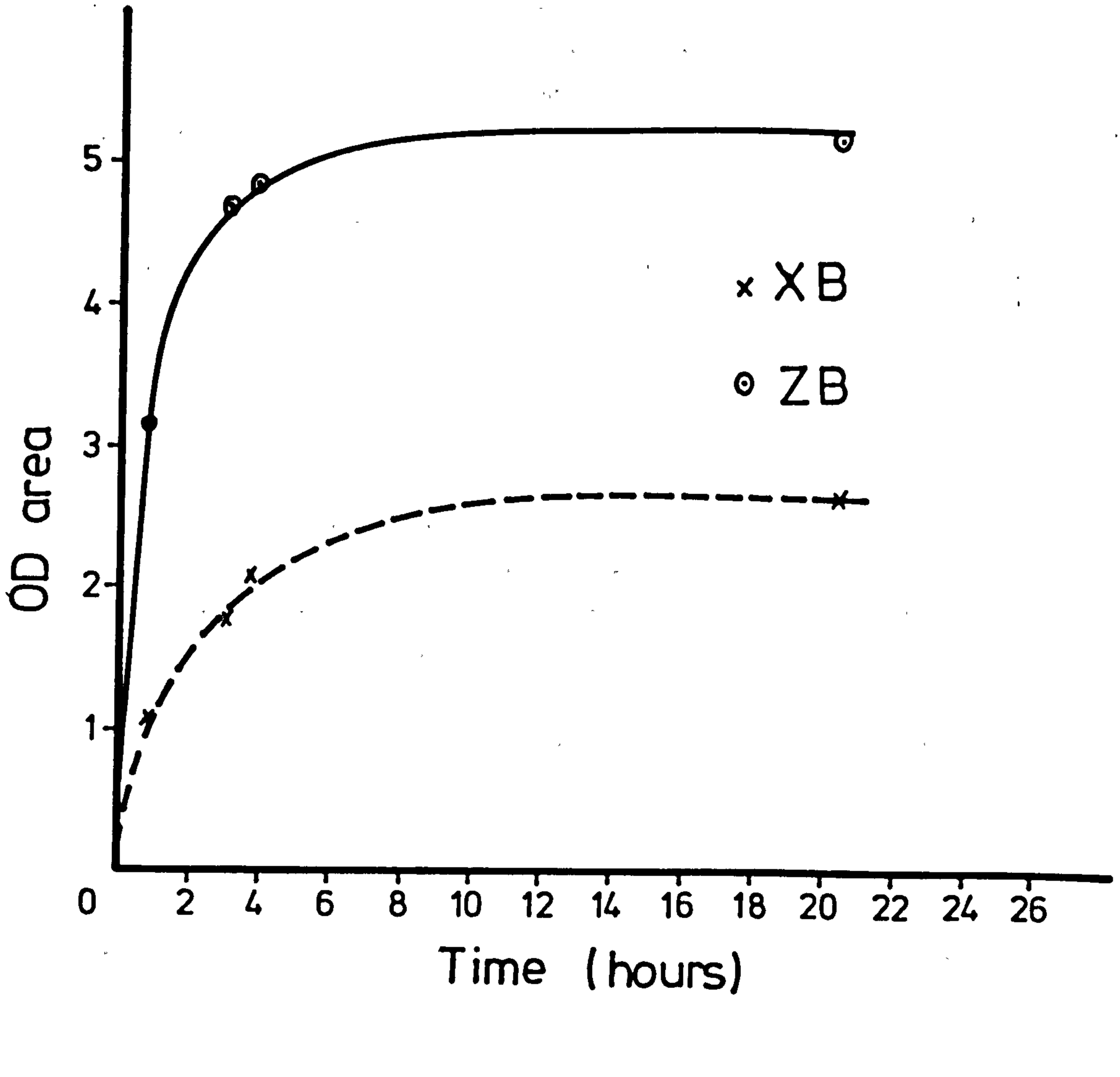

Figure 3.5. Variation In OD– Area With Exposure Time In D_2O Vapour, For The Proton–Exchanged Waveguides XB And ZB *(Both Waveguides Were Fabricated At 155°C For 2hr).*

Infrared spectra of the proton–exchanged waveguide ZZ5 (168°C, 4hr 25min), recorded as a function of the time of exposure of the sample in D_2O vapour, are shown in Figure 3.6. The decrease in the OH–band at $\upsilon_{max}=3505cm^{-1}$ and the growth of an OD counterpart at $\upsilon_{max}=2590cm^{-1}$ indicated isotopic exchange. However, the depth of the waveguide (0.74μm) was such that the proton–deuterium exchange was incomplete. The sharp OH–band at $\upsilon_{max}=3505cm^{-1}$ was unresolved because of the high absorbance (0.2). No isotopic–exchange was observed after a 20hr long exposure. A further 26.5hr long exposure (46.5hr in total) produced no changes in the OH– or OD–bands*.

Exposing the deuterated waveguides to atmospheric water vapour resulted in a decrease in absorbance of the the OD–bands and an increase in the absorbance of the OH–bands, indicating reverse isotopic–exchange between deuterium in the waveguide and hydrogen from atmospheric water vapour. Complete reversal was reached after approximately 20hr in the atmosphere.

It has been shown that isotopic–exchange in x– and z–cut proton–exchanged waveguides occurs over a 20hr long exposure in D_2O vapour. Waveguides with different initial OH hydroxyl concentrations therefore experience limited isotopic–exchange. Virgin x– and z–cut lithium niobate wafers were not measurably affected by exposure to D_2O vapour at room–temperature, although exchange has been observed at 600°C(7). High–temperature isotopic–exchange in x–cut proton–exchanged lithium niobate has been investigated and the results are presented in Chapter 4.

3.4. DEUTERIUM–EXCHANGED LITHIUM NIOBATE WAVEGUIDES.

A study of deuterium–exchanged waveguides in z–cut lithium niobate has been published by Jackel *et al*(3).

* *This work was carried out by G. Hay as part of his final year project, Department Electronic* & Electrical *Engineering, 1987, under the supervision of the author.*

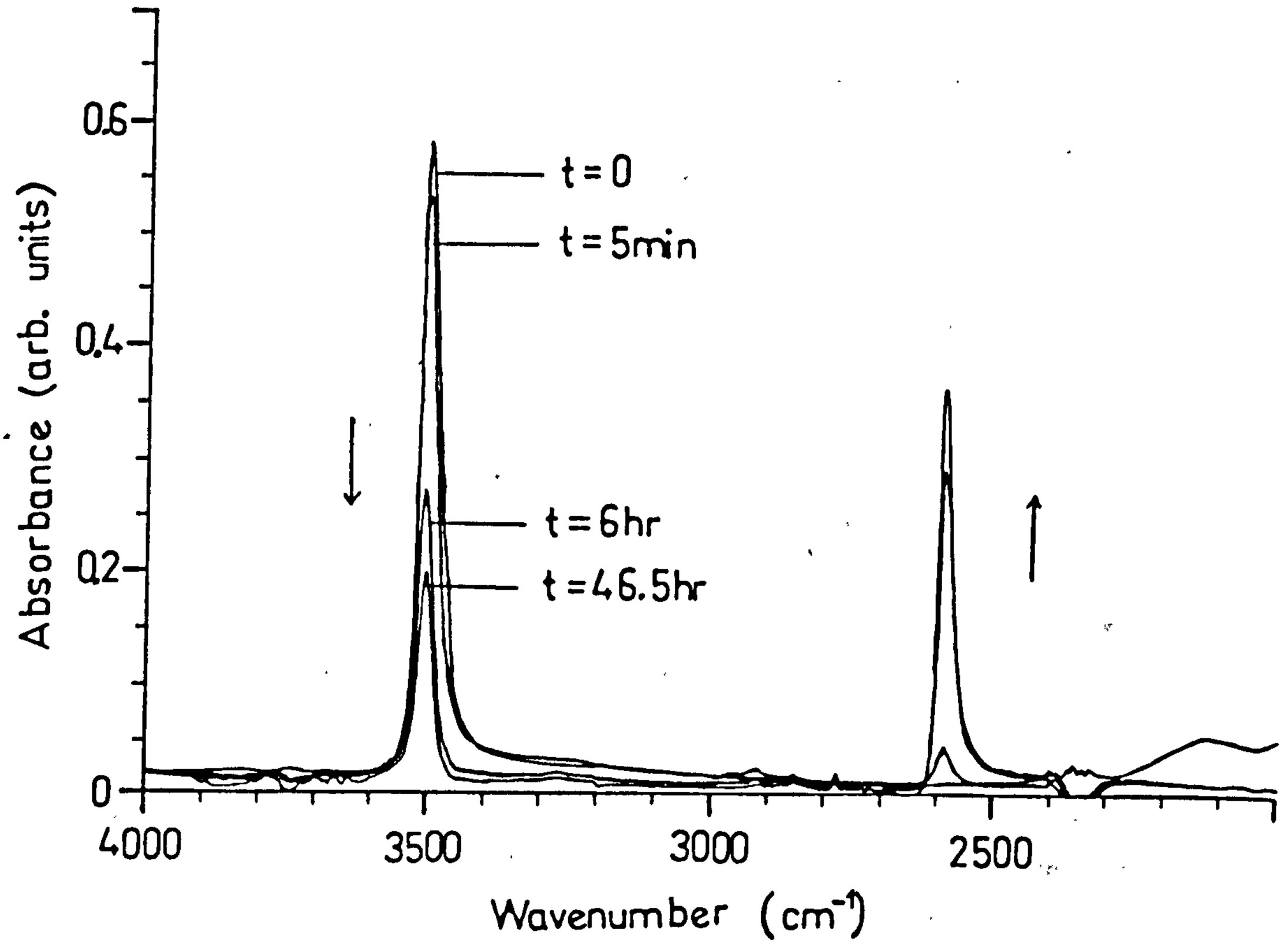

Figure 3.6. Infrared Spectra Of The Z–Cut Proton–Exchanged Waveguide ZZ5, Superimposed As A Function Of The Time Of Exposure Of The Sample In D_2O Vapour ***(The Waveguide Was Fabricated At 168°C For 4hr 25min).***

The latter work[3] used the deuterium concentration/depth profile in the waveguide (measured using a nuclear reaction, see Section 3.5) to give a possible indication of hydrogen profiles in proton–exchanged waveguides. Jackel *et al* claimed that no analytical technique enabling hydrogen profiles to be determined was available to them, although other workers[8,9] had already measured hydrogen profiles in proton–exchanged waveguides using a resonant nuclear reaction (see Section 3.5).

The present work brings into question the similarity between deuetrium exchanged and proton–exchanged waveguides assumed by Jackel *et al*[3]. The results of isotopic–exchange on x–cut deuterium–exchanged lithium niobate suggest that there are differences between the detailed structure of proton–exchanged and deuterium–exchanged waveguides, although the refractive index profiles are similar.

3.4.1. Hydrogen Isotopic–Exchange In Deuterium–Exchanged Waveguides.

The x–cut deuterium–exchanged waveguide sample, XC, was produced under an argon atmosphere using a deuterated benzoic acid melt (218°C, 8hr 11min, Table 3.1) which had previously been prepared by the method given in Section 3.4.2. After fabrication, the waveguide was exposed to ambient atmosphere and the infrared spectrum of the material was recorded as a function of time (Figure 3.7).

The infrared spectrum recorded immediately after fabrication (Figure 3.7) consisted of a sharp OD–band at $\upsilon_{max}=2591cm^{-1}$ and a broad OD–band at $\upsilon_{max}=2416cm^{-1}$ corresponding (respectively) to the free and hydrogen–bonded OH counterparts observed in proton–exchanged lithium niobate (Chapter 2, Section 2.5). At low hydroxyl concentrations there were two closely–spaced OH–bands, separated by $\approx 30cm^{-1}$, and a third OH–band at $\upsilon_{max}=3276cm^{-1}$. The presence of OH–bands in the spectra was due to the fact that the acid used for fabrication was not totally deuterated. The positions of the absorbance bands are summarised in Table 3.2.

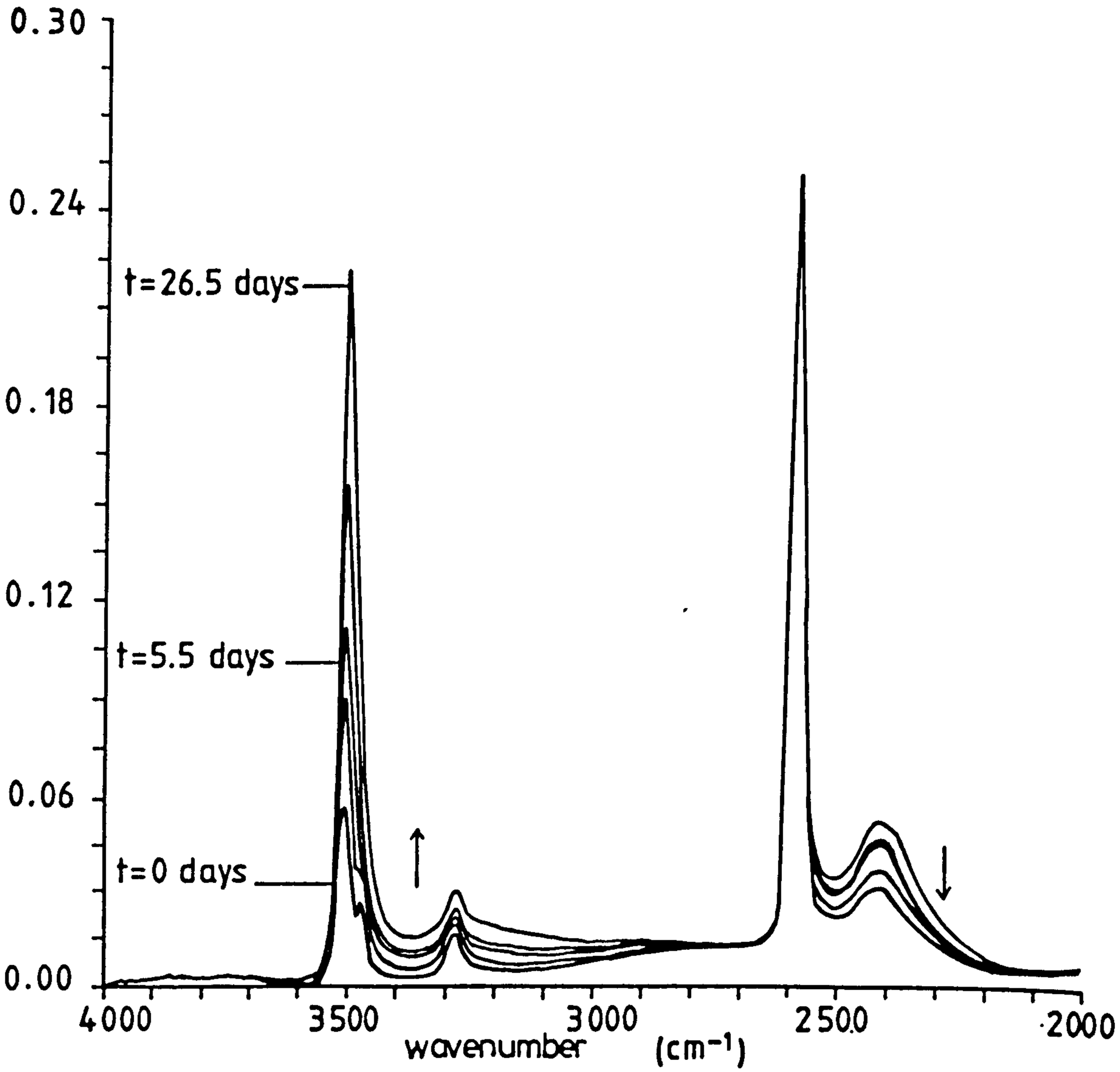

Figure 3.7. Infrared Spectra Of The X–Cut Deuterium–Exchanged Waveguide XC, Superimposed As A Function Of Exposure Time In Ambient Atmosphere *(The Waveguide Was Fabricated At 218°C For 8hr 10min).*

Exposure of the deuterium–exchanged waveguide to atmospheric water vapour resulted in a steady increase in the OH–bands accompanied by a decrease in the broad OD–band at υ_{max}=2416cm^{-1}, with a very much smaller decrease in the sharp OD–band at υ_{max}=2591cm^{-1}. The absorbances of the sharp bands were approximately equal after 624hr. In the spectrum recorded 2yr 5mth after the initial spectrum, the broad OD–band was no longer observable and the sharp OD–band had been significantly reduced.

The results indicate that isotopic–exchange in deuterium–exchanged waveguides is different from isotopic–exchange in proton–exchanged waveguides. When proton–exchanged waveguides were exposed to D_2O vapour, proton–deuterium exchange took place over a 20hr period. However, on exposing a deuterium–exchanged waveguide to atmospheric water vapour, deuterium–proton exchange occurred over a much longer period and to a much lesser extent than was observed in proton–exchanged waveguides exposed to D_2O vapour. It is possible, therefore, that there are differences between the detailed structures of proton–exchanged and deuterium–exchanged waveguides. Structural differences might be due to different OH and OD environments.

Sample	Number of Modes (TE)	Surface Index	Depth (μm)
XD	7	2.325	2.92
XE	6	2.328	2.60
XC	5	2.323	2.05

Table 3.3. Waveguide (Surface) Indices And Depths Of The X–Cut Proton–Exchanged (XD, XE) And Deuterium–Exchanged (XC) Waveguides Measured At λ=0.6328μm.

3.4.2. Optical Waveguide Measurements Of A Deuterium–Exchanged Waveguide.

The optical properties of the deuterium–exchanged waveguide (XC) were assessed at $\lambda = 0.6328\,\mu m$ by the prism–coupling technique. The optical properties of the x–cut proton–exchanged waveguides XD and XE were also measured to give a comparison between deuterium–exchanged and proton–exchanged waveguides, produced under argon (XC, XD) and ambient (XE) atmospheres (Table 3.3).

All the waveguides showed the decline in refractive index expected for guides produced from neat benzoic acid melts[2,9]. For otherwise identical conditions, fabrication in an argon atmosphere produced a shallower waveguide region than in air (Table 3.3). The reason why is unclear. One possibilty is that lithium loss by evaporation from the melt, during fabrication, is facilitated in an open system but is more held in a sealed system. Therefore, the extent of reaction in the sealed system slows down due to a lithium benzoate dilution effect (see Chapter 4). This would, in consequence, give a shallower waveguide.

The proton–exchanged waveguide produced under argon had a greater depth than the deuterium–exchanged waveguide produced under identical conditions (Table 3.3). The different depths of the proton–exchanged and deuterium–exchanged waveguides are presumably a result of a smaller effective diffusion coefficient for the more massive deuterium.

The refractive index profile of the deuterium–exchanged waveguide (Figure 3.8) indicated, in accordance with Jackel *et al*[3], that the extraordinary refractive index change Δn_e, was essentially identical for proton–exchanged and deuterium–exchanged waveguides, i.e. step–like, with $\Delta n_e \simeq 0.125$. The fact that the optical waveguiding properties of proton–exchanged and deuterium–exchanged waveguides are similar is consistent with the suggestion[9,10,11,12] that the factor which primarily determines the change in the refractive index is the extent of the lithium depletion, with uptake of protons (deuterium) in the form of OH (OD) providing a means of charge compensation.

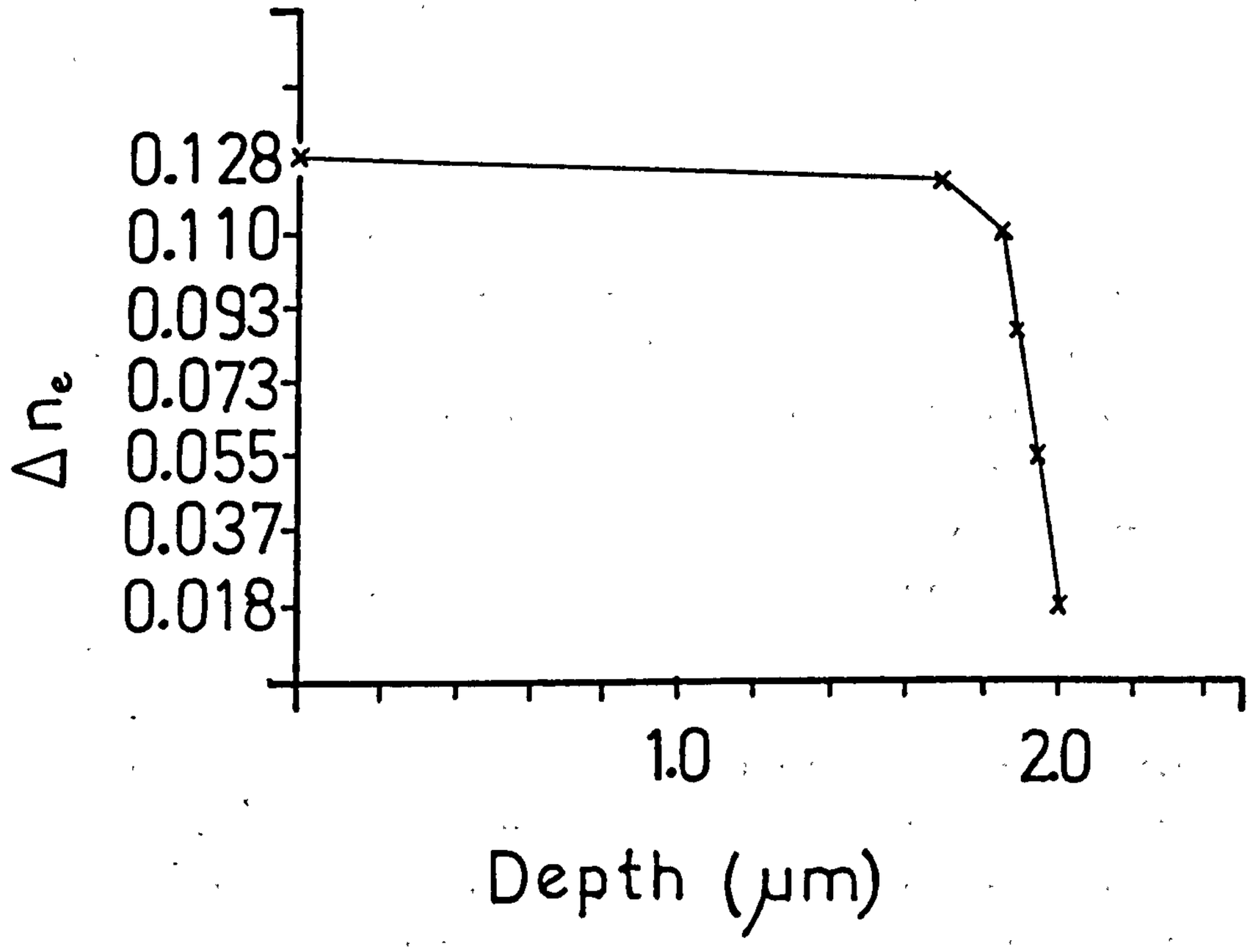

Figure 3.8. Refractive Index Profile Of The X–Cut Deuterium–Exchanged Waveguide XC, Measured At $\lambda = 0.6328\,\mu m$ ***(The Waveguide Was Fabricated At 218°C For 8hr 11min).***

3.5. DISCUSSION.

Reversible hydrogen isotopic–exchange has been observed at room–temperature in neat melt proton–exchanged waveguides, indicating that when a proton–exchanged waveguide is exposed to ambient atmosphere there is a continuous exchange between H in the waveguide and H from atmospheric water vapour. This continuous exchange suggests that protons are free to migrate within the guiding layer at room–temperature.

Migration of protons within the guiding layer could be related to the refractive index instabilities observed in proton–exchanged waveguides[1,2,9]. The latter works[2,9] showed that in proton–exchanged waveguides the effective mode indices decrease with time. Migration of protons from the waveguide into the substrate would not only cause the depth to increase, but may also result in strain–relief. The strain–relief could result in a decrease in effective mode–indices via the elasto–optic effect.

It has been suggested[9] that the migrating protons originate from hydrogen bonded OH groups. Therefore, if a stable waveguide is required, the migration of protons within the waveguide must be stopped, or the hydrogen bonded OH removed from the waveguide. Chapter 4 deals with the subject of waveguide stability in more detail.

Mr. M.A. Foad of the Chemistry Department has shown[13] that room–temperature isotopic–exchange in x– and z–cut deuterium–exchanged lithium niobate is irreversible. When deuterium–exchanged waveguides were exposed to D_2O vapour for 118hr, there was no decrease in OH or increase in OD, although isotopic–exchange in initially proton–exchanged lithium niobate has been shown to be reversible on a comparable time scale. Isotopic exchange in deuterium–exchanged lithium niobate is not therefore, analogous to isotopic–exchange in proton–exchanged lithium niobate. There must, therefore, be differences in the detailed structure of the two types of waveguide, possibly related to different OH and OD environments.

The fact that the sharp OH– band is resolved into two closely– spaced bands at low hydroxyl concentrations whereas the sharp OD– band is unresolved, also indicates different local environments. The differences between OD and OH environments may be related to the different masses of D and H.

It has been shown that an x– cut deuterium– exchanged waveguide reacts with atmospheric water vapour, causing an increase in OH absorption and a decrease in OD absorption. Jackel *et al*[3] showed that exposing a z– cut deuterium– exchanged waveguide to ambient atmosphere for several hours caused no increase in the OH absorption, indicating that the deuterium– exchanged layer did *not* exchange rapidly with atmospheric water vapour. It is unlikely however, from Figure 3.7, that the absorbance would change by a detectable amount in so short a period. It is possible, therefore, that the deuterium– exchanged waveguide used by Jackel *et al* had reacted with atmospheric water vapour at a later period.

As mentioned in reference (6), because of possible structural differences deuterium– exchanged waveguides cannot be used uncritically as an indicator of the characteristics of proton– exchanged waveguides. However, Jackel *et al*[3] used the deuterium concentration profile in a deuterium– exchanged waveguide to give an indication of hydrogen concentration profiles in proton– exchanged waveguides.

The deuterium profile was determined by bombarding the deuterium– exchanged waveguide with 15.089MeV (950keV, centre of mass frame) ^{3}He particles to excite the nuclear reaction[14]:

$$^{3}He + D \dashrightarrow {}^{4}He + p \quad \ldots\ldots(1)$$

and analysing the number and energy distribution of the ^{4}He reaction particles. The deuterium profile was graded in form unlike the step– like hydrogen profiles observed in proton– exchanged waveguides[8,9].
Hydrogen profiling involves[15] bombarding the sample with a beam of less energetic 6.385MeV (402keV, centre of mass frame) ^{15}N particles, resulting in the resonant nuclear reaction:

$$^{15}N + {}^{1}H \longrightarrow {}^{12}C + \alpha + 4.43MeV\ \gamma \ldots\ldots(2).$$

It has been shown[9,16] that heating (annealing) a proton-exchanged waveguide changes the approximate step-like hydrogen profile to a more graded profile. Therefore, because of the highly exothermic nature of reaction (1)[14], it is possible that the deuterium profile is changed during measurement by the energy liberated in the form of heat. This would explain the graded deuterium profile observed in reference (3).

The possibility that the deuterium-exchanged waveguide used in reference (3) had reacted with atmospheric water vapour and therefore contained some H, would explain why the deuterium concentration was lower at the surface of the waveguide (assuming that the H was located at the surface of the waveguide).

In the following chapter, the technique of hydrogen isotopic exchange is used at room-temperature on annealed and dilute melt proton-exchanged waveguides to test if these waveguides react with atmospheric water vapour. The technique is also applied at temperatures commonly used for annealing to determine the role of the annealing atmosphere.

REFERENCES.

(1) A. Yi–Yan, *Index Instabilities in Proton–Exchanged $LiNbO_3$ Waveguides*, Appl. Phys. Lett., 42(8), 633, (1983).

(2) J.L. Jackel, C.E. Rice, *Short– and Long–Term Stabilities in Proton–Exchanged $LiNbO_3$ Waveguides*, SPIE Proc. Guided Wave and Optoelectronic Materials, 460, 43, (1984).

(3) C.E. Rice, J.L. Jackel, W.L. Brown, *Measurement of the Deuterium Concentration Profile in a Deuterium–Exchanged Lithium Niobate Crystal*, J. Appl. Phys., 57(9), 4437, (1985).

(4) J.R. Herrington, B. Dischler, A. Rauber, J. Schneider, *An Optical Study of the Stretching Absorption Near 3μm From OH^- Defects in Lithium Niobate*, Sol. State Commun., 12, 351, (1973).

(5) L. Kovacs, V. Szalay, R. Capelletti, *Stoichiometry Dependence of the OH^- Absorption Band in Lithium Niobate Crystals*, Sol. State Commun., 52, 1029, (1984).

(6) A. Loni, R.M. De La Rue, J.M. Winfield, *Proton–Exchanged Lithium Niobate Planar Optical Waveguides: Chemical and Optical Properties and Room Temperature Hydrogen Isotopic Exchange Reactions*, J. Appl. Phys., 61(1), 64, (1987).

(7) R. Gonzalez, Y. Chen, K.L. Tsang, G.P. Summers, *Diffusion of Deuterium and Hydrogen in Crystalline Lithium Niobate*, Appl. Phys. Lett., 41, 739, (1982).

(8) C. Canali, A. Carnera, G. Della Mea, P. Mazzi, S.M. Al–Shukri, A.C.G. Nutt, R.M. De La Rue, *Structural Characterisation of Proton–Exchanged Lithium Niobate Optical Waveguides*,

(9) A.C.G. Nutt, Ph.D. Thesis, University of Glasgow, (1985).

(10) Yi–Xin Chen, W.S.C. Cheng, S.S. Lau, L. Wielunski, R.L. Holman, *Characterisation of $LiNbO_3$ Waveguides Exchanged in $TINO_3$ Solutions*, Appl. Phys. Lett., 40(1), 10, (1982).

(11) J.G. Bergman, A. Ashkin, A.A. Ballman, J.M. Dziedzic, H.J. Levinstein, R.G. Smith, *Curie Temperature, Birefringence, & Phase–Matching Temperature Variations in Lithium Niobate as a Function of Melt Stoichiometry*, Appl. Phys. Lett., 12, 92, (1968).

(12) I.P. Kaminow, J.R. Carruthers, *Optical Waveguiding Layers in $LiNbO_3$*, Appl. Phys. Lett., 22(7), 326, (1973).

(13) M.A. Foad, First Year Report, Chemistry Department, University of Glasgow, 1987.

(14) D. Diumegard, D. Dubreuil, G. Amsel, *Analysis and Depth Profiling of Deuterium with the D(^{3}He,p)^{4}He Reaction by Detecting the Protons at Backward Angles*, Nucl. Inst. & Methods, 166, 431, (1979).

(15) W.A. Lanford, H.P. Trautvetter, J.F. Ziegler, J. Keller, *New Precision Technique for Measuring the Concentration Versus Depth Profile of Hydrogen in Solids*, Appl. Phys. Lett., 28(9), 566–568, 1976.

(16) C. Canali, A. Carnera, G. Mazzi, P. Mazzoldi, R.M. De La Rue, *Fabrication, Processing, Performances & Stability of Titanium Indiffused and Proton–Exchanged $LiNbO_3$ Optical Waveguides*, IEEE International Workshop on Integrated Optical and Related Technologies for Signal Processing, 17–24, 1984.

CHAPTER 4

Characterisation Of Annealed And Dilute–Melt Proton–Exchanged Waveguides By Prism–Coupler Measurements, Infrared Spectroscopy, And Hydrogen Isotopic–Exchange Reactions.

4.1. INTRODUCTION.

The following sections are concerned with a study of annealed x–cut proton–exchanged lithium niobate waveguides and x–cut waveguides produced using dilute benzoic acid melts. The term "dilute–melt" (when applied to proton–exchange) is commonly used to refer to benzoic acid melts containing small percentages of lithium benzoate. The term "annealing" refers to heating the waveguide material.

The annealing and dilute–melt experiments have been combined in a single chapter since, although they are different processes, the resultant waveguides have similar properties, for example, in their infrared absorption bands, stability of effective mode–indices, and in their waveguide (surface) refractive indices.

Infrared spectroscopic measurements and optical waveguide prism–coupler measurements have been carried out with the annealing temperature and time as parameters. The extent of proton–exchange has been determined with melt–dilution, using infrared spectroscopy and mode–index measurements.

It was suggested in Chapter 3 that the waveguide mode–index relaxation observed in proton–exchanged waveguides[1,2] could, in part, be a result of the migration of protons within the guiding layer. Hydrogen isotopic–exchange in annealed and dilute–melt waveguides has been investigated both at room–temperature and at temperatures commonly used for annealing with a view to determining the origin of the time–varying optical properties.

4.2. ANNEALED PROTON–EXCHANGED WAVEGUIDES.

4.2.1. The Effects Of Annealing On Waveguide Properties.

Many workers have reported on the structural and optical properties of annealed proton–exchanged waveguides[2,3,4,5,6,7]. De Micheli *et al*[7] showed that one of the consequences of annealing was that the waveguide refractive index profile changed from an approximate step–index form to

a more graded–index form, the modification being a function of the annealing temperature and time.

Altering the step–index profile by annealing is desirable for the following reason: because proton–exchanged waveguides have a high index change ($\Delta n_e \simeq 0.125$), single–mode waveguides (at $\lambda = 0.6328\,\mu m$) are shallow, of the order of $0.3\,\mu m$ to $0.6\,\mu m$ (Chapter 2). Therefore, if single–mode proton–exchanged waveguides were used together with single–mode optical fibres, there could be a field mis–match between the waveguide and the fibre, causing power losses if butt–coupling was attempted. A method of increasing the depth of the waveguide while maintaining single–mode operation would be desirable as this should improve fibre–waveguide coupling losses.

One of the disadvantages associated with (unannealed) proton–exchanged waveguides produced using neat benzoic acid melts is the relaxation of effective mode–indices with time[1,2]. Figure 4.1 shows the variation in effective mode–indices with time, for a series of nominally identical z–cut waveguides produced using a neat benzoic acid melt ($T = 212^{o}C$, $t = 3hr$). The decrease in the effective mode–indices agree with results quoted by other workers[1,2,8] and is of the order of 5×10^{-3}, over a 330hr period. Jackel and Rice have shown[2] that the relaxation can be avoided by post–fabrication annealing.

The results of Rutherford backscattering experiments[5,6,8] on x– y– and z–cut proton–exchanged waveguides indicated that the strain in the guiding layer was relieved by annealing. The proton–exchange process creates severe surface damage on y–cut substrates[6]. However, it has been shown[8] that low–temperature annealing of such waveguides forms multimode guides without the surface damage.

Annealed proton–exchanged stripe waveguide cut–off modulators have significantly reduced drive voltages compared to unannealed modulators[9], suggesting that the electro–optic effect in proton–exchanged waveguides (found to be much smaller than the bulk effect, Chapter 5) is restored by annealing.

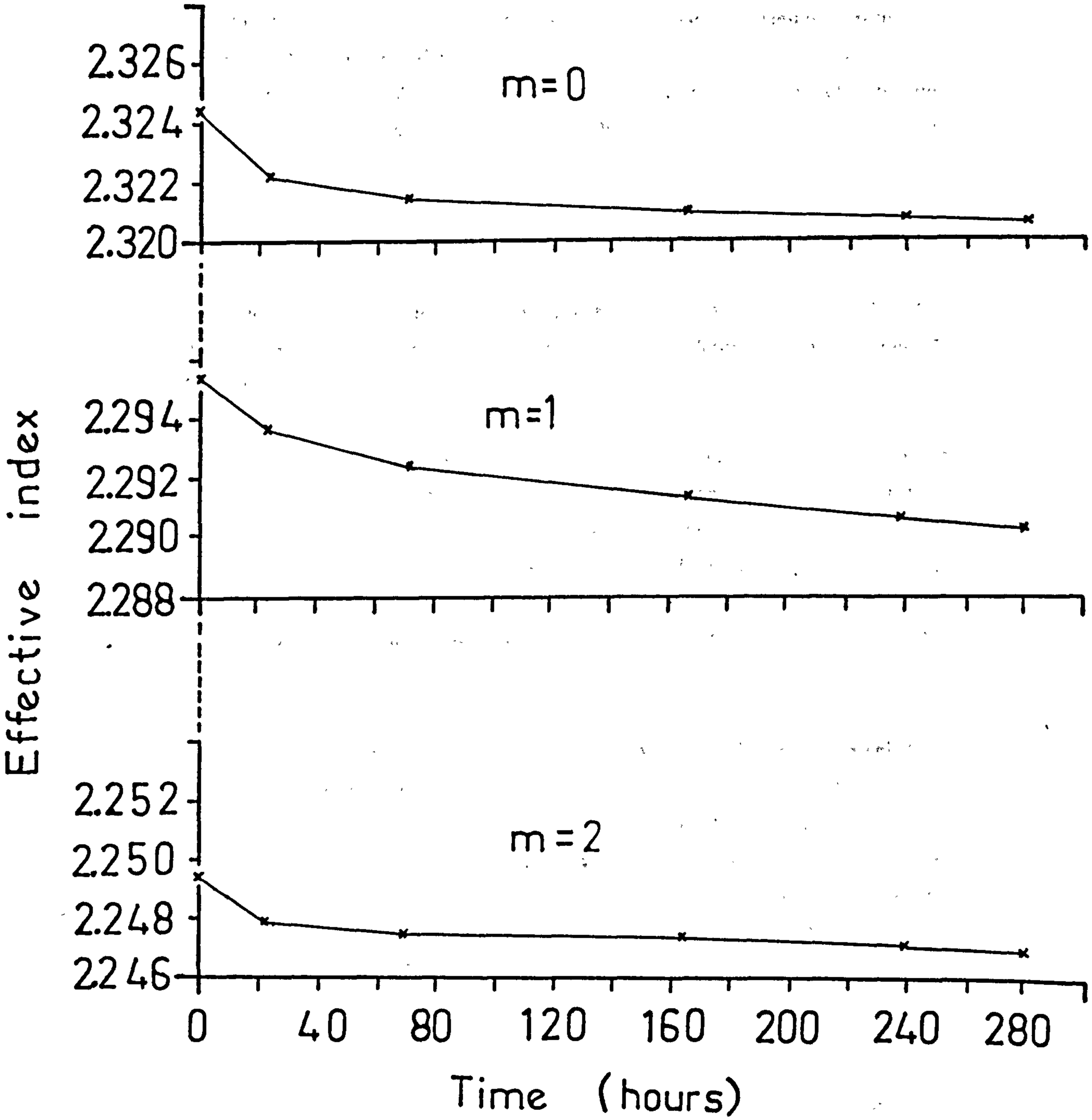

Figure 4.1. Variation In Effective Mode–Indices With Time, For A Series Of Z–Cut Proton–Exchanged Waveguides Fabricated At T=212°C For t=3hr.

In summary, the annealing of proton–exchanged waveguides results in higher quality waveguides, i.e. lower in–plane scattering, lower losses, and waveguide stability[2,5,10,11,12]. A systematic study of annealed proton–exchanged waveguides should help in understanding *why* the annealing process is beneficial.

4.2.2. Annealing Conditions.

The annealing conditions of the x–cut waveguides are given in Table 4.1. The waveguide fabrication conditions were as described in Chapter 2, Section 2.3.

Annealing was carried out in a cylindrical furnace, the temperature of which could be controlled to ±2°C. The furnace was temperature–profiled so that the "hot–spot" position was known for each annealing temperature. Annealing was undertaken in a flowing wet oxygen (O_2) atmosphere obtained by bubbling oxygen through water, at a flow rate of 1.575 litre/min. The water temperature was 60°C. The gas bubbles travelled through approximately 10cm of the water.

The waveguides were mounted in a specially designed stainless steel boat allowing an even flow of vapour over the surfaces of each waveguide. In order to avoid thermal shock on entry and removal, the waveguides were moved slowly along the furnace tube over a period of approximately one minute. The annealing time was defined as the interval between reaching and subsequent removal from the furnace hot–spot. The wet O_2 flow was maintained throughout the entrance and removal periods.

4.2.3. Optical Waveguide Measurements.

The results of optical measurements on annealed proton–exchanged waveguides, presented in this section, confirm much of the previous work[2,3,4,5,6,7]. The results in the present section are, however, important since they are correlated with information obtained from infrared absorption studies on annealed waveguides.

Sample	Annealing Temperature (°C)	Annealing Time	Waveguide (surface) Index	Depth (μm)
X1	–	0	2.3281	0.40
"	250	0.5hr	2.3082	0.70
"	"	1hr	2.3081	0.70
"	"	2hr 37min	2.3036	0.72
X11	–	0	2.3295	0.83
"	250	0.5hr	2.3168	1.14
"	"	1hr	2.3151	1.19
"	"	2hr 37min	2.3098	1.27
X12	–	0	2.3307	1.09
"	250	0.5hr	2.3231	1.41
"	"	1hr	2.3168	1.61
"	"	2hr 37min	2.3153	1.63
X10	–	0	2.3244	0.63
"	320	15min	2.3072	1.02
"	"	1hr	2.2862	1.34
"	"	3hr 11min	2.2763	1.50
X13	–	0	2.3286	1.12
"	320	15min	2.3137	1.85
"	"	1hr	2.3026	2.02
"	"	3hr 11min	2.2882	2.42
X20	–	0	2.3281	1.60
"	320	15min	2.3191	2.35
"	"	1hr	2.3021	2.72
"	"	3hr 11min	2.2992	2.84

Table 4.1. Optical Waveguide Measurements ($\lambda = 0.6328\,\mu$m) And Annealing Conditions For A Series Of X–Cut Proton–Exchanged Waveguides.

The standard prism–coupling technique was used to assess the optical characteristics of the annealed waveguides at $\lambda = 0.6328\,\mu m$. Figure 4.2 shows the dependence of the refractive index profile of an x–cut proton–exchanged waveguide (X13, $T = 175.5^{o}C$, $t = 3hr$) on annealing time and temperature. The waveguide (surface) index decreased by 0.04 after annealing at $320^{o}C$ for 3hr 11min and the depth of the guiding region increased by $1.30\,\mu m$. Although the step–index type profile was preserved after the last annealing run, a tail started to form at the waveguide/substrate boundary, indicating the gradual change to a more graded–index profile.

A consequence of the increase in the depth of sample X13 was an increase in the number of modes supported, from 3 modes (before annealing) to 5 modes (after annealing at $320^{o}C$ for 3hr 11min). After further annealing at $400^{o}C$ for 30min, the tail on the step–like refractive index profile got bigger, indicating that the profile was changing to a more graded–type form. It has been shown[7] that annealing at temperatures greater than $400^{o}C$ for several hours decreases the waveguide (surface) index to a value very close to the substrate index, and causes the waveguide to become highly multimode.

Observations of effective mode–indices (at $\lambda = 0.6328\,\mu m$) and the waveguide depth of sample X13, with the annealing time as a parameter, are represented in Figure 4.3. It can be seen from Figure 4.3 that the second mode ($m = 1$) and the third mode ($m = 2$) had maximum effective indices after approximately 10min and 15min annealing, respectively. The fourth mode ($m = 3$) reached a maximum after approximately 1hr. After reaching a maximum, the effective mode–indices decreased gradually. No initial increase was observed for the fundamental mode ($m = 0$). However, it is possible that the decay–time of the effective index of the fundamental mode was reached at a very early stage, after annealing.

The latter results of effective mode–index variation with annealing time agree with those of Nutt[8], who observed similar effects in y– and z–cut proton–exchanged waveguides. Table 4.1 summarises the waveguide indices and depths as functions of the annealing time and temperature, for the guides used in the present study. The results in Table 4.1

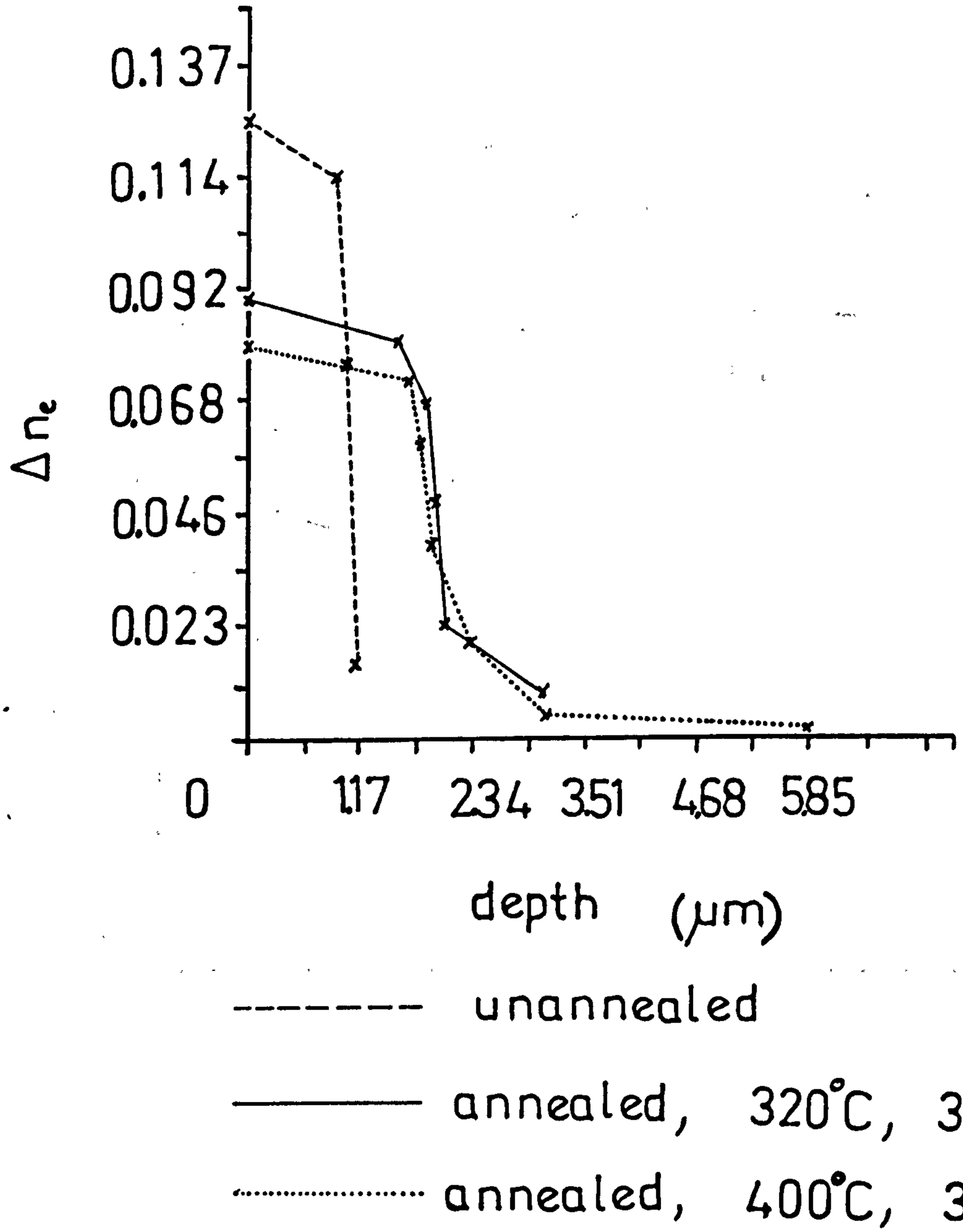

Figure 4.2. Refractive Index Profile ($\lambda = 0.6328\,\mu m$) Of An X–Cut Proton–Exchanged Waveguide (X13, T = 175.5°C, t = 3hr), Measured As A Function Of Annealing Time.

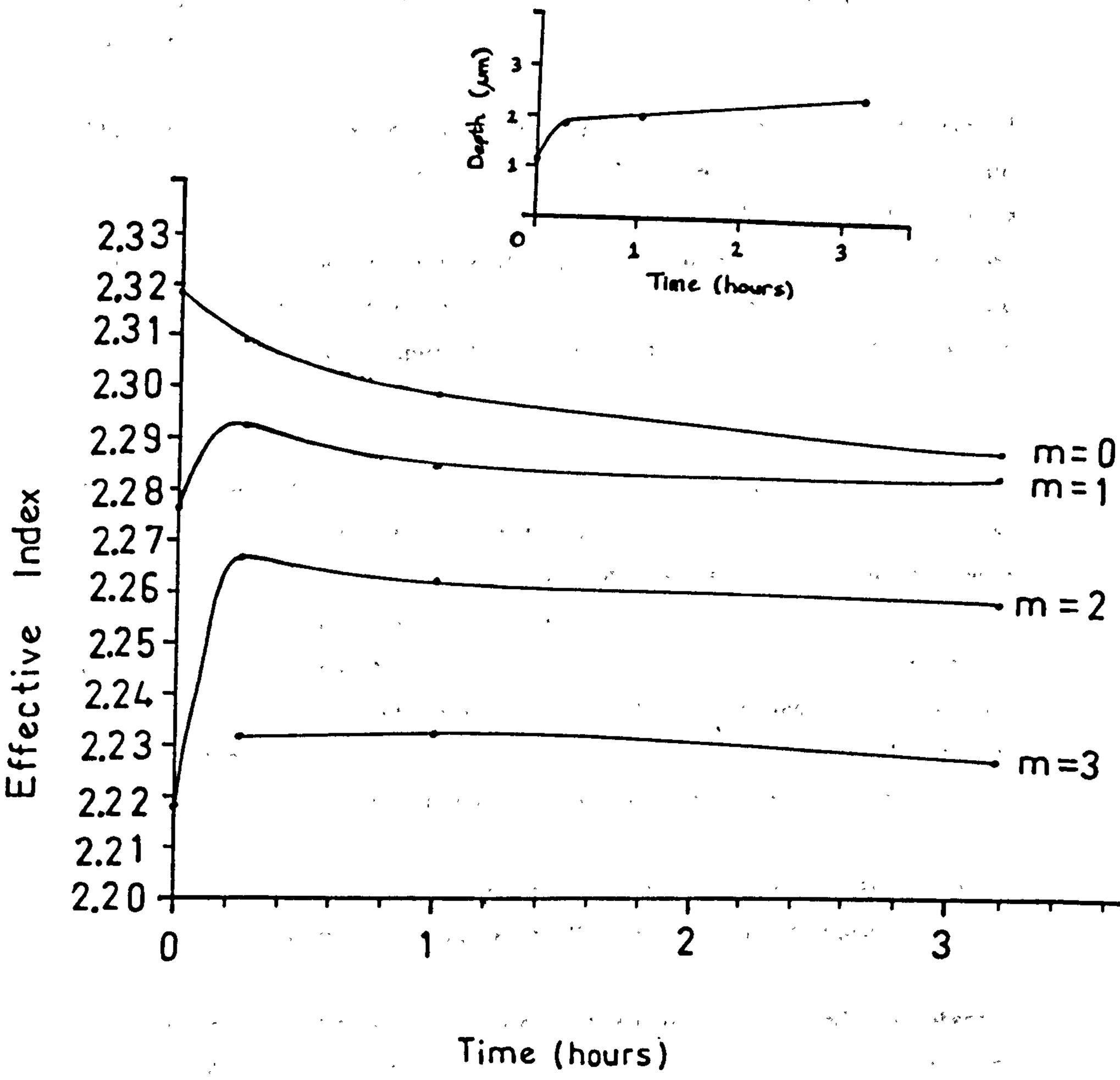

Figure 4.3. Variation In Effective Mode–Indices With Annealing Time For The X–Cut Proton–Exchanged Waveguide, X13 (175.5°C, 3hr).

indicate that, at fixed temperatures, most of the changes in the refractive index profiles take place within the first half–hour of annealing, i.e. there is a very rapid *initial* change. Smaller changes are observed after annealing for greater than 4hr (at fixed temperatures), in agreement with previous work[8].

The fact that annealing increases the depth of a proton–exchanged waveguide indicates that protons migrate from the waveguide region into the substrate. This has been verified[8] by determining proton–concentrations in annealed waveguides using the nuclear reaction technique discussed in Chapter 3. It has also been shown[8] that the rate of diffusion of protons into the substrate is critically controlled by the annealing temperature.

For the annealed x–cut proton–exchanged waveguides in Table 4.1, no decrease in the effective mode–indices was observed (after annealing) with time (over a measurement period of one year), in agreement with previous work[2]. In comparing Figures 4.1 and 4.3, it is evident that the effective index relaxation observed in unannealed proton–exchanged waveguides cannot be considered solely as being the result of very long period annealing at room–temperature, since the effective mode–indices in Figure 4.1 do not vary in the same manner as those in Figure 4.3.

4.2.4. Correlation Between Infrared Absorption Spectra And Optical Waveguide Measurements Of Annealed Proton–Exchanged Waveguides.

In Chapter 2, infrared absorption spectroscopy was used to observe OH–hydroxyl groups in proton–exchanged waveguides. The present section concerns the use of infrared spectroscopy to observe the effects of annealing on the OH–hydroxyl groups. The infrared spectroscopic and optical waveguide prism–coupling measurements were carried out after each annealing run.

Since there was a period of approximately four months between waveguide fabrication and annealing (during which the waveguides were exposed to the atmosphere), the infrared spectra of the waveguides were re–recorded prior to annealing to check for possible changes. The OH absorption

bands (discussed in Chapter 2, Section 2.5) under consideration were at υ_{max}= 3505cm^{-1} (x− and z− cut) and υ_{max}= 3250cm^{-1} (x− cut). No measurable changes in the band absorbances were observed.

After annealing the x− cut proton− exchanged waveguide X11 at 250°C for 0.5hr, the absorbance of the hydrogen− bonded OH− hydroxyl group was reduced (υ_{max}= 3250cm^{-1}, Figure 4.4a). There was no reduction in the absorbance of the free OH− hydroxyl group (υ_{max}= 3505cm^{-1}, Figure 4.4a). Prolonged annealing at the same temperature (Table 4.1) produced further, slight, reductions in the absorbance of the broad band although no further changes were observed 2hr 37min after the initial spectra were recorded. Most of the changes in the refractive index profile of sample X11 occurred after the first 0.5hr of annealing (Table 4.1). For example, the value of Δn_e reduced from 0.1270 after fabrication to 0.1143, and the waveguide depth (d) increased from 0.83μm to 1.14μm. The profile remained step− like after the last annealing period.

After annealing the x− cut proton− exchanged waveguide X12 at 250°C for 0.5hr, there was a substantial reduction in the broad band absorbance at υ_{max}= 3250cm^{-1} from 0.07 absorbance units (after fabrication) to 0.015 absorbance units (Figure 4.4b). No changes in the sharp band were observed. No changes in either band were observed after further annealing at the same temperature. Most of the changes in Δn_e and d for X12 occurred within the first 0.5hr of annealing (Table 4.1). For example, Δn_e= 0.1282 and d= 1.09μm after fabrication and, Δn_e= 0.1206 and d= 1.41μm after annealing for 0.5hr. The profile remained step− like after the last annealing period. Similar effects to those observed in the infrared spectra and optical waveguide measurements of samples X11 and X12 were observed for all the annealed x− cut proton− exchanged waveguides in Table 4.1.

It has been shown in the present section that, in proton− exchanged waveguides, the hydrogen− bonded OH− hydroxyl group responsible for the broad absorption band at υ_{max}= 3250cm^{-1} was removed within the first 0.5hr of annealing at temperatures as low as 250°C. Most of the changes in the refractive index profiles also occurred within 0.5hr annealing. Annealing also increases waveguide depths, presumably due to migration of

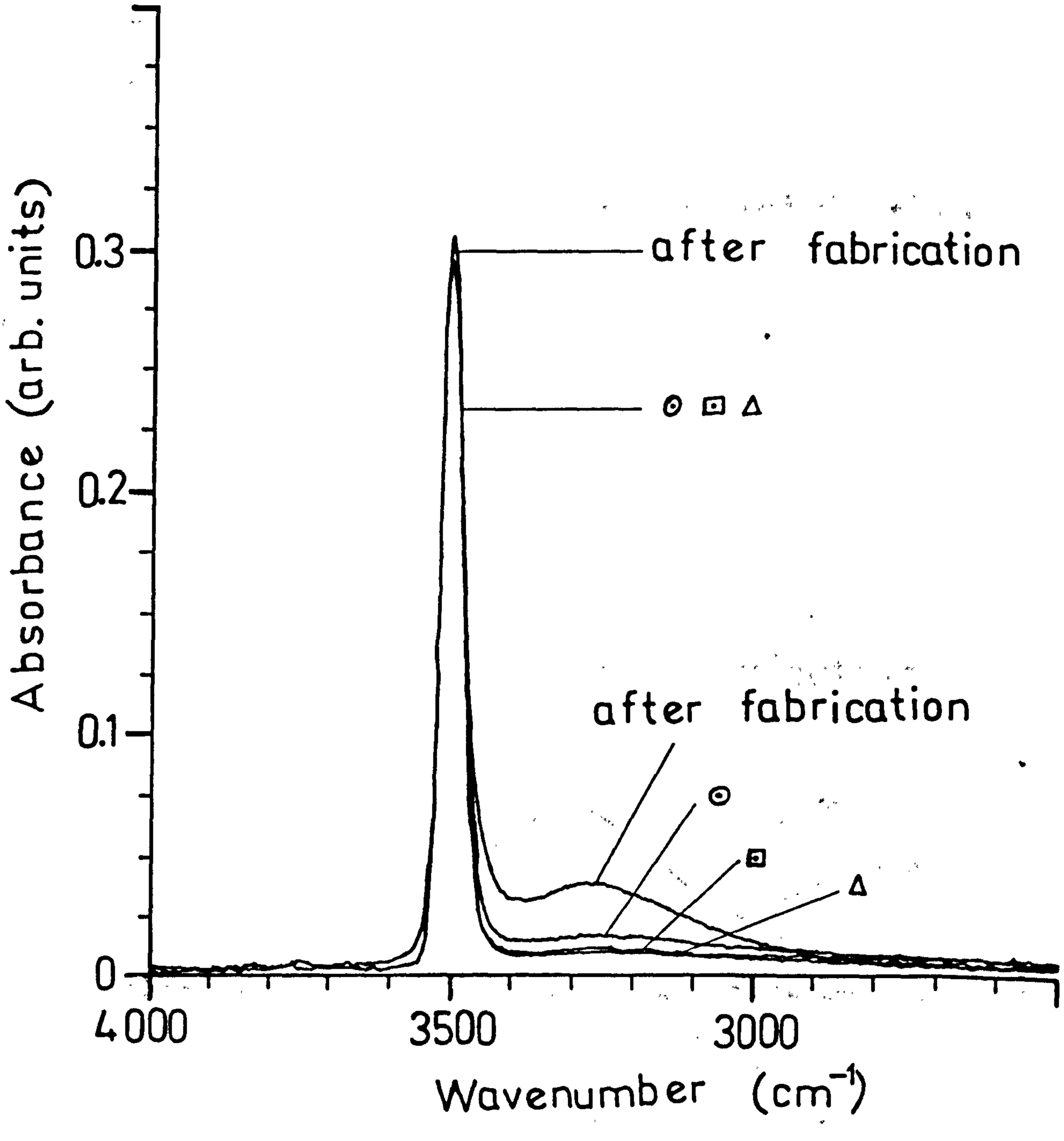

Figure 4.4a. Infrared Absorption Spectrum Of An X–Cut Proton–Exchanged Waveguide (X11, T=168.5°C, t=3hr), Recorded As A Function Of Annealing Time.

The Waveguide Was Annealed At 250°C For ⊙ 0.5hr, ⊡ 1hr, And △ 2hr 37min (Table 4.1).

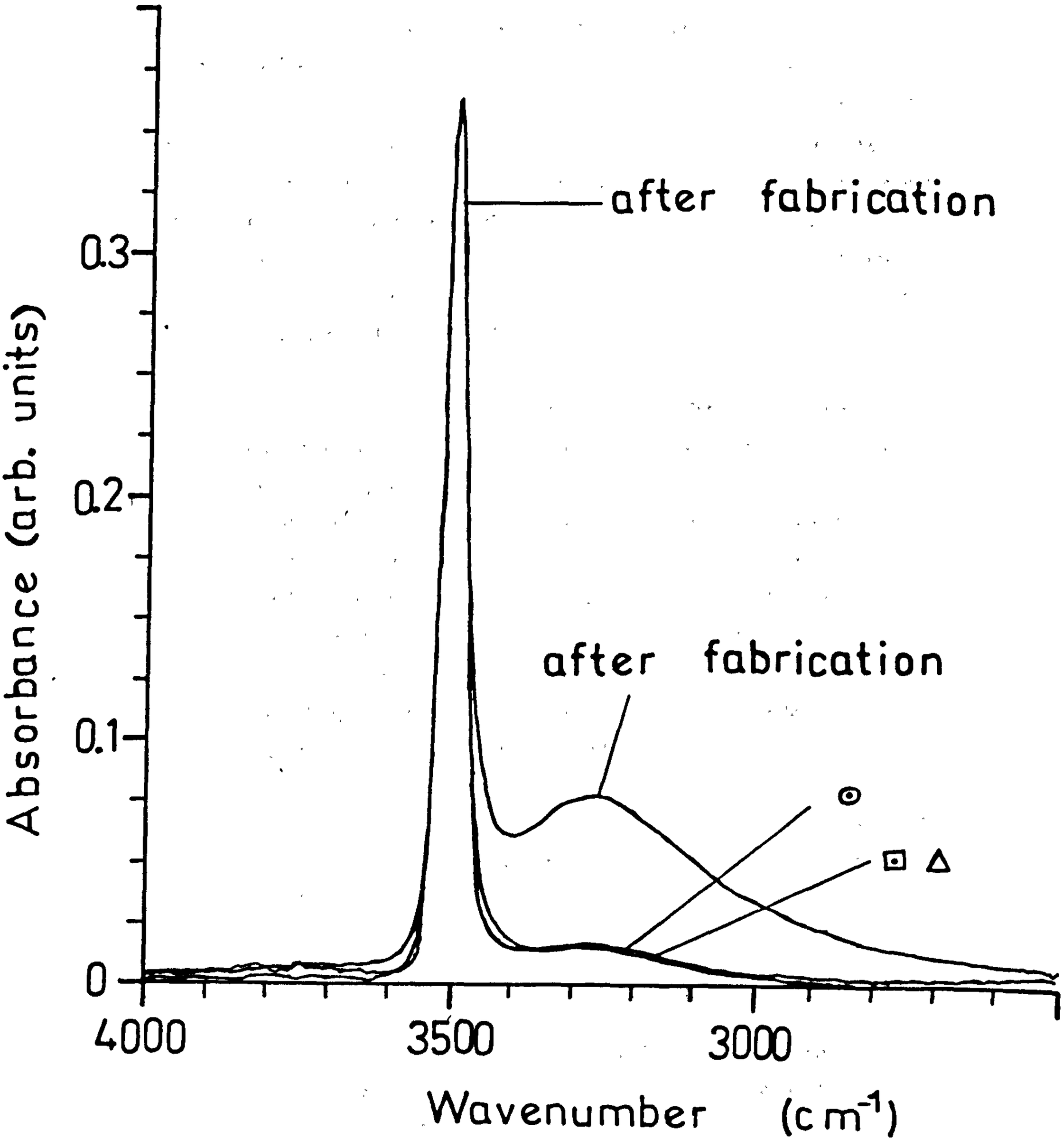

Figure 4.4b. Infrared Absorption Spectrum Of An X–Cut Proton–Exchanged Waveguide (X12, T=168°C, t=6hr), Recorded As A Function Of Annealing Time.

The Waveguide Was Annealed At 250°C For ⊙ 0.5hr, ⊡ 1hr, And △ 2hr 37min (Table 4.1).

protons from the waveguide region into the substrate, and after annealing, the effective mode–indices are stable. As mentioned in Section 4.2.3, annealing a proton–exchanged waveguide is not equivelent to leaving the waveguide for a very long period at room–temperature. This was verified by recording the infrared absorption spectra of unannealed proton–exchanged waveguides and noting, from the broad absorption band at υ_{max}= 3250cm^{-1}, that the hydrogen–bonded OH–hydroxyl groups were still present. If annealing had taken place at some period, there would have been a reduction in the absorbance of the band.

It seems plausible that the removal of the hydrogen–bonded OH–hydroxyl groups could be the reason for the stability of effective mode–indices and the changes in the waveguide refractive index profiles which occurred during the first 0.5hr of annealing. It is possible that, during annealing, hydrogen–bonded OH either diffuses into the substrate or is removed from the waveguide. The former possibility is unlikely since, if hydrogen–bonded OH diffused into the substrate the area under the infrared absorption bands would be conserved, and it is not. Therefore annealing in wet O_2 must remove hydrogen–bonded OH. The role of the annealing atmosphere is discussed in Sections 4.6 and 4.7.

4.3. CHARACTERISATION OF X– AND Z–CUT PROTON–EXCHANGED WAVEGUIDES PRODUCED USING DILUTE–MELTS.

4.3.1. Introduction.

Optical waveguides produced in lithium niobate by proton–exchange with benzoic acid containing small percentages of lithium benzoate have been studied in relation to mode stability[2,13,14], in–plane scattering[13], and the electro–optic effect[13,15,16]. The latter publications collectively refer to such mixtures as *dilute–melts*.

It has been shown that the addition of lithium compounds to benzoic acid reduces the extent of proton–exchange [14,17,18]. Single–mode waveguides are therefore produced at higher temperatures using longer times. It has also been reported[7] that the use of dilute–melts prevents

surface damage, a problem which primarily affects y–cut substrates, and that in–plane scattering levels in x– and z–cut waveguides are reduced[13,15].

The purpose of the work described in the following sections was to determine the extent of proton–exchange in x–cut lithium niobate with melt dilution, temperature, and time as parameters, and to determine the origin of similarities observed between the effective mode–indices of dilute–melt and annealed proton–exchanged waveguides[2,7,13].

In Section 4.2.4, the improved optical properties of annealed proton–exchanged waveguuides were attributed to the removal of hydrogen–bonded OH. It is possible that the improved properties of dilute–melt waveguides are also related to hydrogen–bonded OH. This possibility has been tested by correlating the optical properties of dilute–melt waveguides with infrared spectroscopic measurements.

4.3.2. Dilute–Melt Waveguide Fabrication.

The fabrication procedure for the x–cut dilute–melt proton–exchanged waveguides was as described in Chapter 2, Section 2.3, except that the waveguides were fabricated at 215°C (Table 4.2) and 235°C (Table 4.3). The term used to define the quantity of lithium benzoate added to the benzoic acid melt was the *mole–fraction* (X) given by:

$$X = [L/(L+B)]x100\% \quad \ldots\ldots\ldots\ldots (1),$$

where L= number of moles of lithium benzoate, and B= number of moles of benzoic acid. Tables 4.2 and 4.3 list the samples with their corresponding mole–fractions.

4.3.3. Optical Waveguide Measurements.

The optical properties of the waveguides were assessed at $\lambda = 0.6328\,\mu m$ using the prism–coupling technique. The estimated waveguide depths were plotted as a function of the square–root of the fabrication time to determine whether the process had the same time–dependence observed

Sample	Mole Fraction (%)	Fabrication Temperature (^{o}C)	Fabrication time
51X	0.29	215	2hr 36min
50X	0.28	"	4hr 30min
52X	0.28	"	6hr
49X	0.29	"	7hr 33min
16X	0.49	215	1hr 39min
17X	0.48	"	3hr 2.5min
20X	0.49	"	4hr
18X	0.57	"	6hr
19X	0.50	"	8hr 30min
56X	0.73	215	3hr 45min
54X	0.73	"	4hr 53min
55X	0.74	"	6hr 16.5min
53X	0.73	"	8hr 6.5min
28X	1.01	215	1hr
27X	1.10	"	2hr 30min
26X	1.08	"	4hr 30min
25X	1.01	"	6hr
21X	1.00	"	8hr

Table 4.2. The X–Cut Waveguides Used For Dilute–Melt Proton–Exchange At T= 215^{o}C.

Sample	Mole Fraction (%)	Fabrication Temperature (^{o}C)	Fabrication time
36X	0.28	235	3hr 17.5min
37X	0.28	"	4hr 29.5min
39X	0.28	"	6hr
38X	0.29	"	8hr 1.5min
11X	0.58	235	1hr
12X	0.57	"	3hr 17min
15X	0.53	"	4hr 30min
14X	0.60	"	8hr
40X	0.73	235	4hr 46min
42X	0.73	"	6hr
41X	0.74	"	8hr 3.5min
6X	1.20	235	1hr 4min
7X	1.16	"	3hr
10X	1.09	"	4hr 30min
8X	1.17	"	6hr
9X	1.00	"	8hr 8min

				Index Change Δn_e	Depth (μm)
X01	0.09	235	4hr	0.1147	3.07
X00	0.30	"	"	0.1149	1.92
X03	0.64	"	"	0.1136	1.44
X04	0.76	"	"	0.1118	1.20
X05	1.10	"	"	0.1075	0.93
X06	2.42	"	427hr 10min	0.0870	4.45

Table 4.3. The X–Cut Waveguides Used For Dilute–Melt Proton–Exchange At T=235^{o}C, And The Variation In Step–Index (λ= 0.6328 μm) And Depth With Mole–Fraction For Waveguides X00 To X06.

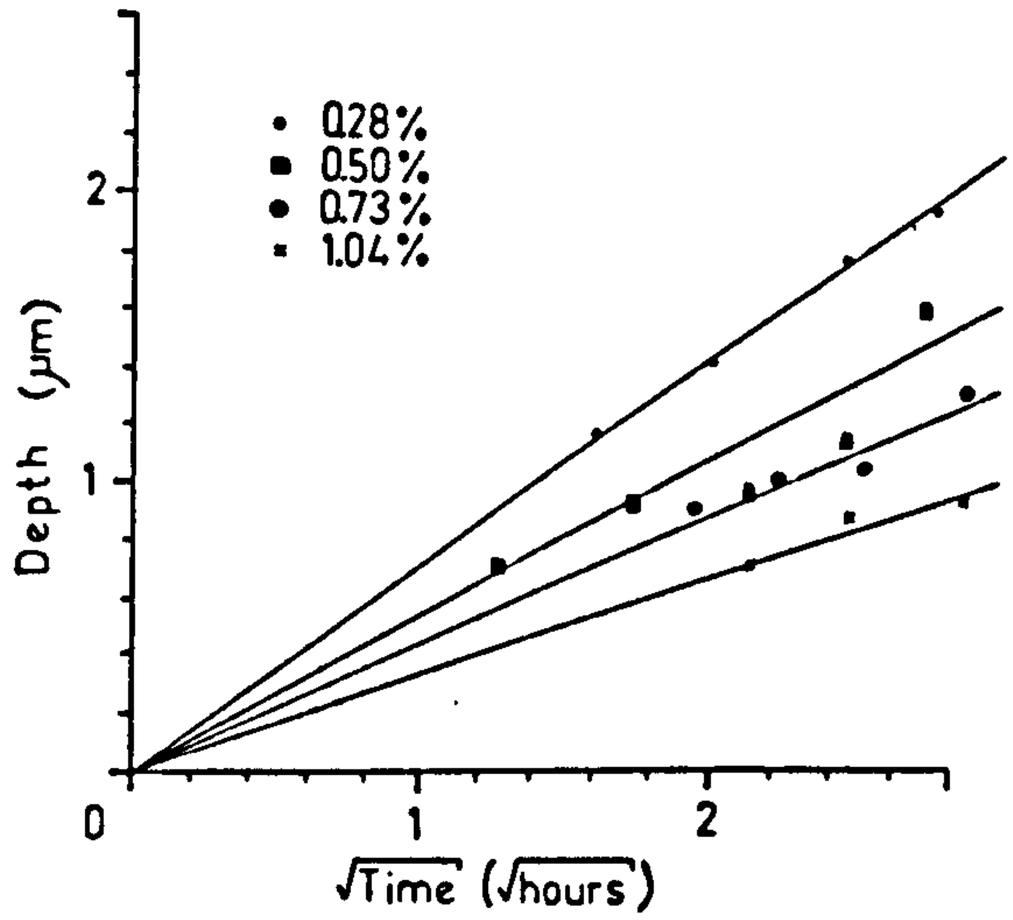

Figure 4.5. Waveguide Depth As A Function Of $t^{1/2}$ And Mole−Fraction, For The X−Cut Dilute−Melt Waveguides Produced At T=215°C (Table 4.2).

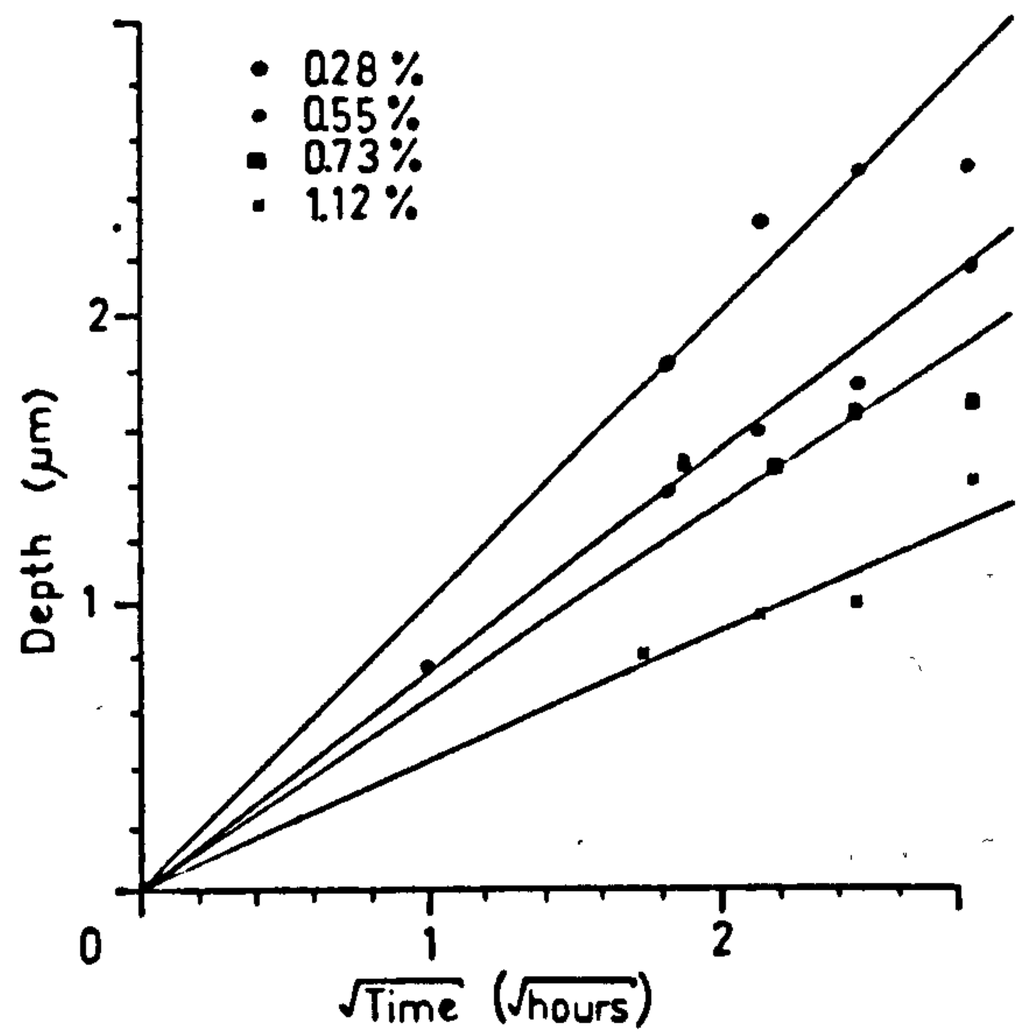

Figure 4.6. Waveguide Depth As A Function Of $t^{1/2}$ And Mole−Fraction, For The X−Cut Dilute−Melt Waveguides Produced At T=235°C (Table 4.3).

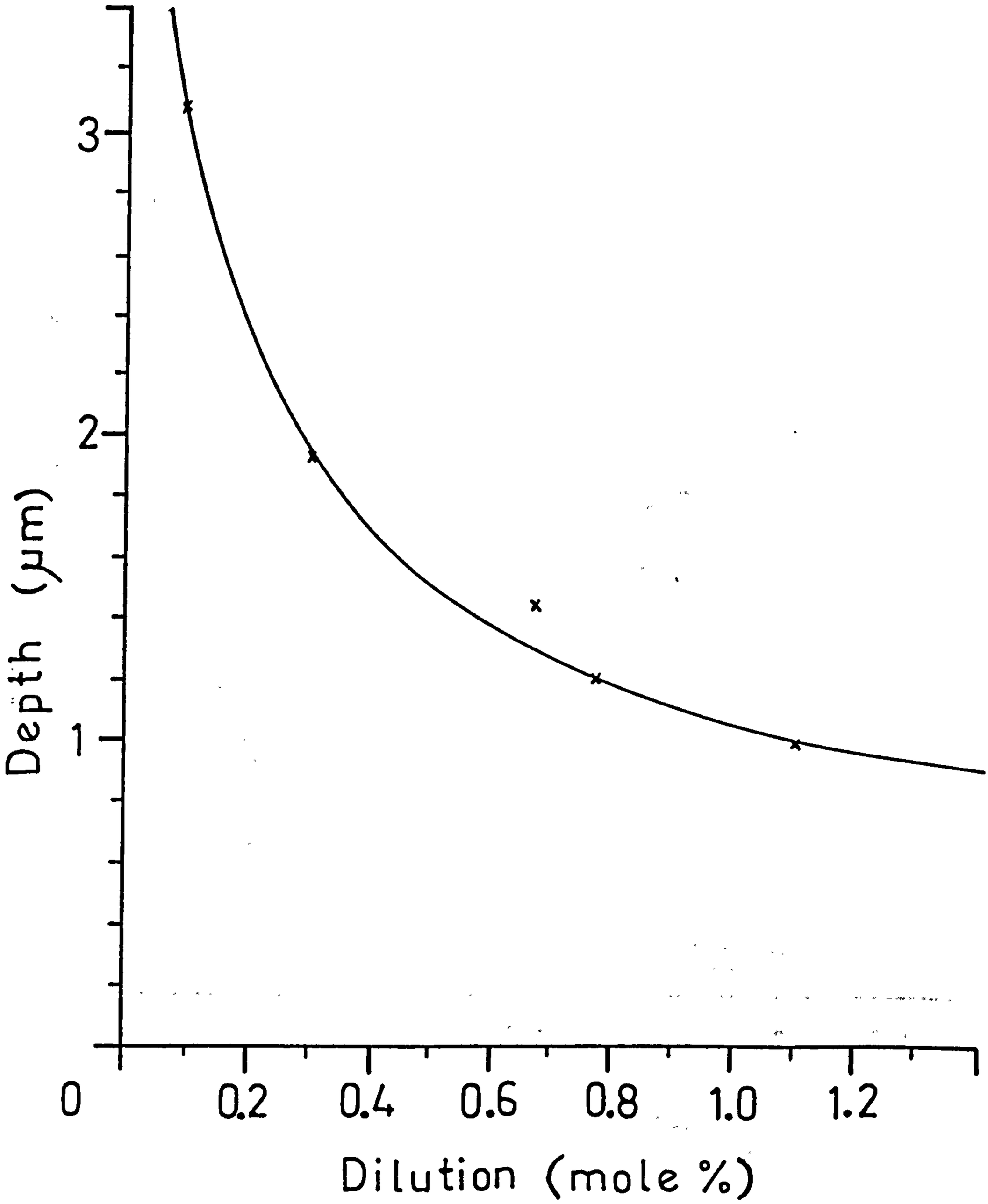

Figure 4.7. Variation In Guide Depth With Mole−Fraction For The X−Cut Dilute−Melt Waveguides Produced At T=235°C For t=3hr (Table 4.3).

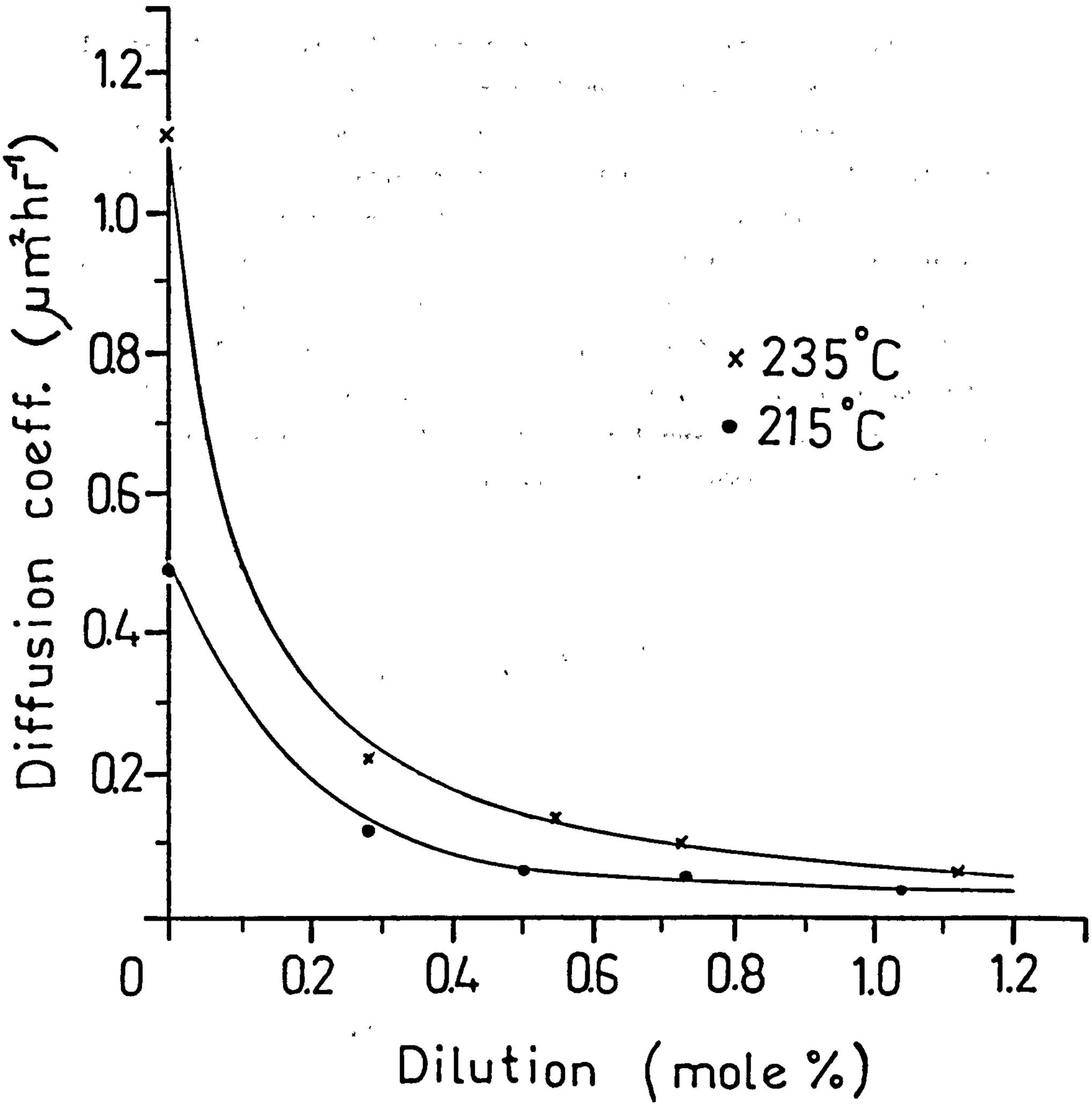

Figure 4.8. Variation In Effective Diffusion Coefficient With Mole– Fraction, At T= 215°C And T= 235°C.

for neat–melt proton–exchange (Chapter 2). The linear variation in the waveguide depth with $t^{1/2}$ (Figures 4.5 and 4.6 for T=215°C and T=235°C, respectively) suggests that the extent of proton–exchange in dilute–melts is also governed by diffusion.

Figure 4.7 shows the variation in the waveguide depth with mole–fraction, for a series of x–cut dilute–melt waveguides fabricated at 235°C for 4hr (Table 4.3). The extent of reaction, represented by the waveguide depths, decreased as the mole–fraction increased. The fact that the depth of the proton–exchanged region depends on the mole–fraction of lithium benzoate added to the melt indicates that the effective diffusion coefficients are dependent on the mole–fraction of lithium benzoate in the melt. The effective diffusion coefficients (D(T)) were calculated from the slopes of the lines in Figures 4.5 and 4.6. The variation in D(T) with mole–fraction (Table 4.4) is shown in Figure 4.8 and confirms that the extent of proton–exchanged depends on the mole–fraction of lithium benzoate in the melt.

Fabrication Temperature (°C)	Mole Fraction* (%)	Effective Diffusion Coefficient ($\mu m^2 hr^{-1}$)
215	0	0.495
"	0.28±0.01	0.123
"	0.51±0.04	0.063
"	0.73±0.01	0.049
"	1.04±0.05	0.028
235	0	1.119
"	0.28±0.01	0.224
"	0.57±0.03	0.138
"	0.73±0.01	0.099
"	1.12±0.08	0.054

Table 4.4. Variation In Effective Diffusion Coefficients With Mole–Fraction, For The X–Cut Dilute–Melt Waveguides In Tables 4.2 And 4.3.

* *mean value and standard deviation.*

Now, it was shown in Chapter 2 that the lithium concentration in benzoic acid melts increased with the proton–exchange time, in effect causing the melt to become progressively more dilute. Therefore, as the proton–exchange time progressed, the effective diffusion coefficients might have decreased. However, the lithium concentration levels in benzoic acid determined after proton–exchange are sufficiently small (Chapter 2, Section 2.6.3) that the effective diffusion coefficients remain approximately constant throughout the period of proton–exchange. For example, the maximum concentration of lithium in benzoic acid, determined after proton–exchange at 210°C for 6hr on x–cut lithium niobate, was 3.5×10^{-4}g lithium in 20g benzoic acid. An equivalent weight of lithium would be found in 6.4×10^{-3}g lithium benzoate, corresponding to a lithium benzoate mole–fraction of 0.02%.

In Section 4.2.3 it was mentioned that no decrease in the effective mode–indices was observed with time after annealing, in agreement with previous workers[2]. Similar results have also been quoted for waveguides produced using dilute–melts[2,13]. Figure 4.9 shows the relationship between the decrease in the effective mode–index (fundamental and first order modes) with time, with the mole–fraction as a parameter (samples X00 to X06, T=235°C, Table 4.3). The degree of stability depends on the mole–fraction. For example, the decrease in the fundamental mode (m=0) index over a period of 410hr was 0.0045 for sample X00 (0.09% mole fraction), and 0.001 for sample X04 (1.10% mole fraction). Jackel *et al*[3,10] showed that no measurable decrease was observed for waveguides produced from melts containing mole–fractions greater than 3.4%.

Another interesting feature of dilute–melt waveguides is that, although the refractive index profiles are step–like, the value of Δn_e varies inversely with the mole–fraction[2,7,16,19]. This is illustrated in Figure 4.10 for the above x–cut waveguides (X00 to X06). The lowest value measured in the present work was $\Delta n_e = 0.085$ for a waveguide produced using a 2.42% mole–fraction.

Extrapolating the results of other workers, the estimated values of Δn_e for X=2.42% are, 0.1100[2], 0.065[7], 0.050[16], and 0.1075[19]. Clearly,

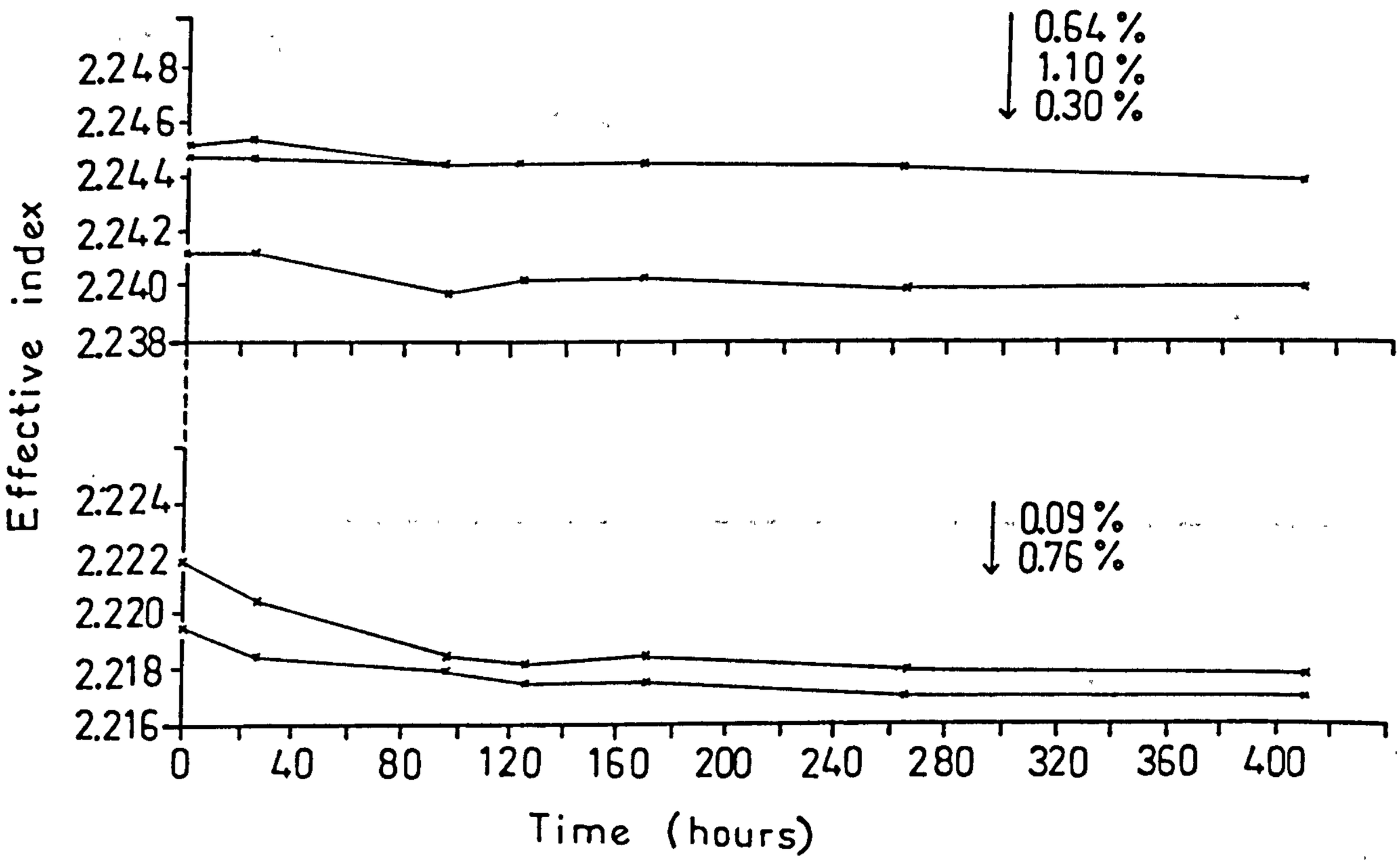

Figure 4.9. Variation In Effective Mode–Indices With Time (As A Function Of Mole–Fraction), For A Series Of X–Cut Dilute–Melt Proton–Exchanged Waveguides Produced At T=235°C For t=4hr (Table 4.3).

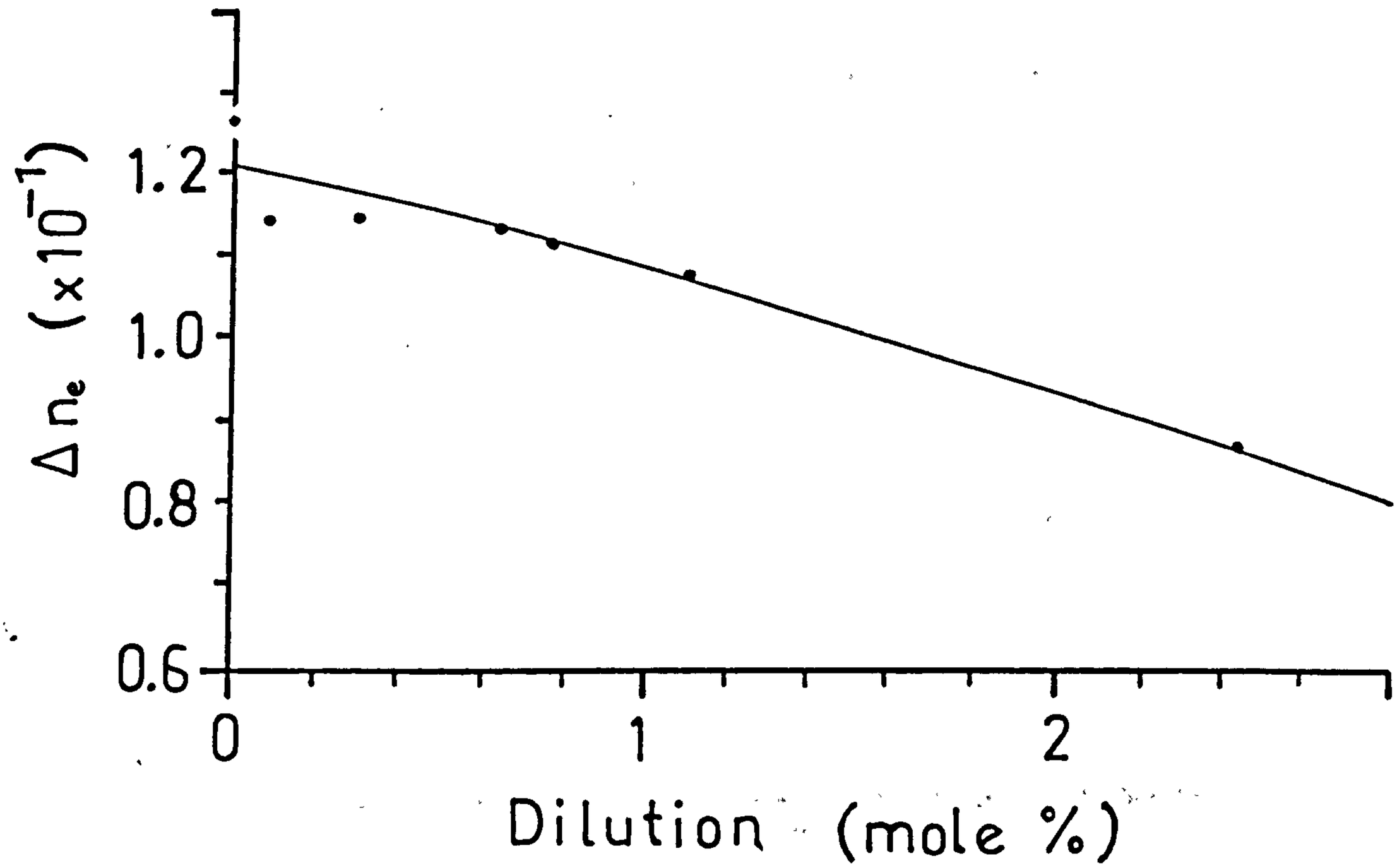

Figure 4.10. Variation In Waveguide (Surface) Index With Mole–Fraction, For A Series Of X–Cut Dilute–Melt Waveguides Produced At T=235°C (Table 4.3).

Sample	Annealing Temperature (°C)	Annealing Time	Step Index Δn_e	Depth (μm)
16X	–	– –	0.1175	0.71
"	250	30min	0.1128	0.82
"	"	1hr	0.1102	0.88
"	"	2hr 37min	0.0778	1.38
26X	–	– –	0.1154	0.71
"	250	30min	0.1097	0.76
"	"	1hr	0.1090	0.79
"	"	2hr 37min	0.0917	2.29
15X	–	– –	0.1156	1.6
"	320	15min	0.1082	1.86
"	"	1hr	0.1032	2.02
"	"	3hr 11min	0.0925	2.28

Table 4.5. Variation In Step–Index Change ($\lambda = 0.6329\mu$m) And Depths With Annealing Time, For X–Cut Dilute–Melt Waveguides.

Initial fabrication conditions were given in Tables 4.2 and 4.3.

the estimated values of Δn_e are somewhat variable, although this may be due to different values of substrate index assumed in the calculations. The reason why the effective index stability and waveguide (surface) refractive index should depend on the mole fraction of lithium benzoate added to the melt is, as yet, unclear. Similar results observed for annealed proton–exchanged waveguides (Section 4.2.3) were related to the removal of hydrogen–bonded OH–hydroxyl groups from the waveguiding layer. Therefore, investigating the infrared absorption spectra of dilute–melt waveguides should help in understanding why these effects are observed.

4.3.4. Infrared Absorption Spectra Of Dilute–Melt Proton–Exchanged Waveguides.

Infrared absorption spectra, superimposed with the waveguide fabrication time as a parameter, are shown in Figures 4.11a and 4.11b for the x–cut waveguides fabricated at T= 215°C using 0.28% and 1.04% mole fractions, respectively (Table 4.2).

It is evident from Figures 4.11a and 4.11b that, although both OH absorption bands at υ_{max}= 3505cm^{-1} and υ_{max}= 3250cm^{-1} are present, the relative intensity of the broad band is much smaller than would be expected for waveguides produced using neat benzoic acid under identical conditions (for example, compare Figures 4.11a and 4.11b with Figure 11 in Chapter 2). The higher the mole–fraction, the lower the relative magnitude of the absorption at υ_{max}= 3250cm^{-1}, indicating that the concentration of hydrogen–bonded OH in the waveguide is inversely proportional to the mole–fraction. The same relationship between the intensity of the hydrogen–bonded absorption band and the mole–fraction was observed in all the x–cut dilute–melt waveguides listed in Tables 4.2 and 4.3.

It has been shown in the preceeding sections that annealed and dilute–melt waveguides can have similar waveguide (surface) refractive indices and stable effective mode–indices, depending on the amount of annealing and the quantity of lithium benzoate added to the benzoic acid melt. The results of infrared spectroscopy indicate that hydrogen–bonded OH is removed by annealing and the extent of its formation is reduced by using benzoic acid melts containing large mole–fractions of lithium benzoate. It seems plausible, therefore, that the presence of hydrogen–bonded OH in proton–exchanged waveguides is associated with the undesirable effects which are observed.

4.4. ANNEALED DILUTE–MELT PROTON–EXCHANGED WAVEGUIDES.

Optical waveguide prism–coupling and infrared spectroscopic measurements were carried out after annealing the dilute–melt waveguides. Annealing

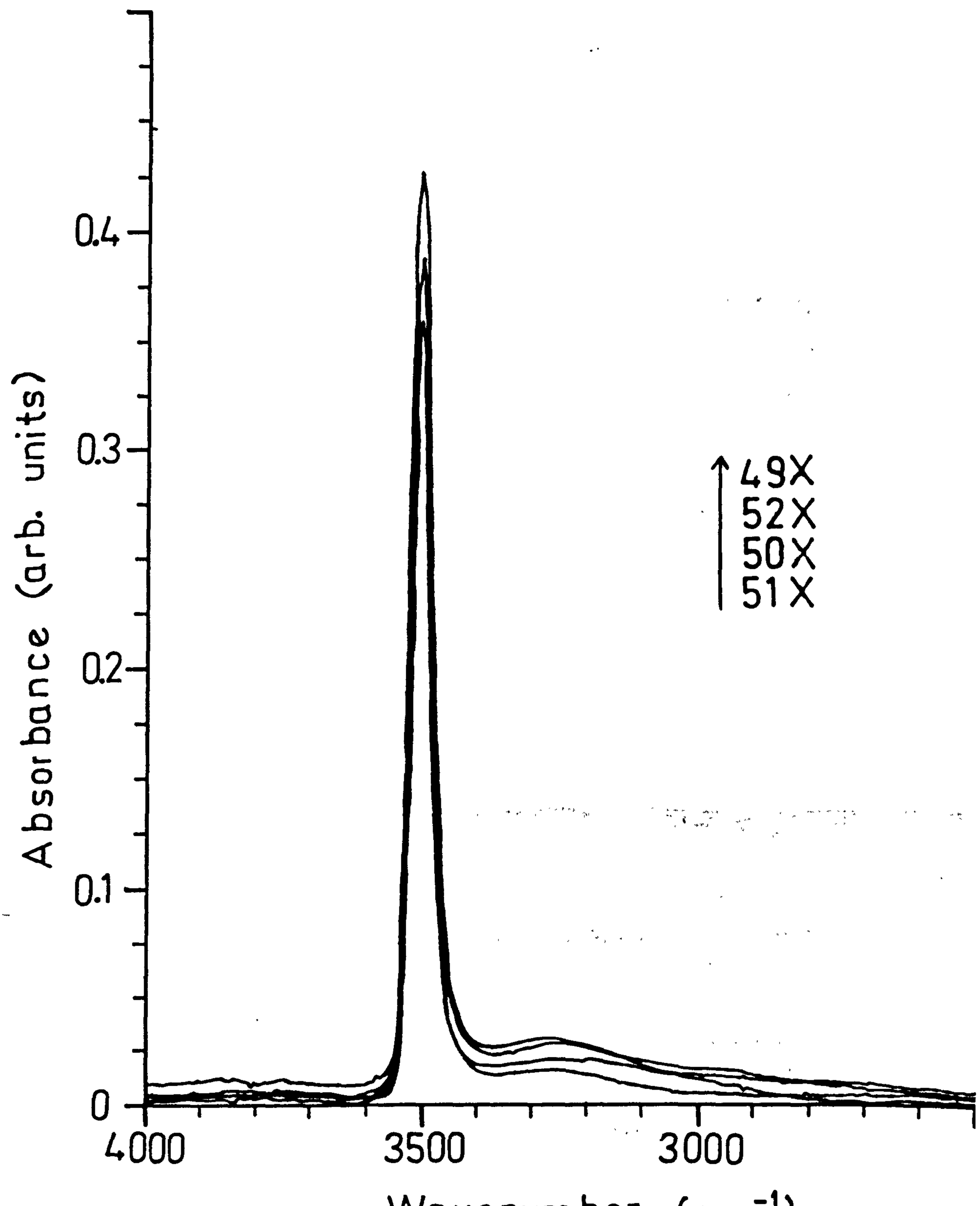

Figure 4.11a. Infrared Spectra, Superimposed As A Function Of Fabrication Time, Of The X–Cut Dilute–Melt Waveguides Produced At T= 215°C.

The Lithium Benzoate Mole–Fraction Was 0.28% (Table 4.2).

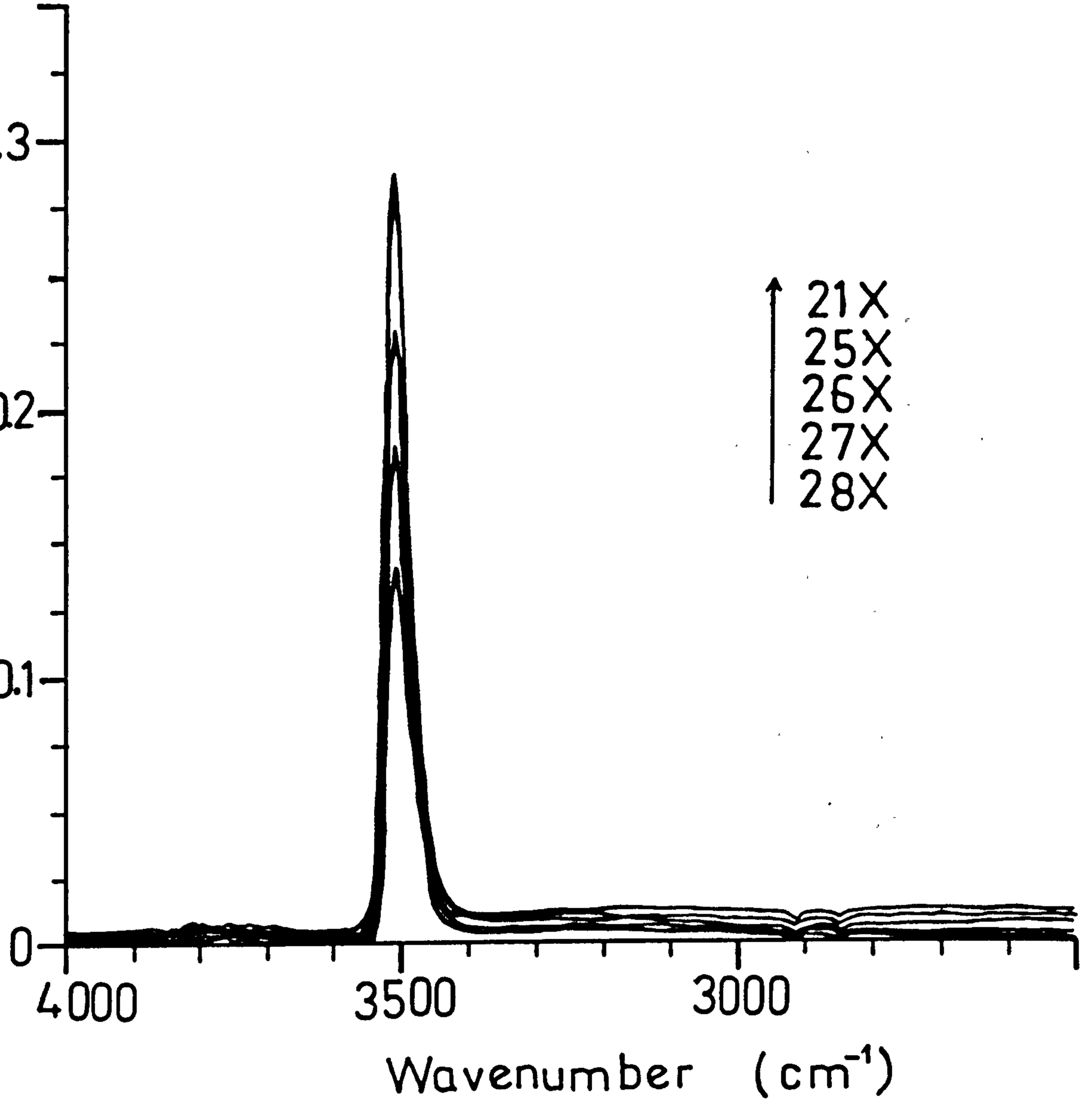

Figure 4.11b. Infrared Spectra, Superimposed As A Function Of Fabrication Time, Of The X–Cut Dilute–Melt Waveguides Produced At T= 215°C.

The Lithium Benzoate Mole–Fraction Was 1.04% (Table 4.2).

conditions were as described in Section 3.2.2. Table 4.5 lists the samples used (fabrication conditions given in Tables 4.2 and 4.3), annealing times and temperatures, and the waveguide indices and depths calculated after annealing.

No measurable changes were observed in the infrared spectra of any of the dilute–melt waveguides after they had been annealed, indicating no removal of OH. There were small changes in the refractive index profiles (Table 4.5), but the decreases in Δn_e were of the same magnitude as observed during the final stages of annealing the proton–exchanged waveguides (i.e. *after* the first 0.5hr). The changes in the refractive index profiles of annealed dilute–melt waveguides are not therefore due to removal of hydrogen–bonded OH but to diffusion of protons (originating from free OH) into the substrate. It is unlikely that protons forming free OH–hydroxyl groups outdiffuse into the atmosphere, since there would be an associated reduction in the absorbance bands.

4.5. HYDROGEN ISOTOPIC–EXCHANGE IN ANNEALED AND DILUTE–MELT PROTON–EXCHANGED WAVEGUIDES.

To test if annealed and dilute–melt proton–exchanged waveguides react with atmospheric water vapour, as do neat melt waveguides[20] hydrogen isotopic–exchange was investigated again. The proton–exchanged (neat–melt) waveguides Z8 (196.9°C, 2hr), ZZ5 (198.6°C, 4hr 25min), and X5 (198.6°C, 1hr) were annealed at 400°C for 0.5hr using the same conditions as outlined in Section 3.2.2. After processing, the latter waveguides, and the dilute–melt waveguides 9X (1.00%, 235°C, 8hr 8min) and 20X (0.49%, 215°C, 4hr), were exposed to D_2O vapour under vacuum (at room–temperature)*.

* *Isotopic–exchange experiments were carried out on samples ZZ5, X5, and 20X by Mr. G. Hay as part of his final year project, Department Electronic & Electrical Engineering, University of Glasgow, 1987, under the supervision of the author. Mr. Hays' work was repeated and verified by the author using samples Z8, 9X, 11X, and X11.*

The infrared absorption spectra of these waveguides indicated that *no* isotopic–exchange had taken place over the respective periods of time of 3hr, for samples 9X and 20X, 3.5hr, for samples X5 and Z8, and 43.5hr for sample ZZ5.

The infrared spectrum of ZZ5 (Figure 4.12), illustrates the fact that no isotopic–exchange was observed. The weak OD–bands at $\upsilon \simeq 2800 cm^{-1}$ in Figure 4.12 were due to the presence of D_2O vapour in the cell. A longer exposure time of two weeks was employed for another two samples, 11X (0.58%, 235°C, 1hr) and X11 (annealed, Table 4.1) but still no isotopic–exchange was observed.

The fact that hydrogen isotopic exchange has not been observed at room–temperature in annealed and dilute–melt waveguides may be related to the non–existence, or much weaker concentration, of hydrogen–bonded OH in these waveguides. This being true, the following isotopic exchange mechanism is proposed for *neat melt* waveguides: H from hydrogen–bonded OH exchanges with D from D_2O vapour; H from free OH then becomes hydrogen–bonded by exchanging with the D in the waveguide, the D then forming a free OH counterpart. The non–existence of hydrogen–bonded OH in annealed and dilute–melt waveguides would therefore imply that, at room–temperature, such waveguides are unable to react with D_2O vapour (and, therefore, atmospheric water vapour).

4.6. HIGH–TEMPERATURE HYDROGEN ISOTOPIC–EXCHANGE AND THE ROLE OF WATER VAPOUR DURING ANNEALING.

It has been shown[8,11] that the refractive index profiles of proton–exchanged waveguides annealed using both wet and dry O_2 were indistinguishable for annealing times of up to 20min. However, after further annealing (40min) there were marked differences: guides annealed in dry O_2 had lower waveguide (surface) refractive indices, although the depth of the guiding region did not depend on the annealing atmosphere. The removal of hydrogen–bonded OH would have occurred during the first 0.5hr of annealing in wet O_2, and, presumably, also when using dry O_2. Further changes in the refractive index profiles must therefore have

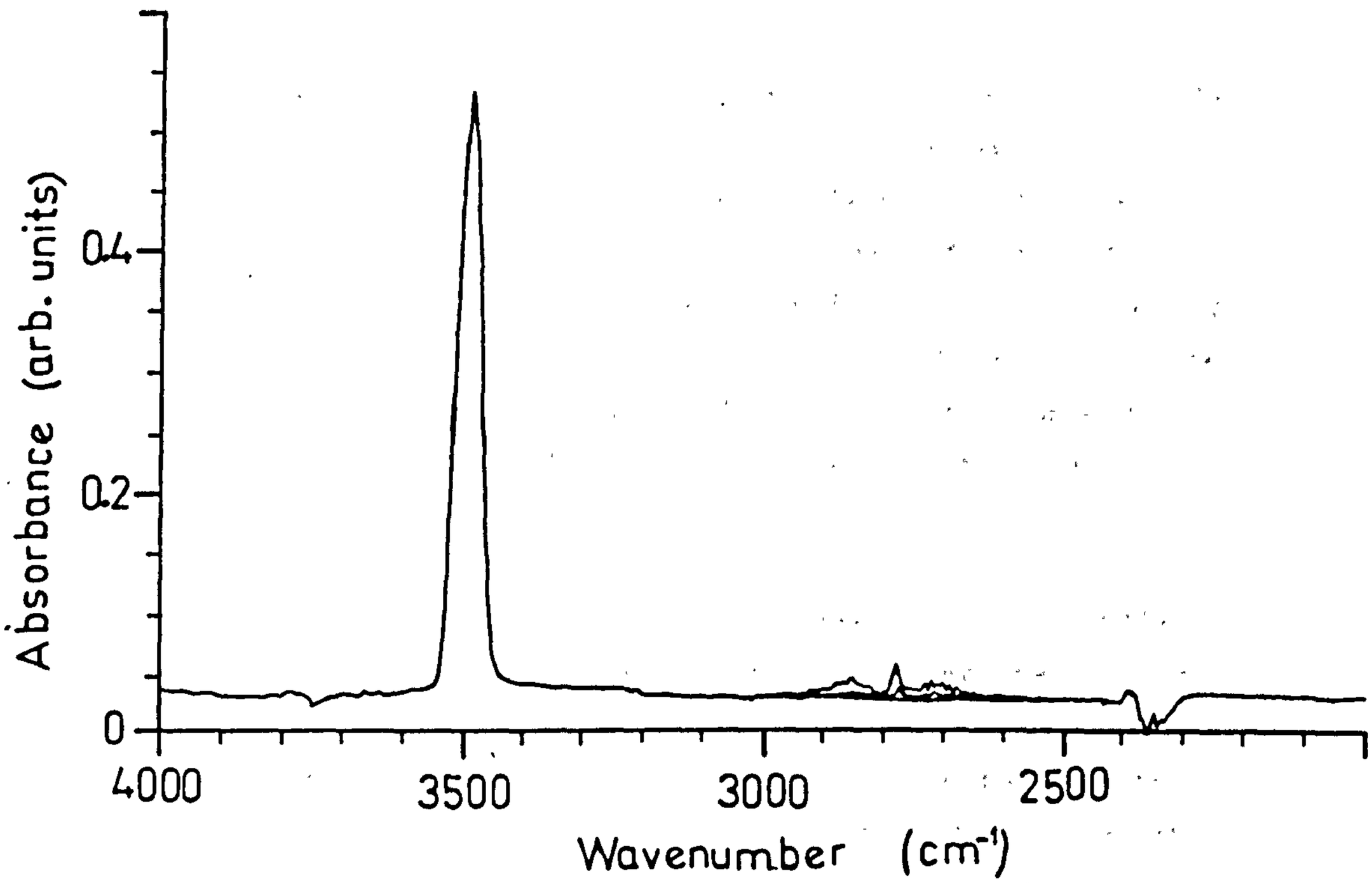

Figure 4.12. Infrared Absorption Spectrum Of A Z–Cut Proton–Exchanged Waveguide (ZZ5, T= 198.6°C, t= 4hr 25min), Recorded After Annealing And Subsequent Exposure To D_2O Vapour For 43.5hr.

been due to migration of protons (originating from free OH− groups) into the substrate, as discussed in Section 4.4. The weaker index profile of guides annealed in dry O_2, observed by Nutt[8], could be due to loss of the free OH− groups from the waveguide region. A method of testing for loss of free OH is to record infrared absorption spectra of waveguides before and after annealing in dry O_2.

The hydrogen isotopic exchange technique has been used to determine the effect of wet O_2 during annealing, by bubbling the O_2 gas through D_2O instead of H_2O and observing any changes in the OH and OD absorption bands. Proton−exchanged (neat−melt) x−cut waveguides XX3 (168.6°C, 15min) and XX13 (168.6°C, 1hr) were annealed at 320°C for 0.5hr in a an O_2 atmosphere, flowing at 1.575 litres/min through D_2O. The water temperature was 60°C and the gas bubbles passed through approximately 10cm of water. Infrared absorption spectra were recorded before and immediately after annealing.

From the infrared absorption spectrum of sample XX3 (Figure 4.13a) it can be seen that the hydrogen−bonded OH was removed after annealing. The sharp band at $\upsilon_{max}=3505cm^{-1}$ decreased significantly, with the growth of an OD counterpart at $\upsilon_{max}=2590cm^{-1}$. In the spectrum of sample XX13 (Figure 4.12b) the broad and sharp OH bands decreased substantially and the decrease was accompanied by the growth of OD counterparts.

The spectra of the waveguides were recorded again after eleven days of exposure to ambient atmosphere and showed *no* changes in the absorption band structures, indicating that, after annealing, no reverse isotopic−exchange occurred, i.e. the waveguides did not react with atmospheric water at room−temperature. Similar results to the above were obtained when dilute−melt and previously annealed (wet O_2) proton−exchanged waveguides were annealed using D_2O at the higher temperature of 375°C, although hydrogen isotopic exchange was not observed in these waveguides at room−temperature.

The presence of OD peaks in the spectra of samples XX3 and XX13 indicates that there was uptake of D from the wet annealing atmosphere

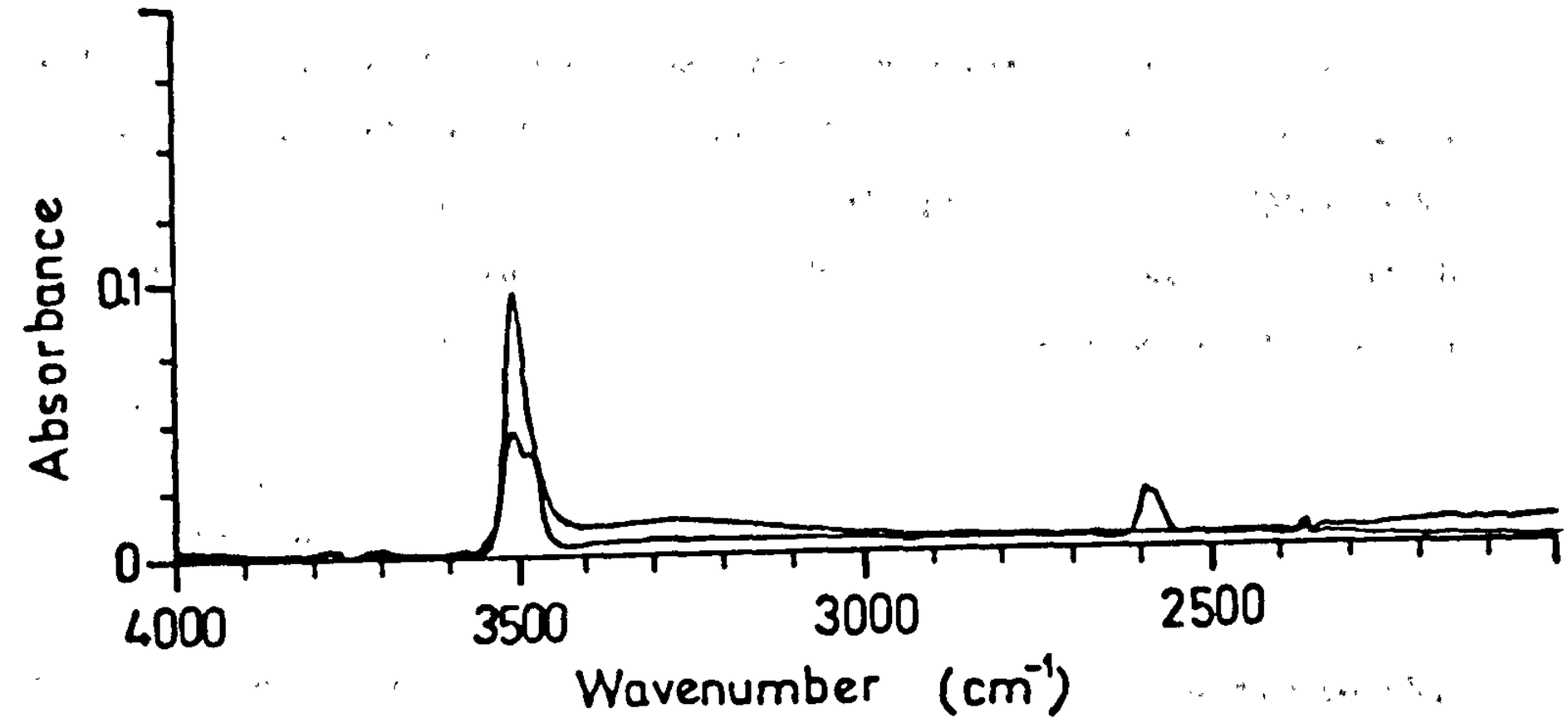

Figure 4.13a. Infrared Absorption Spectra Of An X–Cut Proton–Exchanged Waveguide (XX3, T=168.6°C, t=15min), Recorded Before And After Annealing In D_2O Vapour.

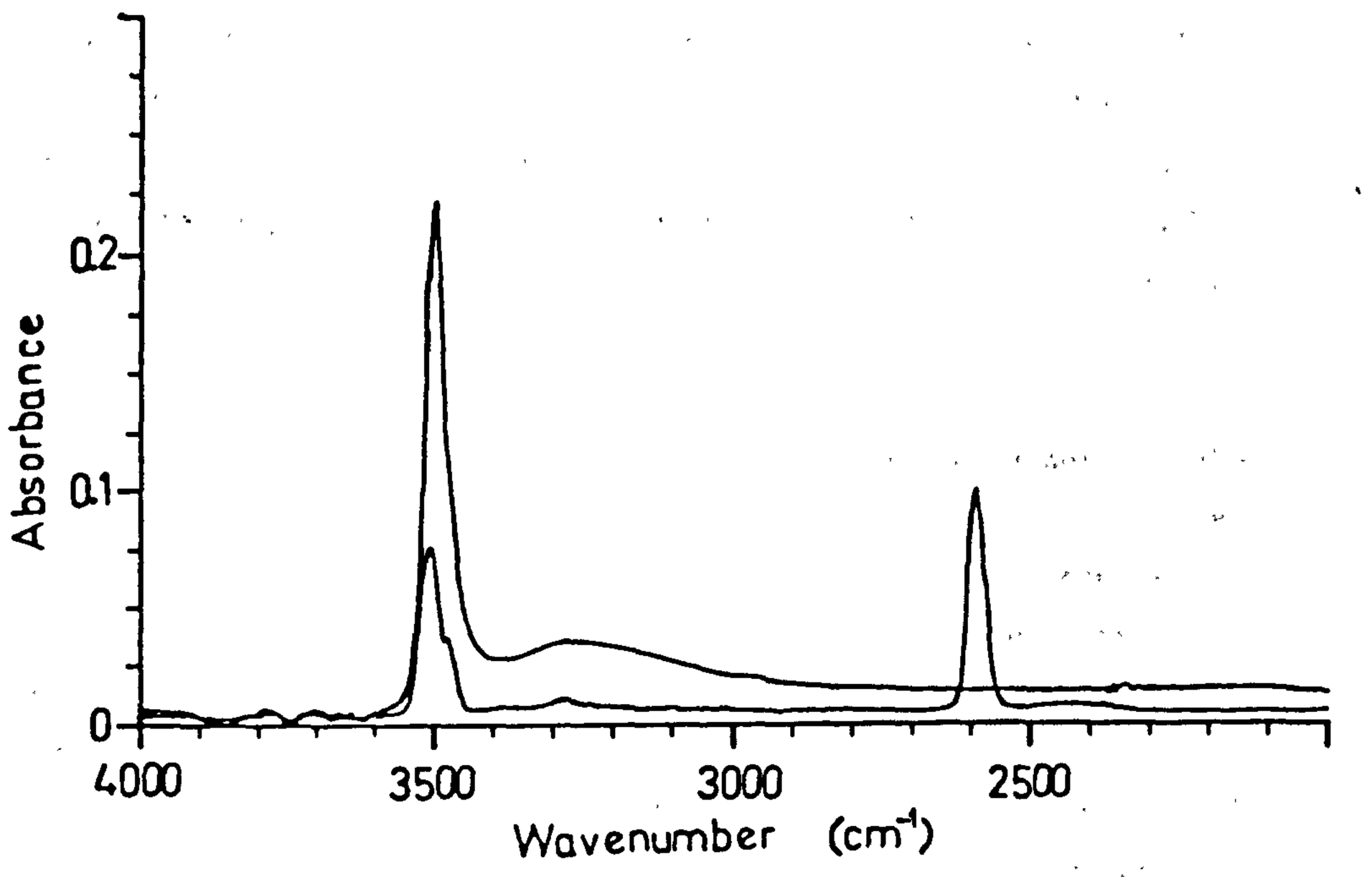

Figure 4.13b. Infrared Absorption Spectra Of An X–Cut Proton–Exchanged Waveguide (XX13, T=168.6°C, t=1hr), Recorded Before And After Annealing In D_2O Vapour.

with the loss of H from the waveguides. Therefore, when waveguides are annealed in wet O_2 (H_2O) there must be uptake of H from the water vapour in turn, suppressing any loss of H from the guide. Waveguides annealed in dry O_2 would be more likely to suffer loss of H, which might explain the differences in the refractive index profiles observed in references (8) and (11).

4.7. DISCUSSION.

It has been demonstrated using optical waveguide prism–coupler measurements and infrared spectroscopy that annealed and dilute–melt x–cut proton–exchanged waveguides can have very similar properties, depending on the amount of annealing and the quantity of lithium benzoate added to the benzoic acid melt. For example, after processing and at room–temperature, the resultant waveguide mode–indices do not vary with time, the waveguide (surface) index decreases as the lithium benzoate mole–fraction is increased and when the guide is annealed, the infrared absorption spectra are similar in that the broad absorption band at $\upsilon_{max}=3250cm^{-1}$ is either removed (annealing) or, the extent of its formation is reduced (dilute–melt), and *no* measurable hydrogen isotopic–exchange takes place at room–temperature. It is plausible, therefore, that the presence of hydrogen–bonded OH contributes to the undesirable effects found in proton–exchanged waveguides.

Annealing removes hydrogen–bonded OH, resulting in the removal of the broad absorption band at $\upsilon_{max}=3250cm^{-1}$. However, in the infrared spectra of unannealed x–cut samples recorded over a 2.5 year period, the broad absorption band was still present, indicating that the time–varying properties cannot be explained simply as the result of very long room–temperature annealing (since, as a consequence, one would expect the band to be eventually removed). Because hydrogen–bonded OH is removed after annealing, it is likely that during annealing, the protons which migrate into the substrate (causing the waveguide depth to increase) originate from free OH. The removal of hydrogen–bonded OH subsequently results in waveguides with stable optical properties.

In unannealed proton–exchanged (neat–melt) waveguides, the guiding layer is highly strained up to a depth which closely agrees with the

optically estimated depth[10,11]. It has been shown, using double–crystal x–ray analysis, that the lattice parameters in the guiding region are heavily modified from the lithium niobate values. For example, $\Delta a/a = 0.6\%$ (x–cut)[11]. However, after annealing there is a sharp decrease in the overall disorder present in the waveguides, as determined from Rutherford backscattering experiments[8,11].

Further, x–ray analysis reveals a decrease in the lattice strain after annealing[10]. Nuclear reaction measurements in x– and z–cut proton–exchanged waveguides have shown[10] that proton–concentration profiles change from a step–like distribution to a more graded–type profile after annealing. In consequence, the proton–concentration in the guiding layer is reduced[10].

Figure 4.14 shows double–crystal x–ray diffraction rocking curves for a series of x–cut samples proton–exchanged and then annealed for 30min at increasing temperatures*. As mentioned in reference (8), the data which can be obtained from double–crystal x–ray diffraction rocking curves are as follows:

(a) the sign of the strain (positive or negative, depending on which side of the main $LiNbO_3$ peak the secondary (satellite) peaks occur)

(b) the intensity of the secondary peaks, giving an indication of the amount of crystal which is strained

(c) the position of the secondary peaks relative to the main peak, giving an indication of the magnitude of the strain (the bigger the deviation, the higher the strain)

(d) the number and position of the secondary peaks, forming an overall picture of the total strain pattern.

* *Reproduced from Reference (10)*

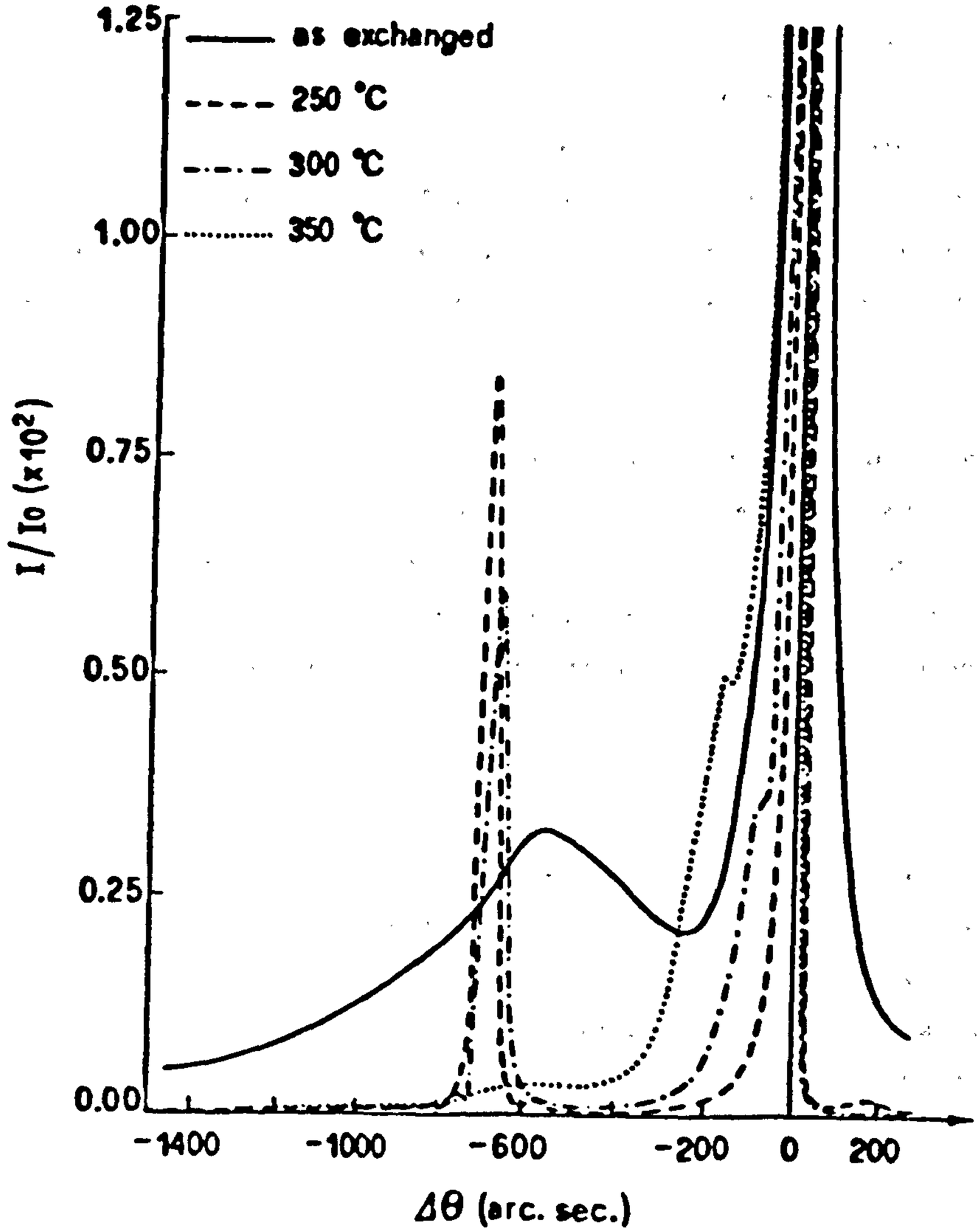

Figure 4.14. Double–Crystal X–Ray Rocking Curves For An X–Cut Proton–Exchanged Waveguide (180°C, 25min), Obtained Before And After Annealing.

The Waveguide Was Annealed For 30min At 250°C, 300°C, And 350°C In A Wet O_2 Atmosphere, Flowing At 2litre/min. (Reproduced From Reference (10)).

In Figure 4.14, the effect of the first annealing stage is reflected in the strong modification of the broad (complex strain pattern), low intensity satellite peak produced by the 'as–exchanged' sample, to the sharp and high peak observed after annealing at 250°C. The shape and position of the latter peak represents a unique and more well–defined positive strain ($\Delta a/a = 0.6\%$) with a step–like depth profile. Increasing the annealing temperature gradually reduces the satellite peak, and a tail appears at the left–side of the substrate diffraction peak. The latter feature indicates that the step–like strain distribution decreases in intensity and a region of lower strain appears in the lattice, most probably at the waveguide/substrate boundary.

In other words, the strain profile is smoothed out in a similar manner as the refractive index and proton–concentration profiles. The depth of the proton–exchanged sample in Figure 4.14 was shallow and, as a consequence, there was only one (broad) satellite peak in the x–ray rocking curves. However, for deeper waveguides, as many as four satellite peaks have been observed[10,11], and strains as high as 1.6% have been estimated for y–cut waveguides[6].

The initial rapid change in the waveguide refractive index profiles observed during annealing can be explained as follows: the pre–annealed waveguide, as well as having free OH–hydroxyl groups, has a large percentage of hydrogen–bonded OH–hydroxyl groups. On annealing the waveguide, the hydrogen–bonded OH is removed and free OH diffuses into the substrate. The waveguide becomes deeper, and the proton–concentration in the guiding layer is reduced.

It is possible that annealing also results in the migration of lithium ions within the guiding layer. If lithium ions from the substrate disperse within the waveguide, the resultant index profile would be weaker due to the increase in the percentage of lithium. A consequence of the removal of the hydrogen–bonded OH by annealing is that the complex series of strains observed prior to annealing disappear except for one well–defined strain.

The annealed waveguide can therefore be interpreted as consisting of different regions distinguished by different proton–concentrations. The largest strain is at the surface of the waveguide, where the proton–concentration is highest and the waveguide structure is closer to the cubic $HNbO_3$ structure. Moving deeper into the waveguide, the strain decreases because the proton–concentration decreases and the structure is closer to virgin lithium niobate.

The mode–index relaxation effect in unannealed proton–exchanged (neat–melt) waveguides is probably caused, in part, by the migration of of protons via hydrogen–bonding with surrounding oxygen anions. However, moving the protons from the guiding region into the substrate may require a higher temperature than room–temperature, where relaxation occurs.

Device instabilities such as the d.c. effect[21] may also be due to the presence of hydrogen–bonded OH–groups. The latter work showed[21] that applying a d.c. voltage of approximately 5 volts (either polarity) to a proton–exchanged stripe waveguide phase modulator resulted in a slow extinction of the guided mode, with time–constants of the order of one minute. Removing the d.c. voltage led to a slow recovery, whereas voltage reversal led to a much more rapid recovery. Such an effect might be caused by the movement of hydrogen–bonded OH (protons) under the influence of an applied electric field.

The distribution of hydrogen–bonded OH is initially uniform within the guiding layer (Figure 4.15A). On applying an electric field, electrostatic forces would redistribute the protons which form the hydrogen–bonded OH. These protons would be attracted by the negative electrode and repelled by the positive electrode (Figure 4.15B). The localisation of protons at the negative electrode might change the step–like refractive index/depth profile (Figure 4.15A) to a more complex profile (Figure 4.15B), perpendicular to the guide depth, resulting in mode extinction.

When the electric field is removed, there would be charge imbalance in the guiding region, producing a 'dipole–effect', and the protons would tend to migrate back to more favourable sites. Such electro–static effects

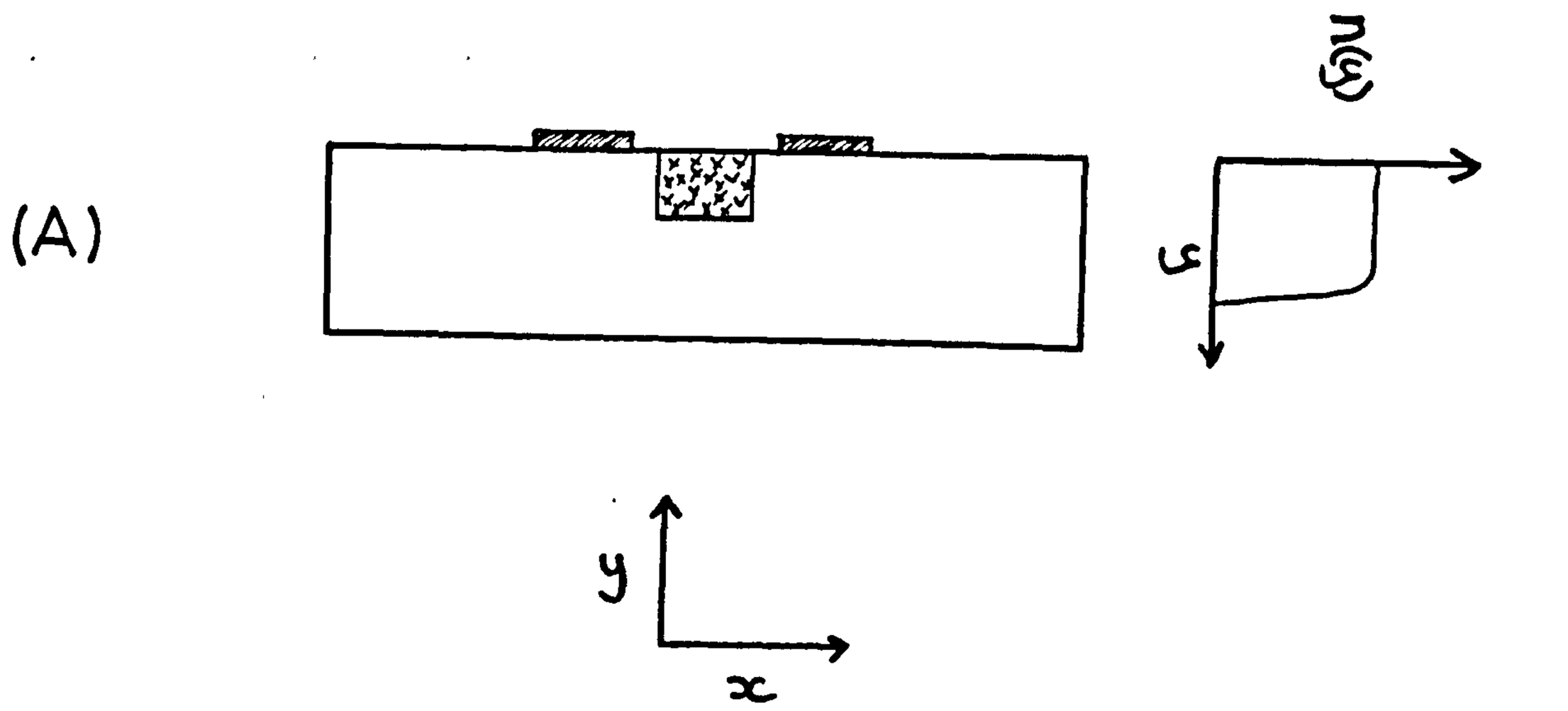

Figures 4.15A And 4.15B. Diagram Showing The Possible Effect On The Refractive Index Profile Of A Proton–Exchanged Strip Waveguide, Due To The Relocation Of Hydrogen–Bonded OH–Hydroxyl Groups On Applying A D.C. Electric Field.

A:– No Field Applied
B:– With A Field Applied

n(y) And n(x) Are The Refractive Index Profiles Along The Y– And X–Axis, Respectively.

have been applied to produce field–assisted proton–exchanged waveguides in lithium niobate[22]. Removing hydrogen–bonded OH by annealing or avoiding their formation by using dilute–melts should improve the performance of proton–exchanged electro–optic devices.

The migration of lithium ions from the substrate into the waveguide, together with migration of protons from the waveguide into the substrate, would, in effect, tend to return the distorted unit cell structure to that of virgin lithium niobate. This would explain why annealed waveguide devices have a restored electro–optic effect[9]. Wong reported[13] that the electro–optic effect in Mach–Zhender interferometric modulators produced by proton–exchange was preserved if dilute–melts were used. However, he noted that unintentional annealing took place during the deposition of SiO_2 buffer layers.

Minakata *et al*[16] reported that the value of the electro–optic coefficient r_{33} could be increased by using dilute–melts. The values quoted in the latter work[16] were: $r_{33}=3.3\times10^{-12}$m/V (neat–melt) and $r_{33}=3.6\times10^{-12}$m/V (1% mole–fraction). If lattice distortion is associated with the reduced electro–optic effect in proton–exchanged waveguides (Chapter 5), then there may indeed be an increase in r_{33} for dilute–melt proton–exchanged devices, since it has been shown[16] that the strain in the guiding region is lower in dilute–melt waveguides, i.e. in z–cut waveguides $\Delta c/c=0.45\%$, (neat–melt), and $\Delta c/c=0.25\%$ (2.5% mole–fraction).

It is likely that annealing has more effect on the electro–optic performance of proton–exchanged waveguide devices, since there is not only a reduction in the concentration of protons in annealed waveguides, but also possible migration of lithium ions from the substrate into the waveguide.

The electro–optic effect and propagation losses of annealed and dilute–melt proton–exchanged waveguides are the subjects of the work presented in Chapter 5.

REFERENCES.

(1) A. Yi–Yan, *Index Instabilities in Proton–Exchanged $LiNbO_3$*, Appl. Phys. Lett., 42(8), 633, (1983).

(2) J.L. Jackel, C.E. Rice, *Short– & Long–Term Stability in Proton–Exchanged Lithium Niobate Waveguides*, SPIE Vol. 460, Guided Wave and Optoelectronic Materials, 43, (1984).

(3) W.E. Lee, N.A. Sanford, A.H. Heuer, *Direct Observations of Structural Phase Changes in Proton–Exchanged $LiNbO_3$ Waveguides Using Transmission Electron Microscopy*, J. Appl. Phys., 59(8), 2629, (1986).

(4) N.A. Sanford, W.E. Lee, *Analysis of Proton–Exchanged Channel Waveguides in $LiNbO_3$*, SPIE Vol. 578, Integrated Optical Circiut Engineering II, 7, (1985).

(5) S.M. Al–Shukri, A. Dawar, R.M. De La Rue, A.C.G. Nutt, M. Taylor, J.R. Tobin, G. Mazzi, A. Carnera, C. Summonte, *Analysis of Annealed Proton–Exchanged Waveguides On $LiNbO_3$ By Optical Waveguide Measurements and Microanalytical Techniques*, Proceedings 7th Topical Meeting on Integrated and Guided Optics, Florida, 24–26 April, 1984, PD7/1..

(6) A. Campari, C. Ferrari, G. Mazzi, C. Summonte, S.M. Al–Shukri, A. Dawar, R.M. De La Rue, A.C.G. Nutt, *Strain and Surface Damage Induced By Proton–Exchange in Y–Cut $LiNbO_3$*, J. Appl. Phys., 58(12), 4521, (1985).

(7) M. De Micheli, J. Botineau, S. Neveu, P. Sibillot, D.B. Ostrowsky, *Independent Control of Index Profiles in Proton–Exchanged Lithium Niobate Waveguides*, Opt. Lett. 8(2), 114, (1983).

(8) A.C.G. Nutt, PhD Thesis, University of Glasgow, (1985).

(9) R. Chen, C.S. Tsai, *Thermally Annealed Single-Mode Proton-Exchanged Channel Waveguide Cut-Off Modulator*, Opt. Lett., 11(8), 546, (1986).

(10) C. Canali, A. Carnera, P. Mazzoldi, R.M. De La Rue, *Lithium Niobate Optical Waveguides Fabricated By Titanium Indiffusion and Proton-Exchange: Process, Performances, and Stability*, SPIE Vol-517, Integrated Optical Circuit Engineering, (1984).

(11) C. Canali, A. Carnera, G. Mazzi, P. Mazzoldi, R.M. De La Rue, *Fabrication, Process, Performances, and Stability of Titanium Indiffused and Proton-Exchanged $LiNbO_3$ Optical Waveguides*, IEEE International Workshop On Integrated Optical & Related Technologies For Signal Processing, (1984).

(12) M.N. Armenise, S.M. Al-Shukri, A. Dawar, R.M. De La Rue, A.C.G. Nutt, *Optical Characterisation of Proton-Exchanged and Titanium Indiffused Proton-Exchanged Slab Waveguides on Lithium Niobate*, IEEE International Workshop On Integrated Optical & Related Technologies For Signal Processing, Tech. Digest, 21, September, 1984, Florence, Italy.

(13) K.K. Wong, *An Experimental Study of Dilute-Melt Proton-Exchanged Waveguides in X- and Z-Cut Lithium Niobate*, GEC J. Res., 3(4), 243, (1985).

(14) J.L. Jackel, C.E. Rice, J.J. Veselka, *Compositional Control in Proton-Exchanged $LiNbO_3$ Waveguides*, Elect. Lett., 19(10), 387, (1983).

(15) M. Minakata, K. Kumagai, S. Kawakami, *Studies On Lattice Constant Changes and Electro-Optic Effects in Proton-Exchanged $LiNbO_3$ Optical Waveguides*, 1st Optoelectronic Conference, Technical Digest, July, 1986, Tokyo.

(16) M. Minakata, K. Kumagai, S. Kawakami, *Lattice Constant Changes and Electro-Optic Effects in Proton-Exchanged $LiNbO_3$*, Appl. Phys. Lett., 49(16), 992, (1986).

(17) C.E. Rice, *The Structure and Properties of* $Li_{1-x}H_xNbO_3$, J. Solid State Chem., 64, 188, (1986).

(18) C.E. Rice, J.L. Jackel, *$HNbO_3$ and $HTaO_3$: New Cubic Perovskites From $LiNbO_3$ and $LiTaO_3$*, J. Sol. State Chem., 41, 308, (1982).

(19) V. Hinkov, E. Ise, *Control of Birefringence in Ti:$LiNbO_3$ Optical Waveguides By The Proton-Exchange of Lithium Ions*, J. Lightwave Tech., LT-4(4), 444, (1986).

(20) A. Loni, R.M. De La Rue, J.M. Winfield, *Proton-Exchanged Lithium Niobate Planar Optical Waveguides: Chemical and Optical Properties and Room-Temperature Hydrogen Isotopic-Exchange Reactions*, J. Appl. Phys., 61(1), 64, (1987).

(21) K.K. Wong, R.M. De La Rue, S. Wright, *Electro-Optic Waveguide Frequency Translator in $LiNbO_3$ Fabricated By Proton-Exchange*, Opt. Lett., 7(11), 546, (1982).

(22) C.W. Pitt, G. Burbie, Tat Wan, *Electric Field Assisted Proton-Exchange Waveguides in Lithium Niobate*, Elect. Lett., 23(19), 988, (1987).

CHAPTER 5

A Study Of Propagation Losses And The Electro-Optic Effect In Proton-Exchanged, Titanium-Indiffused, And Bulk Lithium Niobate.

5.1. INTRODUCTION.

Successful utilisation of guided–wave devices in practical systems requires that the device design be optimised with respect to a number of constraints, e.g. cost, material–processing and, perhaps the most important, actual device performance. As a choice of substrate material for integrated optical devices, lithium niobate has distinct advantages over other materials[1], since it has a relatively high bulk electro–optic effect, and optical waveguides can be fabricated in the material using a number of different techniques.

Active integrated optical devices based on waveguide fabrication by *any* process should ideally have low attenuation (<1db/cm) and should have, for example, good light modulation characteristics. In the following sections a detailed study of the latter two requirements is presented, with a particular emphasis on the properties of proton–exchanged waveguides. A process by which very low losses and good electro–optic light modulation can be achieved (involving the use of dilute–melts and post–fabrication annealing), is also described. The majority of the present work has been carried out at $\lambda = 0.6328\,\mu m$ and propagation losses have been studied more briefly at $\lambda = 1.15\,\mu m$.

5.2. PROPAGATION LOSSES ($\lambda = 0.6328\,\mu m$) OF ANNEALED X– AND Z–CUT PROTON–EXCHANGED WAVEGUIDES PRODUCED USING NEAT AND DILUTE BENZOIC ACID MELTS.

5.2.1. Introduction.

One of the most important basic properties one has to consider when making a choice between different waveguide technologies for device fabrication is how much the guided radiation will be attenuated within the material. Attenuation within a waveguide can be described by the equation:

$$I(y) = I_o \exp(-\alpha y) \quad \ldots\ldots\ldots\ldots\ldots\ldots (1),$$

where I(y) is the intensity of light at a distance y (cm) along the

propagation direction, I_0 is the intensity at y= 0, and α (cm^{-1}) is the waveguide attenuation coefficient. The attenuation is often measured in *decibels/ cm*, defined by:

$$dB/cm = 10\log_{10}[(I(y=1cm)/I_0)].....(2).$$

5.2.2. A Review Of Loss– Measuring Techniques.

A number of interesting techniques are available to measure attenuation in waveguides. One of the most basic (and unattractive) is the cut– back method[2]. More often used when cleaving of the waveguide material is possible (for example, in semiconductor waveguides), the cut– back method involves cutting sections of the material away, each time measuring the intensity of light coming out of the shortened waveguide. The end face of the waveguide must be polished after every cut. Because of the destructive nature of the cut– back method, it is not often used.

Several workers have measured scattered light profiles in waveguides using a single fibre– optic probe to scan the along the light streak[3]. By scanning transversely and longitudinally, a two– dimensional representation of the attenuation can be constructed. However, the optical fibre must be accurately aligned along the direction of the propagating beam and maintained at a constant distance from the surface of the waveguide. The latter problems can be avoided[4] by utilising an optical fibre bundle to image the light away from the waveguide. For the latter case, propagation losses can be determined by scanning along the image with a detector. Methods of estimating propagation losses using optical fibres require a large amount of scattering out of the waveguide plane.

Another method of estimating losses is to image the light scattered from the waveguide using a video camera detection system[5]. The whole of the light streak can then viewed on a television monitor. The peak intensity variation along the streak can be ascertained from the image by scanning along the propagation direction and the loss value is directly aquired from the longitudinal change in intensity. One– dimensional scanning requires setting the sampling line precisely along the streak. However, this problem can be avoided by scanning transversly, i.e. *across*

the light streak. Repeating the procedure at different points along the guide enables a two-dimensional map of the intensity distribution in the waveguide to be constructed.

The technique can be enhanced by spinning a thin-film of poly(methylmethacrylate) which contains a small amount of fluorescent dye onto the surface of the waveguide[6]. The intensity of the unguided fluorescent light is ideally proportional to the optical field intensity in the waveguide. Different dyes absorb at different wavelengths. One such dye, which has been successfully used with potassium ion-exchanged glass[6] waveguides and titanium-indiffused waveguides[7], is Nile Blue A perchlorate[8], which absorbs light centred at $\lambda = 0.63\mu m$ and re-emits at $\lambda = 0.69\mu m$. The main disadvantage of using the latter technique is the expense of the dye (typically a few hundred pounds for approximately 50g of dye). Other adverse factors are that the presence of the dye may modify the properties of the waveguide, and the method is not applicable at any of the wavelengths of major technological interest (as yet).

Obviously the best method of measuring attenuation in waveguides is to measure the transmitted power as a function of the length of the guide. Such measurements can be performed accurately only if the input and output coupling coefficients are kept constant for every measurement (as should also be the case in all of the above methods). The change in length along the waveguide has to be accomplished without disturbing the input coupling, i.e. without taking the guide out of the experimental set-up.

For waveguides with a refractive index of less than 2.0, measurements can be made utilising a sliding output prism[9,10] contacted onto the waveguide with an index-matching fluid. The output signal at different points along the waveguide can then be processed using a logarithmic amplifier, the recorded signal subsequently being linear with length along the waveguide. However, of the index matching fluids currently available, the largest refractive index is approximately 2.0. The refractive index of proton-exchanged waveguides is of the order of 2.328, and so the sliding-prism method cannot be used.

When no suitable index matching fluid is available, a fairly reliable estimate for the attenuation can be achieved by using a clamped output prism to measure the transmitted signal at a number of points along the length of the guide, i.e. the two-prism technique[11]. The difficulty with this approach is that the output coupling coefficient must be the same at every measurement point. Two methods have been proposed which should enable attenuation measurements to be made independent of the output coupling efficiency at individual observation points: the three-prism technique[12], and the modified three-prism technique[13].

The three-prism technique involves the use of fixed input and output prisms placed at each end of the waveguide, with a third (middle) prism which is moved along the waveguide. It is easily shown that the change in intensity along the guide for this arrangement can be written in the form[12]:

$$I(y) = P_2 P_{03} / (P_{03} - P_3) \quad \ldots\ldots\ldots\ldots (3),$$

where P_{03} is the intensity of the signal coupled out by the end prism with *no* middle prism, P_3 is the intensity coupled out by the end prism with the middle prism clamped on at a position y along the guide, and P_2 is the intensity coupled out by the middle prism at this point. By measuring the initial power coupled out by the end prism and the subsequent powers coupled out in the presence of the middle prism, the value of I(y), and hence the attenuation coefficient α, can be calculated.

The modified three-prism technique is essentially identical to the three-prism technique, except that a *symmetrical* middle prism is used, and light is coupled into the waveguide at *either end* via two fixed end prisms. Light from the opposing beams is coupled out via the symmetrical prism. The attenuation for this arrangement is given by[13]:

$$dB/cm = (5/\Delta y) \log_{10} (P_1' P_2 / P_1 P_2') \quad \ldots\ldots\ldots\ldots (4),$$

where Δy is the displacement of the middle prism from position 1 to position 2, and P_1', P_1, P_2', P_2 are the intensities coupled out by the middle prism from positions 1 and 2, respectively. Only two points are

required to measure the attenuation.

The modified three–prism method is complicated to set–up, since the incident beam has to be split into two equal intensity beams and mirrors have to be used to direct one of the split beams onto the face of the other prism. The mirrors have to be precisely aligned so that the correct coupling angle for mode–excitation is achieved. The mirrors reduce the intensity of the reflected beam and, once the beam has been attenuated within the waveguide, it is difficult to detect the output signal. The method is therefore unsuitable for high–loss waveguides. Another adverse factor is the assumption that a measurement between two points is a good representation of the attenuation along the *whole* of the waveguide. If the attenuation along the guide is non–uniform (due, e.g. to localised scattering regions), the method could be unreliable.

Both the three–prism, and modified three–prism methods were used by the author in an attempt to calculate propagation losses in proton–exchanged waveguides, without any success. The particular problem encountered in using the three–prism method was that once the middle prism had been clamped onto the surface of the waveguide, the intensity distribution at the end of the guide (measured by clamping the end prism to different points, perpendicular to the propagating beam axis, and detecting the light coupled out) was of the form depicted in Figure 5.1. Figure 5.1 suggests that the propagating beam diverges into two components which travel at opposite angles with respect to the initial input direction. A similar effect was observed by Duffy[14] when he investigated prism coupling into y–cut proton–exchanged planar waveguides. His observations showed that when the waveguide was rotated about a normal to the substrate plane (i.e. off–axis propagation) the guided–light split into two distinct beams.

The reason for the apparent divergence is unclear, but it may be that the clamping force of the middle prism (exerted from the back face of the waveguide by a screw) is sufficient to cause a local change in waveguide refractive index via the elasto–optic effect. If the pressure point is situated near to the propagating beam axis, the small stress present could cause the light to split into two components. Although the

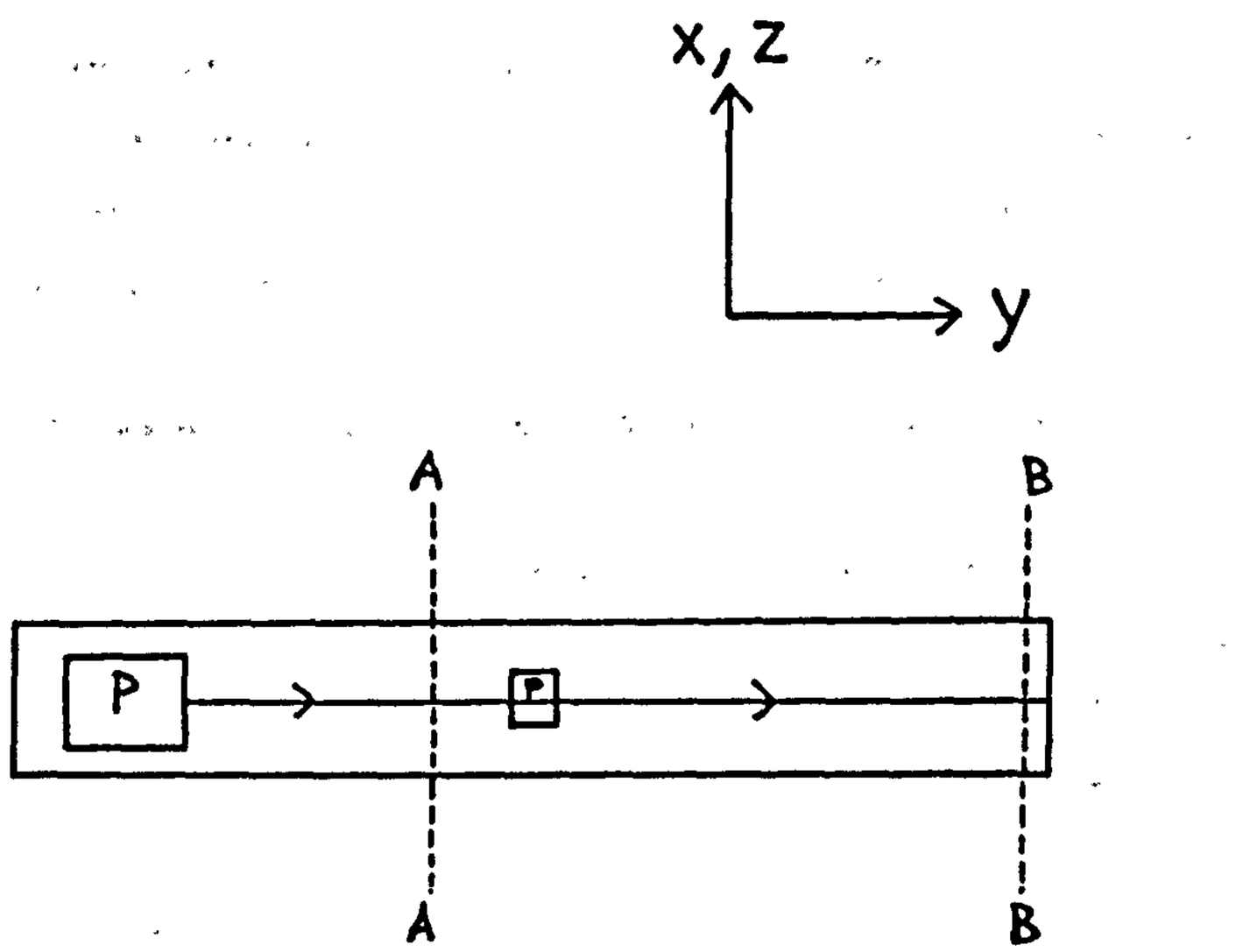

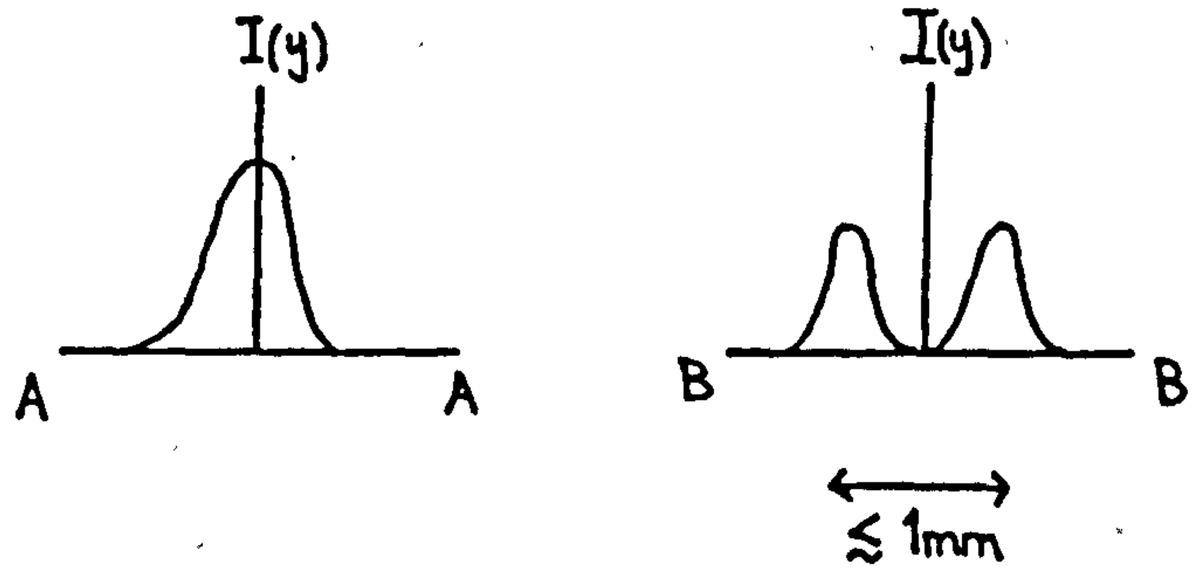

Figure 5.1. Suggested Transverse Intensity Distribution Observed By Clamping An Output Prism To A Proton–Exchanged Waveguide (P– Prism).

modified three–prism technique avoids the latter problem, it is difficult to arrange experimentally. Because of the afore–mentioned difficulties, the two–prism method was adopted. In the following section, a successful and reproducible attempt at measuring propagation losses in proton–exchange waveguides is described, the processing conditions being ultimately optimised to realise waveguides with very low losses (<1db/cm).

5.2.3. Experimental Set–Up And Waveguide Preparation.

The light was mechanically chopped at 1kHz for the purpose of detection and subsequently prism–coupled into the waveguide. The waveguide was placed on a PTFE slab so that a constant position was maintained at each measurement point. A small–base output prism (3mm square) was clamped to the waveguide and the output signal was detected using a photodetector, amplified, and observed using an oscilloscope. The (x,y,z,θ,φ)–stages of the prism–coupling rig were adjusted to optimise the signal at the detector. The pressure on the input prism was increased slowly until the amplitude of the signal on the oscilloscope had reached a maximum, indicating that the maximum input coupling efficiency had been achieved. Any further increase in pressure caused the signal at the detector to decrease. It seems plausible that this decrease was due to a change in the propagation constant of the excited mode, probably via the elasto–optic effect.

The output prism was then removed and clamped to the first measurement point. By using the small–base output prism, the clamp could be placed so that the position of the clamping coincided with the transverse peak intensity in the waveguide. No further adjustments of the translational stages were required if the output prism had been clamped to the peak intensity position. The pressure on the output prism was slowly increased until the amplitude of the signal on the oscilloscope reached a maximum, indicating that the maximum output coupling efficiency had been achieved. The signal was recorded, the output prism was moved along to the next point, and the procedure was repeated.

The coupling point of the output prism should always be at the centre of the transverse intensity distribution. This was easily checked, since altering

the height of the prism–coupling rig caused the amplitude at the detector to increase or decrease, depending on whether the rig was raised or lowered. If the correct position was not achieved, the output prism had to be removed and placed at the required coupling point so that the amplitude at the detector was maximum. The distance along the waveguide (between the edges of the two prisms) was measured with a thin strip of graduated (millimetre) graph paper. With practise the whole operation became relatively quick and easy.

Waveguides were produced in x– and z–cut substrates using neat and dilute benzoic acid melts. All the waveguides were fabricated at an acid temperature of 235°C and were 45mm long. To observe what effect melt–dilution had on propagation losses, different amounts of lithium benzoate were added to the melts, in the range 0% to 1.1%. Mono–mode waveguides were used, to avoid problems associated with inter–modal coupling via scattering. In each case the target waveguide depth was 0.5μm. The results of Chapter 4 were used to estimate the effective diffusion coefficients 'D(T)' expected at 235°C. Having calculated these, the fabrication times 't' required to achieve the target depth were estimated using the standard relationship

$$d = 2[D(T)t]^{1/2} \quad \ldots\ldots\ldots\ldots (5),$$

which was given in Chapter 2.

Immediately after proton–exchange, the waveguide propagation losses were measured. Six output coupling points were used for each waveguide. The measurements were repeated six times so that an average value of the attenuation could be calculated, with the error taken to be the standard deviation. The waveguides were then annealed at 275°C for 30min, 375°C for 15min, and 375°C for 26min, in a flowing wet O_2 atmosphere. The flow–rate was 1.575 litre/min and the water temperature was 60°C. The waveguide losses were re–measured after each stage of annealing. The fabrication times, lithium benzoate mole–fractions, annealing conditions, and the measured loss values are given in Table 5.1 and Table 5.2 for x– and z–cut waveguides, respectively.

5.2.4. Results.

Figures 5.2a, b and 5.3a, b are plots of the natural logarithm of the output signal as a function of distance for two of the samples used, one x–cut and one z–cut. A linear–regression program was used to estimate the equation of the best straight line through the points, the gradient of the line being the value α in Equation (1). Equation (2) was then used to estimate the losses in dB/cm.

Waveguides X4L and X2L were single–mode after the first stage of annealing, and all the waveguides supported two modes after the second and last annealing stages. The waveguide (surface) refractive indices and depths were estimated using the normalised dispersion equations (Chapter 2). The waveguide (surface) indices and depths, and the estimated losses, are given in Table 5.1 and Table 5.2. Because only two modes were supported in the annealed waveguides, accurate waveguide refractive index profiles could not be determined by the IWKB approximation. However, after comparing the annealing conditions and initial waveguide depths with those used for the annealed waveguide studies in Chapter 4, it was assumed that the refractive index profiles of the annealed waveguides used in the present study remained quasi–step–like.

The loss values quoted for the annealed waveguides are those of the *first order mode.* Figure 5.4 shows a comparison between the intensity distributions of the two modes supported in the x–cut sample (XL1) after the final stage of annealing. For this, and all the annealed waveguides, the fundamental mode (m=0) was more lossy than the first order mode (m=1), which is contrary to similar observations in unannealed waveguides[14]. A possible explanation for this effect (with reference to the discussion in Chapter 4) is that the energy distribution of the fundamental mode was localised within a region of higher strain. No attempt was made to measure fundamental mode losses, since they were so high that the modes would be of no practical use. However, the fundamental mode losses were estimated to be >18dB/cm*.

*My thanks to Prof. R.M. De La Rue for helping with this calculation.

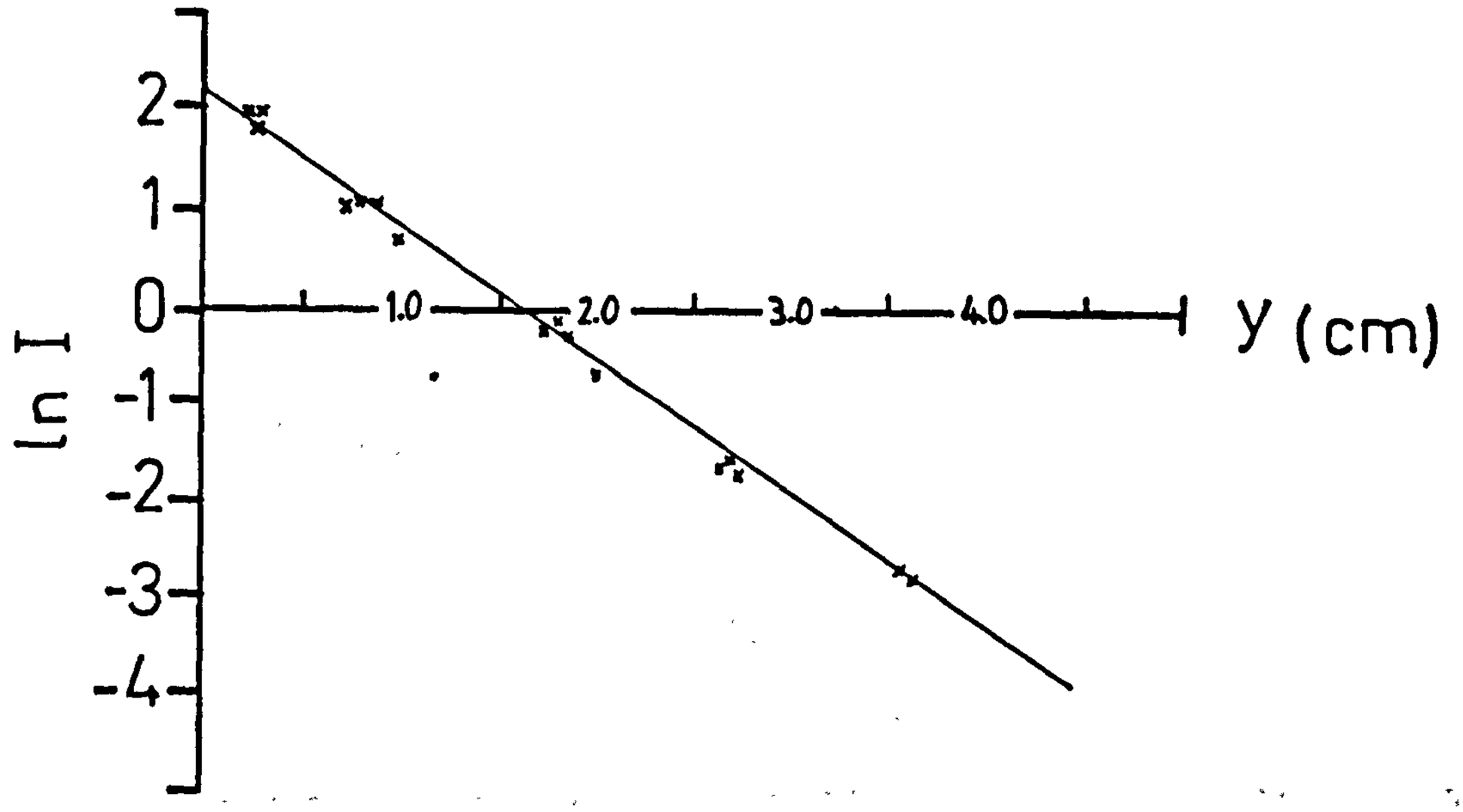

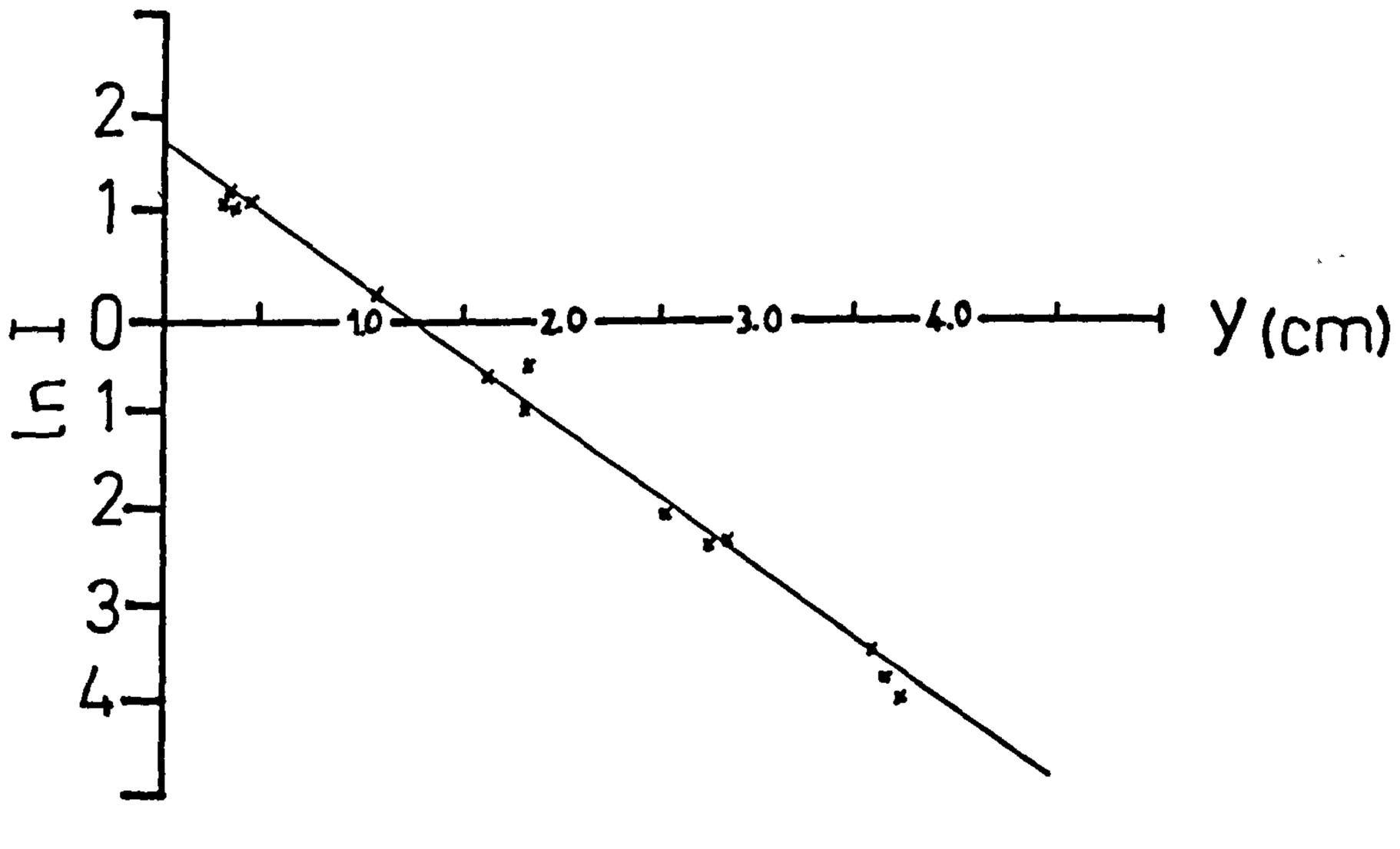

Figure 5.2a. Logarithm Of The Output Signal (Volts) As A Function Of Waveguide Length, Before (Above) And After (Below) Annealing At 275°C For 30min *(The Sample Depicted (X2L) Was Fabricated At 235°C For 30min Using A 0.89% Mole-Fraction).*

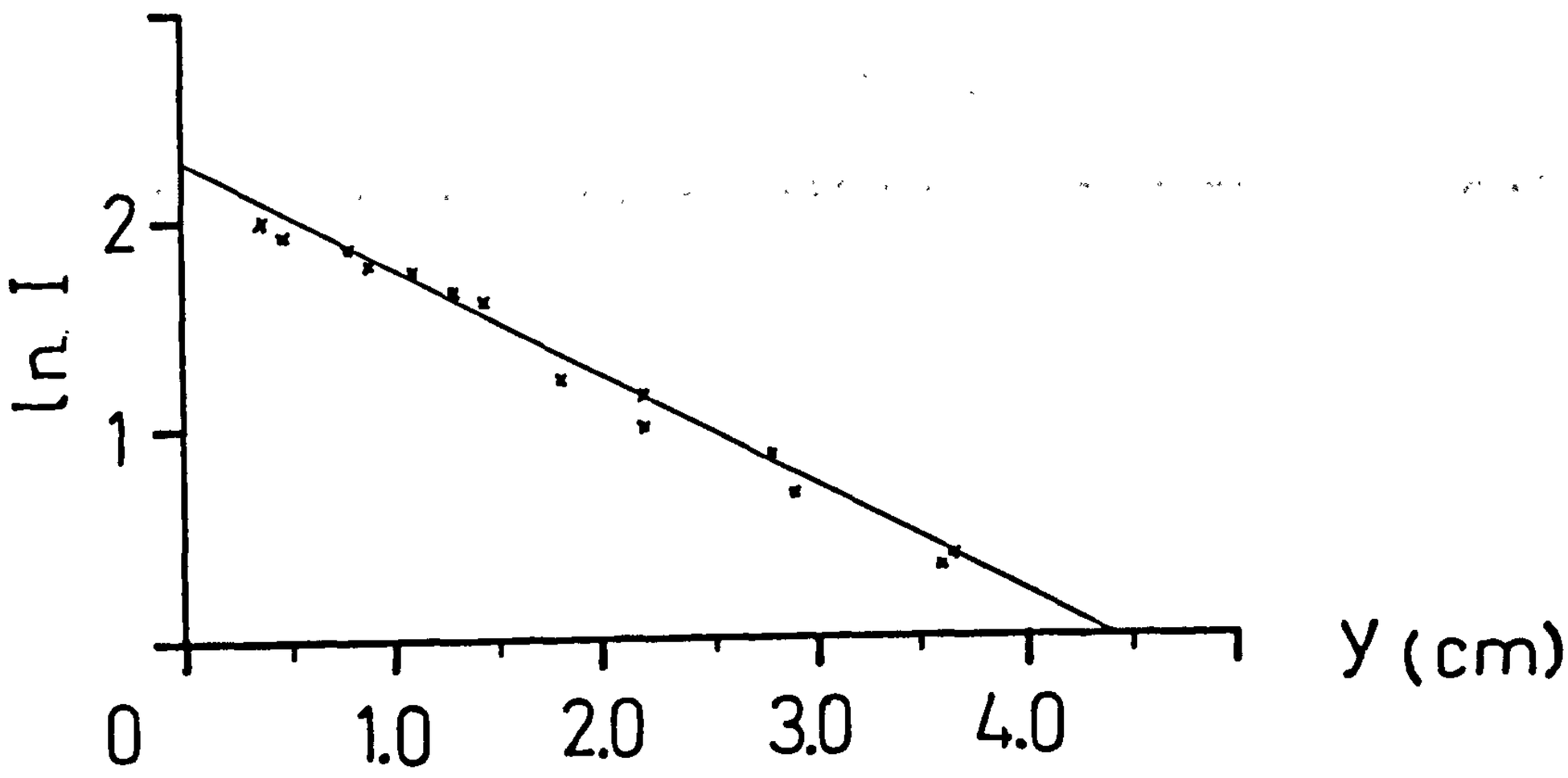

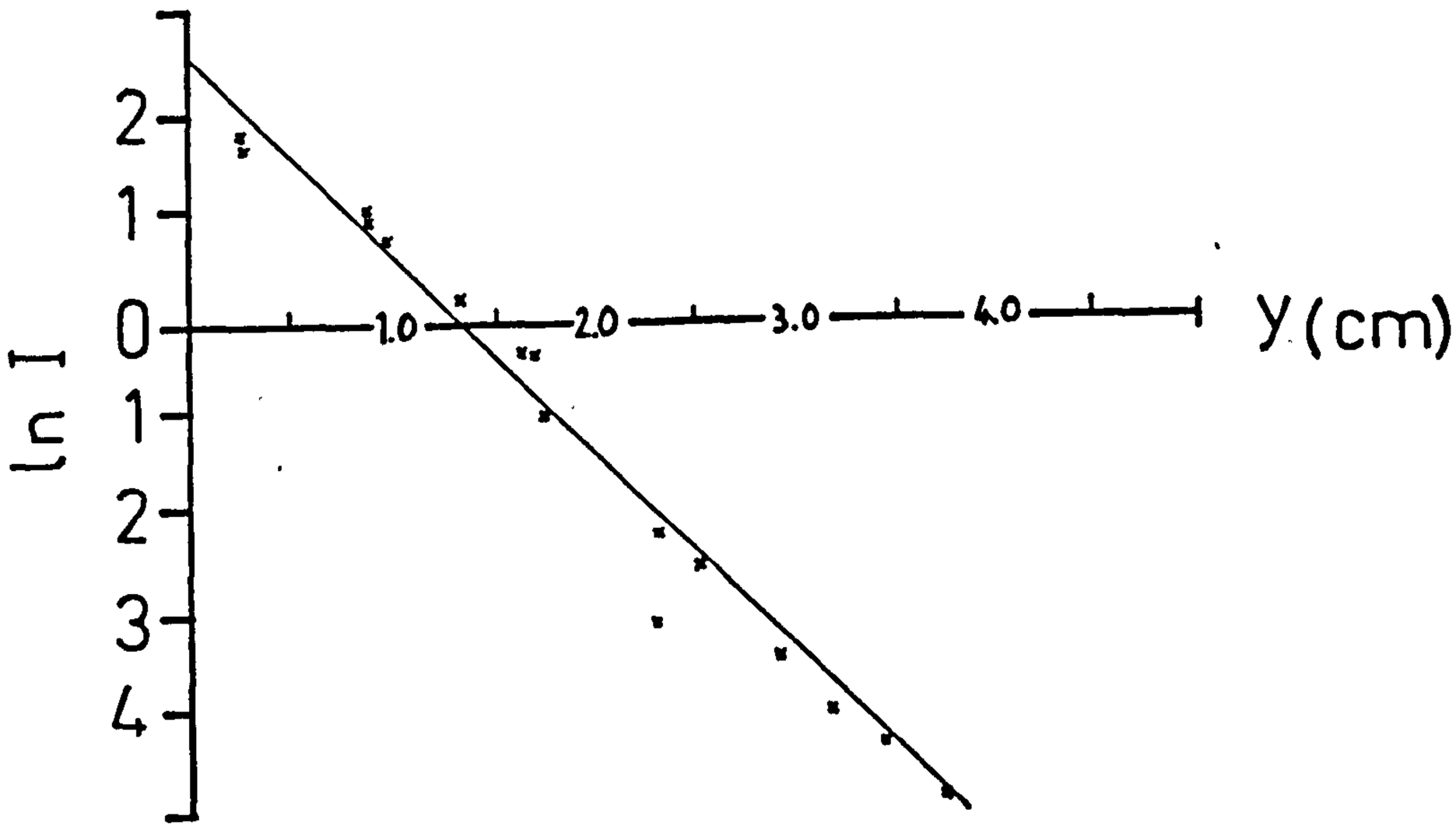

Figure 5.2b. Logarithm Of The Output Signal (Volts) As A Function Of Waveguide Length For Sample X2L After Annealing At 375°C For 15min (Above), And 375°C For 26min (Below).

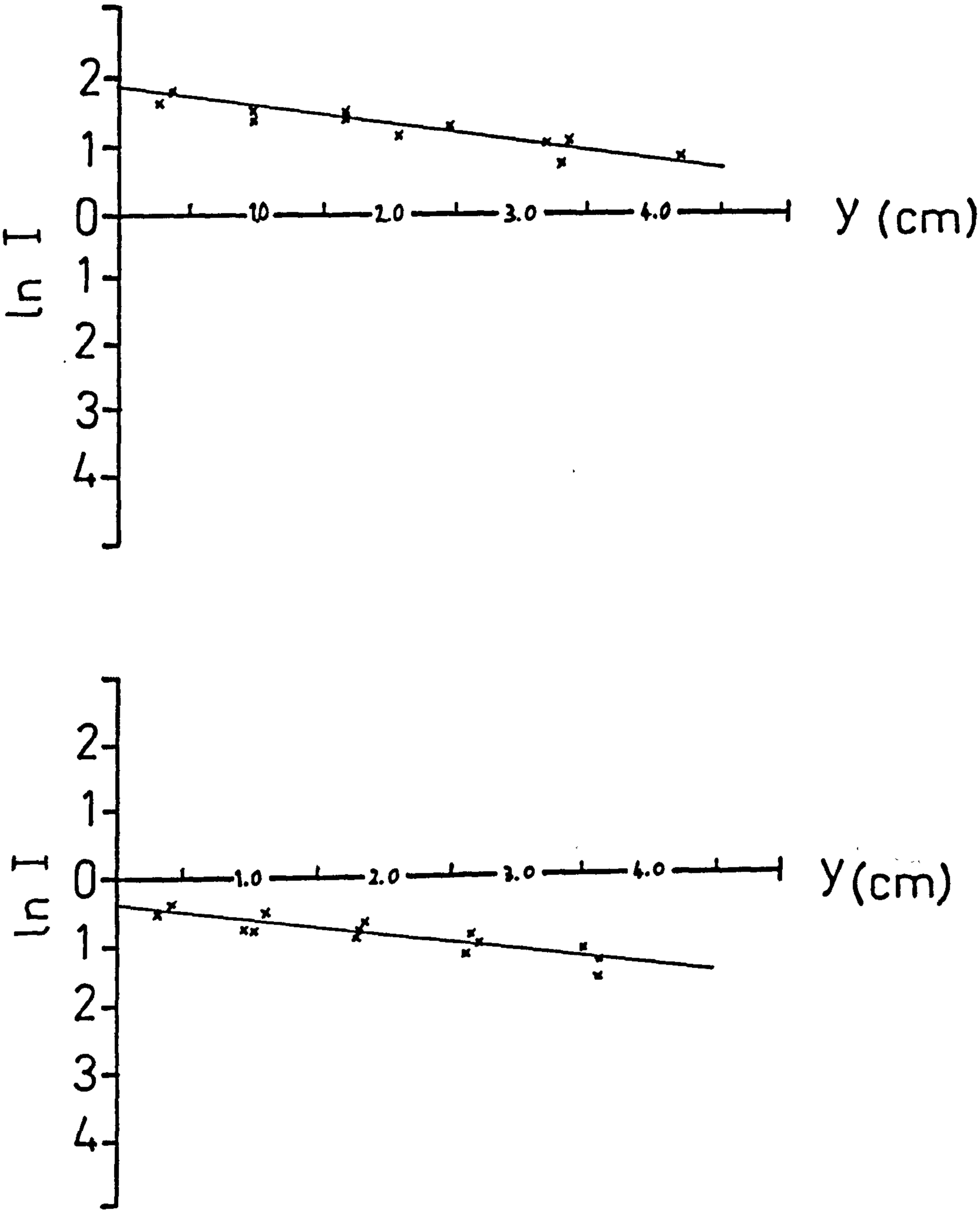

Figure 5.3a. Logarithm Of The Output Signal (Volts) As A Function Of Waveguide Length, Before And After Annealing At 275°C For 30min *(The Sample (Z2L) Was Fabricated At 235°C For 55min Using A 0.96% Mole-Fraction).*

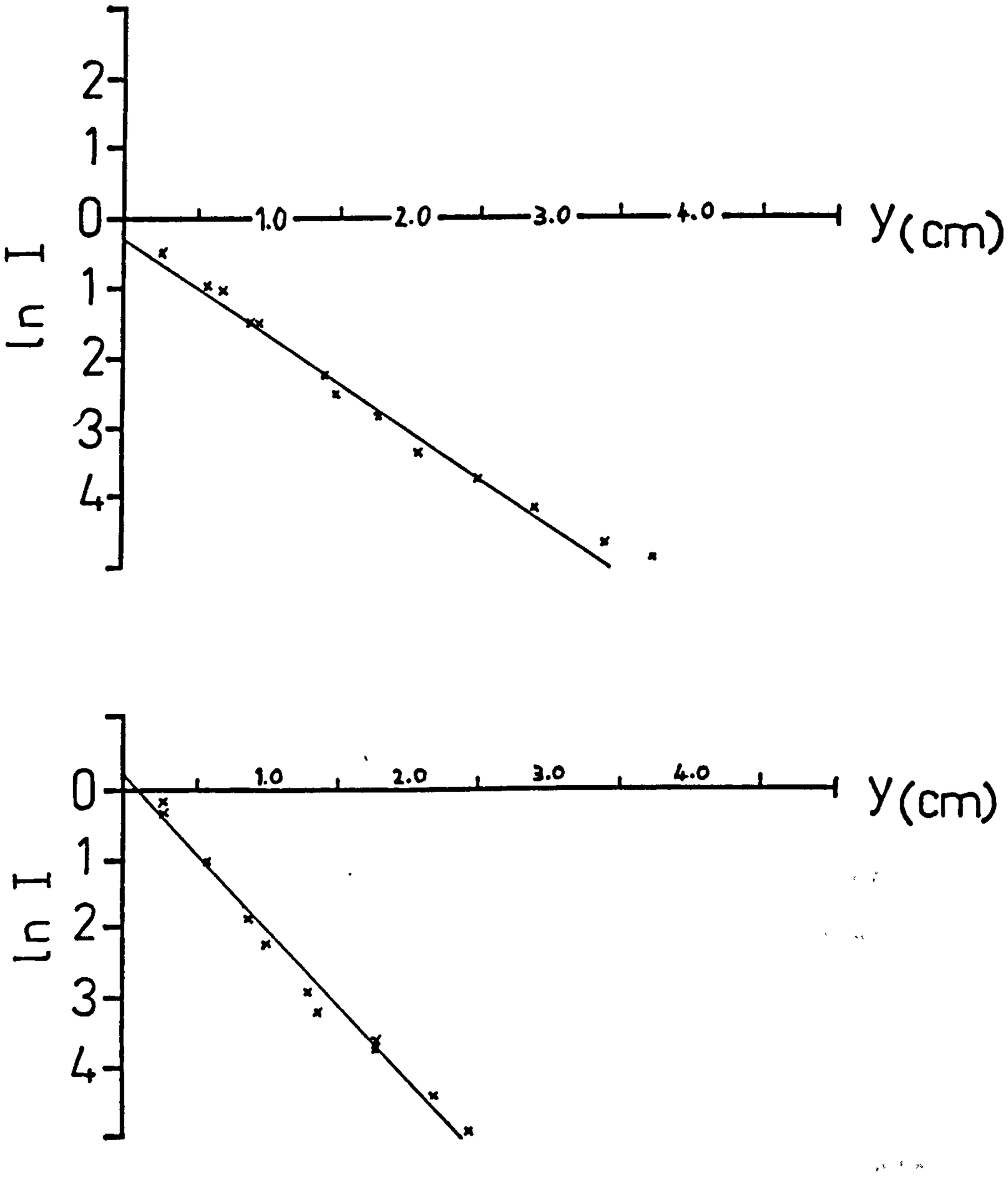

Figure 5.3b. Logarithm Of The Output Signal (Volts) As A Function Of Waveguide Length For Sample Z2L After Annealing At 375°C For 15min (Above), And 375°C For 26min (Below).

Sample		X3L	X1L	X4L	X2L
Mole– Fraction (%)		0	0.48	0.78	0.89
Fabrication Time (min)		4	17	25	30
(a)*	Loss	5.6±0.6	4.3±0.3	5.7±0.2	5.9±0.2
	N_{eff}	2.2769	2.2748	2.2708	2.2688
(b)*	Loss	5.9±0.4	4.9±0.2	6.1±0.1	6.2±0.2
	d (μm)	0.74	0.70	---	---
	n_{guide}	2.3066	2.3060	---	---
(c)*	Loss	5.2±0.2	3.8±0.1	1.4±0.05	2.3±0.1
	d (μm)	0.80	0.83	0.84	0.92
	n_{guide}	2.2915	2.2858	2.2797	2.2742
(d)*	Loss	8.1±0.3	6.7±0.2	6.2±0.1	8.9±0.4
	d (μm)	0.84	0.90	0.92	0.98
	n_{guide}	2.2854	2.2766	2.2699	2.2621

Table 5.1. Propagation Losses (dB/cm) And Waveguide Properties For X– Cut Proton– Exchanged Waveguides, Estimated At $\lambda = 0.6328\mu m$, With Annealing Time And Temperature As Parameters ***(The Waveguides Were Fabricated At 235°C).***

* (a) *unannealed*
(b) *annealed at 275°C for 30min*
(c) *annealed at 375°C for 15min*
(d) *annealed at 375°C for 26min*

Sample		Z3L	Z1L	Z4L	Z2L
Mole– Fraction (%)		0	0.50	0.80	0.96
Fabrication Time (min)		9	27	35	55
(a)*	Loss	1.9±1.1	3.5±0.8	1.6±0.6	1.8±1.0
(b)*	Loss	2.4±0.1	3.3±0.7	2.8±0.6	1.1±0.2
(c)*	Loss	9.4±0.61	3.9±0.1	5.4±0.8	5.6±1.0
(d)*	Loss	3.7±0.05	12.52±0.3	6.61±0.41	9.7±0.2

Table 5.2. Propagation Losses (dB/cm) For Z–Cut Proton–Exchanged Waveguides, Estimated At $\lambda = 0.6328\mu m$, With Annealing Time And Temperature As Parameters *(The Waveguides Were Fabricated At 235°C).*

* (a) *unannealed*
(b) *annealed at 275°C for 30min*
(c) *annealed at 375°C for 15min*
(d) *annealed at 375°C for 26min*

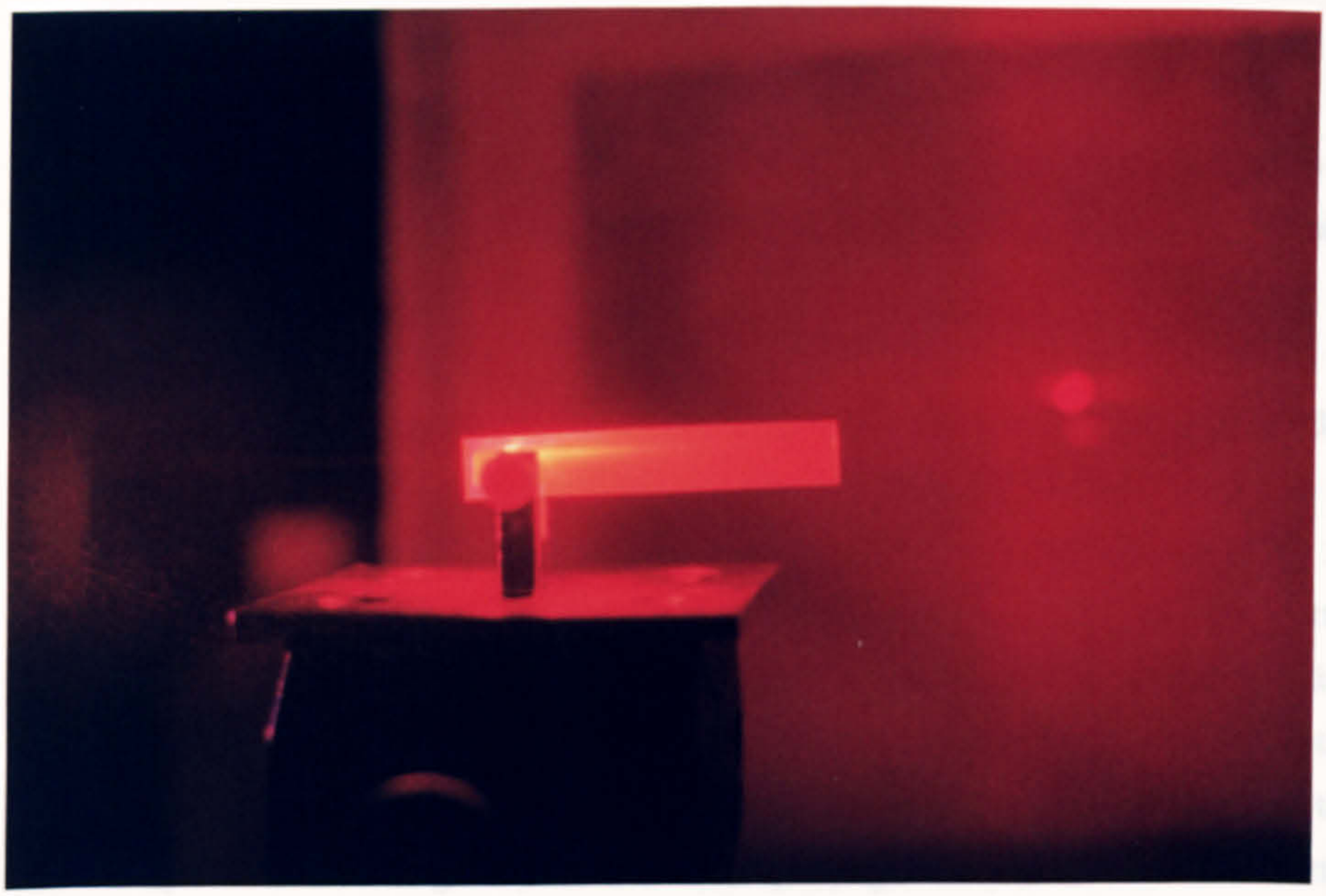

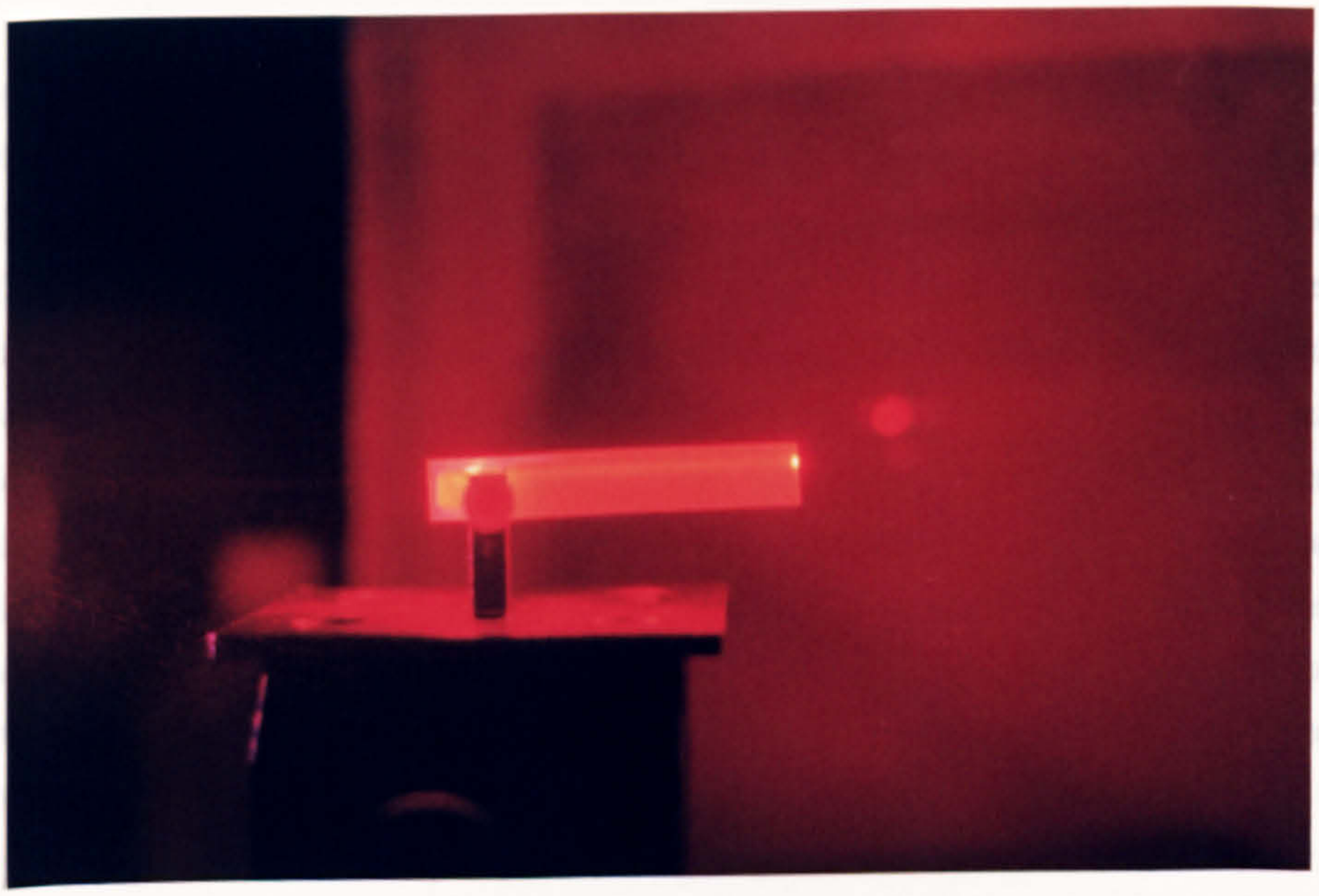

Figure 5.4. Photographs Of The Intensity Of The Fundamental (m= 0) And First Order (m= 1) Mode Supported In Sample X2L, After Annealing At 275°C For 30min And 375°C For 15min (λ= 0.6328 μm).

It is interesting to note that, for both x– and z–cut waveguides, there is no clear relationship between melt–dilution and propagation loss (Tables 5.1 and 5.2).

It was shown in Chapter 4, that the presence of the hydrogen–bonded OH–hydroxyl group responsible for the broad infrared absorption band at υ_{max}= 3250cm^{-1} was removed by annealing and the extent of its formation was reduced by using dilute–melts. The removal of the latter OH–group was accompanied by the gradual relief of strain in the guiding region. For samples X3L and Z3L of the present study, the hydrogen–bonded hydroxyl group would have been removed during the first stage of annealing. However, the propagation losses of the latter waveguides were not reduced by the first annealing stage. It seems plausible then, that hydrogen–bonded OH–hydroxyl groups may play only a small role in the overall strain patterns of unannealed proton–exchanged waveguides, and that the strain–relief observed after annealing was a consequence of the diffusion of free OH–hydroxyl groups (protons) from the waveguide into the substrate.

Assuming that there was no relationship between losses and melt–dilution, the average values of the attenuation (before annealing) were (5.37±0.73)dB/cm for the x–cut proton–exchanged waveguides, and (2.20±0.88)dB/cm for the z–cut proton–exchanged waveguides. After annealing at 275°C for 30min, the losses remained virtually the same with values of (5.78±0.60)dB/cm and (2.40±0.94)dB/cm for the x– and z–cut waveguides, respectively. However, after annealing at 375°C for 15min, the losses of the x–cut waveguides decreased to (3.17±1.67)dB/cm, and the losses of the z–cut guides increased to (6.07±2.34)dB/cm. After annealing at 375°C for a further 26min, the losses of the x– and z–cut waveguides increased to (7.47±1.24)dB/cm and (8.31±3.81)dB/cm, respectively.

5.2.5. Reduced Attenuation Through A Modified Fabrication Process

Many practical devices require single–mode propagation. Therefore, a means of fabricating single–mode waveguides with low attenuation is desirable. However, in the waveguides of the preceeding section, low

losses were only achieved after annealing into multi–mode operation. In the present section, two single–mode waveguides were fabricated using a modified two–step process. The first step involved proton–exchanging to a depth which was below the cut–on depth for single–modes ($\lesssim 0.3\,\mu m$, Chapter 2). The second step involved annealing the proton–exchanged material until a single–mode depth was achieved. The propagation losses of the resulting single–mode waveguides were estimated using the two–prism method.

The two shallow waveguides were formed by proton–exchange with dilute–melts at 235°C. The lithium benzoate mole–fractions used were 0.95% (x–cut, sample X5L) and 0.96% (z–cut, sample Z5L). The initial target depth was $0.1\,\mu m$. The reason dilute–melts were used was that, for shallow depths, the extent of proton–exchange at the temperature used had to be reduced to give a fabrication time which would be much greater than would be required when using neat melts. This would give more accurate control over the fabrication process. For example, to achieve a waveguide depth of $0.1\,\mu m$ using neat benzoic acid at 235°C requires a reaction time of only 8 seconds, whereas the time is approximately 4 minutes for a 0.95% mole–fraction (Chapter 4). The effective diffusion coefficients required to achieve a depth of $0.1\,\mu m$ at 235°C were estimated from the results of Chapter 4.

At a depth of $0.1\,\mu m$ neither sample supported any modes, as expected. After annealing at 275°C for 30min in wet O_2, the samples still did not guide. Only after further annealing at 375°C for 15min did they start guiding. The samples remained single–mode after further annealing at 375°C for 11min. Propagation losses were estimated at $\lambda = 0.6328\,\mu m$ (Table 5.3).

After the second stage of annealing (375°C, 15min), the losses were estimated to be (0.18±0.05)dB/cm for sample X5L and (0.35±0.14)dB/cm for sample Z5L. After the last stage of annealing (375°C, 11min) the losses were unchanged for sample X5L (0.16±0.03)dB/cm, and had increased for sample Z5L (0.98±0.44)dB/cm. These values are significantly lower than those of the single–mode waveguides produced by proton–exchange in the usual manner, by a factor of approximately ten.

Sample	Annealed 275°C 30min	Annealed 375°C 15min	Annealed 375°C 11min
X5L			
Loss	— — —	0.18±0.05	0.16±0.03
Index	— — —	2.2089	2.2092
Z5L			
Loss	— — —	0.35±0.14	0.98±0.44
Index	— — —	2.2046	2.2046

Table 5.3. Propagation Losses (dB/cm) And Effective Mode–Indices For X– And Z–Cut Proton–Exchanged Waveguides, Measured At $\lambda = 0.6328\,\mu m$ *(The Waveguides Were Fabricated At 235°C With An Initial Target Depth Of 0.1*μm).

Sample	*Before annealing	After annealing 400°C for 10min
X1L		
Loss	3.47±0.29	2.52±0.44
Index	2.1717	2.1705
d(μm)	0.90	2.31
X2L		
Loss	---	0.8±0.1
Index	---	2.1655
d(μm)	0.98	2.69
X3L		
Loss	---	2.99±0.05
Index	---	2.1711
d(μm)	0.84	2.30
X4L		
Loss	---	0.79±0.02
Index	---	2.1662
d(μm)	0.92	2.53
Z1L		
Loss	3.59±0.14	2.96±0.18
Index	2.1608	2.1607
d(μm)	---	2.58
Z2L		
Loss	2.1±0.05	1.25±0.19
Index	2.1661	2.1618
d(μm)	---	2.83
Z3L		
Loss	3.96±0.43	2.34±0.05
Index	2.1732	---
d(μm)	---	2.10
Z4L		
Loss	1.94±0.07	1.96±0.01
Index	2.1596	2.1591
d(μm)	---	3.26

Table 5.4. Propagation Losses (dB/cm) And Effective Mode-Indices For X- And Z-Cut Proton-Exchanged Waveguides, Estimated At λ=1.15μm, Before And After Annealing.

**For The Previous Treatment Of These Samples, See Tables 5.1 And 5.2.*

However, since the initial depths and proton–concentrations in the samples X5L and Z5L were lower, an effectively limited–source diffusion model would have been appropriate. Therefore the refractive index profiles of the latter two waveguides are likely to be more modified by the annealing process than the profiles of the other waveguides. The profiles are likely to be much more graded in appearance, with the waveguide (surface) indices substantially reduced from the 'as–exchanged' values. The effective mode–indices of the waveguides were very close to the substrate value (Table 5.3), indicating substantially graded–index profiles.

5.2.6. Propagation Losses Measured At $\lambda = 1.15\mu m$

The operating wavelengths of existing practical systems are in the infrared. To be compatible with such systems, integrated optical devices will have to operate at infrared wavelengths and so will have to have good waveguiding capabilities at infrared wavelengths. Therefore, a brief study of propagation losses at $\lambda = 1.15\mu m$ has been carried out. Loss measurements were carried out as described in Section 5.2.3, using the two–prism technique. Of the samples used in Section 5.2.4 (for measuring losses at $\lambda = 0.6328\mu m$, *excluding* samples X5L and Z5L), only X1L, Z1L, Z2L, Z3L, and Z4L guided at $\lambda = 1.15\mu m$. The losses were measured before and after annealing at 400°C for 10min. All the guides remained single–mode after annealing.

The processing of the waveguides for measurements at $\lambda = 1.15\mu m$ was chosen so that that they might be comparable to the low loss waveguides X5L and Z5L, i.e. initially having a depth below single–mode cut–on and then annealed into the single–mode region. So any losses measured at $\lambda = 1.15\mu m$ *could* be considered lower than would be expected if the guides had been proton–exchanged (without annealing) to a depth for single–mode propagation at $\lambda = 1.15\mu m$.

After the final stage of annealing, the waveguides were characterised at $\lambda = 0.6328\mu m$ so that the waveguide depths could be estimated using the IWKB method. These are given, together with the loss values, in Table 5.4. The losses at $0.6328\mu m$ after annealing at 400°C for 30min were

estimated to be ≥10dB/cm. At 1.15μm, the lowest measured loss before annealing was (1.94±0.07)dB/cm for sample Z4L. The losses of samples X5L and Z5L (the low–loss waveguides of Section 5.2.4) measured at $\lambda = 0.6328\mu$m were less than 0.5dB/cm. Therefore, the losses measured at $\lambda = 1.15\mu$m *cannot* be considered as analogous to X5L and Z5L, since the losses are higher at the longer wavelength.

The higher losses at the longer wavelength could conceivably be because the amount of annealing required to obtain single–mode capability at $\lambda = 1.15\mu$m was much greater than was used for X5L and Z5L at $\lambda = 0.6328\mu$m. The single–mode target depth for 1.15μm operation could have been obtained not by annealing, as above, but by using a longer fabrication time to give an initial exchanged layer below the depth required for single–mode operation at $\lambda = 1.15\mu$m and *then* annealing the waveguide into single–mode operation. In this way, losses lower than those measured for samples X5L and Z5L at $\lambda = 0.6328\mu$m might be achieved.

5.3. THE ELECTRO–OPTIC EFFECT IN BULK LITHIUM NIOBATE.

5.3.1. Theoretical Analysis

Before considering the electro–optic characteristics of proton–exchanged and titanium–indiffused waveguides, measurement of the bulk properties is required. The electro–optic effect in the bulk material can be used as a reference for the electro–optic effect in proton–exchanged and titanium–indiffused waveguides.

A desire to study the electro–optic effect in crystals grown from off–congruent melts, crystals doped with magnesium oxide (MgO), and crystals which had been annealed at high–temperatures (1000°C) had been shown by the author's co–operating industrial body (Barr and Stroud, Ltd), and so the bulk material measurements were carried out on–site.

The electro–optic effect describes a change in the refractive index (or dielectric impermeability) of a medium induced by the application of an

electric field. The change can be represented mathematically by the equation[15]:

$$\Delta B_{ij} = \Delta(1/n^2)_{ij} = r_{ijk} E_k \ldots\ldots\ldots\ldots (6),$$

where B_{ij} is the dielectric impermeability of the material, E_k is the applied electric field in the k– direction (k= x,y, or z), and r_{ijk} is the electro– optic tensor for the material. The subscripts i, j and k run from 1 to 3.

Standard reference works[15,16] show that the impermeability matrix for lithium niobate is symmetrical, i.e. $B_{ij} = B_{ji}$. The components of B_{ij} can then be written: $B_{11} = B_1$, $B_{22} = B_2$, $B_{33} = B_3$, $B_{23} = B_{32} = B_4$, $B_{13} = B_{31} = B_5$, $B_{12} = B_{21} = B_6$. The electro– optic tensor r_{ijk} can then be written in the form:

$$[r_{(ij)k}] = \begin{bmatrix} 0 & -r_{22} & r_{13} \\ 0 & r_{22} & r_{13} \\ 0 & 0 & r_{33} \\ 0 & r_{42} & 0 \\ r_{42} & 0 & 0 \\ -r_{22} & 0 & 0 \end{bmatrix},$$

where $r_{13} = r_{23}$, $r_{22} = -r_{12}$, and $r_{42} = r_{51}$. This is the reduced electro– optic tensor for crystals belonging to the point group 3m, symmetry requiring that eight of the possible eighteen coefficients are non– zero, with only the four coefficients above needed to describe the full electro– optic behaviour of the crystal[15,16].

Because of the piezo– electric nature of lithium niobate, there are two sets of electro– optic coefficients: the d.c. (or zero frequency) coefficients (corresponding to a free crystal), and the high– frequency coefficients (corresponding to a clamped crystal). The two sets of coefficients are related to one another via elastic– optic and piezo– electric effects[16]. Therefore, the application of an electric field across the crystal induces mechanical stress which, in turn, changes the refractive indices and the electro– optic coefficients.

5.3.2. Evaluation Of r_{33}, r_{13}, And r_{22} For Bulk Lithium Niobate..

A number of techniques have been used to measure the value of electro–optic coefficients. These include Senarmont compensation[17,18], Michelson interferometry[19], and optical heterodyning[20]. The most common is the half–wave voltage method[21], and this was used in the present study.

The experimental arrangement for measuring half–wave voltages is depicted in Figure 5.5. Incident light is polarised at 45^{o} to the ordinary and extra–ordinary axes of the crystal and is consequently split into two orthogonal components which travel along n_o and n_e. When an external field is applied in the z–direction (E_z) the refractive indices are changed by an amount which is proportional to the size of the applied field. These changes are, from Equation (6):

$$\Delta n_e = -n_e^3 r_{33} E_z/2, \text{ and } \Delta n_o = -n_o^3 r_{13} E_z/2 \ldots\ldots\ldots(7).$$

The relative phase–change (retardation) between the extraordinary and ordinary waves, after travelling a distance L in the crystal, is given by:

$$\Delta\Gamma = \Gamma_1 - \Gamma_2 = 2\pi L\{(n_o + \Delta n_o) - (n_e + \Delta n_e)\}/\lambda \ldots\ldots\ldots(8)$$

By placing the polariser (analyser) in the path of the emerging beam (as shown in Figure 5.5), the modulation can be detected. The intensities of light emerging from the crystal polarised parallel and perpendicular to the incident polarisation are:

$$I = I_o \cos^2(\Delta\Gamma/2), \text{ and } I = I_o \sin^2(\Delta\Gamma/2). \ldots\ldots\ldots(9),$$

respectively, where I_o is the incident intensity. In Figure 5.5, only the perpendicular polarisation is passed by the analyser. The intensity of light after the analyser is obtained by substituting Equation (8) into Equation (9), giving:

$$I = I_o \sin^2\{\pi L(n_e - n_o)/\lambda - \pi LV(n_e^3 r_{33} - n_o^3 r_{13})/2\lambda d\} \ldots\ldots\ldots(10),$$

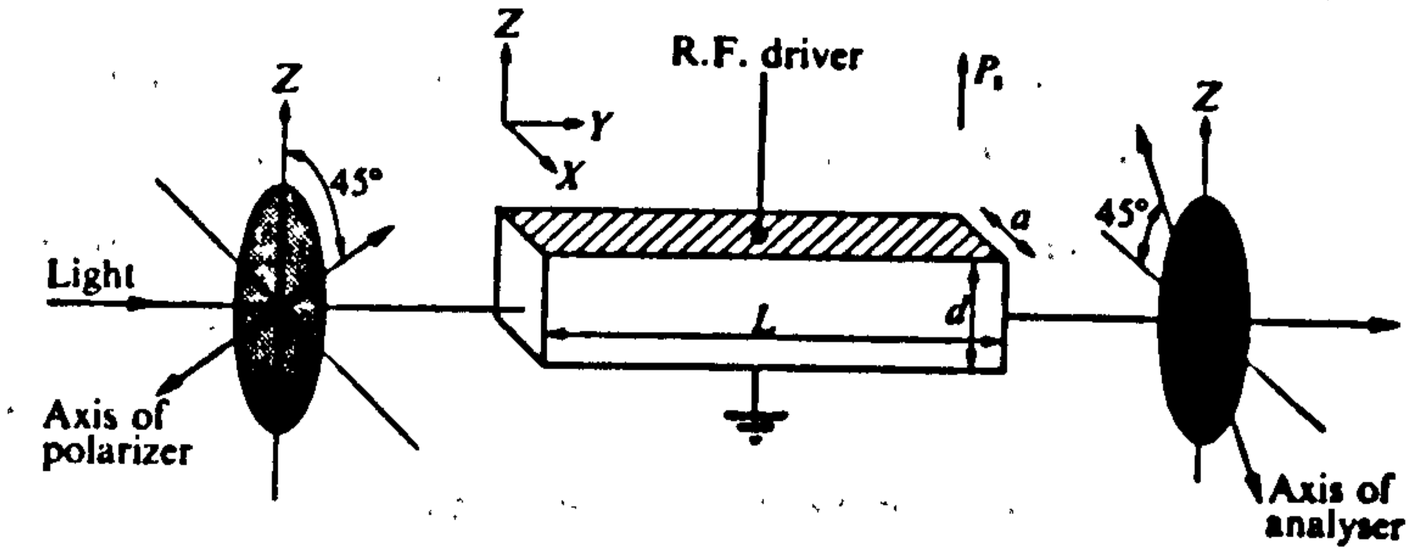

Figure 5.5. Schematic Of A Transverse Bulk Electro–Optic Lithium Niobate Modulator.

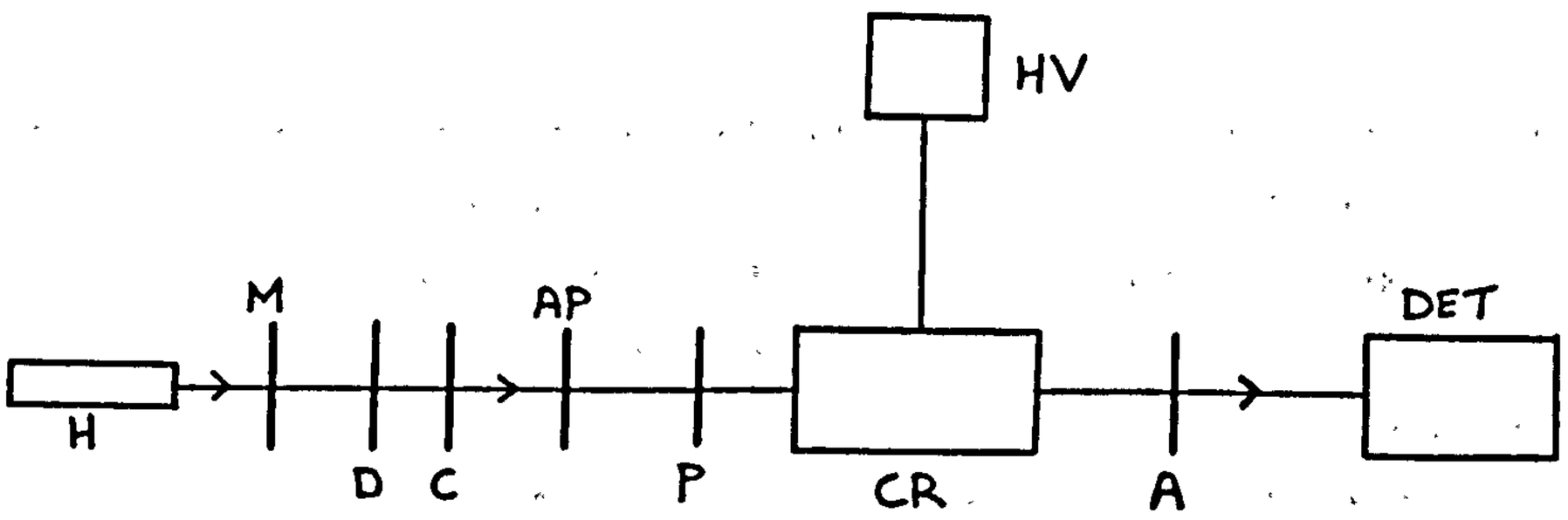

Figure 5.6. Experimental Arrangement For Determining Half–Wave Voltages.

H–Helium/Neon Laser; M–Mechanical Chopper; D–Diverging Lens; C–Converging Lens; AP–Aperture; P–Polariser; A–Analyser; CR–Crystal; HV–Power Supply; DET–Detection/Amplification Equipment.

where V is the voltage applied across a thickness 'd' of the crystal. The voltage required to increase 'I' from zero to unity (or from a minimum to a maximum) is called the *half−wave* voltage ($V\pi$) and, for this configuration, is given by:

$$V\pi = \lambda d/(n_e{}^3 r_{33} - n_o{}^3 r_{13})L \quad \text{.....(11).}$$

The term on the left of the expression in parentheses in Equation (10) is called the *zero−field retardation*, and is simply the retardation caused by the natural birefringence of the crystal. As can be seen, it is independent of the applied voltage but depends directly on the crystal length. This term is an undesirable one for bulk electro−optic modulation, since the natural birefringence is a function of the temperature of the material[22]. The temperature−effect can be compensated for by placing a pair of crystals of identical length, maintained at a common temperature, along the path of the light beam so that the natural birefringence of one crystal cancels out that of the other[23]. In the present study, the temperature−effect was assumed to be negligible.

By choosing suitable substrate orientations and applied field directions the electro−optic coefficients r_{33}, r_{13}, and r_{22} are utilised (Table 5.5). By measuring the variation in intensity (after the analyser) as a function of the applied voltage, the half−wave voltage can be estimated.

The experimental arrangement used for the present study is shown in Figure 5.6. Light from a Helium−Neon laser ($\lambda = 0.6328\,\mu m$) was mechanically chopped at 1kHz for detection purposes. A diverging/converging lens combination was used to provide a collimated beam with a diameter of approximately 2cm. The collimated beam passed through an aperture, the size of which was chosen so that the whole face of the crystal was covered by the incident light. The polariser/analyser assembly was as shown in Figure 5.5.

Each crystal was mounted on an optical stage which had (x,y,z,θ,φ) movements, allowing accurate alignment of the beam through the crystal.

Propagation Direction	Field Direction E_x	E_y	E_z
Parallel to x		$\pi LVn_o{}^3r_{22}/y\lambda$	$\pi LV(n_e{}^3r_{33}-n_o{}^3r_{13})/z\lambda$
Parallel to y		$\pi Vn_o{}^3r_{22}/\lambda$	$\pi LV(n_e{}^3r_{33}-n_o{}^3r_{13})/z\lambda$
Parallel to z	$2\pi LVn_o{}^3r_{22}/x\lambda$	$2\pi LVn_o{}^3r_{22}/y\lambda$	

Table 5.5. Induced Phase Change As A Function Of Light Propagation And Applied Field Direction. ***Crystal Dimensions Are (x,y,z), L Is The Electrode Length, And V Is The Applied Voltage.***

Slab (brass) electrodes were placed in contact with the relevant faces of the crystal and the applied voltage was obtained using a ±(0 to 3.1)kV d.c. supply. The positive and negative polarities of the power supply were used. The output signal was detected by the photodetector, amplified, and viewed on an oscilloscope. The dimensions of each crystal were measured to a precision of ±0.05mm using a Vernier gauge. Several different crystals were used in the experiment and these will now be discussed.

Some of the bulk crystals used were cut from a congruently–grown boule (48.6 mole% Li_2O, corresponding to $(Li/Nb)_{melt}=(Li/Nb)_{crystal}=0.945$[24,25]) grown and supplied by Pilkington Electro–optic Materials (Barr and Stroud) Ltd.

Crystal boules grown by the Czochralski technique often show a variation in stoichiometry along their lengths and any thin–sections subsequently cut from the boule for use as substrates for integrated optical devices are subject to this variation. Since many optical properties are a function of crystal stoichiometry[26], it is clearly of importance to measure what effect crystal stoichiometry has on the electro–optic effect. To test for possible stoichiometry dependence, the electro–optic coefficients of two samples with stoichiometry above and below the congruent composition were measured. The samples had (respectively) 48 mole% Li_2O and 49

mole% Li_2O, corresponding to $(Li/Nb)_{melt}= 0.908$, $(Li/Nb)_{crystal}= 0.933$, and $(Li/Nb)_{melt}= 0.971$, $(Li/Nb)_{crystal}= 0.953$[24,25].

Also examined were two crystals which had been doped with 4.5 mole% MgO. Noda *et al*[27] showed that impurity diffusion of Mg^{2+} into congruent lithium niobate decreased the extraordinary refractive index. Waveguides formed by titanium–indiffusion in MgO–doped lithium niobate are claimed to be less susceptible to laser damage (photo–refractive effect)[28]. The electro–optic effect is another important property which should be studied if MgO–doped material is to be used practical devices.

A consequence of fabricating waveguides by titanium–indiffusion is that the substrate is subjected to high–temperatures (1000°C) for several hours. It has been shown[29] that Li_2O out–diffuses at high–temperature. The properties of the material change depending on the amount of out–diffusion[29], therefore the electro–optic effect might also be effected in some way. In the present study, two samples were heated at 1170°C in wet O_2 (flow rate=1.275 litre/min) and 1120°C in dry nitrogen (at the same flow rate) for 5 hours, and the half–wave voltages re–measured once they had cooled to room–temperature.

5.3.3. Results.

Figure 5.7 shows a typical plot of the output signal as a function of applied voltage for one of the above samples (annealed at 1170°C). From this, and similar plots for the other samples, the half–wave voltages were estimated (Table 5.6). The quoted error limits were estimated using the standard deviation of the mean value of V_π (Figure 5.6). The half–wave voltages can be estimated with better precision if there are many peaks in the output waveform. The number of periodic waveforms can be increased by using crystals of longer length or increasing the range of the applied voltage.

The results in Table 5.6 indicate that the electro–optic coefficients r_{13} and r_{33} are not dependent on either crystal stoichiometry or the addition of MgO in amounts up to 4.5 mole%. However, previous workers[30,31]

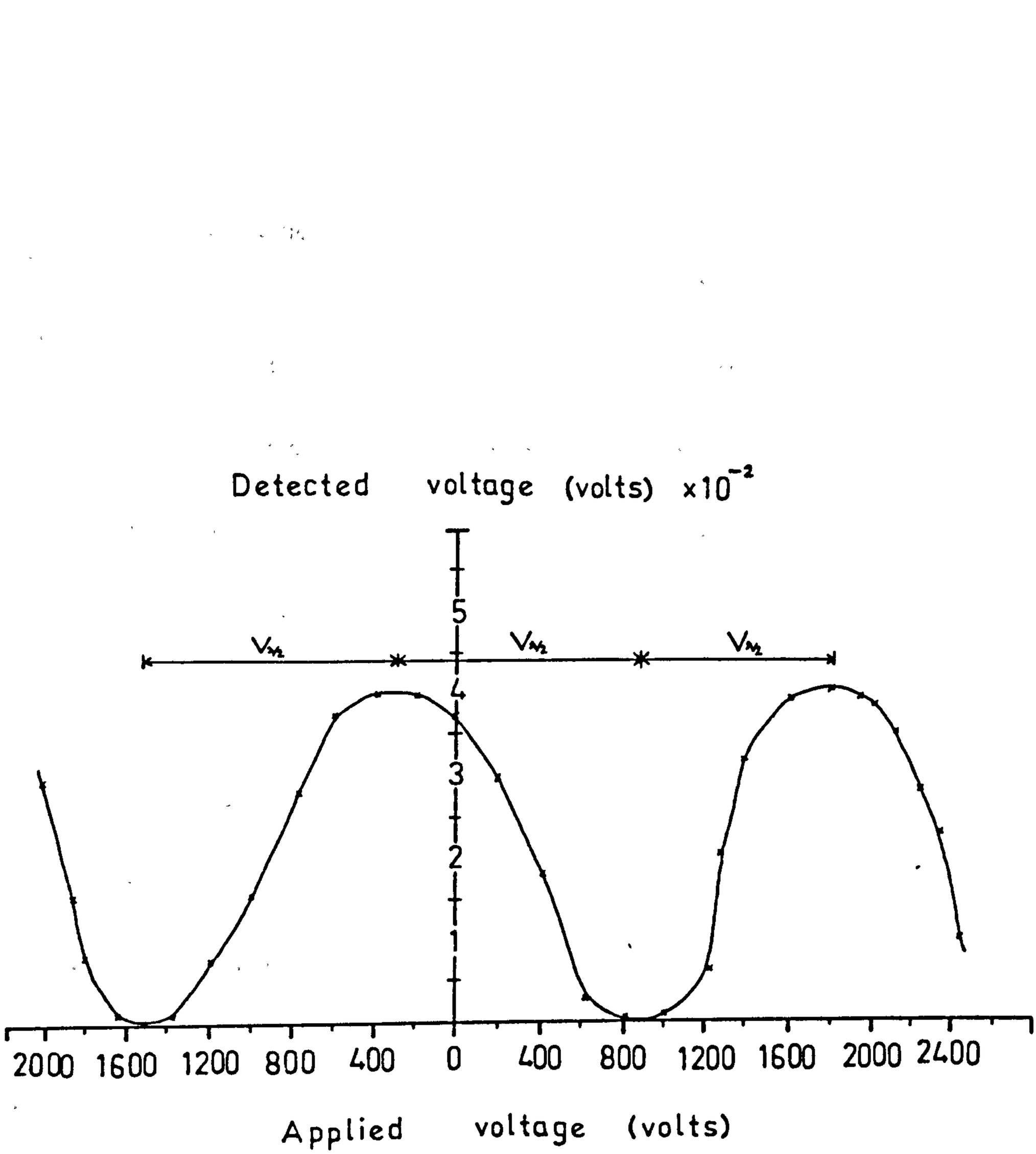

Figure 5.7. Plot Of The Detected Signal As A Function Of Applied Voltage.

The Sample Used Was Annealed At 1170°C For 5hr In Flowing Wet O_2.

Sample Composition	V_π (volts)	$n_o{}^3r_{22}$ (x10^{-12}m/V)	$(n_e{}^3r_{33} - n_o{}^3r_{13})/2$ (x10^{-12}m/V)
Congruent $(Li/Nb)_{melt}$= 0.945	3125±468	---	101±15
Congruent $(Li/Nb)_{melt}$= 0.945	3056±409	---	103±14
Congruent $(Li/Nb)_{melt}$= 0.945	3076±511	---	102±17
Congruent $(Li/Nb)_{melt}$= 0.945	3892±149	---	81±6
Congruent $(Li/Nb)_{melt}$= 0.945	3538±511	---	89±13
Incongruent $(Li/Nb)_{melt}$= 0.908	2883±402	---	109±15
Incongruent $(Li/Nb)_{melt}$= 0.971	3378±693	---	94±20
4.5 mole% MgO	2831±348	---	111±14
4.5 mole% MgO	3313±377	---	95±11
Congruent $(Li/Nb)_{melt}$= 0.945	9765±362	6.48±0.24	---
Congruent $(Li/Nb)_{melt}$= 0.945 Annealed (dry N_2) at 1120°C for 5hr	2980±170	---	106±6
Congruent $(Li/Nb)_{melt}$= 0.945 Annealed (wet O_2) at 1170°C for 5hr	4486±813	---	70±27

Table 5.6. Half-Wave Voltages And Corresponding Electro-Optic Coefficients For Congruent, Off-Congruent, MgO-Doped, And Annealed High-Temperature Lithium Niobate, Estimated At $\lambda = 0.6328\,\mu m$.

reported that the low–frequency dielectric constants and linear electro–optic coefficients in lithium niobate depended *significantly* upon the crystal stoichiometry. In particular it was found that the half–wave voltages decreased with *any* departure from the congruent composition $(Li/Nb)_{melt}= 0.945$. For lithium–rich melts, with the composition $(Li/Nb)_{melt}= 1.1$, V_{π} was estimated to be 1750 volts as compared to 3100 volts for a congruent crystal[30,31].

A later theoretical study[21] showed that any variation in V_{π} over the composition range $(Li/Nb)_{melt}= 0.91$ to 1.08 was likely to be *small* and of the order of ten percent, i.e. 300 volts (greater for compositions above congruent, and smaller for compositions below congruent). The standard deviations of V_{π}, measured in the present work, are larger than the theoretical value, and so the measured half–wave voltages for crystals of different composition are not as clearly differentiated.

The values of V_{π} for the MgO doped lithium niobate were similar to those measured for undoped material (Table 5.6). The similarity could conceivably be due to the fact that magnesium ions are located in lithium sites (assuming that lithium is replaced by magnesium)[27], or that the ionic radii of the two ions are similar (0.60Å, and 0.65Å, respectively[32]). Because magnesium is divalent (Mg^{2+}) and lithium is monovalent (Li^{+}), there is a difference in the impermeability of the two materials (evident from the smaller refractive index observed in MgO doped material[27]), and therefore, the magnitude of the electro–optic coefficients could be different. However, changes in the electro–optic effect may not have been observed because the MgO was present in small concentrations.

The crystals which were annealed at high–temperature showed no obvious changes in the measured values of V_{π} (Table 5.6). Therefore, the high–temperature outdiffusion of Li_2O, observed during titanium–indiffusion, has little effect on the electro–optic properties of the bulk material. However, changes in the electro–optic effect could depend on the extent of Li_2O outdiffusion.

The highest bulk electro–optic coefficient in lithium niobate is r_{33}, with a d.c. value of 32×10^{-12} m/V, and this coefficient is therefore more commonly used for active devices (where a single coefficient only is required). The following section deals with the electro–optic coefficients for proton–exchanged and titanium–indiffused planar waveguides.

5.4. MEASUREMENT OF THE ELECTRO–OPTIC EFFECT IN PROTON–EXCHANGED AND TITANIUM–INDIFFUSED PLANAR WAVEGUIDES.

5.4.1. A Comparison Between The Electro–Optic Effect In Proton–Exchanged And Titanium–Indiffused Waveguides

Many integrated optical devices have been developed for the purpose of phase modulation, intensity modulation, and for switching of light. These devices are based on the use of stripe waveguides with parallel surface electrodes, allowing the phase of propagating light to be changed by applying a voltage to the electrodes. By combining two such structures in the form of a Mach–Zehnder interferometer, the intensity of the light changes when two light waves of variable phase re–combine. Many active electro–optic devices in lithium niobate utilise the r_{33} coefficient.

The most common method of fabricating waveguides for electro–optic devices has been titanium–indiffusion. Only relatively recently (1982 onwards) has proton–exchange been used. The two methods (titanium–indiffused proton–exchanged waveguides) have also been successfully combined[33], and devices like optical frequency translators[34], cut–off modulators[35], directional couplers[36], switches[37], and intensity modulators[38] have been produced.

A comparison between guided–wave Mach–Zehnder intensity modulators fabricated by proton–exchange and titanium–indiffusion was studied by Becker[39]. The electro–optic modulation was determined by measuring the voltage required to cause π differential phase shift (V_π) in the two arms of a single–mode interferometer. By using a number of devices with different electrode lengths and measuring the subsequent V_π, he concluded that, for proton–exchanged devices, the voltage required to

produce a phase change of π was nearly three times that for titanium–indiffused devices, implying a substantial degradation of the electro–optic activity of the proton–exchanged devices.

It has been shown[40] that, in powder samples, a result of proton–exchange is that the material undergoes a structural transformation from the rhombohedral ($LiNbO_3$) to the cubic ($HNbO_3$) unit cell (for complete Li–H substitution). Even partial exchange causes lattice distortion[47,48]. Since the cubic structure is symmetrical about all axes, and therefore has an inversion centre[15], the electro–optic coefficients are non–existent. Hence, r_{33} gradually reduces as the lattice distortion (i.e. the Li–H substitution ratio) increases[43]. It appears that the only way to preserve r_{33} is to limit the percentage of Li–H substitution which takes place, i.e. to limit the proton–concentration in the waveguide layer.

Several workers[42,43,44,45] have used phase modulation and intensity modulation techniques to examine the degradation of the electro–optic effect in proton–exchanged waveguides. The results are in agreement that the magnitude of r_{33} is reduced to approximately one–tenth of the bulk value, i.e. to approximately 3×10^{-12}m/V. However, it has been reported that devices fabricated by dilute–melt proton–exchange have a partially preserved electro–optic effect[42,43,45]. If proton–exchanged waveguide devices are to be used in a reasonable range of practical systems, the electro–optic performance must be comparable to that of waveguide devices fabricated by, for example, titanium–indiffusion.

In the following sections, a method of evaluating the electro–optic coefficients of various waveguide structures is described, and a process whereby the electro–optic effect can be substantially restored in proton–exchanged waveguides is also described.

5.4.2. Experimental Arrangement.

A technique for measuring the electro–optic coefficients of planar waveguides was developed for the present study. The measurement procedure had the advantages of not requiring lithographic electrode fabrication and not requiring detailed calculations or experimental data for

optical modal and electrode field distributions.

The method was based on the detection of phase modulation in planar waveguides using an external interferometric arrangement. The modulation was produced by applying high voltages through the entire substrate and waveguide via slab electrodes. The arrangement is shown schematically in Figures 5.8a and 5.8b for TE and TM modes, respectively.

In the experimental measurements carried out, light from a Helium–Neon laser ($\lambda = 0.6328\mu m$) was split into two equal intensity beams: a sample beam, and a reference beam. The sample beam was prism–coupled into the planar waveguide, excited the required mode, and was prism–coupled out. The sample beam re–combined with the reference beam at the glass slide. The two beams interfered with one another, and interference fringes were observed on the screen. A slightly different configuration had to be used for TM modes because of the geometrical restrictions caused by the smaller coupling angles. This involved the use of a mirror to divert the reference beam (Figure 5.8b).

Slab (brass) electrodes were placed in contact with the surfaces of the crystal substrate so that the applied field direction was normal to the plane of the waveguide, i.e. *through* the substrate and waveguide. Both polarities of a ±(0 to 3.1)kV d.c. power supply were used. The applied field induced a refractive index change (Δn) in the waveguide, and therefore induced a phase change ($\Delta\varphi$) in the propagating mode, given by:

$$\Delta\varphi = 2\pi L\Delta n/\lambda \ldots\ldots\ldots\ldots (12),$$

where L is the electrode length. The phase change was observed as a shift in the fringe pattern, the number of fringe shifts depending on the applied voltage. By counting the number of displaced fringes (in multiples of π) as a function of the applied voltage (V) and using Equation (12), the value of Δn was estimated. Substituting the value of Δn into Equation (7) gave the value of the relevant electro–optic coefficient:

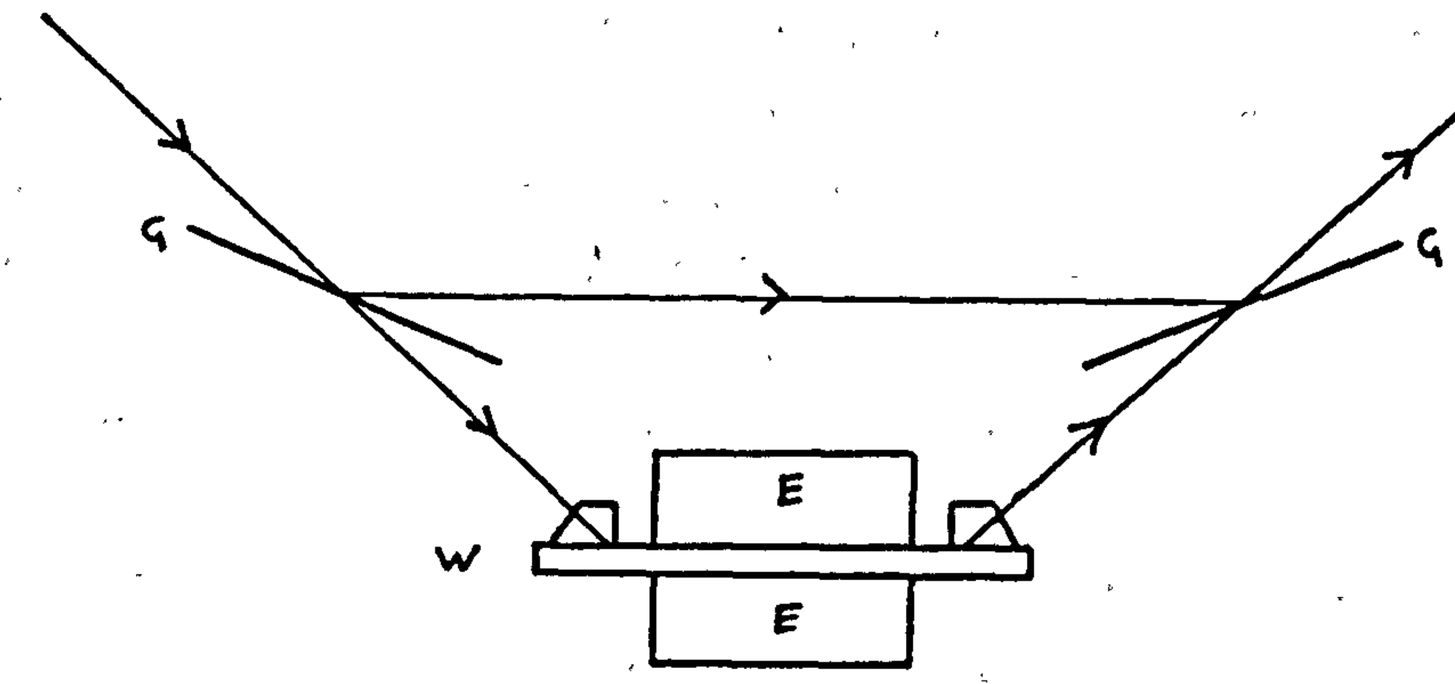

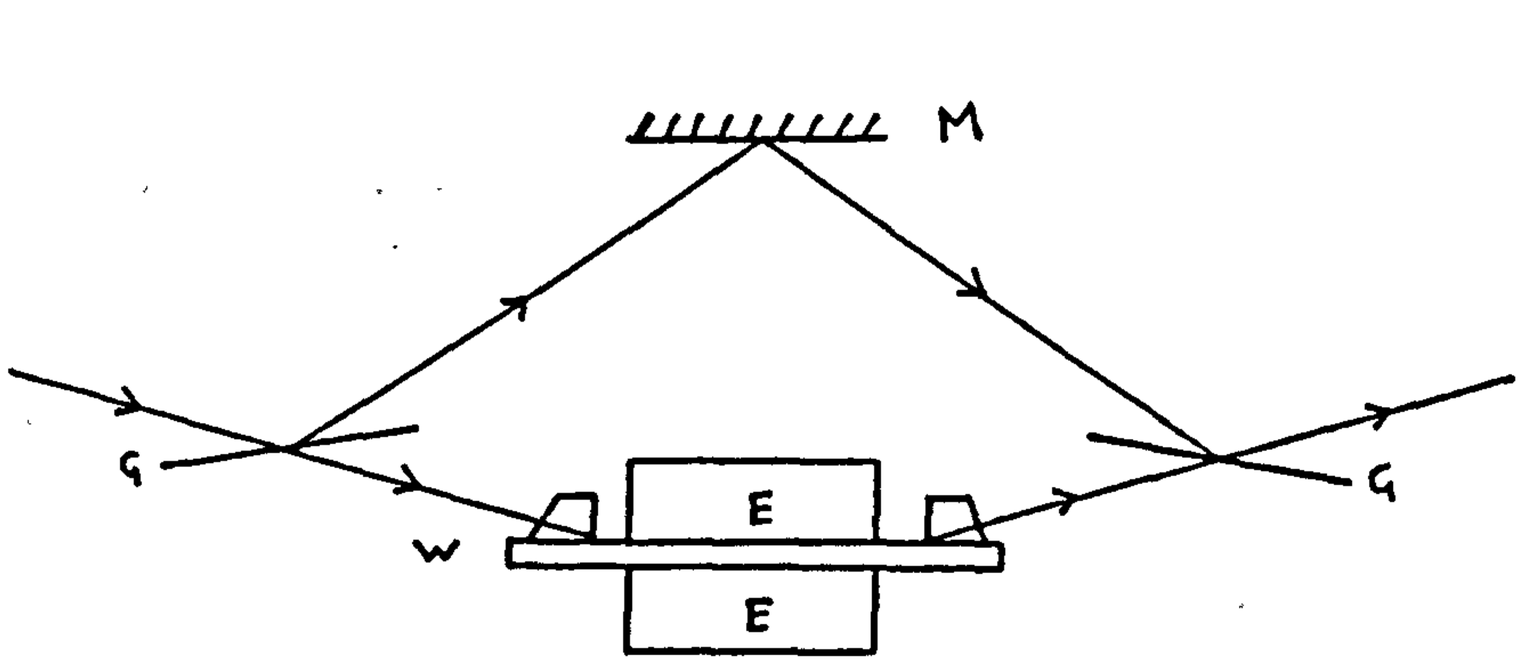

Figure 5.8a (Above, For TE Modes) And Figure 5.8b (Below, For TM Modes). Interferometric/Prism–Coupling Arrangement For Measuring The Electro–Optic Effect In Planar Waveguides.

G–Glass Slide; E–Slab Electrodes; W–Waveguide; M–Mirror.

$$r_{33} = \lambda d \Delta\varphi_1 / \pi L V n_e^3$$

$$r_{22} = \lambda d \Delta\varphi_2 / \pi L V n_o^3 \qquad \text{.....(13)}$$

$$r_{13} = \lambda d \Delta\varphi_3 / \pi L V n_e^3,$$

where d is the thickness of the crystal and V is the applied voltage. Since the applied field was through the whole waveguide, all the propagating light was modulated, corresponding to an overlap integral equal to unity (for strip waveguides). It was assumed that the electric field was linear through the waveguide and substrate. This is a crucial assumption and is discussed in detail in Section 5.5.

The proton–exchange process increases only the extraordinary index (n_e) and so only TE modes can be guided in x–cut material and TM modes in z–cut material. This means that only electro–optically induced changes in n_e can be detected. The only coefficient which can be used for proton–exchange devices is, therefore, r_{33}. Because of the experimental geometry used in the present work, z–cut substrates had to be used, with the electric field applied in the z–direction. Light propagated along the y–axis of the proton–exchanged waveguides.

5.4.3. Sample Processing.

One of the motivations for carrying out this work was to investigate whether there were any measurable differences in r_{33} for proton–exchanged waveguides which had been fabricated using benzoic acid melts containing different quantities of lithium benzoate[42,43,45], and to compare these r_{33} values with those of waveguides fabricated using neat benzoic acid melts.

The lithium benzoate mole–fractions used were 0.94% (sample LZ2), 1.01% (sample LZ4), and 0.55% (sample LZ5). Samples LZ1 and LZ3 were fabricated using neat melts. The fabrication temperature was 235°C. Many practical devices require single–mode propagation. For this reason, the target depth for each waveguide was 0.5μm. The results of Chapter 4 were used to estimate effective diffusion coefficients at 235°C for the above melts, from which the times required to achieve a depth of 0.5μm were calculated.

The fabrication conditions of the proton–exchanged samples were as follows:

(a) sample LZ1:– 0%, t=9min
(b) sample LZ2:– 0.94%, t=55min
(c) sample LZ3:– 0%, t=9min
(d) sample LZ4:– 1.01%, t=55min
(e) sample LZ5:– 0.55%, t=27min.

The titanium–indiffused waveguides were fabricated on y–cut substrates, with the long axis along the x–direction. The electric field was applied in the y–direction and so only changes in n_o were detected. Consequently, the relevant electro–optic coefficient used was r_{22} since, from Equations (7) we have:

$$\Delta n_e = -n_e^3 r_{32} E_y/2 \text{ and } \Delta n_o = -n_o^3 r_{22} E_y/2 \ldots\ldots\ldots(14)$$

for TE and TM modes. Since r_{32} is zero and n_o changes via r_{22}, TM propagation is required for measurements to be possible. The fabrication conditions of the titanium–indiffused samples were as follows*:

(a) TI1:– 300Å titanium, diffused at 1000°C for 4hr in a wet O_2 atmosphere (in the presence of lithium niobate powder)

(b) TI2:– 400Å titanium, diffused at 1000°C for 5hr 20min in a dry O_2 atmosphere

(c) TI3:– 300Å titanium, diffused at 1000°C for 4hr in a dry O_2 atmosphere.

(Flow rates were 1.275 litre/min and the water temperature was 60°C).

The titanium–indiffused waveguides supported (respectively) one TM and two TE modes (samples TI1 and TI3), and 2 TM and 3 TE modes (sample TI2). The sample thicknesses were in the range 0.7mm to 1mm and the fabrication process is given in Table 5.7.

* *I am indebted to Dr. A. Faik for providing these waveguides.*

5.4.4. Results.

A typical fringe pattern is shown in Figure 5.9a (sample LZ1). Fringes were counted with the aid of a Hamamatsu video camera and monitor. Figure 5.9b is a photograph of the detected fringe pattern (sample LZ1), as displayed on the monitor. The bright and dark fringes correspond to regions of constructive and destructive interference, the period between which is π. The errors involved in estimating the electro-optic coefficients were largely due to the precision in counting the number of displaced fringes. A fairly conservative estimate of the precision was $\pm\pi/4$, for a fringe spacing (on the screen) of approximately 3mm. This corresponded to measuring fringe displacements to ±0.75mm. Figure 5.10 shows the linear relationship between fringe displacement and applied voltage for the proton-exchanged sample LZ2. From this, and similar plots for the other waveguides, the values of r_{33} (proton-exchange) and r_{22} (titanium-indiffused) were estimated (Table 5.7).

No relationship between r_{33} and the lithium benzoate mole-fraction was evident for the proton-exchanged waveguides. Assuming that this observation is correct, the average value of r_{33} is $(1.91 \pm 0.40) \times 10^{-12}$ m/V, which is approximately 1/16th of the bulk value. The latter value of r_{33} is slightly lower than that of 1/10th, quoted by Minakata *et al*[43]. However, values quoted by Otsaka *et al*[44] are 1/20th (for guides fabricated in neat benzoic acid melts) and 1/30th (for guides fabricated in pyro-phosphoric acid melts). The value obtained in the present work is between the values given by the other two papers.

Otsaka *et al*'s method[44] was slightly different, in that end-fire coupling into the planar waveguide, and a 50Hz a.c. driving voltage were used. The system was incorporated into one arm of an external Mach-Zehnder interferometer. Minakata *et al*[43] used the phase modulation technique. The values are in agreement that r_{33} is significantly reduced for proton-exchanged waveguides.

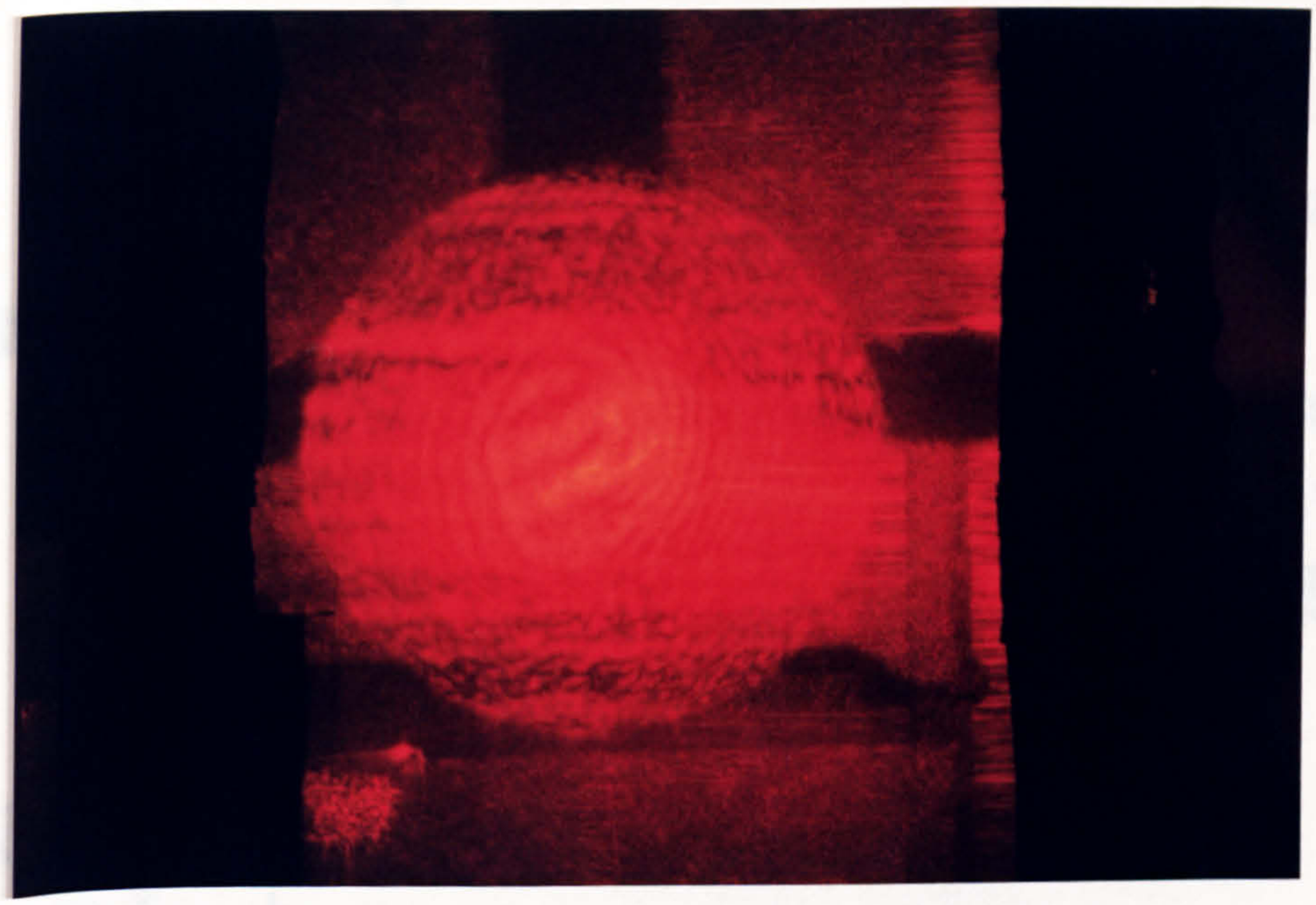

Figure 5.9a. Interference Fringes Observed With The Interferometer Of Figure 5.8.

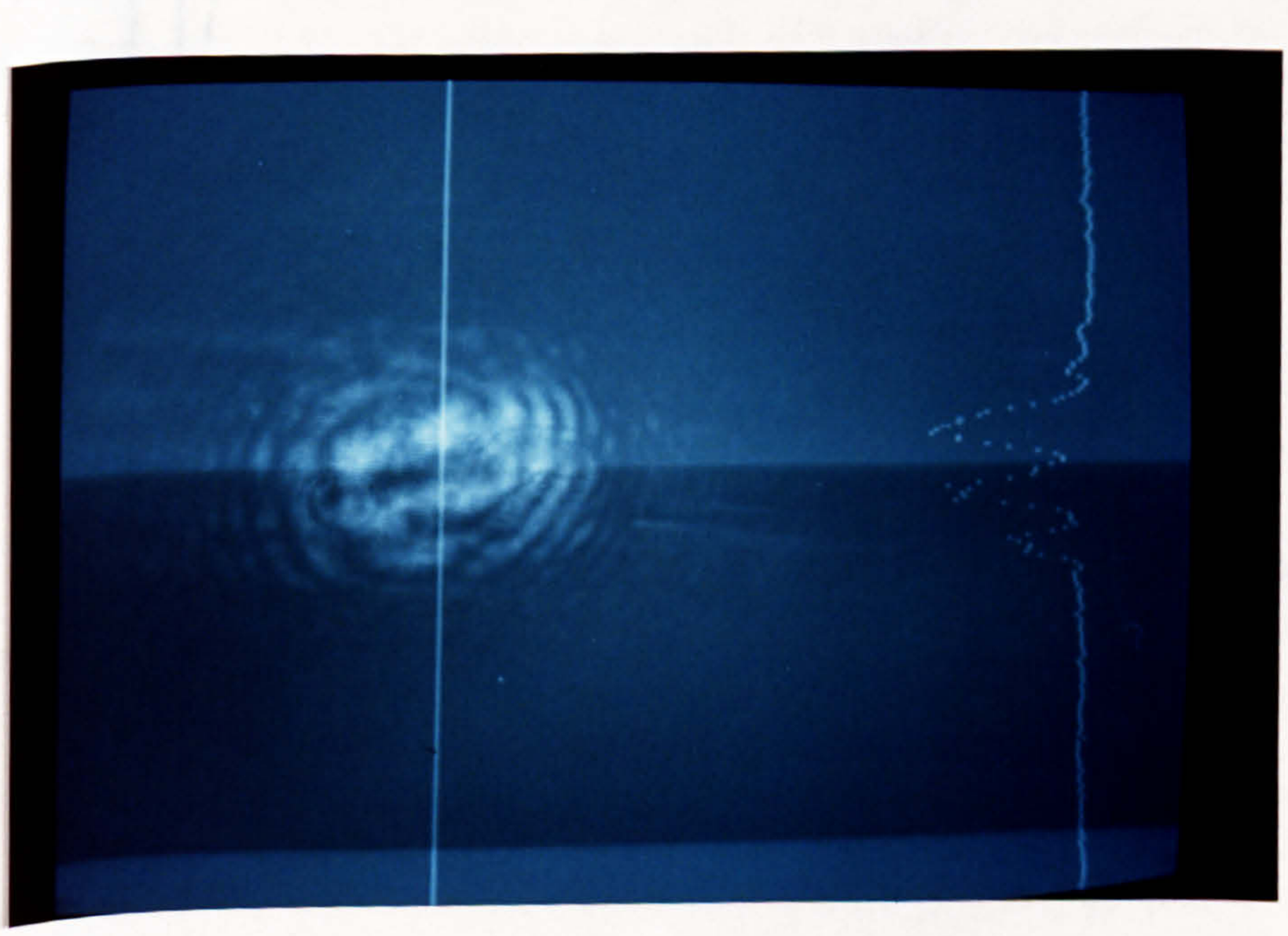

Figure 5.9b. Photograph Of Fringes As Monitored With A Hamamatsu Video Camera And Monitor.

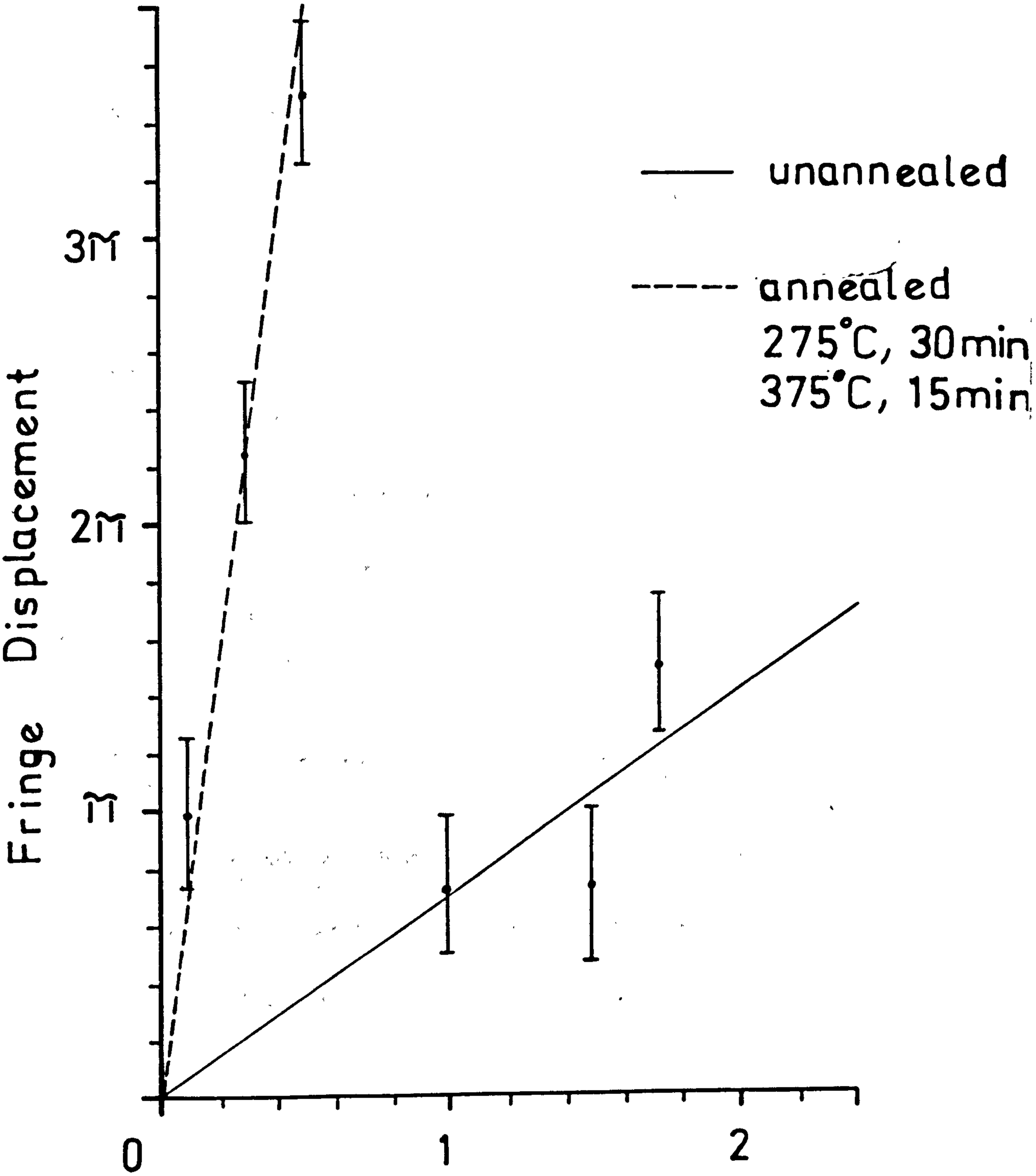

Figure 5.10. Fringe Displacement As A Function Of Applied Voltage For The Z−Cut Proton−Exchanged Waveguide LZ2, Before And After Annealing At 275°C For 30min And 375°C For 15min.

Sample	Description	r_{33}	r_{22}	r_{33}^*
			(x10^{-12}m/V)	
LZ1	PE, 0%	2.46±0.41	---	9.25±0.95
LZ2	PE, 0.94%	1.64±0.41	---	22.33±3.90
LZ3	PE, 0%	2.01±0.40	---	16.09±4.02
LZ4	PE, 1.01%	1.43±0.41	---	24.58±6.14
LZ5	PE, 0.55%	2.02±0.40	---	23.16±4.41
Z5L	*Annealed into single-mode region*		14.81±2.89	
TI1	TI, 300A, 4hr	---	4.40±0.71	---
TI2	TI, 400A, 5hr 20min	---	2.41±0.53	---
TI3	TI, 300A, 4hr	---	3.91±0.81	---

Table 5.7. Electro-Optic Coefficients Of Z-Cut Proton-Exchanged Waveguides (LZ1 To LZ5, And Z5L) And Y-Cut Titanium-Indiffused Waveguides (TI1 To TI3).

TI: *Titanium-Indiffusion Was Carried Out At 1000°C In Wet O_2.*
PE: *Proton-Exchange Was Carried Out At 235°C.*

* *After Annealing At 275°C For 30min And 375°C For 15min.*

Sample	Waveguide Index	Depth (μm)
LZ1	2.2932	0.90
LZ2	2.2948	0.80
LZ3	2.2969	0.95
LZ4	2.2823	0.83
LZ5	2.2763	0.88

Table 5.8. Waveguide Indices And Depths (λ= 0.6328μm) After Annealing At 275°C For 30min And 375°C For 15min.

Assuming there is no relationship between the value of r_{22} and the fabrication conditions of the titanium–indiffused waveguides, the average value is $(3.57 \pm 1.04) \times 10^{-12}$m/V. The bulk d.c. value of r_{22} is 6.8×10^{-12}m/V and the bulk high–frequency value is 3.4×10^{-12}m/V[55]. Measurements carried out on titanium–indiffused stripe waveguides using overlap integral calculations[46] indicate that there is *no* significant reduction in the electro–optic effect.

The lower value determined in the present work could conceivably be due to clamping effects during measurement, although a simple calculation based on the mass of the electrodes did not indicate significant changes*. Clamping effects are less important for r_{33}, since the difference between the low– and high–frequency values is small ($r_{33} = 32.2 \times 10^{-12}$m/V, $r_{33} = 30.8 \times 10^{-12}$m/V, respectively[16]).

5.4.5. A Restored Electro–Optic Effect For Proton–Exchanged Waveguides.

Once the values of r_{33} had been measured, the proton–exchanged waveguides were annealed. Chen *et al*[29] reported that proton–exchanged cut–off modulators which had been annealed had significantly reduced drive voltages compared to their unannealed counterparts, suggesting that annealing had some effect on the electro–optic properties of the waveguide layer. In the present work, the values of r_{33} were re–measured after annealing at 275°C for 30mins, and at 375°C for 15mins. The annealing atmosphere was wet O_2 flowing at 1.575litre/min. The guides remained single–mode after the first stage of annealing and supported two modes after the last stage of annealing.

Measurements were made using both modes in each waveguide. No measurable difference in the value of r_{33} for the fundamental (m=0) and first order mode (m=1) was evident. The fact that each waveguide supported two modes was advantageous, since the waveguide (surface) refractive indices and depths could be estimated. The results are given in Table 5.7 and Table 5.8.

* *Thanks to Prof. R.M. De La Rue for helping with this calculation.*

The linear relationship between fringe displacement and applied voltage is shown in Figure 5.10, for sample LZ1. After the proton–exchanged waveguides were annealed, the magnitude of V_π had decreased substantially (Figure 5.10). The corresponding values of r_{33} increased to an average of $(19.09 \pm 6.37) \times 10^{-12}$ m/V, i.e. to approximately 62% of the bulk value (Table 5.7). The waveguide indices decreased to (2.2887 ± 0.0089). In comparing the latter value with the results of Chapter 4, the refractive index profiles were assumed to be quasi–step–like (Table 5.8).

The value of r_{33} for the sample used in Section 5.2.4, which exhibited very low–loss after annealing into the mono–mode region (sample Z5L), was also measured. The value of r_{33} estimated for this waveguide was $(14.81 \pm 2.89) \times 10^{-12}$ m/V, which is similar to the values quoted for the above two–mode waveguides. The electro–optic performance has not, therefore, been shown to be dependent on the number of modes supported.

5.5. DISCUSSION

Li *et al*[47] have described a new process for realising low–loss proton–exchange waveguides which they call *double–exchange*. This is a two–step procedure carried out in a vacuum–sealed tube at 300°C. They have reported that the large refractive index change is preserved ($\Delta n_e \simeq 0.125$ at $\lambda = 0.6328\,\mu$m) and that there is low inter–modal coupling via scattering.

The first stage consists of proton–exchange in x–cut lithium niobate using a 2.5% lithium benzoate mole–fraction. Because of the large mole–fraction, the fabrication time required to obtain depths which allow even single–mode propagation is long, e.g. up to 14 days. Under these conditions the Li–H substitution is limited to 12%[47], the surface layer $Li_{1-x}H_xNbO_3$ presenting almost the same crystalline structure as the substrate[40]. The resulting waveguides are multi–mode, have low losses ($\leqslant$0.4dB/cm, measured by the *three–prism method*), and have a graded–index profile ($\Delta n_e \simeq 0.025$, $d \simeq 10\,\mu$m)[47].

For the next stage, a lower lithium benzoate mole–fraction is used (1%). The duration of the second stage is chosen according to the required depth. The second stage, alone, would result in a step–index profile with $\Delta n_e \simeq 0.125$, and the Li–H substitution ratio would be between 65% and 75%[47]. When the two stages were superimposed on the same substrate (a double–exchange) the authors reported that, (i) the low–loss obtained from the first stage was preserved, (ii) a high index change resulted from the second stage, (iii) the refractive index profile was step–like, followed by a graded–index tail extending into the substrate and, (iv) there was a very low level of inter–modal coupling via scattering.
The disadvantages of using the double–exchange process are that it is practically inevitable that multi–mode waveguides are produced after the second stage, and that the whole fabrication process itself is difficult and time–consuming. The samples have to be transferred from one sealed–vessel to another, and the fabrication times can be as long as three weeks, depending on the mole–fraction and depth required.

The 12% Li–H replacement, reported by the authors[47], is lower than would be expected for a mole–fraction of 2.5%. The results of Rice *et al*[40] indicate that between 50% and 60% replacement occurs. It is doubtful, from the work presented in Chapter 4, that the values of Δn_e for a 2.5% mole–fraction (first stage) and a 1% mole–fraction (second stage) are, respectively, 0.025 and 0.125. Work performed in the present study (Chapter 4) has shown that the value of Δn_e is closer to 0.08 for a 2.5% mole–fraction and 0.10 for a 1% mole–fraction.

Campari *et al*[50] showed that in proton–exchanged waveguides, where an approximate step–index profile is produced, the strains are distributed at the waveguide/substrate boundary. The sharp interface could, therefore, contribute to high propagation losses. Li *et al*[47] suggested that by distributing the strain through a graded–index tail (over approximately a few microns), the losses could be reduced. However, the strains are unlikely to be solely at the interface region, since the Li–H substitution has taken place within the *whole* layer. The strain would, therefore, be distributed *throughout* the layer, and not localised at the interface between substrate and waveguide, as Li *et al* suggest[47].

The low losses of samples X5L and Z5L (Section 5.2.5) may be explained as follows. From the results of Rice *et al*[40], the value of 'x' in the layer $Li_{1-x}H_xNbO_3$, for the proton-exchanged waveguides used in Section 5.2.4 was 0.75 for neat-melts and 0.65 for a 1% dilute-melt, leaving a surface layer with the (approximate) composition $Li_{0.3}H_{0.7}NbO_3$. For the low-loss samples X5L and Z5L of Section 5.2.5, 'x' was estimated to be[40] 0.65. However, it has been shown (Chapter 4) that annealing causes protons to diffuse from the guiding layer into the substrate, with the possibility of lithium ion migration from the substrate into the waveguide. Therefore, 'x' effectively decreases as a result of annealing, more so in samples X5L and Z5L since the proton-concentration in the latter samples was lower than in the other waveguides. The much smaller value of 'x', together with the fact that the waveguides were single-mode, could conceivably result in lower losses.

The method of achieving low-loss proton-exchanged waveguides by annealing into single-mode operation (Section 5.2.5) is clearly more attractive than Li *et al*'s method, since only *short* fabrication times and *lower* fabrication temperatures are required, with a minimum amount of experimental work. Although the waveguide index is relatively low (2.2225), there are no problems associated with inter-modal scattering (since the waveguides are single-mode).

Contrary to other workers[42,43,45], the present work has shown that there is no clear experimental evidence suggesting that the value of r_{33} for proton-exchanged waveguides depends on mole-fractions of up to 1.1%. It has been reported[43] that the value of r_{33} is 3.3×10^{-12}m/V for 0% (neat benzoic acid) and 3.6×10^{-12}m/V for a 1% mole-fraction. This is a small difference, and *no* experimental errors were assigned. It is doubtful that the absolute value of r_{33} can be measured with enough accuracy to say that these numbers are truly different.

Wong[45] reported that r_{33} is preserved in Mach-Zehnder intensity modulators fabricated using dilute-melts, although he noted that this may have been a result of some annealing which had taken place during the deposition of SiO_2 buffer layers. The *presence* of an SiO_2 dielectric

buffer layer could, itself, have an effect on the performance of an electro–optic device. For example, if the buffer layer is not highly conductive, the potential drop could occur mainly in the buffer layer rather than in the waveguiding material. The thickness of the buffer layer (which is generally greater than the thickness of the waveguiding region) could therefore be of importance.

In Chapter 4 it was shown that the hydrogen–bonded OH–hydroxyl group responsible for the broad infrared absorption band at $\upsilon_{max} = 3250cm^{-1}$ was removed by annealing and the extent of its formation was reduced by using dilute–melts. Assuming that the presence of hydrogen–bonded OH contributes, in part, to the lattice strain, the subsequent removal could lead to lower losses and a partially restored electro–optic effect.

The strain present in waveguide layers has been shown by several workers to decrease as the lithium benzoate mole–fraction is increased. For example[43,48], in the c–axis direction the strain $\Delta c/c$ was measured to be 0.47% and 0.27% for neat and 2.5% dilute benzoic acid melts, respectively. Any strain present as a result of lattice distortion can be substantially relieved by annealing[49]. This may, in part, explain why the electro–optic effect and propagation losses can be improved more by the annealing process than by using dilute–melts.

In the method of measuring electro–optic coefficients used in the present study, the applied electric field was assumed to be linear through the waveguide and substrate. It was suggested in Chapter 4 that hydrogen–bonded OH–hydroxyl groups (protons) could be influenced by the presence of an electric field. The migration of the latter protons under the influence of an applied field could result in a charge build–up at the electrode/waveguide boundary or the waveguide/substrate boundary (Figures 5.8a and 5.8b), due to ionic conductivity. This could, therefore, act as a possible source of non–linearity for the applied electric field.

Charge build–up is more likely to take effect in the stripe waveguide/surface electrode configuration, since the field is through the waveguide alone. In the present study, the field was through the lithium niobate

substrate (in addition to the waveguide), which is essentially an insulator at room–temperature. Therefore, ionic conductivity in the planar waveguide would occur to a lesser extent.

In the present chapter it has been demonstrated that the electro–optic effect can be partially restored in *planar* proton–exchanged waveguides. The method of restoration has yet to be tested for stripe waveguide configurations. The methods described above have now potentially brought the proton–exchange reaction into direct competition with other technologies in terms of propagation losses and electro–optic modulation. For example, at $\lambda = 0.6328\mu m$, titanium–indiffused waveguides have reported losses of 0.3dB/cm[47]; silver ion–exchanged soda–lime glass waveguides[51] and helium implanted waveguides in lithium niobate[52] both have measured losses of 2dB/cm; potassium ion–exchanged soda–lime glass waveguides have losses of 1dB/cm[6]; and thin–film waveguides produced by sputtering or evaporation of ZnO and ZnS onto silicon wafers have losses of the order of 1.5dB/cm and 5.23dB/cm, respectively[4].

Although the afore–mentioned waveguide losses have been measured using a range of techniques, it is clear that waveguides produced by the process described in Section 5.2.4 have, in some cases, much lower losses. Combined with the improved electro–optic effect (observed after annealing), large refractive index changes, and the possibility of refractive index profile modification by annealing or by using dilute–melts, proton–exchange becomes, potentially, one of the most attractive processes to date.

REFERENCES.

(1) R.L. Holman, L.M. Althouse Johnson, D.P. Skinner, *Desirability of Electro–Optic Materials For Guided–Wave Optics*, Opt. Eng., 26(2), 134, (1987).

(2) P.K. Tien, *Light–Waves in Thin–Films and Integrated Optics*, Appl. Opt., 10, 2395, (1971).

(3) M. Kartzow, T. Le Hiep, R.Th. Kerston, *Losses of Optical Multi–Mode Strip Waveguides Made By Thick–Film Technology*, Opt. Commun., 29(2), 160, (1979).

(4) M.D. Himel, U.J. Gibson, *Measurement of Planar Waveguide Losses Using a Coherent Fibre Bundle*, Appl. Opt., 25(23), 4413, (1986).

(5) Y. Okamura, s. Yashinaka, S. Yamamoto, *Measuring Mode Propagation Losses of Integrated Optical Waveguides: A Simple Method*, Appl. Opt., 22(23), 3892, (1983).

(6) Y. Okamura, S. Sato, S. Yamamoto, *Simple Method of Measuring Propagation Losses of Integrated Optical Waveguides: An Improvement*, Appl. Opt., 24(1), 57, (1985).

(7) Unpublished work carried out by GEC Marconi Research Centre (U.K.) under the JOERS program *Improved Lithium Niobate for Integrated Optics.*

(8) F.P. Schafer, *Dye Lasers*, (Springer, New York, 1973).

(9) F. Zernik, J.W. Douglas, D.R. Olson, *Transmission Measurements In Optical Waveguides Produced By Proton Irradiation of Fused Silica*, J. Opt. Soc. Am., 61, 678, (1971).

(10) H.P. Weber, F.A. Dunn, W.N. Leibolt, Appl. Phys., 12, 755, (1973).

(11) T. Tamir, *Topics in Applied Physics: Integrated Optics*, (Springer, Verlag, New York,1975).

(12) Y.H. Won, P.C. Jaussuad, G.H. Chartier, *Three–Prism Loss Measurements of Optical Waveguides*, Appl. Phys. Lett., 37(3), 269, (1980).

(13) E.A. Artunyan, S.Kh. Gabyan, *New Method For Loss Measurements In Optical Waveguides*, Opt. Commun.,57(6), 391, (1986).

(14) J.F. Duffy, Ph.D thesis, University of Glasgow, 1986.

(15) I.P. Kaminow, *Introduction to Electrooptic Devices*, (A.P. New York, 1974), also J.F. Nye, *Physical Properties of Crystals* (OUP, London, 1957).

(16) J.T. Milek, M. Neuberger, *Linear Electro–optic Modulator Materials*, (IFI/Plenum, New York, 1972).

(17) E. Bernal, G.D. Chen, T.C. Lee, *Low–Frequency Electro–Optic & Dielectric Constants Of* $LiNbO_3$, Phys. Lett., 21(3), 259, (1966).

(18) P.V. Lenzo, E.G. Spencer, K. Nassau, *Electro–Optic Coefficients In Single–Domain Ferroelectric Lithium Niobate*, J. Opt. Soc. Am., 56(5), 633, (1966).

(19) J.D. Zook, D. Chen, G.N. Otto, *Temperature–Dependence & Model Of The Electro–Optic Effect In* $LiNbO_3$, Appl. Phys. Lett., 11(5), 159, (1967).

(20) E.H. Turner, *High–Frequency Electro–Optic Coefficients of Lithium Niobate*, Appl. Phys. Lett., 8(11), 303, (1966).

(21) E.H. Turner, F.R. Nash, P.M. Bridenbaugh, *Dependence of Linear Electro–Optic Effect & Dielectric Constant on Melt Composition of Lithium Niobate*, J. Appl. Phys. 41(13), 5278, (1970).

(22) J. Warner, *The Temperature–Dependence of Optical Birefringence in $LiNbO_3$*, Phys. Lett., 20(2), 163, (1966).

(23) M.E. Lines, A.M. Glass, *Principles and Applications of Ferroelectrics and Related Materials*, (O.U.P., 1977).

(24) J.R. Carruthers, G.E. Peterson, M. Grasso, P.M. Bridenbaugh, *Non–Stoichiometry & Crystal Growth of $LiNbO_3$*, J. Appl. Phys., 42(5), 1846, (1971).

(25) S.C. Abrahams, P. Marsh, *Defect Structure Dependence on Composition in Lithium Niobate*, Acta Cryst., B42, 61, (1986).

(26) J.E. Midwinter, *Lithium Niobate: Effects of Composition on the Refractive Indices & Optical Second Harmonic Generation*, J. Appl. Phys., 39(7), 3033, (1968).

(27) J. Noda, H. Iwasaki, *Impurity Diffusion Into Lithium Niobate*, Proc. 2nd Meeting on Ferroelectric Materials and Their Applications, 24th–26th May, 1979, Kyoto.

(28) D.A. Bryan, R. Gerson, H.E. Tomaschke, *Increased Damage Resistance in $LiNbO_3$*, Appl. Phys. Lett., 44(9), 847, (1984).

(29) J.R. Carruthers, I.P. Kaminow, L.W. Stultz, *Diffusion Kinetics & Optical Waveguide Properties of Out–Diffused Layers in Lithium Niobate*, Appl. Opt., 13(10), 2333, (1974).

(30) H. Hirano, Japan. J. Appl. Phys., 8, 339, (1969).

(31) H. Hirano, *Melt Composition Dependence of the Pockels Effect in Lithium Niobate Crystals*, J. Phys. Soc. Japan Suppl. 28, 10, (1970).

(32) R.E. Dickenson, H.B. Gray, G.P. Haight, Jr., *Chemical Principles* (2nd Edition, W.A. Benjamin, Inc., Calif., 1978, page 117).

(33) M. De Micheli, *Non–Linear Effects in TIPE Lithium Niobate Waveguides for Optical Communications*, J. Opt. Commun., 4(1), 25, (1983).

(34) K.K. Wong, R.M. De La Rue, S. Wright, *Electro–Optic Waveguide Frequency Translator in Lithium Niobate Fabricated By Proton–Exchange*, Opt. Lett., 7(11), 546, (1982).

(35) R. Chen, C.S. Tsai, *Thermally Annealed Single–Mode Proton–Exchanged Channel Waveguide Cut–Off Modulator*, Opt. Lett., 11(8), 546, (1986).

(36) M. Papuchon, Y. Combemale, X. Mathieu, D.B. Ostrowsky, L. Reiber, A.M. Roy, B. Sejourne, M. Warner, *Electrically Switched Optical Directional Coupler: COBRA*, Appl. Phys. Lett., 27(5), 289, (1975).

(37) R.V. Schmidt, R.C. Alfernesse, *Directional Coupler Switches, Modulators, & Filters Using Alternating $\Delta\beta$ Techniques*, IEEE Trans. Circ. Syst., CAS–26(12), 1029, (1979).

(38) R.A. Becker, *Guided–Wave Optics in $LiNbO_3$: Physical Properties, Devices, & Signal Processing Systems*, SPIE Proc. Int. Opt. Cir. Eng., vol. 517, (1984).

(39) R.A. Becker, *Comparison of Guided–Wave Interferometric Modulators Fabricated on $LiNbO_3$ Via Titanium–Indiffusion and Proton–Exchange*, Appl. Phys. Lett., 43(2), 131, (1983).

(40) C.E. Rice, J.L. Jackel, *The Structure & Properties of $Li_{1-x}H_xNbO_3$*, Mat. Res. Bull., 19, 591, (1984).

(41) J.L. Jackel, C.E. Rice, J.J. Vesselka, *Compositional Control in Proton–Exchanged Lithium Niobate Waveguides*, Elect. Lett., 19, 387, (1983).

(42) M. Minakata, K. Kumagai, S. Kawakami, *Studies on Lattice Constant Changes & Electro-Optic Effects in Proton-Exchanged $LiNbO_3$ Optical Waveguides*, 1st Optoelectronics Conference, Technical Digest, July, 1986, Tokyo.

(43) M. Minakata, K. Kumagai, S. Kawakami, *Lattice Constant Changes & Electro-Optic Effects in Proton-Exchanged $LiNbO_3$*, Appl. Phys. Lett., 49(16), 992, (1986).

(44) Y. Otsuka, H. Li, Y. Fujii, *personal communication/ unpublished work.*

(45) K.K. Wong, *An Experimental Study of Dilute-Melt Proton-Exchange Waveguides in X- and Z-Cut Lithium Niobate*, GEC J. Res. 3(4), 243, (1985).

(46) Unpublished work carried out by Plessey (Caswell) under the JOERS program *Improved Lithium Niobate for Integrated Optics.*

(47) M.J. Li, M. De Micheli, D.B. Ostrowsky, M. Papuchon, *High Index Low-Loss $LiNbO_3$ Waveguides*, Opt. Commun., 62(1), 17, (1987).

(48) M. De Micheli, J. Botineau, S. Neveau, P. Sibillot, D.B. Ostrowsky, M. Papuchon, *Independent Control of Index Profiles in Proton-Exchanged $LiNbO_3$ Waveguides*, Opt. Commun., 8, 114, (1983).

(49) M.N. Armenise, S.M. Al-Shukri, A. Dawar, R.M. De La Rue, A.C.G. Nutt, *Optical Characterisation of Proton-Exchanged and Titanium-Indiffused Proton-Exchanged Slab Waveguides on $LiNbO_3$*, IEEE International Workshop on Integrated Optical & Related Technologies for Signal Processing, Technical Digest, 21, Italy (1984).

(50) A. Campari, C. Ferrari, G. Mazzi, C. Summonte, S.M. Al-Shukri, A.L. Dawar, R.M. De La Rue, A.C.G. Nutt, *Strain & Surface Damage Induced By Proton-Exchange in Y-Cut Lithium Niobate*, J. Appl. Phys., 58(12), 4521, (1985).

(51) T.J. Cullen, C.D.W. Wilkinson, *Radiation Losses From Single–Mode Optical Y–Junctions Formed By Silver–Ion Exchange in Glass*, Opt. Lett., 10, 134, (1984).

(52) B.L. Weiss, J.L. Flint, *The Characterisation of Optical Waveguides Fabricated in Y– and Z–Cut* $LiNbO_3$ *By* He^+ *Implantation*, J. Appl. Phys., 60(1), 464, (1986).

CHAPTER 6

Summary, Conclusions, And Future Work

The crystal structure of congruent lithium niobate (above and below the Curie temperature) and the growth of single–crystal lithium niobate by the Czochralski technique have been discussed, with reference to the published literature.

The possibility of non–stoichiometric growth and the relationship between melt composition and solid (crystal) composition were discussed. The congruent melting composition of lithium niobate (i.e. when the melt cools to give a solid of the same stoichiometry) is 48.6 mole% Li_2O. Some of the properties which depend on the composition of the crystal have been discussed.

The processes available for waveguide fabrication in lithium niobate, namely lithium oxide (Li_2O) outdiffusion, ion–implantation, metal–indiffusion, and proton–exchange have been reviewed, with comparisons made between the fabrication procedures and the properties of the resultant waveguides. The problems associated with proton–exchange have been briefly described, and some of the active and passive devices fabricated by proton–exchange have been discussed.

It was mentioned that, when considering proton–exchange for fabricating waveguide devices, the major problems which have to be avoided are relaxation effects in effective mode–indices, high propagation losses, and the greatly reduced electro–optic effect. A study of the latter three effects was targeted as part of the work to be carried out in the thesis.

The object of the work carried out in Chapter 2 was to determine the extent of proton–exchange as a function of temperature and time using three different techniques: optical waveguide prism–coupler measurements, infrared absorption spectroscopy and atomic absorption spectroscopy.

Effective diffusion coefficients (at temperatures in the range 167°C to 211°C) and activation energies were estimated using data obtained from both prism–coupling measurements (assuming a step–like refractive index profile) and infrared absorption spectra of proton–exchanged waveguides. Agreement between the latter two methods was good. However, the effective diffusion coefficients and activation energies were different from values quoted by previous workers. The differences were shown to be due to discrepancies between oil–bath temperatures and acid temperatures, the latter being lower by as much as 10°C.

From the polarisation dependence of the absorption bands, the free OH− hydroxyl group vibration at $\upsilon_{max}=3505cm^{-1}$ was found to be localised mainly in the (x− y)− plane, while the hydrogen− bonded OH− hydroxyl group absorption band at $\upsilon_{max}=3250cm^{-1}$ had vibrational components along the x− y− and z− axes of the crystal. A linear relationship between the area under the infrared absorption bands and $t^{1/2}$ was established, confirming that proton− exchange is a diffusion process. A relationship between waveguide depth and the area under the infrared absorption bands was given, for both x− and z− cut proton− exchanged waveguides, enabling the depth of proton− exchanged regions to be estimated simply by recording the infrared spectrum.

The extent of proton− exchange was determined with temperature and time by using atomic absorption spectroscopy to estimate lithium concentrations in benzoic acid, after proton− exchange. The results indicated, as expected, that the lithium concentration in the acid increases with temperature and time. The value of 'x' in the equation $Li_{1-x}H_xNbO_3$ was estimated to be approximately 0.33, corresponding to 33% of the original lithium ions in the waveguide layer exchanging with protons. The latter value was lower than the value (of between 65% and 75%) quoted by other workers using different techniques.

It is suggested that the low value could have been explained by loss of lithium in some form during proton− exchange. The latter suggestion has been tested, however further work has yet to be carried out in order to determine conclusively whether or not lithium is actually lost from the melt.

There has recently been an interest in proton− exchange waveguides fabricated using pyro− phosphoric acid. Yamamoto *et al*[1] reported that waveguides produced using pyro− phosphoric acid had a larger refractive index change ($\Delta n_e=0.145$, $\lambda=0.6328\mu m$) than guides produced using benzoic acid ($\Delta n_e=0.125$, $\lambda=0.6328\mu m$), and that the pyro− phosphoric acid waveguides had significantly lower propagation losses (e.g. 0.7dB/cm, $\lambda=0.6328\mu m$). The author of this thesis has carried out a brief study on z− cut proton− exchanged waveguides produced using ortho− phosphoric acid. The results of prism− coupling measurements and infrared absorption spectroscopy indicate that the ortho− phosphoric waveguides are no different from waveguides produced using benzoic acid. Work at Glasgow is continuing using pyro− phosphoric acid.

A hydrogen isotopic–exchange reaction was employed to investigate the stability of proton–exchanged waveguides at room–temperature. The extent of proton (hydrogen)–deuterium exchange with time was observed using infrared absorption spectroscopy, and was shown to be reversible. The experiments clearly showed that waveguides produced using neat benzoic acid melts reacted with atmospheric water vapour. The free OH–hydroxyl group absorption band at υ_{max}=3505cm^{-1} was resolved into two bands separated by approximately 30cm^{-1}, indicating the existence of two slightly different free OH–hydroxyl environments.

An x–cut deuterium–exchanged waveguide, prepared using deuterated benzoic acid, was shown to have a refractive index profile similar to that of proton–exchanged waveguides. The deuterium–exchanged waveguide was formed at a much slower rate (at a given temperature), as expected from the heavier mass of deuterium. The behaviour of the deuterium–exchanged waveguide with respect to reaction with atmospheric water vapour was not the same as for proton–exchanged waveguides, indicating possible structural differences between proton–exchanged and deuterium–exchanged waveguides.

The object of the work carried out in Chapter 4 was to study the properties of annealed proton–exchange waveguides and waveguides produced using dilute–melts. The extent of proton–exchange was determined as a function of time, at temperatures between 215°C and 235°C, for x–cut dilute–melt waveguides produced using lithium benzoate mole–fractions of up to 1.1%. Effective diffusion coefficients were estimated as a function of lithium benzoate mole–fraction, for the above temperatures. Experiments to estimate effective diffusion coefficients for y– and z–cut dilute–melt waveguides should also prove useful.

It was shown that annealed and dilute–melt waveguides could have very similar optical properties, depending on the amount of annealing and the mole–fractions used. For example, no relaxation of effective mode–indices was observed for waveguides which had been annealed. The extent of relaxation was reduced for waveguides produced using larger lithium benzoate mole–fractions. Annealing was shown (eventually) to reduce the waveguide (surface) refractive index, while the value of the waveguide index was shown to vary inversely with the lithium benzoate mole–fraction.

The infrared absorption spectra of annealed and dilute–melt waveguides were similar in that the absorption band of hydrogen–bonded OH–hydroxyls (υ_{max}= 3250cm^{-1}) was removed after annealing and the extent of its formation was reduced for dilute–melt waveguides, the amount of reduction being dependent on the mole–fraction. Isotopic–exchange experiments were carried out on annealed and dilute–melt waveguides. No measurable uptake of deuterium has been observed in either case, at room–temperature (although partial proton–deuterium exchange has been observed at temperatures between 300°C and 400°C). It is suggested that isotopic–exchange occurred via hydrogen–bonded OH, and that the non–existence of the latter hydroxyl group results in no isotopic–exchange. It is suggested that the relaxation effects and problems associated with electro–optic device operation (such as d.c. drift) are caused, in part, by migration of protons via hydrogen–bonding, and that combining the annealing and dilute–melt processes should improve waveguide performance.

Propagation losses and the electro–optic effect in proton–exchanged waveguides were the subjects of the work in Chapter 5. Observations were made on x– and z–cut waveguides produced using neat and dilute (up to 1.1%) benzoic acid melts, before and after annealing. The results of Chapter 4 were used to estimate effective diffusion coefficients (at 235°C) for the different lithium benzoate mole–fractions used. Single–mode waveguides were fabricated with closely similar exchanged region depths (0.5μm), in order to determine the relationship (if any) between melt–dilution and propagation loss. Propagation losses were obtained using a two–prism method at λ= 0.6328μm, with a brief study at λ= 1.15μm.

Observations (at a wavelength of 0.6328μm) on x–cut proton–exchanged waveguides showed that, after annealing at 275°C for 30min, there was relatively little change in the propagation losses (4dB/cm to 6dB/cm). Losses as low as 1.4dB/cm (for a waveguide produced using a 0.8% dilute–melt) were estimated after a second stage of annealing at 375°C for 15min, with substantial reductions in the losses of the other x–cut waveguides. A final stage of annealing (375°C, 26min) produced a dramatic increase in propagation loss to values above 6dB/cm. The fundamental mode (m= 0) losses were very high (≥18dB/cm) after annealing. The effects of annealing on z–cut proton–exchanged waveguides were different. Losses were initially lower (2dB/cm), but increased steadily through the same annealing routine as used for the x–cut samples.

A method yielding much lower propagation losses has been established. The method involved fabricating a thin (0.1μm) proton–exchange (dilute–melt, 1%) region, in which no modes were supported, and annealing the layer from below cut–off into the single–mode region (λ= 0.6328μm). Observations on one x–cut and one z–cut waveguide showed that two annealing stages were required to induce single–mode guiding (275°C, 30min followed by 375°C, 15min) and that very low losses were obtained– 0.18dB/cm for the x–cut waveguide, and 0.35dB/cm for the z–cut waveguide. The latter combination is not at all unique, since clearly a single annealing stage, with appropriate conditions, would suffice. The resulting waveguide index differences were, as expected, much lower (of the order of 10^{-2}) than the values of up to 0.125 found in unannealed waveguides. Comparably good results were not obtained at λ= 1.15μm, although this should be a straightforward achievement if the fabrication times are adjusted properly.

A method of estimating the electro–optic coefficients of planar waveguides was established. The method was an adaptation of a technique used for electro–optic measurements of bulk lithium niobate, involving the use of an external interferometer configuration. Measurements were made on samples which had been fabricated by proton–exchange, to a depth of 0.5μm (single–mode), using melts containing up to 1.1% lithium benzoate mole–fractions, before and after annealing.

Initially (using the TM mode on z–cut material), an estimated r_{33} value of 1.91×10^{-12}m/V was obtained– a massive reduction from the bulk value of 30.8×10^{-12}m/V. Subsequent annealing at 275°C for 26min and 375°C for 15min (giving two–mode waveguides) gave an estimated *ten–fold increase* in r_{33}, to a value of 19.09×10^{-12}m/V, i.e. approximately 2/3 of the bulk value. In the z–cut sample which became single–mode after annealing, the r_{33} value was reasonably comparable, at 14.81×10^{-12}m/V.

While it is not possible to assert that the low losses and large r_{33} values obtained are the ultimate limits for proton–exchanged waveguides, the results indicate clearly that useful performance is possible and that more investigations should be worthwhile. For example, propagation losses and r_{33} could be estimated for a range of annealing times and temperatures. An attempt at optimising the annealing conditions might result in waveguides with better optical properties.

An initial target depth of 0.1μm was chosen to fabricate the low-loss x- and z-cut waveguides. Using the combined results of Chapter 2 and Chapter 4 to estimate diffusion coefficients and fabrication times (at fixed temperatures), target depths of other than 0.1μm could be used. By optimising the annealing conditions, waveguides with losses lower than 0.18dB/cm (λ= 0.6328μm) ought to be achievable.

A more thorough investigation of propagation losses at infrared wavelengths (e.g. λ=1.15μm) should be carried out. The method of fabricating a proton-exchange region with a depth below cut-on for the fundamental mode and annealing the layer into the single-mode region could be used. This would require an independent set of experiments to determine optical properties of unannealed waveguides as a function of the extent of proton-exchange, at the particular wavelength required. These experiments should enable depths below and above the single-mode cut-on depth to be estimated for the required wavelength.

The present work has been concerned mainly with planar waveguides. Investigations should also be carried out for proton-exchanged strip waveguides. For example, lower insertion losses might be achieved by annealing the guide into single-mode propagation. Clearly, the method of restoration of the electro-optic effect in proton-exchanged (planar) waveguides should be tested for planar or strip waveguides, where the use of parallel surface electrodes and the different electric field configuration could present some problems. Consider, for example, the possible effects of ionic conductivity on electric fields applied via surface electrodes. Ionic conductivity in the waveguide could lead to a build-up of charge below the negative electrode (assuming the mobile ions are positively charged). The voltage drop would therefore take place (eventually) mainly below the negative electrode, and electro-optic modulation could not be applied in the guiding region.

An alternative electrode configuration yet to be investigated is one which involves strip waveguides with one (surface) electrode in direct contact with the proton-exchanged region and the other electrode in contact with the opposite face of the substrate. The latter configuaration is analogous to the method used to determine the electro-optic effect in planar waveguides, established in the present work. The lithium niobate substrate has to be polished to a thickness which enables the small voltages (±10 volts) applied via the electrodes to have any effect. Substrates have been polished down to a thickness of approximately

40μm at Glasgow University.

Charge build–up due to ionic conductivity would be less of a problem in the latter method, since the electric field would be applied *through* the waveguide and substrate. Because the conductivity of lithium niobate is extremely low at room–temperature, the bulk material between the waveguide and electrode would act essentially as an insulator. Mr. Scott McMeekin is currently investigating the electro–optic effect in both proton–exchanged and titanium–indiffused waveguides produced on thin lithium niobate substrates as part of his research for the degree of PhD.

REFERENCES.

(1). Y. Yamamoto, T. Taniuchi, *New Proton–Exchange Technique For $LiNbO_3$ Waveguide Fabrication*, Proc. Optical Fibre Communications Conference/Internatial Conf. Integrated Optics & Optical Fibre Communications, Nevada, January, 1987.

PUBLICATIONS.

A. Loni, R.M. De La Rue, J.M. Winfield, *Proton–Exchanged Lithium Niobate Planar Optical Waveguides: Chemical And Optical Properties And Room–Temperature Hydrogen Isotopic–Exchange Reactions*, J. Appl. Phys., 61(1), 64, (1987).

R.M. De La Rue, A. Loni, A. Lambert, J.F. Duffy, S.M. Al–Shukri, Y.L. Kopylov, J.M. Winfield, *Proton–Exchange In Lithium Niobate And Lithium Tantalate*, 4th European Conference On Integrated Optics, May 11th–13th, Glasgow, 1987.

A. Loni, R.M. De La Rue, J.M. Winfield, *Very Low–Loss Proton–Exchange Waveguides With A Substantially Restored Electro–Optic Effect*, to be published.